UNIVERSITY OF GAZİANTEP

GRADUATE SCHOOL OF

NATURAL & APPLIED SCIENCES

BUCKLING EFFECT INVESTIGATION OF HYBRID LAMINATED COMPOSITE PLATES

Ph.D THESIS

IN

MECHANICAL ENGINEERING

BY

EYÜP YETER

DECEMBER 2013

Buckling Effect Investigation of Hybrid Laminated Composite Plates

Ph.D Thesis

in

Mechanical Engineering

University of Gaziantep

Supervisor

Assist. Prof. Dr. Ahmet ERKLİĞ

by

Eyüp YETER

December 2013

REPUBLIC OF TURKEY
UNIVERSITY OF GAZİANTEP
GRADUATE SCHOOL OF NATURAL & APPLIED SCIENCES
MECHANICAL ENGINEERING DEPARTMENT

Name of the thesis: Buckling effect investigation of hybrid laminated composite plates

Name of the student: Eyüp YETER

Exam date: 27.12.2013

Approval of the Graduate School of Natural and Applied Sciences

Assoc. Prof. Dr. Metin BEDİR

Director

I certify that this thesis satisfies all the requirements as a thesis for the degree of Doctor of Philosophy.

Prof. Dr. M. Sait SÖYLEMEZ

Head of Department

This is to certify that we have read this thesis and that in our consensus/majority opinion it is fully adequate, in scope and quality, as a thesis for the degree of Doctor of Philosophy.

Assist. Prof. Dr. Ahmet ERKLİĞ

Supervisor

Examining Committee Members	Signature
Prof. Dr. İbrahim H. GÜZELBEY	.....
Assoc. Prof. Dr. Abdulkadir ÇEVİK	.....
Assoc. Prof. Dr. Faruk ŞEN	.....
Assist. Prof. Dr. M. Akif KÜTÜK	.....
Assist. Prof. Dr. Ahmet ERKLİĞ	.....

I hereby declare that all information in this document has been obtained and presented in accordance with academic rules and ethical conduct. I also declare that, as required by these rules and conduct, I have fully cited and referenced all material and results that are not original to this work.

Eyüp YETER

ABSTRACT

BUCKLING EFFECT INVESTIGATION OF HYBRID LAMINATED COMPOSITE PLATES

YETER, Eyüp
Ph.D. in Mechanical Engineering
Supervisor: Assist. Prof. Dr. Ahmet ERKLİĞ
December 2013 , 144 page

In this study, laminated hybrid composite plates have been produced using different combinations of Carbon, S-glass and Aramid fibers with epoxy resin (as a matrix) and effects of fiber types and their combinations on the buckling and lateral buckling have been investigated.

Hybrid plates have been produced using vacuum supported production unit (has been designed and produced). The hybrid plates are prepared having $[(0/90)_3]_s$, $[(30/-60)_3]_s$, $[(45/-45)_3]_s$ and $[(0/90)_6]_{us}$ symmetrical and unsymmetrical ply orientations. Buckling and lateral buckling test specimens have been prepared from produced hybrid plates and buckling and lateral buckling characteristics of produced hybrid composite plates have been determined. Comparisons of different hybrid configurations are performed to see effects of various combinations of fibers on buckling and lateral bucking. Hybrid configurations which have the highest and the smallest buckling and lateral buckling strength are determined.

Numerical studies have been performed using ANSYS finite element program. A parametric study is performed to see effects of various parameters such as hybrid plate thickness, plate aspect ratio, cutout type, size and location of cutouts are examined. Square, circular, triangular and elliptical cutouts are used during the analyses.

Key Words: Hybrid composite plates, buckling, lateral buckling

ÖZET

HİBRİD KOMPOZİT PLAKALARIN BURKULMA ETKİSİNİN ARAŞTIRILMASI

YETER, Eyüp
Doktora Tezi, Makine Mühendisliği Bölümü
Tez Yöneticisi: Yrd. Doç. Dr. Ahmet ERKLİĞ
Aralık 2013, 144 sayfa

Bu çalışmada, Karbon, S-cam ve Aramid fiberlerinin farklı kombinasyonları ve matris olarak epoksi reçinesi kullanılarak tabakalı hibrit kompozit plakalar üretilmiş, farklı fiber kombinasyonlarının burkulma ve yanal burkulma yüklerine etkileri araştırılmıştır.

Simetrik ($[(0/90)_3]_s$, $[(30/-60)_3]_s$, $[(45/-45)_3]_s$) ve simetrik olmayan ($[(0/90)_6]_{us}$) yönlenme açılarıyla hibrit plakalar vakum destekli üretim sistemi ile üretilmiştir. Üretilen plakalardan deney numuneleri hazırlanıp, plakaların burkulma karakteristikleri belirlenmiştir. Hibrit plakalardaki farklı fiber kombinasyonlarının burkulma ve yanal burkulma yüklerine etkileri incelenmiş ve sonuçlar karşılaştırılmıştır. En yüksek ve en düşük burkulma ve yanal burkulma mukavemetine sahip dizilim belirlenmiştir.

ANSYS sonlu elemanlar programı kullanılarak nümerik çalışmalar yapılmıştır. Hibrit plaka kalınlığı, plaka boy/en oranı, kesit tipi, boyu ve konumu parametrelerinin burkulma ve yanal burkulma yüklerine etkileri araştırılmıştır. Analizler sırasında, kare, daire, üçgen ve eliptik kesit tipleri kullanılmıştır.

Anahtar Kelimeler: Hibrid kompozit plakalar, burkulma, yanal burkulma

To My Mother (1962- 2009)

ACKNOWLEDGEMENTS

I would like to express my debt of the gratitude to Assist. Prof. Dr. Ahmet ERKLİĞ for his guidance, advice, criticism, encouragements, insight and suggestions throughout the research and preparation of this thesis.

I would also like to thank Prof. Dr. İbrahim H. GÜZELBEY and Assoc. Prof. Dr. Abdulkadir ÇEVİK for serving in my thesis committee and providing valuable contributions to the study.

I would like to thank all my coworkers in the Mechanic Department of Mechanical Engineering. In particular, I would like to thank Assoc. Prof. Dr. Bahattin KANBER, Assist. Prof. Dr. M. Akif KÜTÜK, Assist. Prof. Dr. Ö. Yavuz BOZKURT, research assistants İbrahim GÖV, M. Hanifi DOĞRU and Mehmet BULUT for their contributions to me.

I would also like to thank to my family for their supports during this study and all my educational life.

I would like to thank my wife for her continuous love and supports during the study.

This study was supported by Scientific Research Project Center of Gaziantep University (No: MF.11.07). Special thanks are due to the financial support of Scientific Research Project Center of Gaziantep University.

LIST OF CONTENTS

LIST OF FIGURES

FIGURES Page

LIST OF TABLES

TABLES Page

CHAPTER 1

INTRODUCTION

1.1 General Introduction

Materials are generally classified into three main groups which are namely metals, ceramics and plastics. Each of these three groups has different properties. Also they have some weakness or superiority from each others.

Due to gather superior properties of these groups in one material or to get a new feature from these groups, they combine at the macro level and these new structure is called as composite. There are several comments that define composite materials. Some of them are:

- A composite is a structural material that consists of two or more combined constituents that are combined at a macroscopic level and are not soluble in each other. One constituent is called the *reinforcing phase* and the one in which it is embedded is called the *matrix*. The reinforcing phase material may be in the form of fibers, particles, or flakes [1].
- The word composite in the term composite material signifies that two or more materials are combined on a macroscopic scale to form a useful third material [2].

Composite materials have been used for thousands of years. An early example of application of composites is bricks made of clay and reinforced with straw used by Israelites. The other early example is that mud walls reinforced with bamboo shoots used by Egyptians (1500 B.C.). Also, woven sticks bonded with cow dung and muds were used in the construction of house walls in England [3]. Similarly, Eskimos have used moss to improve the strength of ice while they are building their igloos.

More recently, in the 20th century civil engineers placed steel bars in cement and aggregate to make a well-known composite material, i.e., reinforced concrete [4]. The first composites in modern concern were used (in the production of boats and aircraft) when glass fibers reinforced with matrix (resin) in 1930s. This composite is generally called as fiberglass. When carbon, boron and aramid fibers developed in 1970s, the usage areas of composites increased rapidly.

Nowadays, engineering applications of composites have been increased since new composites have excellent properties and they have new and more applicable manufacturing methods comparing the ones used earlier. Some of the usage areas of composites are aerospace, automotive, marine and healthcare industry.

1.2 Definition of Hybrid Composite

The hybrid composite materials are composite materials that have more than one fiber (glass, boron, Kevlar or carbon) or more matrixes (polyester, epoxy and ect.) in its production stage. Using hybrid composite can increase some of the properties of which cannot be achieved by using traditional composite materials. Also hybrid composites can be more cost-effective (by using less cost fibers with more durable and more expensive ones) from the traditional composites or conventional materials.

In other words, the hybrid composites (in the aspect of Polymer Matrix Composites) are combinations of different fibers such as glass, boron, Kevlar and carbon in a matrix which can be thermoplastic or thermosetting. Hybrid composites are generally used to meet some design requirements (for example to have high strength with high toughness or high compressive strength with good fatigue or impact properties etc.) with less cost or sometimes with easy production advantages. There are four basic types of hybrid composites:

- Interply hybrids, that consists of plies from two or more different unidirectional composites stacked according to a specific sequence.
- Intraply hybrids, consisting in two or more different fibers mixed in the same ply.
- Interply-intraply hybrids, in which interply and intraply hybrids are stacked according to a specific sequence.

- Super hybrids, that are resin-matrix composite plies stacked according to a specific sequence.

1.3 Definitions of Buckling and Lateral Buckling

Buckling phenomenon can be defined as sudden failure of columns, beams or plates without main effects of stress in elastic or inelastic region. In the aspect of the plates, when a flat plate is subjected to in-plane compressive load, it remains flat and in equilibrium condition up to a critical value of load. At that load value, the equilibrium is eventually changed and the plate becomes unstable. The magnitude of the compressive load at which the plate becomes unstable is called the "critical buckling load".

When a cantilever beam is loaded with a lateral force, the end of the beam will deflect in downward direction normally. However, if the beam is long enough and thickness/height ratio of the cross-section of the beam is sufficiently small, the beam will collapse in a twisting mode. This is due to the compression in the bottom fibers of the beam which causes the fibers to buckle sideways. So this phenomenon is called as **lateral buckling**.

1.4 Importance of the Study

Advances in technology require materials with unique property combinations that cannot be achieved with conventional metal alloys, ceramics, or polymeric materials. This is particularly true for applications that require durability under extreme conditions such as aerospace, automobile, and infrastructure industry.

Superior mechanical, physical and chemical properties are achieved using composites and hybrid composites. The main advantages that drive the use of composites are weight reduction, corrosion resistance, wear resistance, part-count reduction, easy of handling, excellent damage tolerance and impact resistance great specific strength (high strength with less weight or more generally, it has high stiffness with less weight), enhanced fatigue life and low thermal expansion.

There have been many studies on the laminated composite structures as given in the following chapter (literature survey) due to the fact that composite structures have lots of application areas such as aerospace industry, automotive industry, marine applications, sporting goods industry, construction and civil structures and healthcare industry (like biomedical). In others words, they are used nearly all of the engineering based applications.

Buckling and lateral buckling characteristics of structures are very important research areas of engineers since this phenomenon have important value in the stability of composite structures. Sometimes buckling characteristic can be the most important design criteria in the engineering applications.

More durable and less buckling affected materials can be obtained with the use of hybrid composite material. Material distribution in layers, required number of layers and fiber orientation angles to avoid buckling can be determined. In this way, the benefits of hybrid laminated composites for automotive and aircraft industry can be determined.

1.5 Methods and Outline of the Study

In this study, laminated hybrid composite plates have been produced using different combinations of Carbon, Aramid and S-glass fibers with epoxy resin. In the production part, vacuum supported production unit (has been designed and produced) is used. Then buckling and lateral buckling characteristics of produced hybrid composite plates have been determined with different fiber orientation angles and symmetrical and unsymmetrical ply orientations. A parametric study is performed to see effects of various parameters such as hybrid plate thickness, plate aspect ratio, cutout type, size and location of cutouts. Study has been divided into 8 chapters.

General introduction and definitions on composites materials and buckling and lateral buckling are given in the first chapter. First chapter also includes importance of the study and outline of the study.

Literature review is given in chapter 2. Literature review has been grouped in four sections; general studies about composite plates, studies on buckling of composite plates, studies on lateral buckling of composite plates and studies on hybrid composite plates.

In chapter 3, derivation of buckling formulations for thin plates and application to composites are given.

Information about designed and produced vacuum supported production unit and production methods of composite and hybrid composites are given in chapter 4. Also mechanical properties, standards and test methods to determine these mechanical properties are given in this chapter.

Buckling experiments and results of buckling experiments which were conducted to see effects of different hybrid configurations on buckling are given in chapter 5 for different fiber orientation angles, symmetrical and un-symmetrical ply orientations.

In chapter 6, lateral buckling experiments and their results are given for different fiber orientation angles, symmetrical and un-symmetrical ply orientations.

Numerical studies on the buckling and lateral buckling of hybrid composites and comparison with the results which determined from experiments are given in chapter 7. This chapter is divided into the three main sections; numerical buckling studies, numerical lateral buckling studies and parametric study on numerical buckling and lateral buckling.

General conclusions and future works are given in chapter 8 and 9, respectively.

CHAPTER 2

LITERATURE SURVEY

2.1. Introduction

A brief literature review related with composite, hybrid composite materials, buckling and lateral buckling of composite materials are presented in this chapter. Literature review has been grouped in four sections. General studies on composite plates are reviewed in section 2.2. The literature review on buckling of composite plates is given in section 2.3. The literature review on lateral buckling of composite plates is given in section 2.4. Studies on hybrid composite plates are reviewed in section 2.5.

2.2. Literature Review on General Composite Studies

Parallel to the increase of the usage areas of composite materials, studies about the composites are increasing. In this section, some studies about composite materials are given.

Becenen [5] produced composite materials by combining trimmed glass fibers with thermoset plastic matrixes and the effects of resin chemical structure, variety of reinforcement, thickness of material and post-cure process on mechanical properties of composite materials were studied. The test results of produced composite materials were compared with the mechanical values of composite materials used in tractors.

Aktas and Karakuzu [6] investigated the effects of temperature on mechanical properties (tensile, compressive, shear) of glass/epoxy composite plates. The used temperatures of experiments were 20°C, 40°C, 60°C, 80°C, and 100°C. Laminated

composite plates were cured at constant pressure of 250 kPa with a constant temperature of 120 °C and a curing time of 2h. Then, laminated composite plates were cooled to room temperature at constant pressure of 250 kPa. It was concluded that increasing temperature cause to reduction of mechanical properties.

Kuş [7] studied mechanical properties of composites which were produced using cast iron and low carbon steel wire (as reinforcement). The aim of selecting fiber with low carbon was to decrease forming graphite and improve mechanical properties. Effect of heat treatment temperatures on mechanical properties of composite materials is examined.

2.2.1 Studies about Investigating General Effect of Joint on Strength of Composites

Okutan [8] studied failure characteristics of laminated composites (E/glass–Epoxy) including mechanically fastened joints. Specimens having $[0/90/0]_s$ and $[90/0/90]_s$ stacking sequences were prepared from manufactured composites and then mechanical properties were determined experimentally. It was shown that fiber orientation and geometries of composites were important for composites that have pinned joints. Okutan and Karakuzu [9] also investigated effects of pinned joints on strengths (bearing, shear and tension) of composites (E-glass/Epoxy) using specimens with 20 different geometric dimensions (formed changing the edge distance and the width with respect to hole diameter considering hole diameter constant) having $[0/-45]_s$ and $[90/-45]_s$ stacking sequences.

İçten and Karakuzu [10] investigated failure strength of laminated composites (Carbon/Epoxy) with pinned-joints. By using specimens having different fiber orientations, failure characteristics (failure load and mode) were determined. Içten et al. [11] continued this study searching failure characteristics of woven Kevlar/Epoxy composite plates including joints. Failure loads and modes were obtained experimentally and compared with the results which were obtained by numerically using 2D finite element method (FEM) (developed to predict damage initiation and progression). Moreover, Karakuzu et al. [12, 13] studied on failure characteristics (bearing strength, load and mode) of composite plates (woven glass/ vinyl ester)

having circular holes [12] and two parallel circular holes [13]. Effects of the hole position (distance of hole from free end) and size (ratio of hole diameter to length of plate) on failure characteristics were determined numerically and experimentally. Both results were compared and shown good agreement.

Whitworth et al. [14] studied on bearing strength of composite having pinned joints. Point stress failure criterion was used to obtain characteristic lengths in tension and compression. Stress distribution around the fastener hole was obtained by using 2D finite element analysis (FEA).

Ahn et al. [15] performed an investigation on the failure analysis of composite materials (unidirectional woven) which used in airplane control rod by experimentally and numerically. Specimens having nine different geometries (formed changing the ratio of width to hole diameter and the ratio of edge distance to hole diameter considering hole size constant) were used in the tests. Failure modes and loads were determined by testing under pin loading and effects of different geometries were obtained. Also numerical analyses were done and results were compared.

Effects of joint geometry on the load bearing capacity were considered by Yılmaz [16]. Fiber type, fiber orientation, and type of polymer matrices, effects of parameters related with joint geometry were investigated for load bearing performance of the pin connected composites. Load bearing capacities and changes in failure formation mechanisms related to variations in geometric parameters were investigated.

Dursun [17] developed a 3D damage modeling program to investigate the behavior of laminated composite plates which have bolted connection and to determine the failure modes and maximum load carrying capacities under tensile loading. Both stress and failure analyses have been performed using this program in conjunction with a general finite element code, ANSYS.

Adin [18] studied on an adhesively bonded inverse Z type joint. The material of support and horizontal plate which were members of joint was manufactured to be

composite materials. The FEM was used in analysis. In analysis, the variations of peak stresses have been investigated for overlap distance, model breadth, model thickness band overlap angle. Experimental results and numerical results were compared and found quite reasonable.

Sen [19] studied failure response (bearing strength) of composite plates which is pin-loaded. Effects of ply orientation, geometry of joint and preload moments on the failure initiation and bearing strength were parametically investigated. It was seen that increasing geometric parameters increased the magnitudes of bearing strengths. Also Sen and Sayman [20] investigated failure analyses of composite plates (Glass/Epoxy) which have two-serial bolt connections. Effects of hole position (distance from free end), hole size, distance between holes were considered parametrically. It was shown that material parameters, geometric parameters and magnitude of pre-load moments effected on the joints which have two-serial bolt connections.

Koruvatan [21] investigated joint behaviour of composite plates (Glass/Epoxy) which were pin/bolt loaded and produced with different cure cycles and with different geometric dimensions. Experimental and numerical studies were done. It was shown that the composite plates which pin/bolt loaded and manufactured at high level temperatures and high level period (120 ºC temperature and 4 h period) had more high bearing strengths than the others.

Ataş et al. [22] researched failure behaviour of composite plates (Glass/Polyester) which have two parallel circular holes. Experimental and numerical studies were done considering different geometries (created changing edge distance, plate width, and the distance between two parallel holes with respect to hole diameter) and stacking sequences. Effects of the hole location (distance from free end) and distance between holes with constant hole diameter on failure characteristics were determined numerically (using Lusas. 13.6 finite element software) and experimentally.

2.2.2. Some Studies about Impact, Vibration and Fatigue Performance of Composites

Icten [23] studied impact response of laminated composites constructed from orthotropic layers containing collimated unidirectional fibers or woven fabrics made of glass fabrics and epoxy matrix. The effects of following parameters on impact resistance of the composite plates have been studied; the angle between adjacent layers, weaving gaps, the curing pressure, the size of weaving cell, the stitching reinforcement through the composite thickness and the weaving angle between fill and warp yarns.

Thermal impact behaviors (using Fractovis Plus impact) test machine of unidirectional laminated composite plates (Glass/Epoxy) under different temperatures were investigated by Aktas [24]. The used temperatures were 20°C, 40°C, 60°C, 80°C, and 100°C. In addition, mechanical properties of the composite plates were obtained under mentioned temperature conditions. Fourteen impact energies from 5 J to 70 J were selected for impact tests. Results from experiments were compared with results from numerical studies (obtained from 3D finite element code) which shown good agreement.

Khalili et al. [25] studied on impact characteristics of uniaxial graphite-epoxy composites. Uni-axial and bi-axial tensile prestresses were taken into consideration and their influences were determined.

Free vibration problems of simply supported rectangular plates made of composite materials were studied by Çırak [26]. In this study, the density of plate and Young's modulus were changed dependent on thickness coordinate. In general case, fundamental relations, dynamic stability and compatibility equations were obtained for anisotropic plates including transversal shear deformations made of non-homogeneous materials and in simply supported rectangular orthotropic plates.

Gharagoni [27] studied the free vibration analysis of composite plates (Graphite/Epoxy) with FEM (ANSYS software). The clamped and simple supported boundary conditions were considered in the study.

Özakıncı [28] studied vibration analysis of composite plates which are in plane stress condition by using trigonometric function as the admissible function, using Rayleigh – Ritz method. Obtained results were compared with the ones obtained from numerically using ANSYS. The effect of ratio of width to thickness, material anisotropy, the angle-ply, pate dimensions and boundary conditions upon non-dimensional frequency parameters have been examined.

Effects of different geometrical and material parameters on natural frequencies of a composite plate strip with macro crack were studied by Eren [29]. Boundary value problems concerned were examined under two different boundary conditions. For the state of plane strain, mathematical modeling of the problems was implemented in the scope of the exact equations of the Theory of Elasticity. Due to the fact that discussed boundary value problems are incomputable with analytical approach, FEM was used for numerical solutions. So as to retrieve the solutions, a computer program was coded in MATLAB®. Numerical solutions were obtained for different boundary conditions, number of finite elements, composite material constants, size and location of the cracks. Acquired results for undamaged and cracked were compared.

Eruslu [30] studied on free vibration characteristics of composite plates. Short fibers were used as reinforcement in the cross ply laminated composite square plates. The analysis was performed for different plate span to thickness ratio. Numerical analyses were given for glass reinforced epoxy composites. It was concluded that the natural frequency for unidirectional aligned composites were affected by fiber content and aspect ratio.

Tolun [31] derived equation of motion of composite plates using Kirchhoff Plate Theory. In this study, finite difference method was used with various boundary conditions. Effects of the plate dimension (ratio of width to length), the thickness (ratio of length to depth), and length to depth ratio, fiber orientation angle on the natural frequency of composite plates were investigated.

Grimmer [32] investigated the use of carbon nanotubes (CNTs) in conventional glass fiber composites as an additive that can improve the fatigue strength. The research

described here was focused on the development, testing and modeling of CNT / glass-fiber hybrid composites, a novel material exhibiting both low cost and improved properties under fatigue loading. A manufacturing process for small-scale production of these hybrid composites was developed for the purpose of evaluating their relative benefits. The hybrid composites were subjected to uniaxial fatigue and cyclic delamination tests and their performance was compared to that of traditional glass-fiber composites.

Erkal et al. [33] performed fatigue analyses to find optimum fiber orientation angle of symmetric composite cylinders (Eglass/Epoxy). Specimens having $[\pm 750]_2$, $[\pm 60°]_2$, $[\pm 55°]_2$, and $[\pm 45°]_2$ stacking sequences were prepared symmetrically and then burst pressures were determined experimentally using alternating internal pressure. It was concluded that fiber orientation angle have important effects on fatigue characteristics.

2.2.3 Studies about Investigating Effect of Perforation (Cutout) on Strength of Composites

An analytical investigation was used to study the stress analysis of composite plates with different central cutout by Rezaeepazhand and Jafari [34]. Particular emphasis was placed on flat square plates subjected to a uni-axial tension load. The results based on analytical solution were compared with the results obtained using finite element methods. The effect of cutout geometry (circular, square, or special cutouts), material properties (isotropic and orthotropic), fiber angles, and cutout curvature were considered. The important result was that for triangular cutout change in the maximum stress is higher than two other configurations (square and hexagonal cutouts) with respect to fiber orientation angle.

Rezaeepazhand and Jafari [35] also concentrated on problems associated with the maximum stresses in perforated composite plates with quasi-square shaped cutouts. Parametric studies were conducted to investigate the effects of variation in cutout bluntness and orientation, material properties, and loading direction on the location and the value of the maximum stress in a flat composite plate subjected uniaxial tension load. Based on results presented herein, the maximum normalized stress of

perforated composite plates could be significantly changed by using proper combination of material properties, fiber orientation, loading angle, cutout bluntness, and orientation.

2.3. Literature Review on Buckling of Composites

Buckling characteristics of structures are very important research areas of engineers since this phenomenon has important value in the stability of composite structure. Sometimes buckling characteristic can be the most important design criteria as being in the aircraft design. So investigations on that subject have increased rapidly with the increase of usage percentage of composite materials in the engineering applications.

The first paper on the buckling of columns is produced by Euler in 1744. Then Walker studied on buckling by doing experiments [36]. The first original plate equation about buckling was founded by Lagrance and Navier. The first theoretical examination including energy about plate buckling was by Bryan [37]. Since then many investigations have done on this subject.

2.3.1. Literature Review on General Effects of Production Parameters on Buckling of Composites

Papila and Akgün [38] studied buckling and post-buckling characteristics of composites theoretically. Galerkin's method was used in the derivation of post-buckling response which was considered as magnification of buckling analysis.

Effect of layer numbers, lamina thickness, ratio of Young's modulus in plane and lateral direction and fiber orientations (cross-ply and angle-ply) on buckling were researched using FEM (using high-order shear deformable finite strip) by Zou and Lam [39].

Elaldı [40] studied exploration of buckling and post-buckling responses of composite panels. This panel had two different stiffener types (J- and hat-stiffened). By giving definition structural efficiency, experimental results of these two types were

compared. Also buckling and post buckling characteristics of composite panels were compared with analytical results.

Ray [41] researched buckling response of composite materials numerically. The effect of fiber weight ratio in lamina on buckling was researched parametrically and compared with studies from the literature.

The effects of ballistic penetration on composite plates (woven E-glass/Epoxy) subjected simultaneously to in-plane compressive loading were investigated by Wiedenman and Dharan [42]. A portable hydraulic press and fixture were designed to apply compressive preloads during ballistic penetration. Samples without simultaneous compressive preload were subjected to ballistic penetration alone and then compressively loaded to failure. Finally, samples that had previously undergone ballistic testing at varying levels of compressive preloads were loaded in compression to determine the residual compressive failure strength. It was concluded the effect of simultaneous preload and ballistic penetration results in a greater extent of damage propagation than for ballistic penetration alone, increasing the possibility of initiating buckling failure of the loaded plate.

Chakrabarti and Sheikh [43] studied buckling responses of composite plates subjected to in-plane partial edge compression using a refined plate theory. In this theory, transverse shear stresses were continuous at the layer interfaces along with stress-free conditions at the top and bottom surfaces of the plate.

Singh and Verma [44] analyzed the buckling characteristics of composite plate including temperature and moisture effects. In the study, FEM (using high-order shear deformation theory) were used to derive buckling equations. Influences of span to thickness ratio, stacking sequences, plate dimensions on the hydrothermal buckling were investigated. Also different boundary conditions were examined.

Tarjan et al. [45] performed the local buckling response investigation on composite beams (FRP) numerically. The structures used in this study have thin-walled open or closed section. Approximate expressions were presented for the local buckling

analysis of thin-walled composite beams subjected to transverse loads. Some numerical model was prepared to verify the method.

Kim et al. [46] studied on buckling characteristics of composite cylinders (produced by filament-winding) which exposed to external hydrostatic pressure using FEM. Also some experimental tests were carried out and results were compared with FEM results.

2.3.2. Studies on Investigating Effect of Perforation (Cutouts) on Buckling of Composites

Lin and Kuo [47] examined effects of circular holes on buckling of composite plates (having symmetric or anti-symmetrically stacking sequences) by numerically. First-order shear deformation theory (FSDT) was used in the derivations, and 9-node Lagrangian FEM was used to obtain critical loads. Effects of hole dimensions, plate thickness, Young modulus, stacking sequences, loading types, and boundary types were searched.

Buckling response of biaxial- and shear-loaded anisotropic composite panels having central elliptical cutout was investigated by Britt [48]. Study was composed of two sections, a prebuckling section and a buckling section. Results of a parametric study were presented for rectangular panels having elliptical cutouts. The effects of panel aspect ratio, cutout shape, cutout size, cutout orientation, laminate anisotropy, and combined loading on the buckling load were examined.

Critical buckling loads of FRP square panels were determined using FEM by Srivatsa and Murty [49]. Different boundary conditions, stacking sequences (using $[\pm\theta]_{6s}$ laminates), cut-out sizes were taken in consideration.

Lee and Hyer [50] searched failure characteristics of composites having a central circular cutout including postbuckling deflections. The study was numerical and experimental. It was seen that failure of composites having $(\pm 45/0/90)_{2S}$ and $(\pm 45/0_2)_{2S}$ stacking sequences was due to fiber compression failure and was predictable. The failure load was, for the most part, independent of response

configuration. It was seen that the $(\pm 45/0_6)_S$ laminate failed due to interlaminar shear along the simple support, while the response and failure of the $(\pm 45)_{4S}$ laminate was governed to a large degree by material nonlinearities and progressive failure.
Buckling responses of composites having central square hole was examined by Akbulut and Sayman [51]. Different hole dimensions, different stacking sequences (angle ply and cross ply), different thicknesses and simple or clamped boundary conditions, varied modulus ratios were taken in consideration.

Kong et al. [52] performed buckling and post buckling analysis for composite plates having a hole numerically and experimentally. In the FEA, the updated Lagrangian formulations and 8-node shell elements were used. To determine failure response, maximum stress criterion was used. Experimental results were compared with FEM results and which shown good agreement.

Yazıcı et al. [53] searched effects of cutout shapes (U-shaped) on the buckling stability of Glass/Epoxy composite plates Simply supported boundary condition and various stacking sequences were taken in consideration during the analysis. Also plates having no cutouts were used to verify theoretical, experimental and FE results. According to results, influences of cutout depth were higher than that of the cutout size on buckling loads. Yazıcı [54] also studied the effects of square cut-out upon the buckling response of composites which produced by polypropylene reinforced with steel numerically and experimentally. FE and experiment results were given for various different stacking sequences and boundary types. It was concluded that buckling load was affected higher by square cutouts under clamp-clamp boundary types than by the pinned-pinned case. Moreover, Yazıcı [55] studied the influences of square cutouts on the buckling response of rectangular composites (polymer type). Simple supported boundary type and various stacking sequences with different cut-out corner fillets were taken in consideration during the analysis. According to results, buckling loads were not affected from stacking sequences and cut-out corner fillets.

Jain and Kumar [56] studied the postbuckling characteristics of composites having centric cutouts (circular and elliptical) exposed uniaxial compression using FEA. The formulation was based on Mindlin's plate theory and von Karman's equations to

include geometric nonlinearity. Newton–Raphson method was used on the solution of FE equations. Influences of cutout type, dimensions and cutout positions on the buckling were examined. It was observed that these have substantial influence on the strength which laminates possess beyond buckling.

Ghannadpour [57] investigated effect of the circular cut-out on the buckling loads of laminated composites which have symmetric cross-ply orientation. FEA was performed to estimate the influences of cutouts on the buckling loads. Some overall important findings were that composites that have no cut-outs can buckle with less buckling loads than corresponding loads of composites having cut-outs.
Baltacı et al. [58] studied on buckling of composite circular plates including circular holes and exposed to uniform radial load using the FEM. Influences of hole dimensions, positions of the holes, different thickness and different boundary types on buckling load of the composites were investigated.

Elaldi and Alecakir [59] evaluated influences of cut-out and stacking sequences on the buckling response and damage tolerance of composite (Carbon/Epoxy) panels. FEA was performed and experimental results were compared with FEA results and which shown good agreement.

The influence of boundary types on the buckling loads for composite (E-glass/epoxy) plates of different cutout shapes, span/thickness ratio, and stacking sequences were investigated by Baba [60] numerically (using ANSYS) and experimentally. Clamped-clamped, simple-supported and combination of these boundaries were considered. Comparisons were made between experiment results and results based on FEA. Baba and Baltaci [61] investigated effects of cut-outs on the buckling response of composites (E-glass/Epoxy). The buckling load was examined for symmetrical and anti-symmetrical composites subjected to in-plane compression load. [90/45/−45/0] and $[90/45/-45/0]_s$ stacking sequences, various cut-out types (circular and semi-circular), different span/thickness ratios and different boundary types (clamp-clamp , clamp–simple supported and simple supported–simple supported). Experimental results were verified with results obtained from FEA (using ANSYS).

The buckling response of metal matrix composite (MMC) plates with a centric square cut-out was studied with compressive bi-axial loads using FEM by Yeh et al. [62]. Effects of hole dimensions, boundary types, fiber orientations and plate length on the buckling of MMC were examined. $[90/0/0/90]_2$ and $[45/-45/-45/45]_2$ fiber orientations were considered in the study. Some important findings were that buckling capacity of MMC having centric cutout increased with free-free boundary types when cut-out dimensions were increased.

Buckling characteristics of composites having circular cut-outs were investigated by Yapıcı et al. [63]. Two different reinforced materials (galvanized steel wire and a woven galvanized wire) were used. The FEM was used for the solution. First critical buckling load of an orthotropic plate with and without hole subjected to unidirectional compression were found.

Buckling responses of composite plates having corner circular notches under compressive load were investigated by Akbulut and Ural [64]. FEM was also used to estimate the influences of notch lengths, different thicknesses, varied modulus ratios loads, different stacking sequences and simply-supported boundary type.

Effects of circular hole diameter and position on the buckling response of composites (woven E-glass/epoxy) were researched by Sahin [65] by numerically (using ANSYS 11.0) and experimentally.

Topal and Uzman [66] studied on design of pinned-pinned symmetric laminated composite plates having centric circular holes. Aims of the design were getting maximum buckling load using stacking sequences as design parameters and using modified feasible direction method. Bending– twisting coupling were also considered. The influences of various layer numbers, boundary types, width thickness, and length width and cutout diameter width ratios on the buckling loads were researched.

The effects of cutout geometry, span/thickness ratio, and stacking sequences and span/width ratio on buckling behaviours of composites (woven Glass/Epoxy) were studied experimentally by Kumar [67]. Clamp-Clamp boundary type was used during

the study. Various cutout types (circular, square and rectangular) were considered. After buckling tests micro electroscope were used to determine failure types.

Selek [68] studied buckling analysis of laminated orthotropic composites having a centric rectangular hole applying in-plane loading (uniaxial compression). Initially, the critical buckling coefficients of the laminated plates were obtained by FEM. Artificial neural networks were used to obtain buckling coefficients. A PASCAL computer program was used for training and testing procedure of neural networks, and finally good results were achieved.

Qablan et al. [69] evaluated influences of cutout dimension and position, stacking sequences and different loads on buckling response of square cross-ply layered composites having circular cut-outs. Uni-axial compression, bi-axial compression and shear loads were performed. Some important findings were that buckling loads decrease using higher cut-out dimension with shear loads and it was less in other loading types with respect to this loading. It was also concluded that cut-outs near the clamped edge increased buckling loads for small dimension ones. But for large dimension ones buckling loads were increased when cut-out were in the center.

Buckling analysis was performed to layered composites (glass/polyester) having circular and elliptical cutouts by Komur et al. [70] using FEM. Types and locations of cutouts having $[(0/90)_2]_s$, $[(15/-75)_2]_s$, $[(30/-60)_2]_s$ and $[(45/-45)_2]_s$ stacking sequences were investigated parametrically. It was concluded that higher cutout size decrease the buckling strength.

Kumar and Singh [71] studied the effects of boundary types on buckling and post-buckling responses of composites with $(+45/-45/0/90)_{2s}$ stacking sequence different cutout types and dimensions using FEM. The finite element formulation was derived using FSDT and von Karman's equations to include nonlinearities. Laminate failures were determined by using Tsai-Hill and interlaminar theories. It was seen that models with clamp-clamp and pinned-pinned both edges had higher and the smallest buckling and post-buckling loads, respectively, independent from the cut-out types and dimensions.

2.3.3. Studies on Investigating Effect of Delaminations on Buckling

Delamination effects on compressive failure response of composites were determined by Sun et al. [72] numerically. Derived FE equations using Mindlin's theory and Von Karman's equations to include nonlinearities was used to find buckling, post buckling, contact influences of delaminated region, progress of delaminated region, fiber and matrix cracking. Progress of delaminated region was considered by using a fracture theory which controls energy dissipated during fracture along delaminated region. It was concluded that delamination growth is influenced seriously from boundary types, and stiffness degradation have considerable effects on buckling strength.

Hwang and Mao [73] studied buckling and post buckling characteristics (modes and loads) and delamination progress of composite plates produced reinforced Epoxy with unidirectional carbon fibers. Non-linear FE buckling analysis containing contact elements to prevent over-lapping was used to estimate buckling loads. Buckling and post buckling responses of layered composites having multi delaminated regions were analyzed by Hwang and Liu [74] experimentally. Through width multiple triangular geometry delaminated regions were used to see impact failures. Experimental results were verified using non-linear FE buckling analysis. Critic delamination growth loads of multi delaminated regions were determined with post buckling analysis.

Zor [75] studied influences of the strip delamination on the buckling responses of composites produced with layered Carbon-Epoxy composites. Three-dimensional (3D) FE models of the layered plates were prepared. Delaminations were placed between 2^{nd} and 3^{rd} layers. Also plates having no delamination were used to verify theoretic and FE results. Then, buckling loads were obtained to various stacking sequences. It was concluded that buckling loads decreased with increase of delaminated region size. Also, Zor et al. [76] evaluated influences of the strip vertical or horizontal delaminated region width on the buckling responses of pinned-pinned composites produced woven steel-reinforced thermoplastic. 3D FE models having $[0]_4$, $[15/-15]_s$, $[15/-15]_2$, $[30/-30]_s$ and $[30/-30]_2$, $[45]_4$ and $[45/-45]_s$ fiber

orientations were used. Moreover, Zor [77] analyzed the influences of multi delaminations size on the buckling responses of composites produced with woven steel-reinforced thermoplastic which have lateral delaminations between each layers. The critic delamination giving higher delamination dimensions and tolerance value in the structure without decreasing compressive strength was determined.

Buckling behavior of 3 layer beams having 2 over-lapped delaminated regions was studied by Msrao et al. [78]. Non-dimensional parameters, axial and bending stiffnesses and slenderness ratios were given parametrically. Influences of span-wise delamination position on buckling response were given for 3 layer composite beams which produced with carbon and glass fibers and epoxy matrix.

Wright [79] studied buckling and post buckling loads of composite strut having delamination using four DOF non-linear Rayleigh Ritz formulation. It was given that depend on thickness of delaminated region overall buckling may exist in post buckling regime.

Arman et al. [80] done experimental and numerical study on layered composites delaminated circularly around a circular cutout to investigate buckling response. 3D buckling analysis was performed to find critic delamination sizes. Cross-ply layered delaminated and without any delamination composites were manufactured and clamped-clamped boundary conditions were used in the tests and results were verified with numerical results. It has been seen that the results obtained the numerically are close to experimental results. Also various delamination sizes and stacking sequences were studied numerically and it was concluded that buckling strength of the plates decreases significantly with the increase of delamination size and stacking sequences have important effects.

Euler Bernoulli beam and classical lamination theories (CLT) were used to derive the analytical model that used to determine buckling response of composite beam having delamination by Yap and Chai [81]. Eight node shell elements with contact pairs were considered in the FEA. Effects of fiber orientations, through width position and length of the delaminated region were investigated. It was noted that precision of the study were effected from length of delaminated region.

Suemasu et al. [82] researched post buckling characteristics of rectangular multi circular delaminated composites experimentally and numerically. The plate was clamped from loading edges and pinned from the other edges using compression after impact tests. Delaminations were positioned orderly in the thickness direction at central part.

Effects of circular hole diameter and position on the buckling response of composites (woven E-glass/epoxy) were researched by Sahin [83] by numerically (using ANSYS 11.0) and experimentally. Aslan and Sahin [84] also studied the influences of the delaminated region dimensions on buckling response and failure load of composites (E-glass/Epoxy) having multi large delaminated regions by numerically and experimentally. $[0/90/0/90]_s$ and cross ply layered composites having multi large delaminated regions and plates without any delaminated region were manufactured using hand lay-up method. Clamped-clamped boundary conditions were used in the experimental study and results were verified with FE (ANSYS 11.0 used) results. It was seen that buckling loads were affected from bigger and near surface delaminations.

Post-buckling response of layered composites having embedded delamination with uniaxial compression loads were studied by Hosseini-Toudeshky et al. [85]. Delamination initiation and progress was modeled with softening behavior of interface elements. A FE program was developed to obtain the buckling characteristics.

Kharazi et al. [86] studied buckling behavior of the composite laminates with through the width delaminations by using different plate theories. The analytical method is based on the CLPT, FSDT and HSDT plate theories. The formulation was developed on the basis of the Rayleigh–Ritz technique by the implementation of the simple polynomial series. The three-dimensional FEM analysis was also performed and the results were compared with those obtained by the analytical models.

Ovesy et al. [87] investigated buckling characteristics of layered composites having embedded delaminated regions. The method used in this study is derived using FSDT

and Rayleigh-Ritz approximation method adding simple and complete polynomials. Local (delamination part) and general buckling of plate were solved by using derived equations. Also 3D FEA (by ANSYS 5.4) was used in the study and analytically obtained results were verified with these results.

Chirica and Beznea [88] researched effects of elliptic delaminations on the buckling behavior of ship deck plates produced by composites. A model containing delaminated region were prepared with surface to surface contact option (using COSMOS). Numerically obtained results were verified with results obtained by tests.

Damghani et al. [89] studied the critic buckling loads of composites having through/length delaminations using exact stiffness analysis. It was concluded that numerically obtained results for longitudinal, transverse and shearing loads show a transition from general to local buckling modes as the delaminated region sizes were increased. Also it was seen that critic buckling loads were decreased when delamination was placed near surface.

Kroflic et al. [90] studied on 3D composite column model containing delamination and considering extensional and bending stiffness couplings and transverse shearing influences to obtain in-plane buckling loads. Linearized stability theory was used to determine buckling loads. Influences of shearing, delaminated region location, rotation angle of delaminated region and elastically to shearing modulus ratios were investigated parametrically.

Schnabl and Planinc [91] studied on mathematical model to determine buckling responses of perfectly-elastic 2 layers composite columns containing inter-layer slipping between layers. This model was derived using linearized stability theory and could be used to predict critic buckling loads.

2.3.4. Buckling Analysis of Laminated Composite Plates Under Thermal Loading

Li et al. [92] investigated the axisymmetric vibrations of a statically buckled polar orthotropic circular plate due to uniform temperature rise. Laura and Rossit [93]

worked on thermal bending of thin, anisotropic, clamped elliptic plates and their study deals with the exact analytical solution of thermal bending. Lee [94] derived governing buckling equations from the variational principle and a finite element method to analyze thermal buckling of laminated composites by using a layer-wise theory.

Singha et al. [95] maximized buckling temperatures of layered composite (Graphite-Epoxy) plates. Fiber orientations and relative thicknesses of layers were considered as design factors. Thermal buckling analysis was performed using FEM and genetic algorithm (GA) was used to optimize ten factors to 5 layered plates. Study results revealed that buckling loads were affected from fiber orientation and thickness.

Kabir et al. [96] extended developed [97] 3 node plate element to determine thermal buckling loads of layered composite square and skew plates. The method used in this study is derived using FSDT which can be used thick plates, however it could also be used for thin plates. Thermal buckling loads containing critic ones and mode shapes were obtained using numeric equations. The results were verified with NASTRAN and ANSYS.

Le-Chung and Shih-Yao [98] studied thermal buckling responses of sandwich composite plates using new 36 DOF high order element containing displacements because of bending and shearing deformations. It was concluded that buckling load and modes affected from stacking sequences and length/width ratios.

Shariyat [99] investigated thermal buckling responses of rectangular multi-laminated composites exposed uniform temperature rise with layer wise plate theory. Von Karman's assumptions were considered. It was previously verified that layer wise theory was suitable with the 3-D theory of elasticity results.

A closed form solution was presented to determine thermal buckling characteristics of symmetrical angle ply composites having fixed from one side and free from other side by Barton [100].

Le-Chung et al. [101] studied thermal stability characteristics of layered composite plates using FEM. The thermal buckling shapes of cross ply and angle ply composites having different modulus and length/width ratios, ply orientations, and boundary types were investigated.

Aydogdu [102] researched the thermal buckling analysis of rectangular cross-ply laminated beams subjected to different sets of boundary conditions by applying the Ritz method. Yapici [103] studied on the thermal buckling analysis of symmetric and antisymmetric angle-ply laminated hybrid composite plates with an inclined crack subjected to a uniform temperature rise. Avci et al. [104] performed the thermal buckling analysis of symmetric and antisymmetric cross-ply laminated hybrid composite plates with an inclined crack subjected to a uniform temperature rise. Avci et al. [105] extended their work on the thermal buckling analysis of symmetric and antisymmetric laminated composite plates with clamped and simply supported edges, and containing a hole. Then, Avci et al. [106] studied on the thermal buckling analysis of symmetric and antisymmetric cross-ply laminated hybrid composite plates with a hole subjected to a uniform temperature rise for different boundary conditions. Sahin [107] worked on thermal buckling analysis of symmetric and antisymmetric laminated hybrid composite plates with a hole subjected to a uniform temperature rise for different boundary conditions.

2.4. Literature Review on Lateral Buckling of Composites

Bauld and Tzeng [108] presented a Vlasov type theory for thin-walled beams with open cross sections made from midplane symmetric fiber-reinforced laminates. Ma and Hughes [109] developed an energy method using nonlinear elastic theory to analyze the lateral buckling behavior of beams subjected to distributed vertical load. Mottram [110] compared short-term critical loading for linear elastic lateral-torsional buckling of an E-glass reinforced polymer I-beam with theoretical predictions derived using the finite difference approach and thin-walled beam theory. Davalos et al. [111] investigated flexural-torsional buckling behavior of full-size pultruded fiber-reinforced plastic (FRP) I-beams. Energy principles and the total potential energy equations for the instability of FRP I-beams using nonlinear elastic theory were used.

Roberts and Al-Ubaidi [112] presented an approximate theory for quantifying the influence of shear deformation on the restrained torsional warping of pultruded FRP bars of open cross-section and theory was validated by a series of bending and torsion tests. Qiao et al. [113] analytically and experimentally studied on the lateral buckling of pultruded FRP composite cantilever I-beams. An energy method based on nonlinear plate theory is developed with shear effect and bending–twisting coupling. Brooks and Turvey [114] performed lateral buckling tests on pultruded glass-fiber reinforced plastic (GRP) I-section cantilever beams and test results were compared with theoretical and finite element analysis. Turkey [115] also investigated effects of load position on the lateral buckling response of pultruded GRP cantilevers. Roberts and Masri [116] determined the flexural and torsional buckling properties of pultruded FRP profiles. Silva and Silvestre [117] presented the combination of shear deformation effects into a generalized beam theory to analyze the structural behavior of composite thin-walled columns made of laminated plates and displaying arbitrary orthotropy. Elastic coupling effects, warping effects, cross-section in-plane deformation and shear deformation were included into the theory. Correia et al. [118] reported an experimental study on the first-order, buckling and post buckling behaviors of I-section beams made of GFRP pultruded profiles. Silva et al. [119] studied numerical modeling of the GFRP pultruded beams, by means of shell and beam finite element analyses based on a recently developed generalized beam theory formulation.

Kabir et al. [120,121] investigated optimal fiber orientation which affecting lateral buckling capacity of laminated channel beams using an analytical solution. Lee et al. [122,123] developed a general analytical model applicable to the lateral buckling of an I-section composite beam subjected to various types of loadings. Effects of fiber orientation, location of applied load, and types of loads on the buckling capacity was considered. Sapkas and Kollar [124] studied the stability analysis of simply supported and cantilever, thin walled, open section, orthotropic composite beams subjected to concentrated end moments with concentrated forces or uniformly distributed load. Lee and Lee [125] developed a general analytical model applicable to thin-walled I-section composite beams subjected to vertical and torsional loads.

Mohri et al. [126] studied thin-walled beams with open sections using a nonlinear model developed in the context of large displacements and small deformations by accounting for bending-bending and bending-torsion couplings. Machado and Cortinez [127] and Machado [128] developed a geometrically non-linear theory for thin-walled composite beams for both open and closed cross-sections considering shear flexibility (bending and warping shear).

Lawson et al. [129] presented simplified equations for web-post buckling based on a compression field or strut model, which is validated with finite element analyses (FEA). Kim et al.[130,131] developed a stability theory for the analysis of thin-walled composite beam with arbitrary lamination including the restrained warping and Wagner effects based on concepts of the semi tangential rotations and semi tangential moments. Minghini et al. [132] presented a numerical beam model for overall buckling analysis of orthotropic FRP open-section beams subjected to in-plane and lateral loads. Kabir and Seif [133] presented an analytical solution of lateral-torsional buckling of an FRP I-beam based on total potential energy and applying the Rayleigh-Ritz method.

Lee [134] developed a general geometrically nonlinear model for thin walled laminated composites with arbitrary open cross-section and general laminate stacking sequences based on the classical lamination theory. Machado [135] derived analytical solutions for the lateral stability analysis of cross-ply laminated thin-walled beams subjected to combined axial and bending loads based on seven-degree-of-freedom shear deformable beam model considering moderate bending rotations and large twist. Effects of the variation of load height parameter and fiber angle orientation on the lateral stability of thin-walled composite beams were investigated. Karaağac et al. [136] investigated the effects of crack ratios and positions on lateral buckling loads and fundamental frequencies of slender cantilever Euler beams with a single-edge crack. Eryigit and Eryigit et al. [137, 138] researched the buckling behaviors of the layered composite beams having circular hole. Beam was restricted as at one side and the vertical load is applied from the other side. Firstly, the lateral critical buckling loads of beams were obtained theoretically, experimentally and numerically. After that the experimental results of the beam with circular hole in the middle were compared with the finite element analysis results.

2.5 Literature Review on Hybrid Composite Plates

Hwang and Mao [139] studied buckling characteristics of inter-ply hybrid composites (Carbon/Epoxy and E-glass/Epoxy) including delamination. It was concluded that nonlinear buckling analysis were given close results with experimental results.

Stability analysis of symmetrical and antisymmetrical cross-ply layered hybrid composites (E-glass/Epoxy and Boron/Epoxy) plates having incline crack was studied by Önal [140]. The buckling characteristics were determined using FSDT and FE technics.

Fatigue characteristics of hybrid composite rods containing unidirectional carbon and glass fibers were searched by Kar et al. [141]. The rods were comprised of a carbon fiber core surrounded by a glass fiber shell. Damage characteristics were determined by considering stiffness reduction as a function of cycles, and fatigue failure was given with strength variation. Acoustical emission technic and microscopic examination were employed to determine damage progression and failure characteristic.

Impact behaviors of hybrid composites were investigated with low velocity impact loads by Hosur et al. [142]. Hybrid composites were manufactured with twill-weave carbon and plain weave S2 glass fibers. Square plates having dimensions 100x100 mm and thickness 3mm were exposed to low velocity impact loads at 4 energy levels of 10, 20, 30 and 40 J. It was concluded that there were important increase on load carrying capability with small decrease in stiffness.

Sayer and Bektaş [143] investigated impact characteristics of Carbon/Epoxy and Glass/Epoxy hybrid composites with different temperatures and increasing impact energies. The increasing impact energies were applied to the specimens at various temperatures as -20, 0, 20 and 40 ^{0}C until perforation took place of specimens. Those specimens were composed by two types of fiber orientation with eight laminates hybrid composites. Energy profile diagram were used to show relation between impact and absorbed energy.

Failure characteristics of woven-hybrid composites impacted by drop weights at 4 velocity levels were investigated by Sevkat et al. [144] by experimentally and numerically (using 3D non-linear FEM). Hybrid panels were manufactured using S2-glass/Epoxy and IM7-graphite/Epoxy using 177 ^{0}C curing temperature. Instron Dynatup 8520 drop-weight impact test machine were employed during the experiments. Results determined experimentally were verified using 3D dynamic non-linear FE software (LS DYNA) which shown close agreement.

Sayer et al. [145] investigated the impact characteristics of hybrid composites manufactured using (glass-carbon/epoxy). The increased impact energy was performed on two types of hybrid composite plates until complete perforation of specimens. The failure processes of damaged specimens for different impact energies were evaluated by comparing load–deflection curves and images of damaged samples taken from impacted sides and non-impacted sides. Cross-sections of damaged specimens were also inspected visually and discussed to assess the extent of damage, such as fiber fracture in layers, expansion of delaminations between adjacent layers.

The influences of hybrid composite beams containing various delaminated region and locations were studied by Ghasemnejad et al. [146]. The Charpy impact tests were conducted to see energy absorption ability of composite beams having delaminations. Hybrid composite beams were manufactured by combining Glass/Epoxy and Carbon/Epoxy. Results were shown that composite beams containing delaminated region near to impacted surface were absorbed higher energy than other locations.

Durao et al. [147] evaluated effect of drilling to delamination formations. In this work two types of laminates (Carbon/Epoxy and Glass/Epoxy) were drilled using different machining parameters and comparing drill geometries. Results showed the importance of a careful selection of these variables when drilling of composites is involved.

2.6. Conclusion on Literature Review

The following conclusions can be derived from the literature review:

- In literature, there are more studies on polymer matrix composites.
- There are also some studies about hybrid composites but studies on hybrid composites are less comparing to composite materials.
- Buckling of composites has been investigated by many researchers.
- In the literature, the hybrid composites having two different type of fiber have been studied.
- It is seen from literature review that curing pressure, curing temperature and curing time are very important parameters on the production of composite and hybrid composite plates.

In this study, hybrid composite plates having three different types of fiber have been produced. The main goal of this thesis is to investigate buckling characteristic of hybrid composites. The specific objectives are:

- To produce hybrid composite plates using different combinations of Carbon, S-glass and Aramid. And to investigate effects of fiber types on buckling of hybrid composite plates,
- To examine buckling behavior of hybrid composites experimentally.
- To examine lateral buckling behavior of hybrid composites experimentally.
- To produce composite materials which are more stable on the compressive loads,
- To investigate effects of geometrical properties (plate length, plate width, thickness etc.), type and mechanical properties of the fiber on a layer (volume ratio, fiber angle, etc.) on buckling and lateral buckling,
- To do also numeric studies on buckling of hybrid composite and to compare with experiments.
- To see effects of cutouts, cutout types, size and location on buckling and lateral buckling.

CHAPTER 3

PLATE BUCKLING

3.1 Derivation of thin plate buckling load [148]

A rectangular thin plate is considered to begin to the derivation of thin plate theory. The plate is referred to rectangular cartesian coordinates x, y, z where x and y lie on the middle plane of the plate and z is measured from the middle plane and a, b, and h are width, length and thickness, respectively (Figure 3.1).

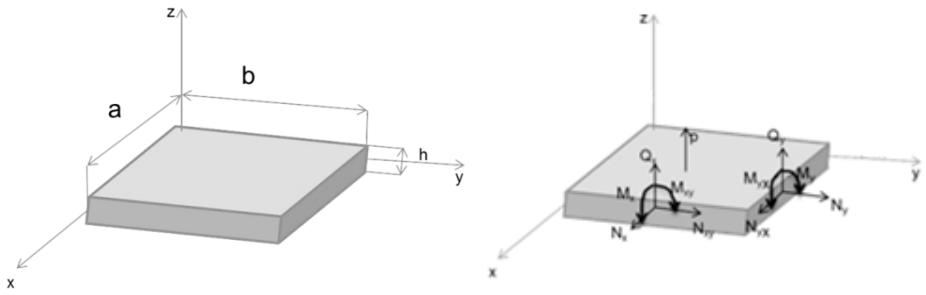

(a) (b)

Figure 3.1 Thin plate (a) coordinate system and dimensions, (b) forces and moments on the plate element

The object of thin plate theory is reducing a 3D problem to an approximate 2D one. Assumptions given below are considered while deriving thin plate theory:

1. The material of the plate is elastic, homogeneous, and isotropic.
2. The plate is initially flat.
3. The deflection (the normal component of the displacement vector) of the midplane is small compared with the thickness of the plate. The slope of the deflected surface is therefore very small and the square of the slope is a negligible quantity in comparison with unity.

4. Normals to the undeformed middle plane are assumed straight, normal, and in extensional during the deformation, so that transverse normal and shear strains may be negligible while deriving the plane kinematic relations.
5. Transverse normal stresses (the stress normal to the middle plane) are assumed to be small compared with the other normal stress components, so that they may be ignored in the stress strain relations.
6. Since the displacements of a plate are small, it is assumed that the middle surface remains unstrained after bending.

These approximations are called as the **Kirchhoff's assumptions**.

The forces and moments act on the edges of the plate element dx dy, as shown figure 3.1.b, are expressed per unit distance. The internal forces acts on the edge of plate element are given by related with internal stresses as;

$$N_x = \int_{-h/2}^{h/2} \overline{\sigma}_x \, d_z \; ; \; N_y = \int_{-h/2}^{h/2} \overline{\sigma}_y \, d_z \; ; \; N_{xy} = \int_{-h/2}^{h/2} \overline{\tau}_{xy} \, d_z \; ;$$

$$N_{yx} = \int_{-h/2}^{h/2} \overline{\tau}_{yx} \, d_z \; ; \quad Q_x = \int_{-h/2}^{h/2} \overline{\tau}_{xz} \, d_z \; ; \; Q_y = \int_{-h/2}^{h/2} \overline{\tau}_{yz} \, d_z \; ; \tag{3.1}$$

$$M_x = \int_{-h/2}^{h/2} \overline{\sigma}_x \, z d_z \; ; \; M_y = \int_{-h/2}^{h/2} \overline{\sigma}_y \, z d_z \; ; \; M_{xy} = \int_{-h/2}^{h/2} \overline{\tau}_{xy} \, z d_z \; ; \; M_{yx} = \int_{-h/2}^{h/2} \overline{\tau}_{yx} \, z d_z$$

Where;

N_x, N_y, N_{xy}, = in plane normal and shear force intensities (N/mm)

Q_x, Q_y= transverse shearing force intensities, N/mm

M_x, M_y= bending moment intensities, Nm/mm

M_{xy}, M_{yx} = twisting moment intensities, Nm/mm

Symbol $\bar{\sigma}_x$, $\bar{\sigma}_y$, etc., are denote the stress constituents at any point on the plate along thickness, and σ_x, σ_y and etc., which refer to corresponding ones at the center (which

means z equals to zero). Since $\tau_{xy}= \tau_{yx}$, it follows from Equation (3.1) that $N_{xy}= N_{yx}$ and $M_{xy}= M_{yx}$.

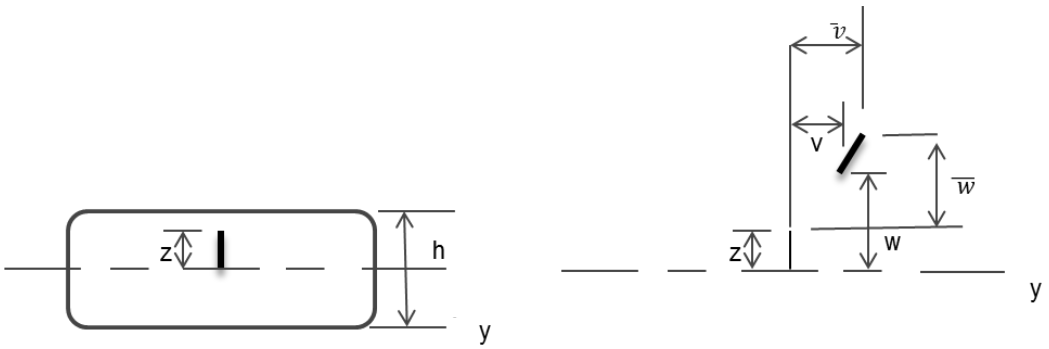

Figure 3.2 Normal to plate middle surface before and after deformation

As a consequence of the **Kirchhoff's third assumption**, $\bar{u}$, $\bar{v}$ and $\bar{w}$ are the displacement constituents at any point in the plate (Figure 3.2) and, u, v, w are the corresponding ones at middle plane and can be given as below:

$$\begin{aligned} \bar{u} &= u + z\beta_x \\ \bar{v} &= v + z\beta_y \\ \bar{w} &= w \end{aligned} \qquad (3.2)$$

since $\beta_x = -\frac{\partial w}{\partial x}$ and $\beta_y = -\frac{\partial w}{\partial y}$

Then,

$$\begin{aligned} \bar{u} &= u - z\frac{\partial w}{\partial x} \\ \bar{v} &= v - z\frac{\partial w}{\partial y} \\ \bar{w} &= w \end{aligned} \qquad (3.3)$$

Where; β_x and β_y are rotations relative to the y and x coordinate directions, respectively.

The intermediate class of deformations is defined by the limitations that the strains be small compared with unity, the rotations rexpect to the x and y directions small, and rotations to z direction small (negligible). For such deformations the $\bar{\varepsilon}_x, \bar{\varepsilon}_x \; and \; \bar{\gamma}_{xy}$ constituents of the strain displacement relations for a 3D medium ignoring negligible small high-order terms are:

$$\bar{\varepsilon}_x = \bar{u}_{,x} + \frac{1}{2}\bar{w}_{,x}{}^2 = \frac{\partial \bar{u}}{\partial x} + \frac{1}{2}\left(\frac{\partial \bar{w}}{\partial x}\right)^2$$

$$\bar{\varepsilon}_y = \bar{v}_{,y} + \frac{1}{2}\bar{w}_{,y}{}^2 = \frac{\partial \bar{v}}{\partial y} + \frac{1}{2}\left(\frac{\partial \bar{w}}{\partial y}\right)^2 \qquad (3.4)$$

$$\bar{\gamma}_{xy} = \bar{u}_{,y} + \bar{v}_{,x} + \bar{w}_{,x}\bar{w}_{,y} = \frac{\partial \bar{u}}{\partial y} + \frac{\partial \bar{v}}{\partial x} + \frac{\partial \bar{w}}{\partial x}\frac{\partial \bar{w}}{\partial y}$$

Substituting Equation (3.3) into Equation (3.4) yields

$$\bar{\varepsilon}_x = \varepsilon_x + z\kappa_x$$

$$\bar{\varepsilon}_y = \varepsilon_y + z\kappa_y \qquad (3.5)$$

$$\bar{\gamma}_{xy} = \gamma_{xy} + 2z\kappa_{xy}$$

Where; $\bar{\varepsilon}_x, \bar{\varepsilon}_x \; and \; \bar{\gamma}_{xy}$ are extensional and shear strain constituents at any point through the plate thickness and $\varepsilon_x, \varepsilon_x \; and \; \gamma_{xy}$ are ones at the middle plate only, and

$$\bar{\varepsilon}_x = u_{,x} + \frac{1}{2}\beta_x{}^2 = \frac{\partial u}{\partial x} + \frac{1}{2}\beta_x{}^2$$

$$\bar{\varepsilon}_y = v_{,y} + \frac{1}{2}\beta_y{}^2 = \frac{\partial v}{\partial y} + \frac{1}{2}\beta_y{}^2$$

$$\gamma_{xy} = \left(u_{,y} + v_{,x}\right) + \beta_x\beta_y = \frac{\partial u}{\partial y} + \frac{\partial v}{\partial x} + \beta_x\beta_y \qquad (3.6)$$

$$\beta_x = -w_{,x}\,;\; \beta_y = -w_{,y}$$

$$\kappa_x = -\beta_{x,x} = \frac{\partial \beta_x}{\partial x} = -\frac{\partial^2 w}{\partial x^2};\;\; \kappa_y = -\beta_{y,y} = \frac{\partial \beta_y}{\partial y} = -\frac{\partial^2 w}{\partial y^2}$$

$$\kappa_{xy} = \frac{1}{2}\left(\beta_{x,y} + \beta_{y,x}\right) = -\frac{\partial^2 w}{\partial x\,\partial y}$$

Equations (3.6) are the kinematical relations for the plate. Also, $u_{,x}$ is first derivation of displacement with respect to x (in the following equations "$_{,x}$", "$_{,xx}$" "$_{,y}$" and "$_{,yy}$" are used for first and second derivation of parameters with respect to x or y) . The generalized Hooke's law for the strain components$\bar{\varepsilon}_x$, $\bar{\varepsilon}_y$ and $\bar{\gamma}_{xy}$ in a 3D isotropic medium has the form**;**

$$\bar{\varepsilon}_x = \frac{1}{E}\left[\bar{\sigma}_x - \nu(\bar{\sigma}_y + \bar{\sigma}_z)\right]$$

$$\bar{\varepsilon}_y = \frac{1}{E}\left[\bar{\sigma}_y - \nu(\bar{\sigma}_z + \bar{\sigma}_x)\right] \qquad (3.7)$$

$$\bar{\gamma}_{xy} = \frac{2(1+\nu)}{E}\bar{\tau}_{xy}$$

Where; ν is Poisson's ratio. As a result of the approximation of thin-plate theory, σ_z is negligibly small. Omission of σ_z from Equation (3.7) and rearrangement gives:

$$\overline{\sigma}_x = \frac{E}{1-\nu^2}(\overline{\varepsilon}_x + \nu\overline{\varepsilon}_y)$$

$$\overline{\sigma}_y = \frac{E}{1-\nu^2}(\overline{\varepsilon}_y + \nu\overline{\varepsilon}_x) \qquad (3.8)$$

$$\overline{\tau}_{xy} = \frac{E}{2(1+\nu)}\overline{\gamma}_{xy}$$

Substituting Equations (3.8) and (3.5) into Equation (3.1) and integration yield the equations;

$$N_x = C(\varepsilon_x + \nu\varepsilon_y) \qquad M_x = D(\kappa_x + \nu\kappa_y)$$

$$N_y = C(\varepsilon_y + \nu\varepsilon_x) \qquad M_y = D(\kappa_y + \nu\kappa_x) \qquad (3.9)$$

$$N_{xy} = C\frac{1-\nu}{2}\gamma_{xy} \qquad M_{xy} = D(1-\nu)\kappa_{xy}$$

Where; $C \equiv \frac{Eh}{1-\nu^2}$ $D \equiv \frac{Eh^3}{12(1-\nu^2)}$

Equations (3.9) are the constitutive relations for the plate. The coefficients C and D are termed extensional and bending stiffness parameters, respectively.

3.2 Summation of Forces and Moments [148]

To take into account the nonlinear effects between forces and rotations, the equations of equilibrium of forces and moments must be derived for the plate element in a deformed configuration, as can be seen in Figure 3.3. Force and moment intensities are given in separate sketches, and the plate element is drawn as an element of surface without thickness. The double-headed vector notation is used to denote directions of the couples (right-hand rule). The force and moment intensities are given in Figure 3.3 in their positive directions; sign conversion is chosen so that all the terms on the right sides of Equations (3.1) are positive. The rotations β_x and β_y in Figure 3.3, each represent the angle between a coordinate direction and corresponding tangent to the center surface of plate element at upper corner, as shown. The force and moment intensities and rotations vary across the element, and the notations N_x^+ is used to denote ($N_x + N_{x,x}dx$), etc.

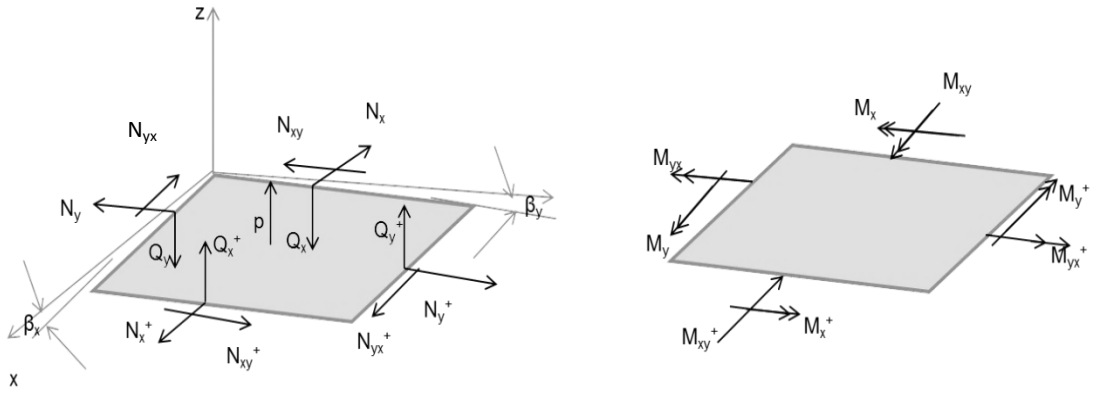

Figure 3.3 Plate element in deformed configuration

The angles of rotation (β_x and β_y) are small. So, sines and cosines of the angles can be changed with the angle itself and unity, respectively. Quadratic terms representing non-linear effects between the small transverse shear forces and the rotations are so small (negligible). Summing of forces in the x direction gives:

$$-\mathrm{N}_x d_y + \left(\mathrm{N}_x + \mathrm{N}_{x,x}\right)d_y - \mathrm{N}_{yx}d_x + \left(\mathrm{N}_{yx} + \mathrm{N}_{yx,y}d_y\right)d_x = 0 \tag{3.10}$$

On dividing out the quantity dxdy, Eq. (3.10) becomes

$$\mathrm{N}_{x,x} + \mathrm{N}_{yx,y} = 0 \tag{3.11}$$

Similarly, from summing of the forces in the y direction gives:

$$\mathrm{N}_{xy,x} + \mathrm{N}_{y,y} = 0 \tag{3.12}$$

Summing of the forces in the z direction gives:

$$\begin{aligned}
&\mathrm{N}_y d_x \beta_y - \left(\mathrm{N}_y + \mathrm{N}_{y,y}d_y\right)d_x\left(\beta_y + \beta_{y,y}d_y\right) + \mathrm{N}_x d_y \beta_x - \left(\mathrm{N}_x + \mathrm{N}_{x,x}d_x\right)d_y\left(\beta_x + \beta_{x,x}d_x\right) \\
&-\mathrm{Q}_y d_x + \left(\mathrm{Q}_y + \mathrm{Q}_{y,y}d_y\right)d_x - \mathrm{Q}_x d_y + \left(\mathrm{Q}_x + \mathrm{Q}_{x,x}d_x\right)d_y \\
&+\mathrm{N}_{xy} d_y \beta_y - \left(\mathrm{N}_{xy} + \mathrm{N}_{xy,x}d_x\right)d_y\left(\beta_y + \beta_{y,x}d_x\right) \\
&+\mathrm{N}_{yx} d_x \beta_x - \left(\mathrm{N}_{yx} + \mathrm{N}_{yx,y}d_y\right)d_x\left(\beta_x + \beta_{x,y}d_y\right) + p d_x d_y = 0
\end{aligned} \tag{3.13}$$

Regrouping and omission of higher-order terms in Equation (3.13) gives

$$\begin{aligned}
&\left(\mathrm{N}_{x,x} + \mathrm{N}_{xy,y}\right)\beta_x - \left(\mathrm{N}_{yx,x} + \mathrm{N}_{y,y}\right)\beta_y - \mathrm{N}_x \beta_{x,x} \\
&-\mathrm{N}_{xy}\beta_{y,x} - \mathrm{N}_{yx}\beta_{x,y} - \mathrm{N}_y \beta_{y,y} + \mathrm{Q}_{x,x} + \mathrm{Q}_{y,y} = -p
\end{aligned} \tag{3.14}$$

The terms containing derivatives of N_x, N_{xy}, N_{yx} , and N_y in Equations (3.11) and (3.12), and they are omitted in subsequent equations.

Summations of moments with respect to x and y coordinate directions, gives the equations:

$$-\mathrm{M}_{xy,x} - \mathrm{M}_{y,y} + \mathrm{Q}_y = 0$$

$$+\mathrm{M}_{yx,y} - \mathrm{M}_{x,x} - \mathrm{Q}_x = 0 \tag{3.15}$$

Collection of the five equilibrium equations and rearrangement gives (also considering $\mathrm{N_{yx}} = \mathrm{N_{xy}}$ and $\mathrm{M_{yx}} = \mathrm{M_{xy}}$)

$$\mathrm{N_{x,x}} - \mathrm{N_{xy,y}} = 0 \tag{3.16a}$$

$$\mathrm{N_{xy,x}} - \mathrm{N_{y,y}} = 0 \tag{3.16b}$$

$$\mathrm{Q_{x,x}} + \mathrm{Q_{y,y}} - \mathrm{N_x}\beta_{\mathrm{x,x}} - \mathrm{N_{xy}}\left(\beta_{\mathrm{y,x}} + \beta_{\mathrm{x,y}}\right) - \mathrm{N_y}\beta_{\mathrm{y,y}} = -\mathrm{p} \tag{3.16c}$$

$$\mathrm{Q_y} = \mathrm{M_{y,y}} + \mathrm{M_{xy,x}} \tag{3.16d}$$

$$\mathrm{Q_x} = \mathrm{M_{x,x}} + \mathrm{M_{xy,y}} \tag{3.16e}$$

Several of the variables are readily eliminated. Putting Equations (3.16d) and (3.16e) into Equaction (3.16c) gives

$$\mathrm{M_{x,xx}} - 2\mathrm{M_{xy,xy}} + \mathrm{M_{y,yy}} - \mathrm{N_x}\beta_{\mathrm{x,x}} - \mathrm{N_{xy}}\left(\beta_{\mathrm{y,x}} + \beta_{\mathrm{x,y}}\right) - \mathrm{N_y}\beta_{\mathrm{y,y}} = -\mathrm{p} \tag{3.17}$$

Adding appropriate constitutive and kinematic relations for the moment intensities and rotations Eq. (3.17) reduces to the form:

$$\mathrm{D}\nabla^4 w - \left(\mathrm{N}_x \mathrm{w}_{,xx} + 2\mathrm{N}_{xy}\mathrm{w}_{,xy} + \mathrm{N}_y \mathrm{w}_{,yy}\right) = \mathrm{p} \tag{3.18}$$

Where; $\mathrm{D}\nabla^4 w = \mathrm{w}_{,xxxx} + 2\mathrm{w}_{,xxyy} + \mathrm{w}_{,yyyy}$

With these simplifications the equations of equilibrium can be rewritten in the relatively compact form;

$$\mathrm{N_{x,x}} - \mathrm{N_{xy,y}} = 0 \tag{3.19a}$$

$$\mathrm{N_{xy,x}} - \mathrm{N_{y,y}} = 0 \tag{3.19b}$$

$$\mathrm{D}\nabla^4 w - \left(\mathrm{N}_x \mathrm{w}_{,xx} + 2\mathrm{N}_{xy}\mathrm{w}_{,xy} + \mathrm{N}_y \mathrm{w}_{,yy}\right) = \mathrm{p} \tag{3.19c}$$

$$D\left(\frac{\partial^4 w}{\partial x^4}+2\frac{\partial^4 w}{\partial x^2\,\partial y^2}+\frac{\partial^4 w}{\partial y^4}\right)-\left(N_x\frac{\partial^2 w}{\partial x^2}+2N_{xy}\frac{\partial^2 w}{\partial x\,\partial y}+N_y\frac{\partial^2 w}{\partial y^2}\right)=p \qquad (3.19c)$$

3.3 Buckling Load of Composite Plate [4]

For a specially orthotropic plate the equation (3.19 c) is modified as;

$$D_1\frac{\partial^4 w}{\partial x^4}+2D_3\frac{\partial^4 w}{\partial x^2\partial y^2}+D_2\frac{\partial^4 w}{\partial y^4}=p(x,y)+N_x\frac{\partial^2 w}{\partial x^2}+2N_{xy}\frac{\partial^2 w}{\partial x\,\partial y}+N_y\frac{\partial^2 w}{\partial y^2} \qquad (3.20)$$

It is clearly seen that there is a connection between the axial loads and lateral deflection. Looking now at Equation (3.20) for the buckling of the composites under an in-plane load per unit width only (Since Nx=- P_x /b and N_{xy} , N_y =0 and $p(x,y)$ were ignored) Equation (3.20) turns:

$$D_1\frac{\partial^4 w}{\partial x^4}+2D_3\frac{\partial^4 w}{\partial x^2\partial y^2}+D_2\frac{\partial^4 w}{\partial y^4}-N_x\frac{\partial^2 w}{\partial x^2}=0 \qquad (3.21)$$

The simple-supported boundary conditions give the following equations:

w and $Mx = 0$ when $x = 0$ and $x = a$(length of the plate)

w and $My = 0$ when $y = 0$ and $y = b$(width of the plate)

Where:

Mx= -EI($w_{,xx}$+v$w_{,yy}$) and My=-EI($w_{,yy}$+v$w_{,xx}$). Therefore, the boundary-conditions are;

$w = w_{,xx} = 0$ when $x = 0$ and $x = a$ (3.22a)

$w = w_{,yy} = 0$ when $y = 0$ and $y = b$ (3.22b)

For the plate simple- supported from edges one assumes the Navier solution:

$$w(x,y)=\sum_{m=1}^{\infty}\sum_{n=1}^{\infty}A_{mn}sin\frac{m\pi x}{a}\,sin\frac{n\pi y}{b} \qquad (3.23)$$

Substituting Equation (3.23) into Equation (3.21), one gets critical load as in the Equation (3.24);

$$P_{cr}=-N_{x_{cr}}=\frac{\pi^2a^2}{m^2}\left[D_1\left(\frac{m}{a}\right)^4+2\,D_3\left(\frac{m}{a}\right)^2\left(\frac{n}{b}\right)^2+D_2\left(\frac{n}{b}\right)^4\right] \qquad (3.24)$$

Where;

$$D_1 = D_{11}\,, \qquad D_2 = D_{22}\,, D_3 = D_{12} + 2D_{66}\,, \tag{3.25}$$

Putting Equation (3.25) to the Equation (3.24), one gets the Equation (3.26) as;

$$P_{cr} = \pi^2[D_{11}\left(\frac{m}{a}\right)^2 + 2\,(D_{12} + 2D_{66}\,)\left(\frac{n}{b}\right)^2 + D_{22}\left(\frac{n}{b}\right)^4\left(\frac{a}{m}\right)^2\,] \tag{3.26}$$

Equation (3.26) is a homogeneous equation. Value of *n* and *m* is important for determining smallest critical buckling load. For the case of loaded edges are fixed and unloaded edges are free, n is taken as equal to 2. However *m* is the smallest one which gives smallest buckling load and changeable with respect to value of the flexural stiffness D_{11}, D_{12}, D_{22} and D_{66} and the length to width ratio of the plate, *a/b*. So value of m can be obtained with respect to these parameters.

Then taking *n*=2 the Equation (3.26) turns to:

$$P_{cr} = \pi^2[D_{11}\left(\frac{m}{a}\right)^2 + 2\,(D_{12} + 2D_{66}\,)\left(\frac{2}{b}\right)^2 + D_{22}\left(\frac{2}{b}\right)^4\left(\frac{a}{m}\right)^2\,] \tag{3.27}$$

Where D_{11}, D_{12}, D_{22}, and D_{66} are components of bending stiffness matrices [*D*] and calculated by using Equation (3.28):

$$D_{ij} = \frac{1}{3}\sum_{k=1}^{n}[\overline{Q}_{ij}]_k\,(\;{h_k}^3 - {h_{k-1}}^3\,)\,, i = 1,2,6; \quad j = 1,2,6; \tag{3.28}$$

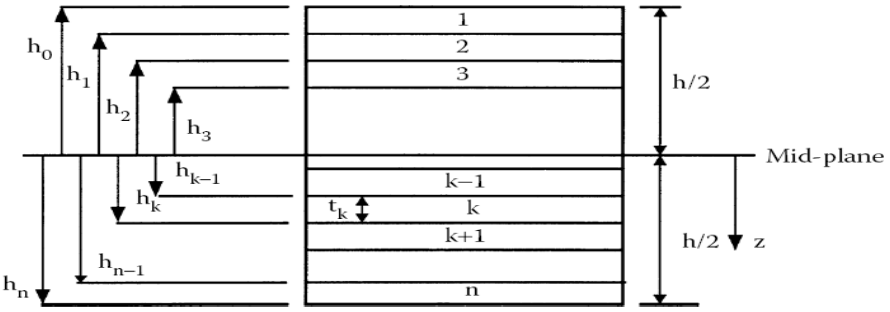

Figure 3.4 Coordinate locations for layered composite

h values can be shown in figure 3.4 and formulas are;

$$h = \sum_{k=1}^{n} t_k \quad ; \quad h_0 = -\frac{h}{2}(top\ surface)\,; h_1 = -\frac{h}{2} + t_1(top\ surface);\ h_2 = -\frac{h}{2} + t_2\,; \ldots \tag{3.29}$$

$$h_{k-1} = -\frac{h}{2} + \sum_{1}^{k-1} t\ (top\ surface)\ \ ; h_k = -\frac{h}{2} + \sum_{=1}^{k} t\ (bottom\ surface)\ ;\ k = 2,3,\ldots,n-2,n-1 \tag{3.30}$$

Then to find the $[Q]$ which is called as reduced stiffness matrix for each ply orientations, Equations (3.31) below are used.

$$Q_{11} = \frac{E_1}{1 - v_{21}v_{12}} \quad ; \quad Q_{12} = \frac{v_{12}E_2}{1 - v_{21}v_{12}} \quad ; \quad Q_{22} = \frac{E_2}{1 - v_{21}v_{12}} \; ; \qquad Q_{66} = G_{12} \tag{3.31}$$

Finally to calculate the transformed reduced stiffness matrix $[\bar{Q}]$ of Equation (3.28), the below equations are used:

$$\overline{Q}_{11} = Q_{11}\cos^4\theta + Q_{22}\sin^4\theta + 2(Q_{12} + 2Q_{66})\sin^2\theta\cos^2\theta$$

$$\overline{Q}_{12} = (Q_{11} + Q_{22} - 4Q_{66})\sin^2\theta\cos^2\theta + Q_{12}(\cos^4\theta + \sin^2\theta)$$

$$\overline{Q}_{22} = Q_{11}\sin^4\theta + Q_{22}\cos^4\theta + 2(Q_{12} + 2Q_{66})\sin^2\theta\cos^2\theta \tag{3.32}$$

$$\overline{Q}_{16} = (Q_{11} - Q_{12} - 2Q_{66})\cos^3\theta\sin\theta - (Q_{22} - Q_{12} - 2Q_{66})\sin^3\theta\cos\theta$$

$$\overline{Q}_{26} = (Q_{11} - Q_{12} - 2Q_{66})\cos\theta\sin^3\theta - (Q_{22} - Q_{12} - 2Q_{66})\cos^3\theta\sin\theta$$

$$\overline{Q}_{66} = (Q_{11} + Q_{22} - 2Q_{12} - 2Q_{66})\sin^2\theta\cos^2\theta + Q_{66}(\cos^4\theta + \sin^4\theta)$$

Where; $[Q]$ is the reduced stiffness matrix and θ is ply orientation angle.

CHAPTER 4

EXPERIMENTAL STUDIES PART I: PRODUCTION OF COMPOSITE PLATES AND DETERMINATION OF MECHANICAL PROPERTIES

4.1. Introduction

This chapter deals with the production of composite plates and determination of mechanical properties of these laminates.

4.2. Production of Composite Plates

In the production of composite plates plain S-Glass woven fibers (200 g/m^2), plain Carbon fibers (200 g/m^2) and twill Aramid woven fibers (170 g/m^2) have been used. The epoxy resin and hardener used in the production of composite plates are MGS L285 and MGS H285, respectively. Mechanical properties of fibers are given in the Table 4.1.

Table 4.1 General properties of fibers

Fiber Type	Weight (g/m^2)	Tensile Strength (MPa)	Young's Modulus (GPa)	Density (g/cm^3)
S-glass	200	3000-5000	72-82	2.48-2.60
Carbon	200	2500-3000	200-700	1.75-1.96
Aramid	170	2750-3000	82-124	1.44

The setup which is shown in Figure 4.1 has been used for production of composite laminates. As can be seen in the figure, the unit is combination of pressure, heat and vacuum. Curing pressure and temperature for composite plates have been determined experimentally by comparing tensile strength of produced

laminates. The optimum curing pressure and temperature were 0.2 MPa and 80 °C, respectively. So while producing laminates, these pressure and temperature have been applied during 1 hour (curing time). Then, composite laminates are cooled to room temperature under pressure. A typical curing cycle is given in the Figure 4.2.

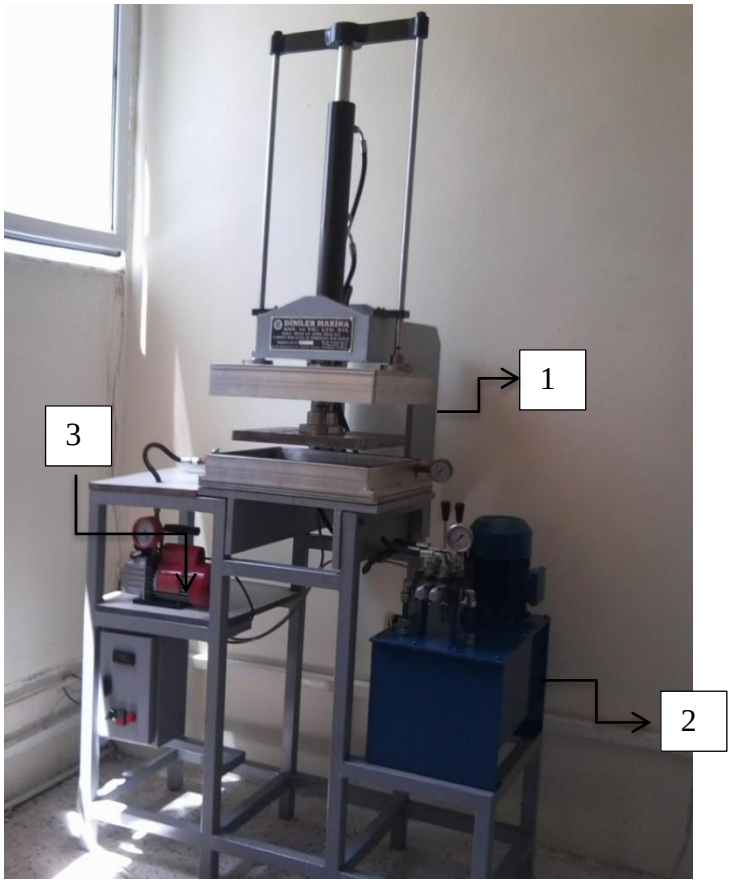

Figure 4.1 Vacuum supported composite production unit. (1) Combination of heat, pressure and vacuum, (2) Hydraulic unit, (3) Vacuum pump

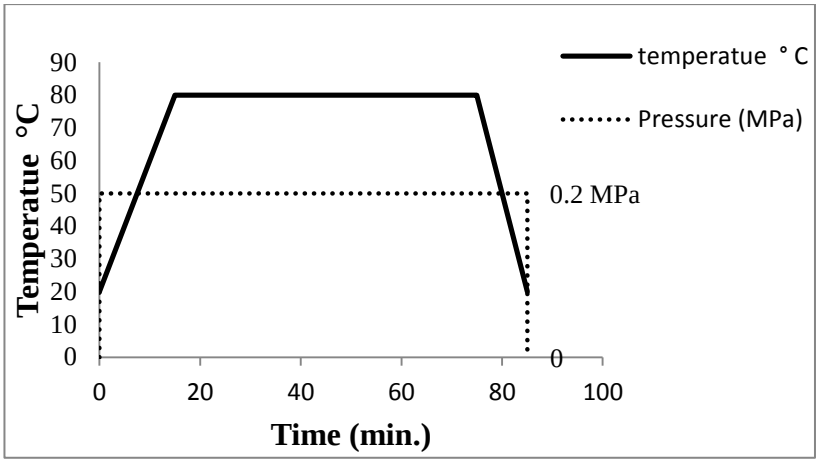

Figure 4.2 Cure cycle

Before production of plates, fibers are cut to desired specimen dimensions using EC fiber cutter as shown in the Figure 4.3. The epoxy and hardener ratio has been taken as 100:40 by weight. During production process, resin has been applied to fibers using a spatula (brush) as shown in the Figure 4.4 (a). In this process, it is so important to remove all air bubbles. After applying resin, the laminates have been cured in the production unit (Figure 4.4 (b)).

(a) (b)

(c)

Figure 4.3 Cutting fibers a) Aramid, b) Carbon c) S-glass

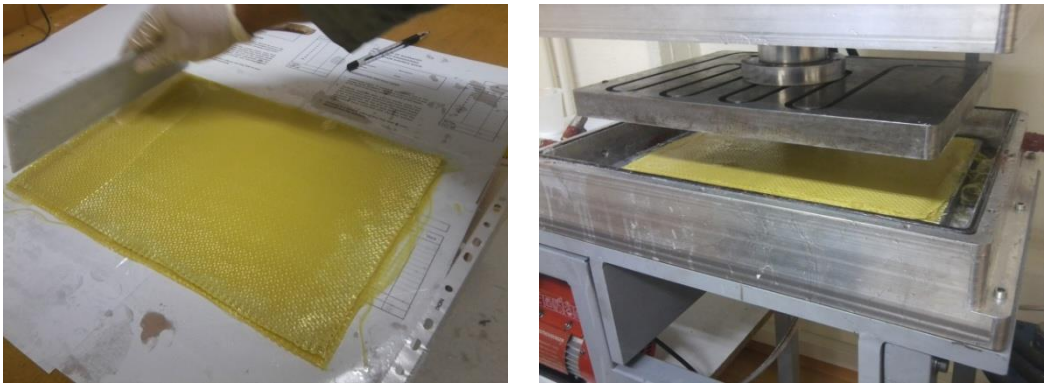

(a) (b)

Figure 4.4 Composite production a) resin application b) production unit

4.3 Production of Hybrid Composites

In the production of hybrid composite plates, the same production stages have been used. To see effect of all fiber types, different configurations of Carbon, Aramid and S-glass have been used with $[(0/90)_3]_s$, $[(\pm45)_3]_s$ and $[(30/-60)_3]_s$ stacking sequences. The used configurations are given in the Table 4.2. The plates have been produced with 240 mm x 350 mm dimensions and then specimens have been cut using CNC machine. 4 plates have been produced from each configuration. Example of produced composite and hybrid composite plates are given in Figure 4.5 and 4.6.

Table 4.2 Composite and Hybrid composite configurations

Configurations	Naming
$[0_G/90_G/0_G/90_G\ /0_G/90_G]_s$	G_{12}
$[30_G/-60_G/30_G/-60_G\ /30_G/-60_G]_s$	$(G_{12})^{30}$
$[45_G/-45_G/45_G/-45_G\ /45_G/-45_G]_s$	$(G_{12})^{45}$
$[0_A/90_A/0_A/90_A\ /0_A/90_A]_s$	A_{12}
$[30_A/-60_A/30_A/-60_A\ /30_A/-60_A]_s$	$(A_{12})^{30}$
$[45_A/-45_A/45_A/-45_A\ /45_A/-45_A]_s$	$(A_{12})^{45}$
$[0_C/90_C/0_C/90_C\ /0_C/90_C]_s$	C_{12}
$[30_C/-60_C/30_C/-60_C\ /30_C/-60_C]_s$	$(C_{12})^{30}$
$[45_C/-45_C/45_C/-45_C\ /45_C/-45_C]_s$	$(C_{12})^{45}$
$[0_G/90_G\ /0_C/90_C\ /0_A/90_A]_s$	GCA
$[30_G/-60_G\ /30_C/-60_C\ /30_A/-60_A]_s$	GCA^{30}
$[45_G/-45_G\ /45_C/-45_C\ /45_A/-45_A]_s$	GCA^{45}
$[0_G/90_G\ /0_A/90_A\ /0_C/90_C]_s$	GAC
$[30_G/-60_G\ /30_A/-60_A\ /30_C/-60_C]_s$	GAC^{30}
$[45_G/-45_G\ /45_A/-45_A\ /45_C/-45_C]_s$	GAC^{45}
$[0_C/90_C\ /0_G/90_G\ /0_A/90_A]_s$	CGA
$[30_C/-60_C\ /30_G/-60_G\ /30_A/-60_A]_s$	CGA^{30}
$[45_C/-45_C\ /45_G/-45_G\ /45_A/-45_A]_s$	CGA^{45}
$[0_C/90_C\ /0_A/90_A\ /0_G/90_G]_s$	CAG
$[30_C/-60_C\ /30_A/-60_A\ /30_G/-60_G]_s$	CAG^{30}
$[45_C/-45_C\ /45_A/-45_A\ /45_G/-45_G]_s$	CAG^{45}
$[0_A/90_A\ /0_G/90_G\ /0_C/90_C]_s$	AGC
$[30_A/-60_A\ /30_G/-60_G\ /30_C/-60_C]_s$	AGC^{30}
$[45_A/-45_A\ /45_G/-45_G\ /45_C/-45_C]_s$	AGC^{45}
$[0_A/90_A\ /0_C/90_C\ /0_G/90_G]_s$	ACG
$[30_A/-60_A\ /30_C/-60_C\ /30_G/-60_G]_s$	ACG^{30}
$[45_A/-45_A\ /45_C/-45_C\ /45_G/-45_G]_s$	ACG^{30}
$[0_G/90_G\ /0_C/90_C\ /0_A/90_A/0_G/90_G\ /0_C/90_C\ /0_A/90_A]$	GCA*
$[0_G/90_G\ /0_A/90_A\ /0_C/90_C/0_G/90_G\ /0_A/90_A\ /0_C/90_C]$	GAC*
$[0_C/90_C\ /0_G/90_G\ /0_A/90_A/0_C/90_C\ /0_G/90_G\ /0_A/90_A]$	CGA*

Table 4.2 (Continued)

Configurations	Naming
$[0_C/90_C\ /0_A/90_A\ /0_G/90_G/0_C/90_C\ /0_A/90_A\ /0_G/90_G]$	CAG*
$[0_A/90_A\ /0_G/90_G\ /0_C/90_C/0_A/90_A\ /0_G/90_G\ /0_C/90_C]$	AGC*
$[0_A/90_A\ /0_C/90_C\ /0_G/90_G/0_A/90_A/0_C/90_C\ /0_G/90_G]$	ACG*
G: glass fiber **, C:** carbon fiber**, A:**Aramid fiber ^{30} **:** means the $\mathbf{[(30/\text{-}60)_3]_s}$ stacking sequences ^{45} **:** means the $\mathbf{[(\pm 45)_3]_s}$ stacking sequences *: means the configuration is unsymmetrical	

Figure 4.5 Example of produced symmetrical hybrid plates.

Figure 4.6 Example of produced un-symmetrical hybrid plates.

4.4 Determination of the Mechanical Properties

S-Glass/Epoxy, Carbon/Epoxy and Aramid/Epoxy composite materials having $[(0/90)_3]_s$ stacking sequences have been produced to determine mechanical properties. Then, specimens have been prepared from produced composites plates. The main mechanical properties of laminated composite plates are tensile strength (σ_t), compressive strength ($\sigma_{c)}$, density (ρ), longitudinal Young's modulus (E_1), transverse Young's modulus (E_2), poison's ratio (ν), in-plane shear modulus (G_{12}). These mechanical properties are determined according to the American Society for Testing and Materials (ASTM) standards.

4.4.1 Determination of Tensile Properties

Tensile properties of specimens of plates are determined according to the ASTM D638–10 [149] standard test method. Suitable dimensions for this standard are given in the Figure 4.7. Type 1 configuration of ASTM 638-10 standard have been used considering specimen dimensions (Figure 4.7 and 4.8) as width of narrow section (W) 13 mm, length of narrow section (L) 57 mm, overall width (WO) 19 mm, overall length (LO) 165 mm, gage length (G) 50 mm, distance between grips (L) 115 mm and radius of fillet (R) 76 mm.

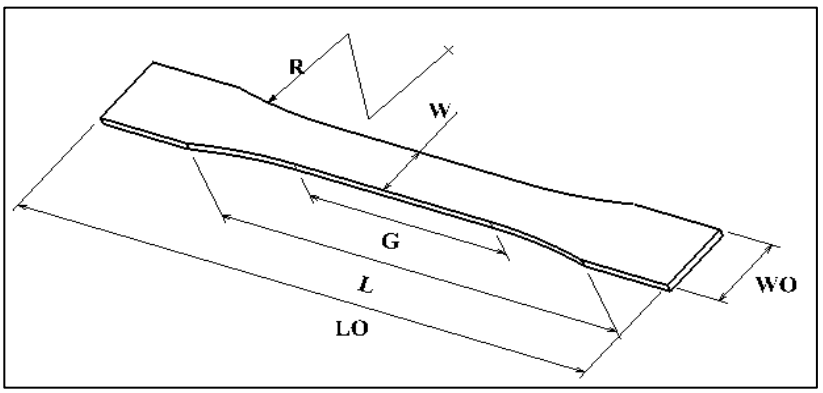

Figure 4.7 The dimensions of the tensile specimens according to ASTM 638-10 [2]

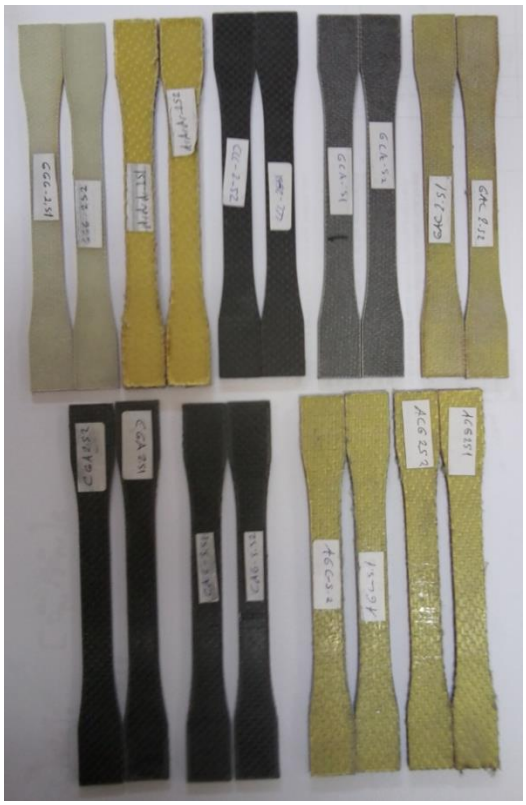

Figure 4.8 Examples of tensile test specimens

Mechanical properties of samples are obtained using Shimadzu AG-X series testing machine and Ni-9237 data acquisition card (Figure 4.9). To determine tension properties, specimens are loaded in tension direction with the 1 mm/min speed up to failure. Then tensile strength (σ_t), longitudinal Young's modulus (E_1), transverse Young's modulus (E_2) and poison's ratio (ν) are determined using the stress and strain data's obtained from testing machine and data acquisition card.

Figure 4.9 Test set-up (1) Shimadzu AG-X series testing machine, (2) Ni-9237 data acquisition card

4.4.2 Determination of Compressive Properties

Compressive properties of specimens are determined according to the ASTM D3410/D3410M – 03 [150] standard test method. Suitable dimensions for this standard are given in the Figure 4.10. Compressive test specimen dimensions (Figure 4.10 and 4.11) are taken as width (W) 10 mm, overall length (LO) 140 mm, gage length (G) 10 mm, Tab length (TL) 65 mm and Tab thickness (Tt) 1.5 mm. To determine compressive properties, specimens are loaded in compressive direction up to failure. Then compressive strength (σ_c) is determined by dividing failure load to the cross-sectional area using stress and strain data's obtained from testing machine and data acquisition card.

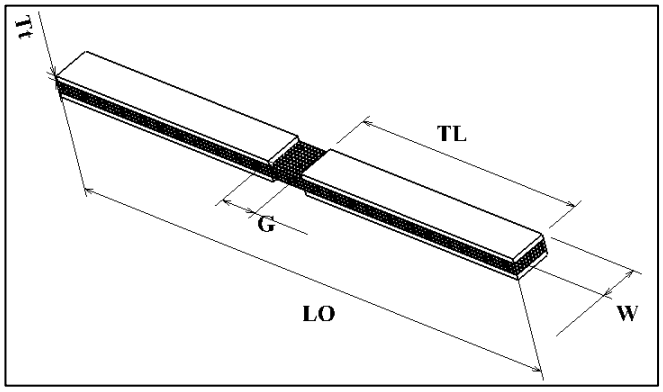

Figure 4.10 The dimensions of the compressive specimens suitable to ASTM D3410/D3410M – 03

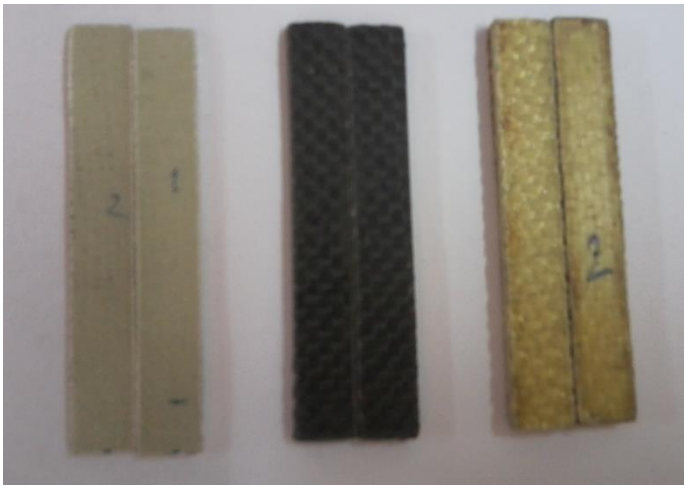

Figure 4.11 Examples of Compressive test specimens

4.4.3 Determination of Shear Properties

To determine shear properties, specimens are prepared with $[(\pm45)_3]_s$ stacking sequences in the same dimensions of tension test specimens according to D3518/D3518M – 94 [151]. The specimens are loaded in tension direction up to failure. Then the in-plane shear modulus (G_{12}) is calculated using equation (4.1).

$$G_{12} = \frac{1}{\left(\frac{4}{E_x} - \frac{1}{E_1} - \frac{1}{E_2} + \frac{2\nu_{12}}{E_1}\right)} \tag{4.1}$$

Where:

E_1 and E_2 denote longitudinal Young's modulus and transverse Young's modulus of $[(0/90)_3]_s$ stacking sequences laminate, respectively. ν_{12} is the poison ratio. E_x is longitudinal Young's modulus of $[(\pm45)_3]_s$ stacking sequences laminate.

4.4.4 Determined Mechanical Properties

Mechanical properties determined using the procedures and standards given above sections are given in the Table 4.3.

Table 4.3 Mechanical Properties of Composites

Composite Type	Tensile Strength (MPa)	Young's Modulus ($E_1 = E_2$) (GPa)	In plane shear modulus (G_{12}) (GPa)	Poisson' ratio ν_{12}
S-glass/Epoxy	310±10	19.65	3.80	0.14
Carbon/Epoxy	790±10	49.65	5.00	0.10
Aramid/Epoxy	440±10	26.78	2.56	0.095

CHAPTER 5

EXPERIMENTAL STUDIES PART 2: BUCKLING EXPERIMENTS

5.1. Introduction

This chapter deals with the buckling experiments and their results. The specimens having G_{12}, A_{12}, C_{12}, GCA, GAC, CGA, CAG, AGC and ACG configurations (Figure 5.1), specimens having $(G_{12})^{30}$,$(G_{12})^{45}$, $(A_{12})^{30}$, $(A_{12})^{45}$, $(C_{12})^{30}$, $(C_{12})^{45}$, GCA^{30}, GCA^{45}, GAC^{30}, GAC^{45}, CGA^{30}, CGA^{45}, CAG^{30}, CAG^{45}, AGC^{30}, AGC^{45}, ACG^{30} and ACG^{45} (Figure 5.2) configurations and specimens having GCA^{*}, GAC^{*}, CGA^{*}, CAG^{*}, AGC^{*} and ACG^{*} (Figure 5.3) configurations are prepared to carry out buckling experiments.

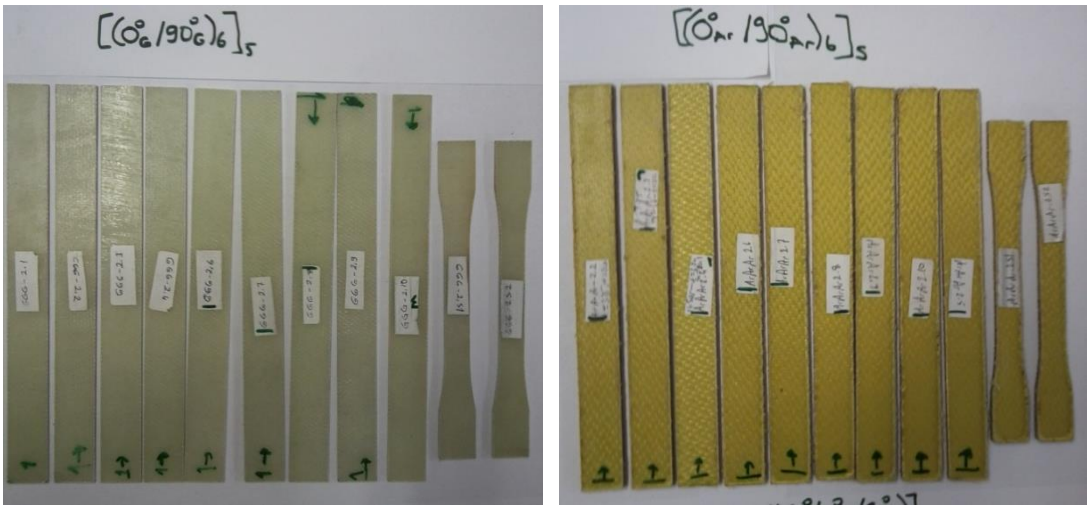

(a) (b)

(c)

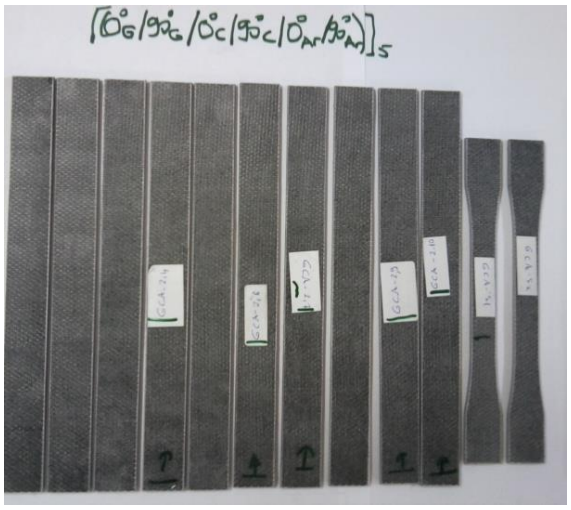

(d)

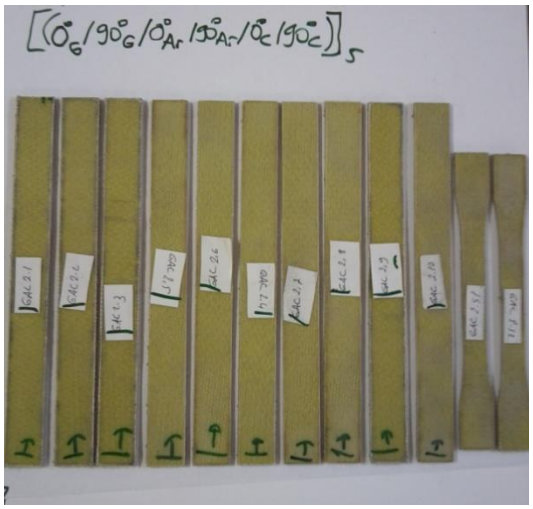

(e)

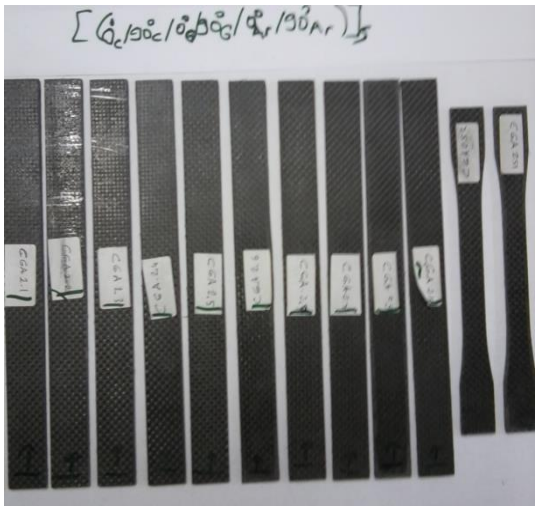

(f)

(g)

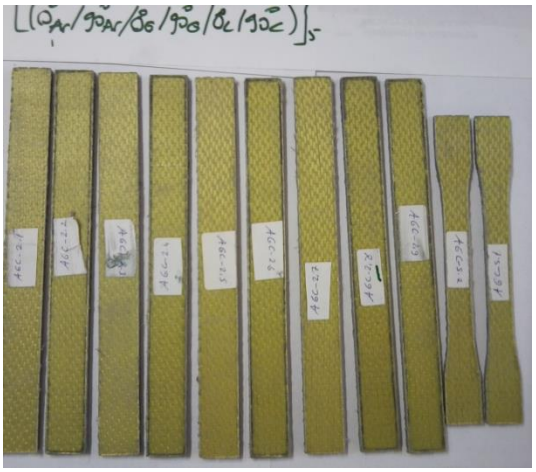

(h)

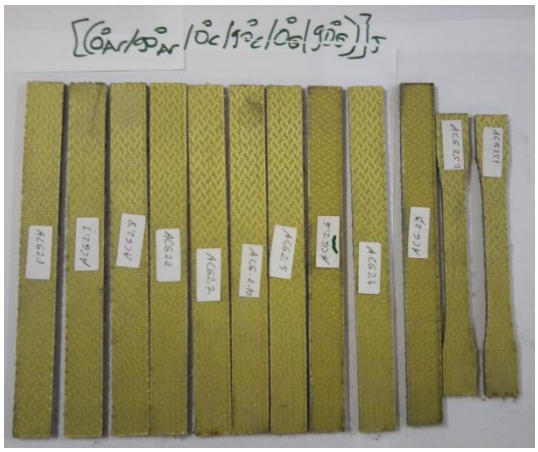

(ı)

Figure 5.1 Experiment specimens a) G_{12}, b) A_{12}, c) C_{12}, d) GCA, e) GAC, f) CGA, g) CAG, h) AGC, ı) ACG

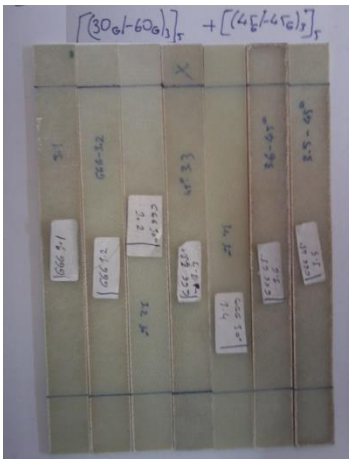

(a)

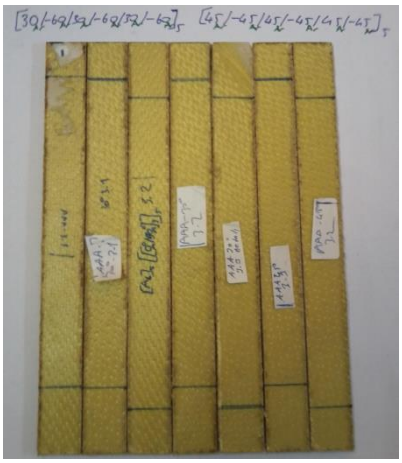

(b)

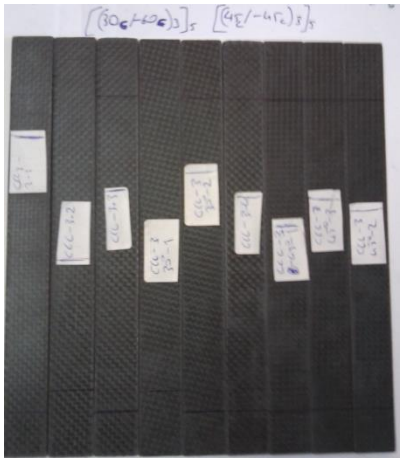

(c)

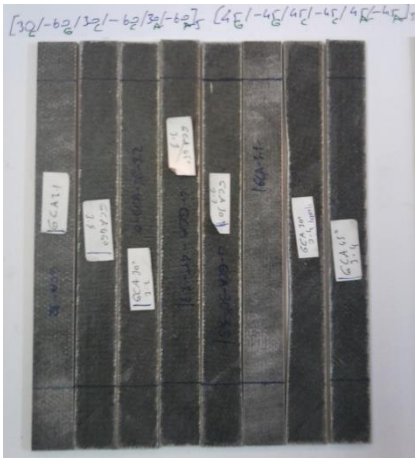

(d)

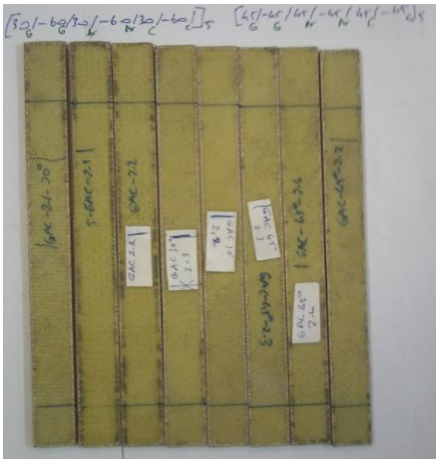

(e)

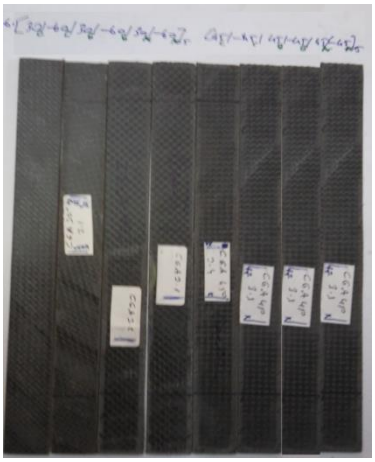

(f)

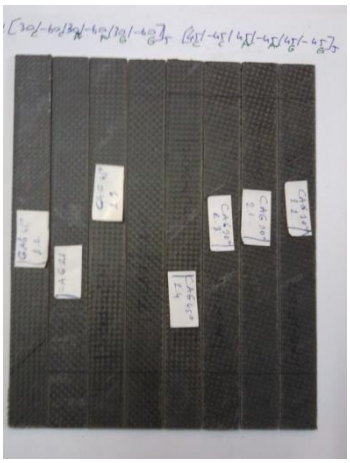

(g)

(h)

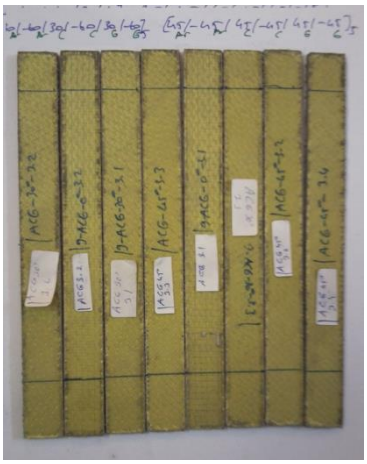

(ı)

Figure 5.2 Experiment specimens a) $(G_{12})^{30}$ and $(G_{12})^{45}$, b) $(A_{12})^{30}$ and $(A_{12})^{45}$, c) $(C_{12})^{30}$ and $(C_{12})^{45}$, d) GCA^{30} and GCA^{45}, e) GAC^{30} and GAC^{45}, f) CGA^{30} and CGA^{45}, g) CAG^{30} and CAG^{45}, h) AGC^{30} and AGC^{45}, ı) ACG^{30} and ACG^{45}

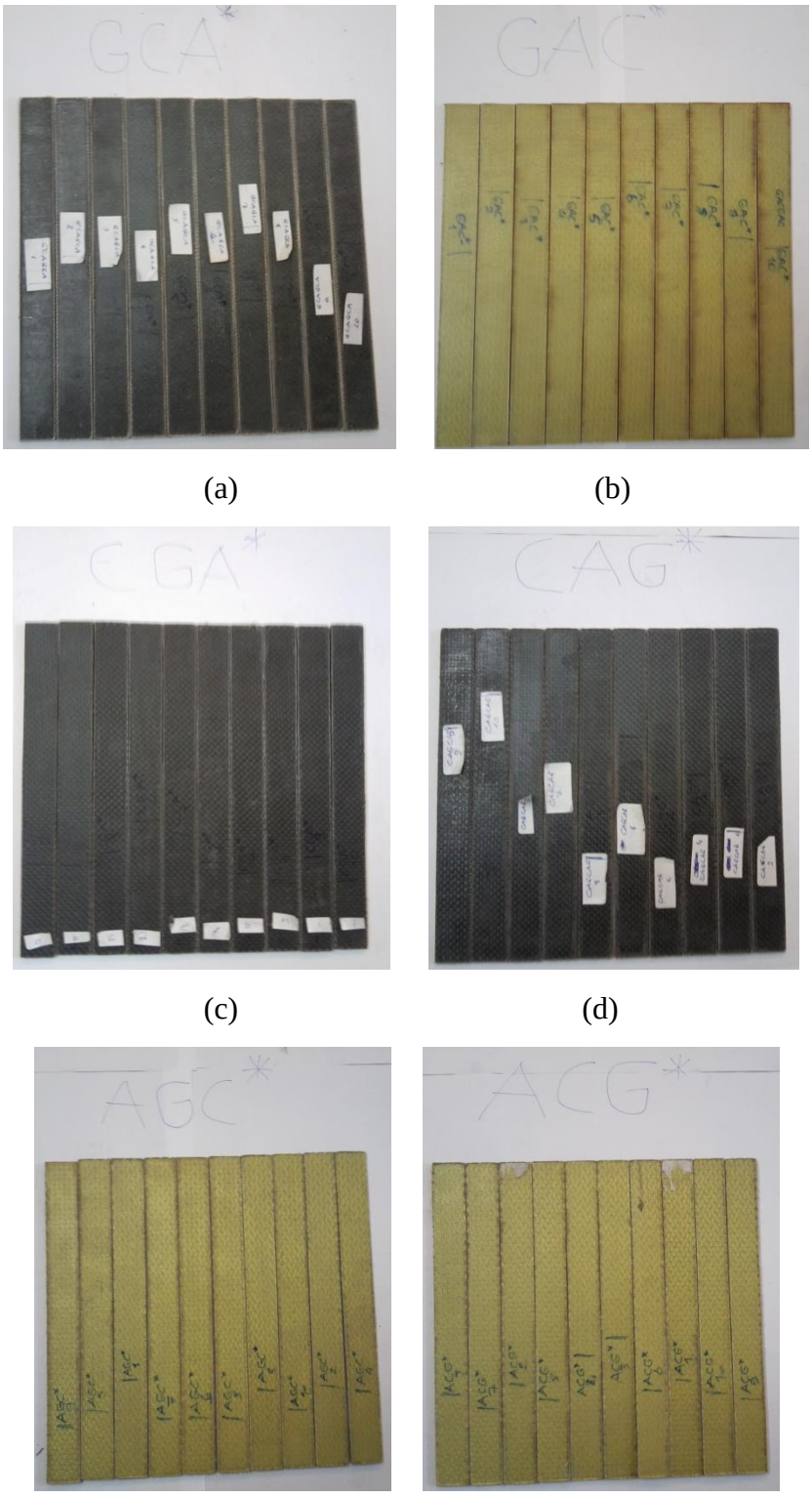

(a) (b)

(c) (d)

(e) (f)

Figure 5.3 Experiment specimens a) GCA*, b) GAC*, c) CGA*, d) CAG*, e) AGC*, f) ACG*

5.2 Buckling Experiment Results of Composites and Hybrid Composites Having $[(0/90)_3]_s$ Stacking Sequence

Buckling experiments are performed using Shimadzu AG-X series testing machine (Figure 5.4). During the experiments, the specimens have been fixed both from bottom grip and top grip and loaded in compressive direction (as given in the Figure 2.2) with the 0.25 mm/min speed up to buckling occurs.

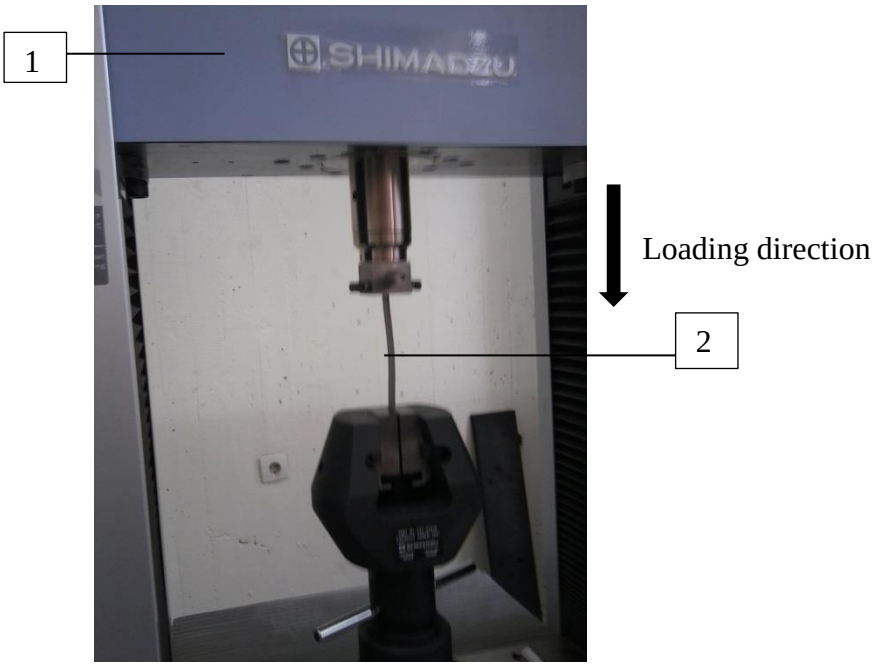

Figure 5.4 Experiment set-up of Buckling (1) Shimadzu AG-X serial testing machine, (2) Specimen

The produced G_{12}, A_{12} and C_{12} plate thicknesses are 2.20 mm, 3.30 mm and 2.60 mm, respectively. Thicknesses of hybrid composite plates produced from different combinations of S-Glass, Aramid and Carbon are 2.70 ±0.2 mm. Buckling test specimen dimensions are taken as width (W) 20 mm, overall length (LO) 200 mm and gage length (G) 155 mm.

In the Figure 5.5, the buckling load-displacement diagrams of composite and hybrid composite specimens (G_{12}, A_{12}, C_{12}, GCA, GAC, CGA, CAG, AGC and ACG) having $[(0/90)_3]_s$ stacking sequences are given. The load that the curve directly begins to return the down is the buckling load. In other words, buckling will occur when the slop of the curve change side (positive to negative or vice versa). As can

be seen in the figure 5.5, the position and magnitude of the critical buckling load changes for the different hybrid configurations.

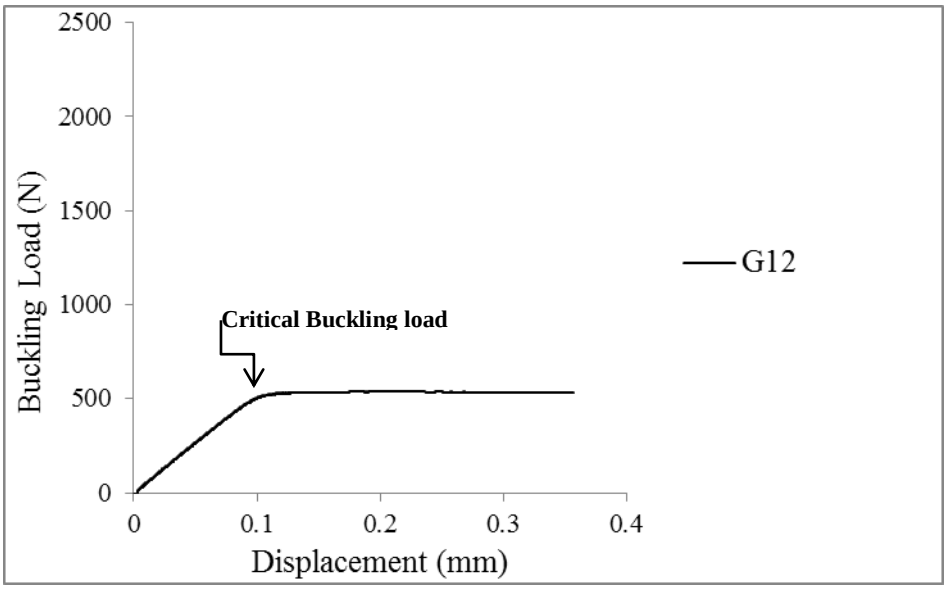

(a)

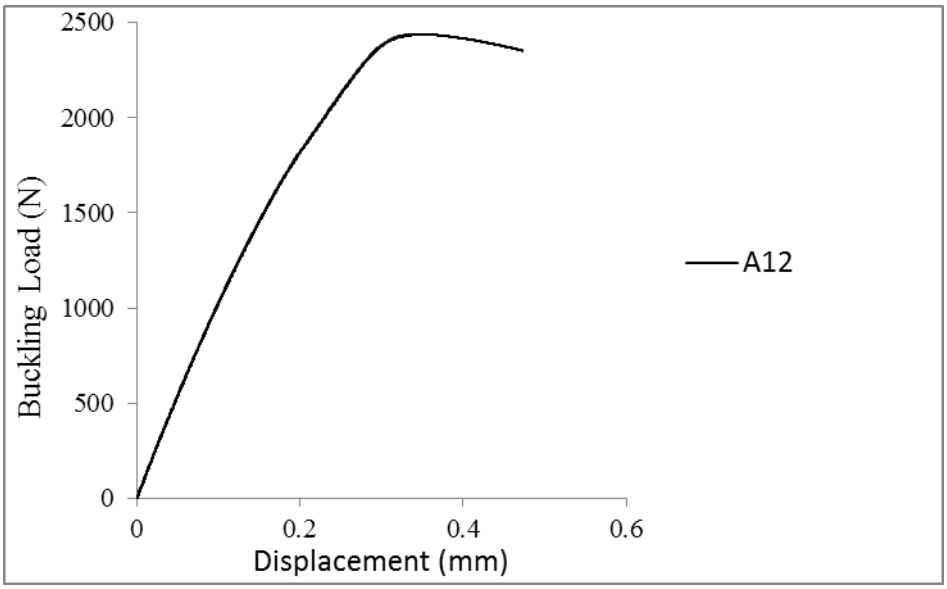

(b)

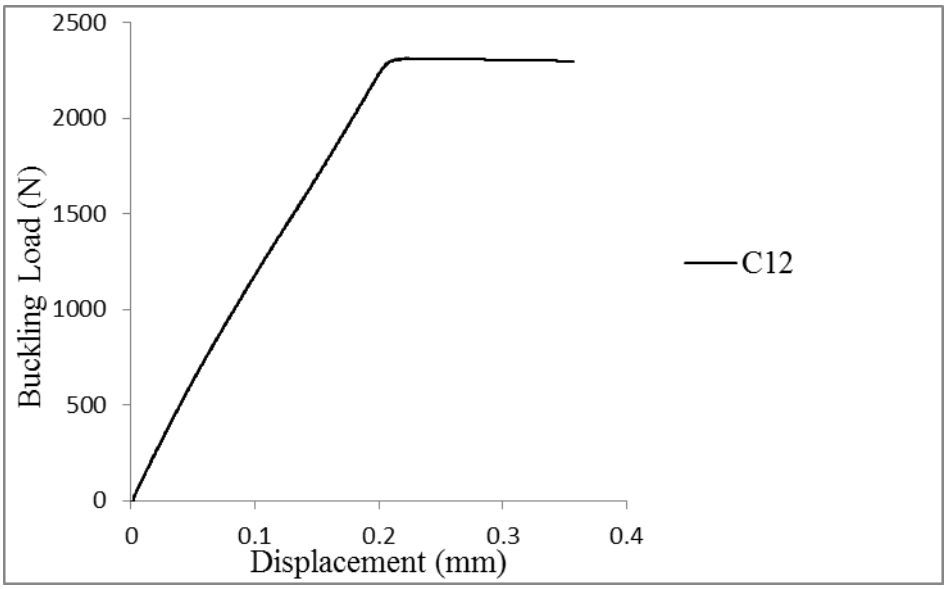
2500
2000
1500
1000
500
0
Buckling Load (N)
0
0.1
0.2
0.3
0.4
Displacement (mm)
C12

(c)

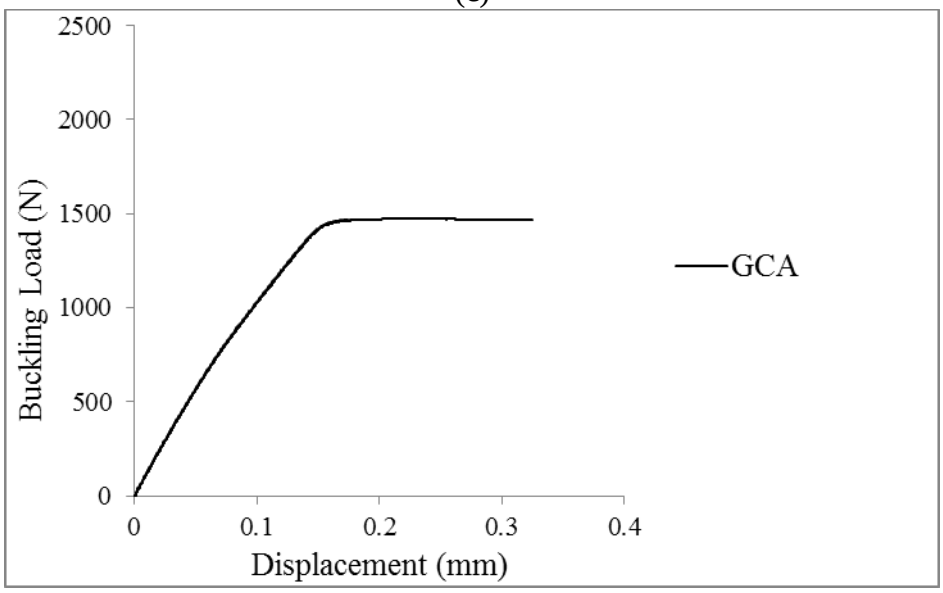
2500
2000
1500
1000
500
0
Buckling Load (N)
0
0.1
0.2
0.3
0.4
Displacement (mm)
GCA

(d)

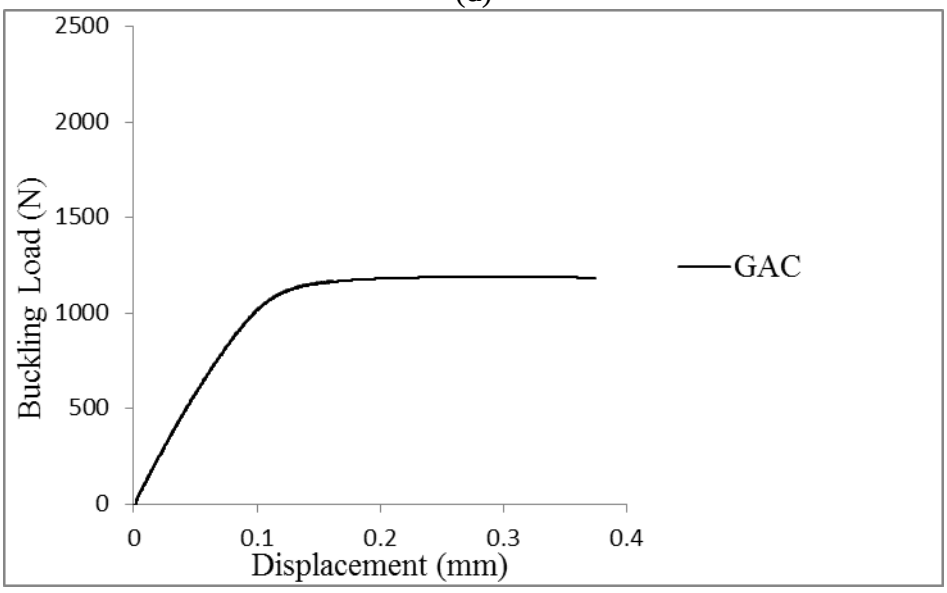
2500
2000
1500
1000
500
0
Buckling Load (N)
0
0.1
0.2
0.3
0.4
Displacement (mm)
GAC

(e)

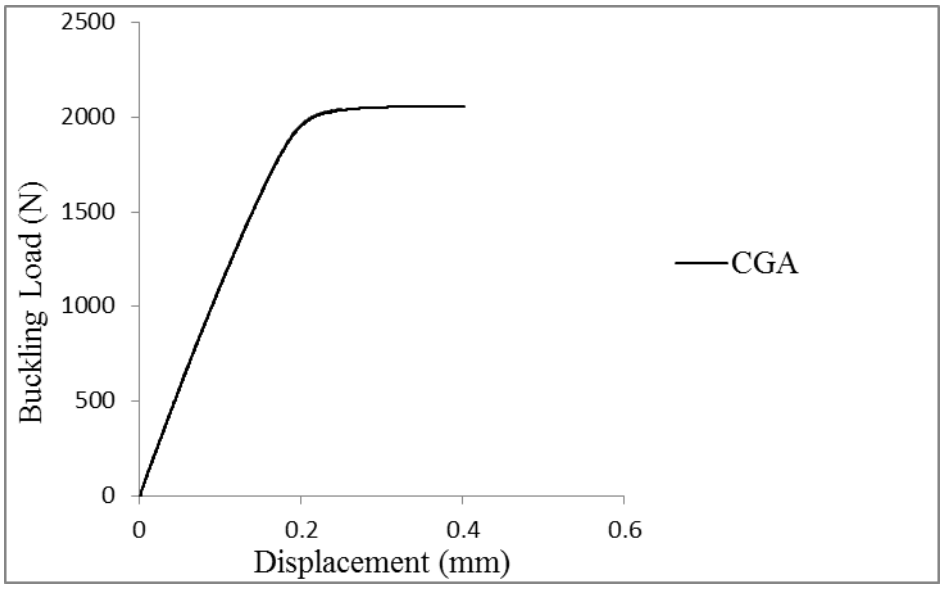
2500
2000
1500
1000
500
0
Buckling Load (N)
0
0.2
0.4
0.6
Displacement (mm)
CGA

(f)

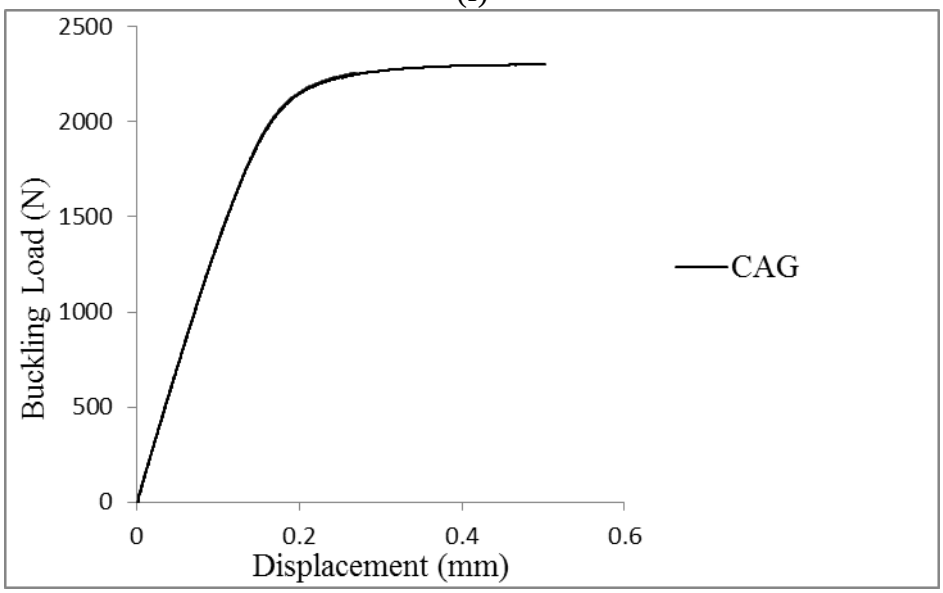
2500
2000
1500
1000
500
0
Buckling Load (N)
0
0.2
0.4
0.6
Displacement (mm)
CAG

(g)

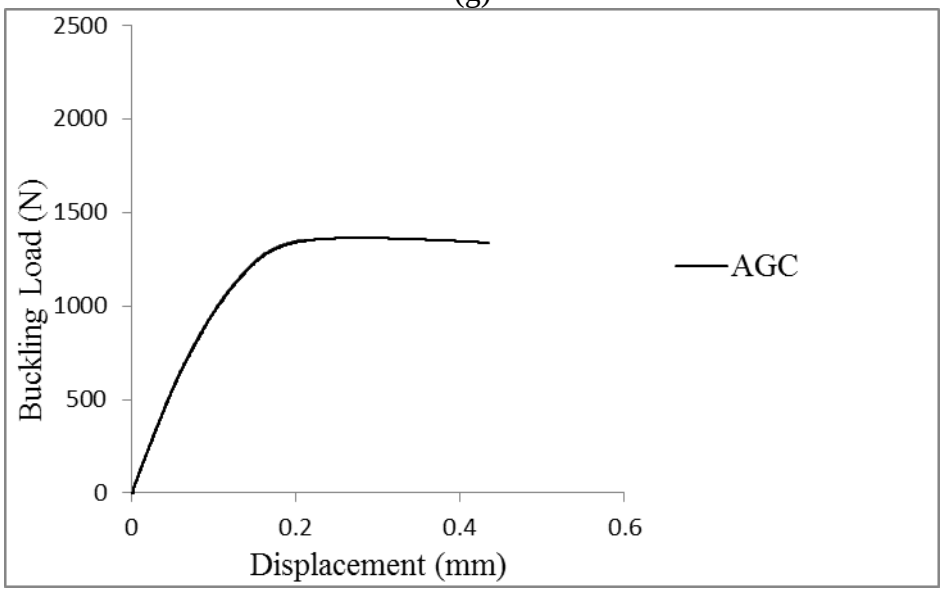
2500
2000
1500
1000
500
0
Buckling Load (N)
0
0.2
0.4
0.6
Displacement (mm)
AGC

(h)

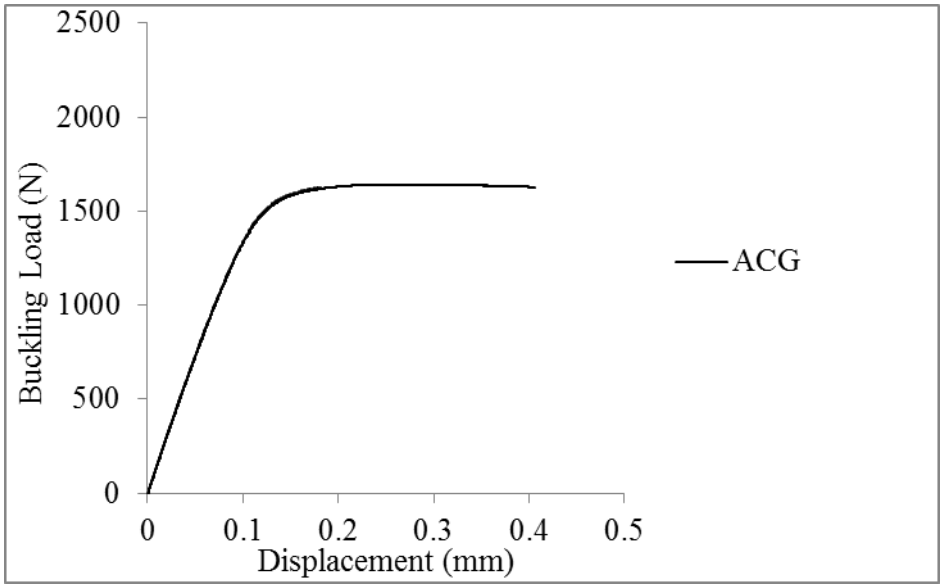

(ı)

Figure 5.5 Buckling load - displacement diagram of a) G_{12}, b) A_{12}, c) C_{12}, d) GCA, e) GAC, f) CGA, g) CAG, h) AGC, ı) ACG

In the Figure 5.6, buckling load-displacement curves of hybrid specimens are given together. As can be seen from figure 5.6, CAG has the highest buckling load and GAC has the smallest buckling load. In other words, CAG is the most durable, and GAC is the less durable with respect to buckling characteristic. The ratio of buckling load of CAG to GAC is nearly 1.9 and buckling load of CAG is nearly 47 % higher than GAC.

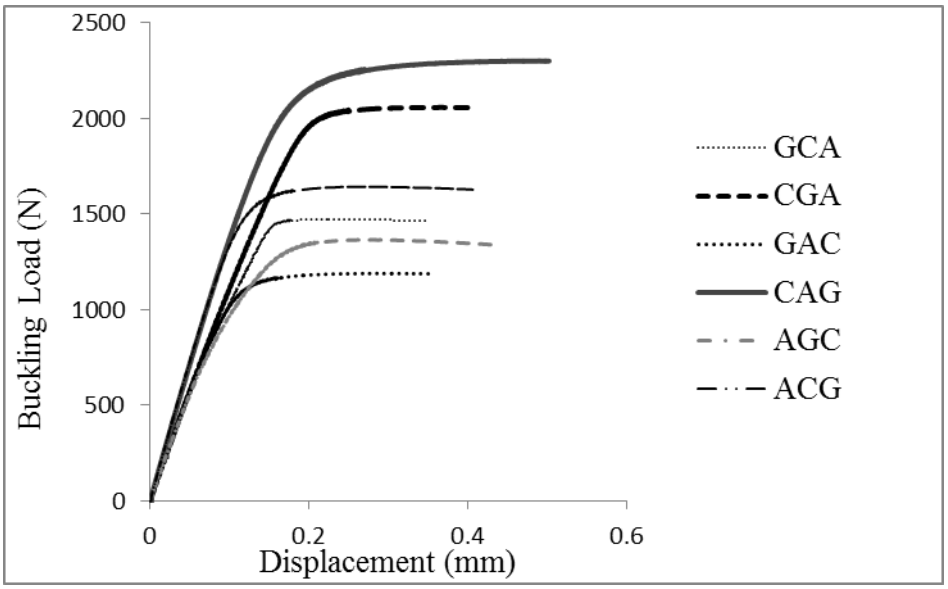

Figure 5.6 Comparison of buckling load- displacement curves of 6 different hybrid configurations ($[(0/90)_3]_s$).

Experiment results of 3 different specimens of each hybrid composite configurations are given in Figure 5.7 and Table 5.1. Buckling loads can be ordered from the highest buckling load to the smallest buckling load as; CAG, CGA, ACG, GCA, AGC, GAC, respectively.

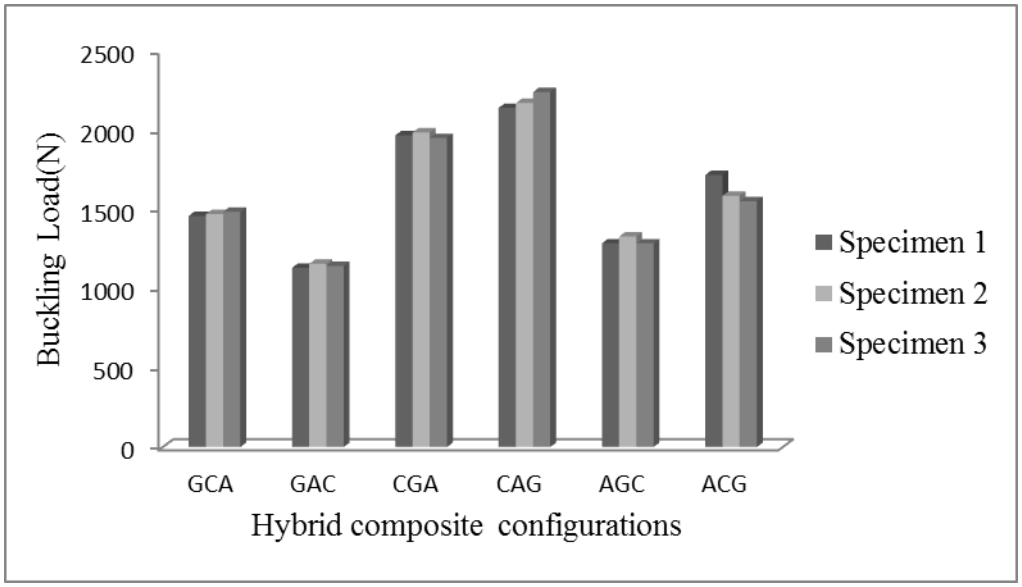

Figure 5.7 Comparison of buckling load- displacement curves of 6 different hybrid configurations with 3 different specimens

Table 5.1 Critical buckling loads of Composite and hybrid composite specimens having $[(0/90)_3]_s$ stacking sequences

	Buckling Load (N)		
Hybrid composite configurations	**Specimen 1**	**Specimen 2**	**Specimen 3**
G_{12}	578.022	524.502	513.798
A_{12}	2347.177	2355.115	2380.154
C_{12}	2280.469	2292.633	2234.237
GCA	1459.624	1471.356	1485.189
GAC	1131.577	1157.074	1143.718
CGA	1968.691	1986.260	1951.440
CAG	2141.485	2172.078	2242.441
AGC	1286.164	1329.657	1286.164
ACG	1718.299	1585.998	1552.592

5.3 Buckling Experiment Results of Composites and Hybrid Composites Having $[(30/-60)_3]_s$ and $[(45/-45)_3]_s$ Stacking Sequences

In this section, experiment results of composite and hybrid composite having $[(30/-60)_3]_s$ and $[(45/-45)_3]_s$ stacking sequences are given. In Figure 5.8, the buckling load-displacement diagrams of composite and hybrid composite specimens $(G12)^{30}$, $(A12)^{30}$, $(C12)^{30}$, GCA^{30}, GAC^{30}, CGA^{30}, CAG^{30}, AGC^{30} and ACG^{30} which have $[(30/-60)_3]_s$ stacking sequences are given.

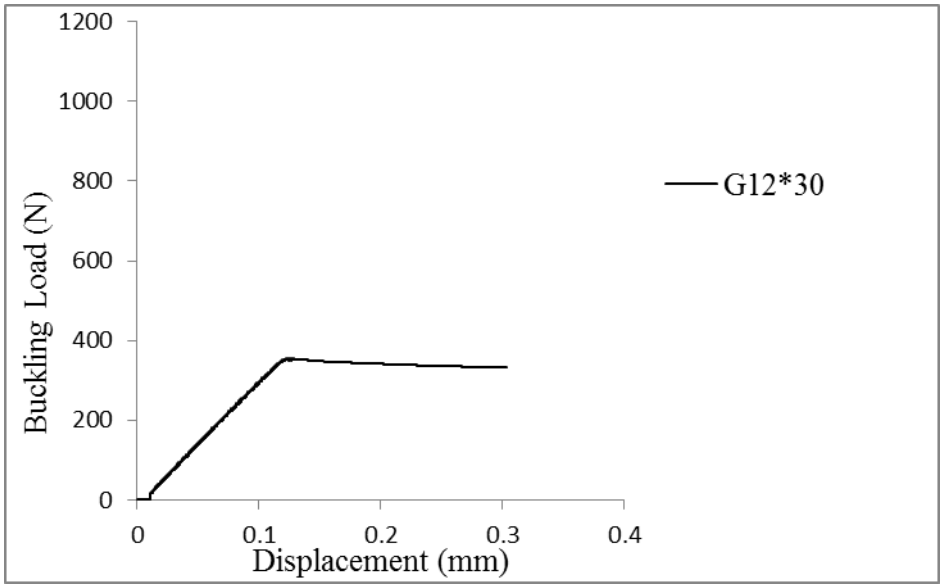

(a)

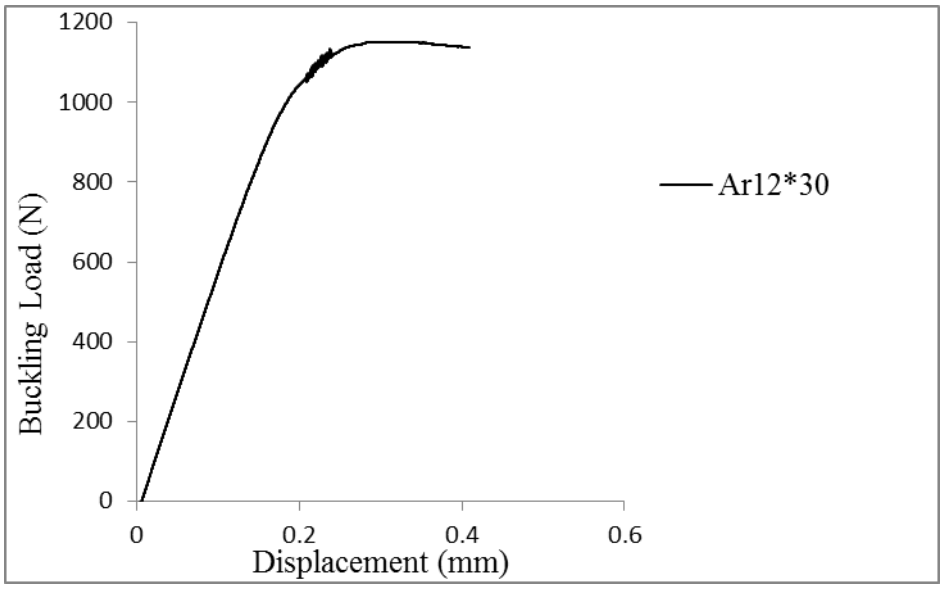

(b)

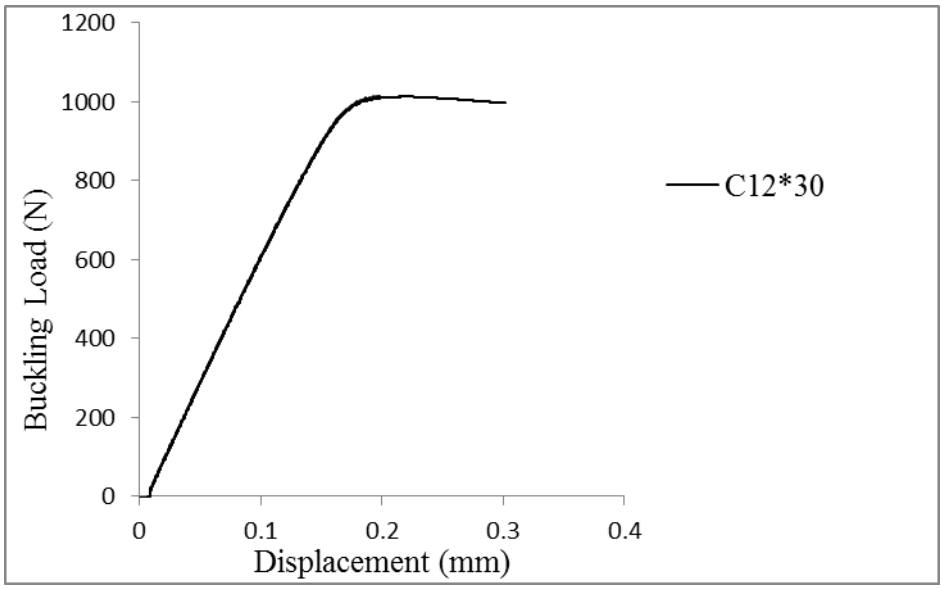
1200
1000
800
600
400
200
0
Buckling Load (N)
0
0.1
0.2
0.3
0.4
Displacement (mm)
C12*30

(c)

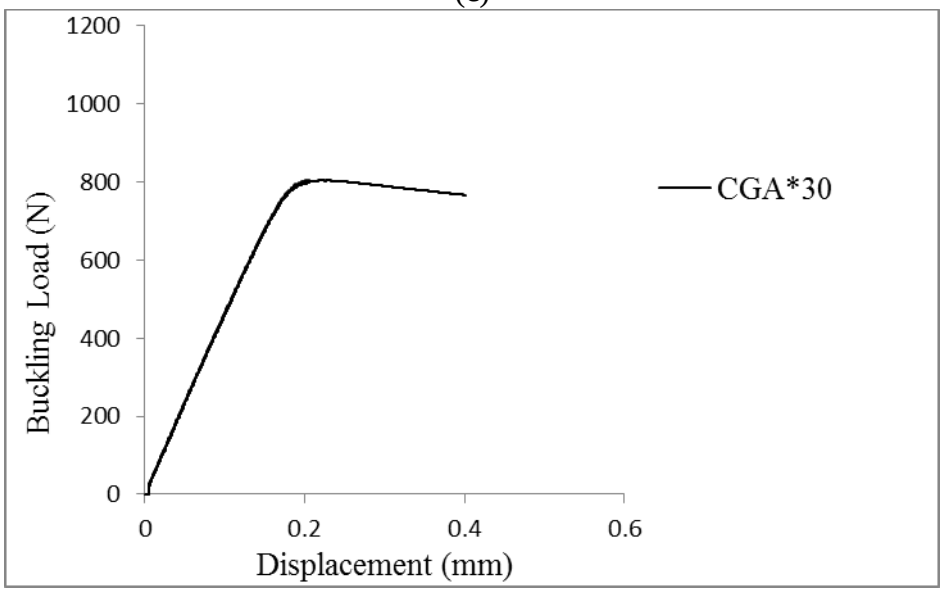
1200
1000
800
600
400
200
0
Buckling Load (N)
0
0.2
0.4
0.6
Displacement (mm)
CGA*30

(d)

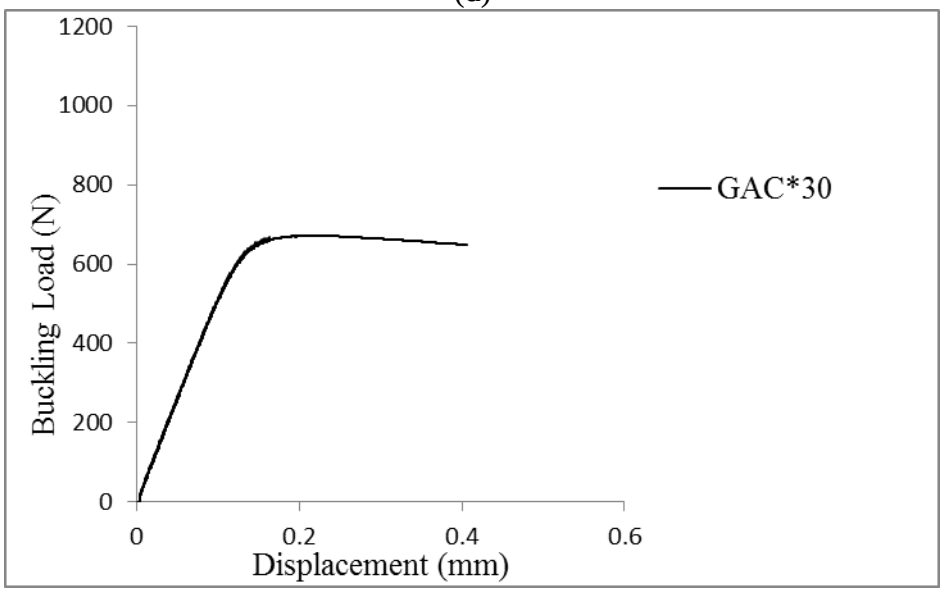
1200
1000
800
600
400
200
0
Buckling Load (N)
0
0.2
0.4
0.6
Displacement (mm)
GAC*30

(e)

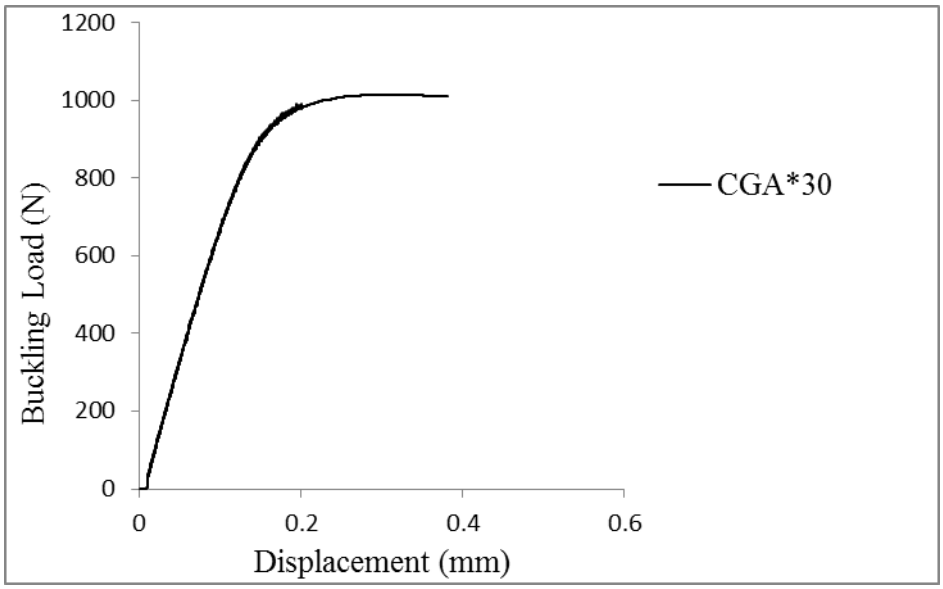
1200
1000
800
600
400
200
0
Buckling Load (N)
0
0.2
0.4
0.6
Displacement (mm)
CGA*30

(f)

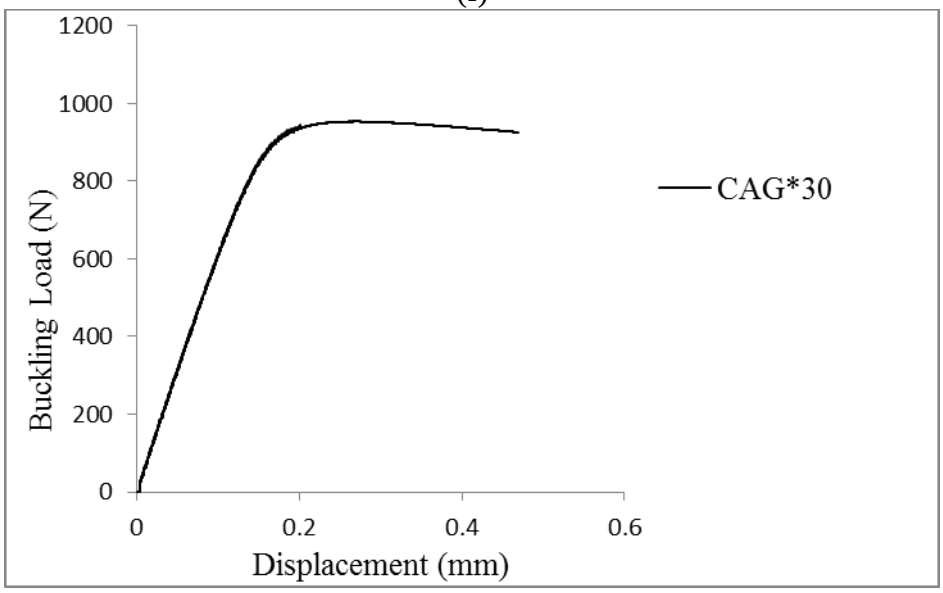
1200
1000
800
600
400
200
0
Buckling Load (N)
0
0.2
0.4
0.6
Displacement (mm)
CAG*30

(g)

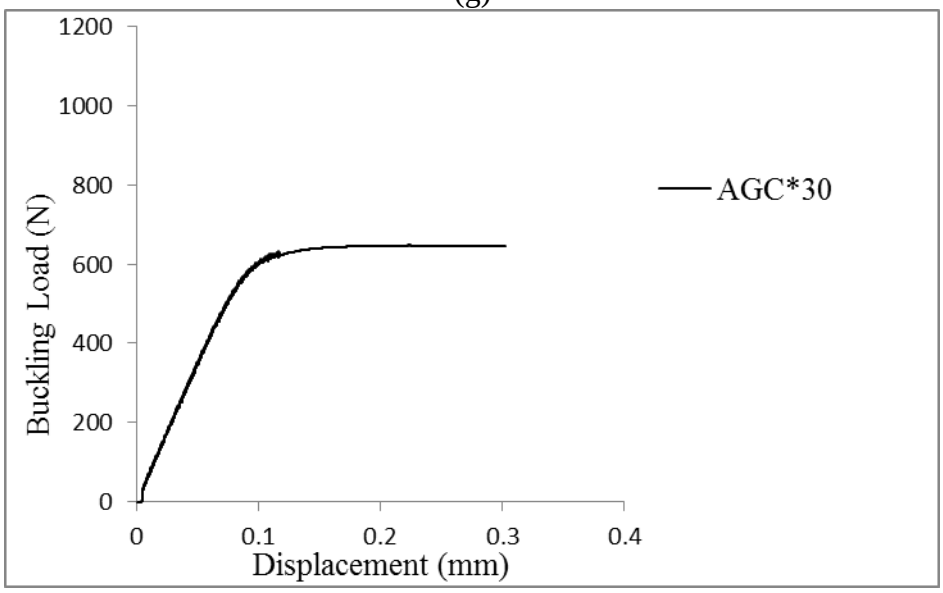
1200
1000
800
600
400
200
0
Buckling Load (N)
0
0.1
0.2
0.3
0.4
Displacement (mm)
AGC*30

(h)

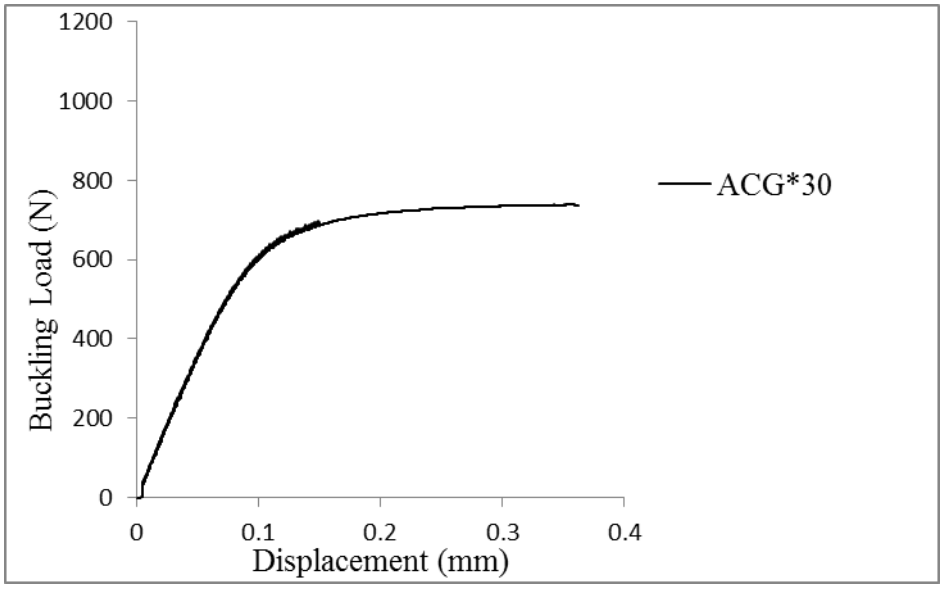

(ı)

Figure 5.8 Buckling load - displacement diagram of a) $(G_{12})^{30}$, b) $(A_{12})^{30}$, c) $(C_{12})^{30}$, d) GCA^{30}, e) GAC^{30}, f) CGA^{30}, g) CAG^{30}, h) AGC^{30}, ı) ACG^{30}

In Figure 5.9, the buckling load-displacement diagrams of composite and hybrid composite specimens $(G_{12})^{45}$, $(A_{12})^{45}$, $C_{12})^{45}$, GCA^{45}, GAC^{45}, CGA^{45}, CAG^{45}, AGC^{45} and ACG^{45} which have $[(45/-45)_3]_s$ stacking sequences are given.

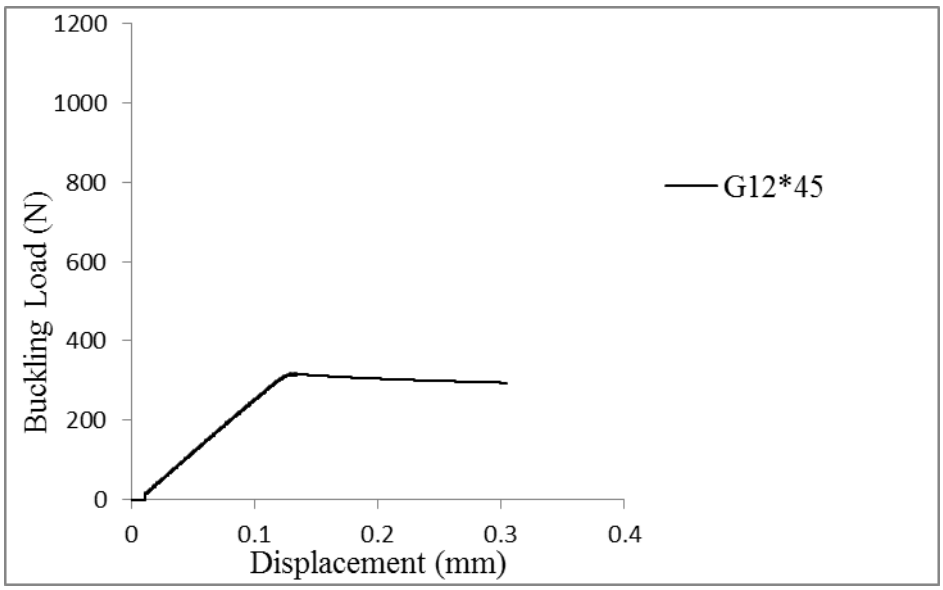

(a)

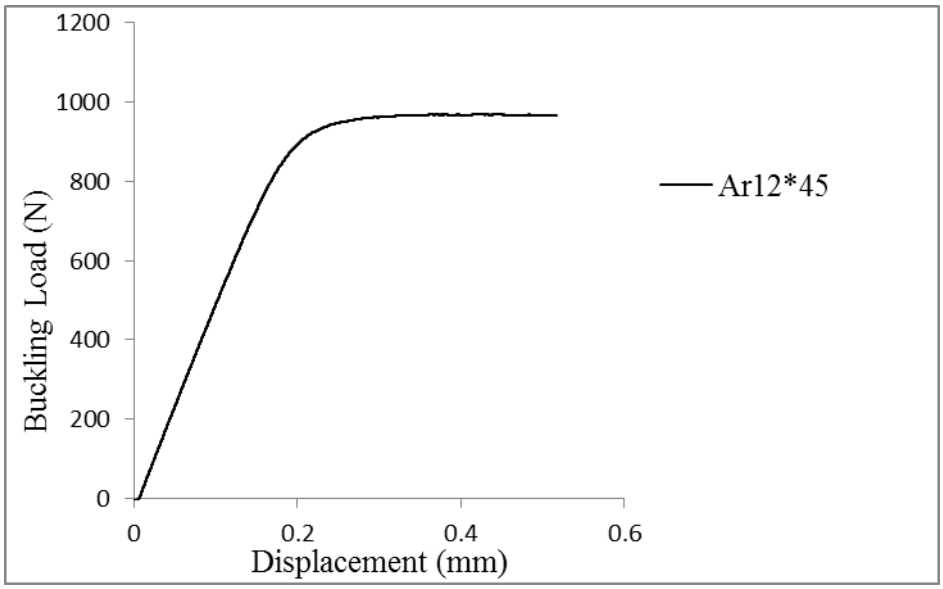
1200
1000
800
600
400
200
0
Buckling Load (N)
0
0.2
0.4
0.6
Displacement (mm)
Ar12*45

(b)

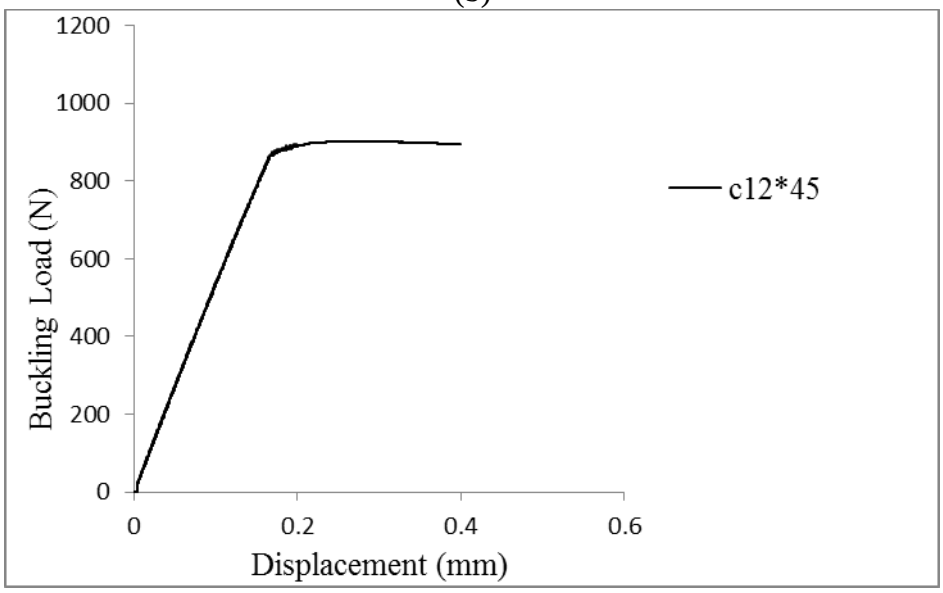
1200
1000
800
600
400
200
0
Buckling Load (N)
0
0.2
0.4
0.6
Displacement (mm)
c12*45

(c)

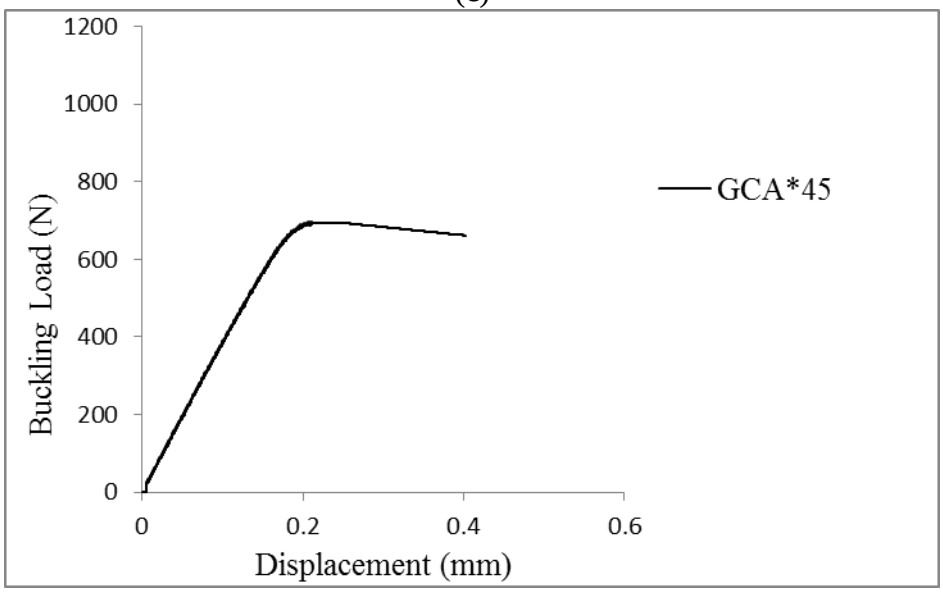
1200
1000
800
600
400
200
0
Buckling Load (N)
0
0.2
0.4
0.6
Displacement (mm)
GCA*45

(d)

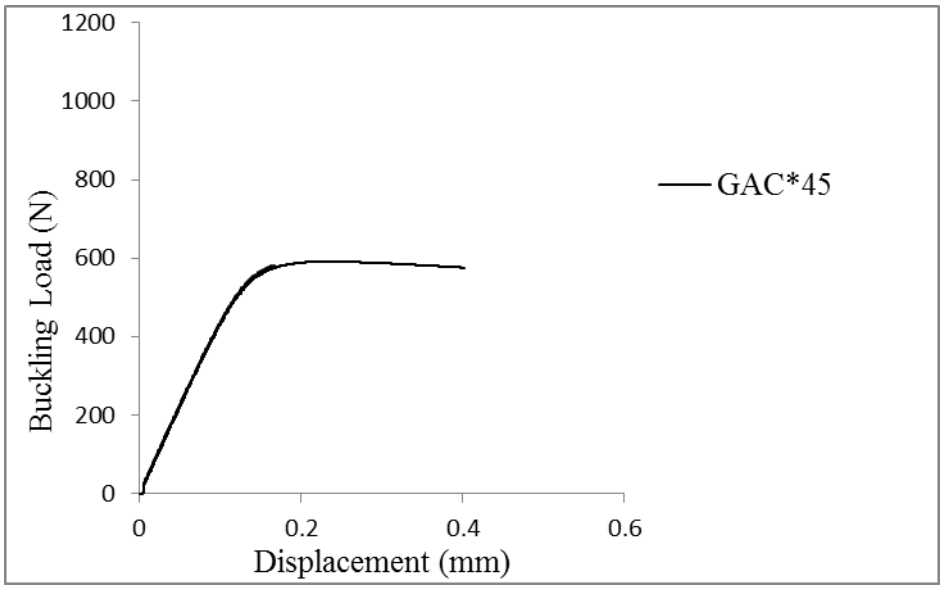
1200
1000
800
600
400
200
0
Buckling Load (N)
0
0.2
0.4
0.6
Displacement (mm)
GAC*45

(e)

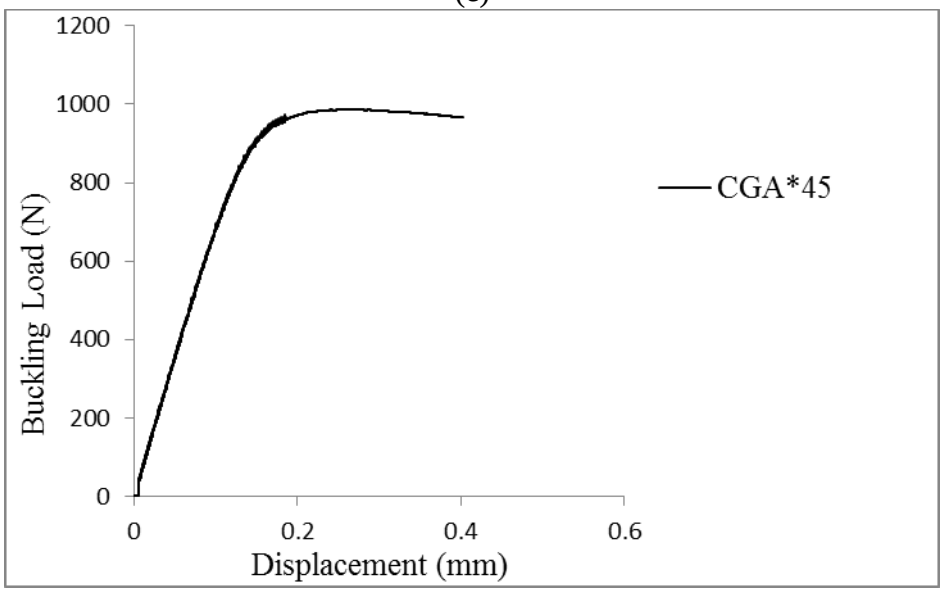
1200
1000
800
600
400
200
0
Buckling Load (N)
0
0.2
0.4
0.6
Displacement (mm)
CGA*45

(f)

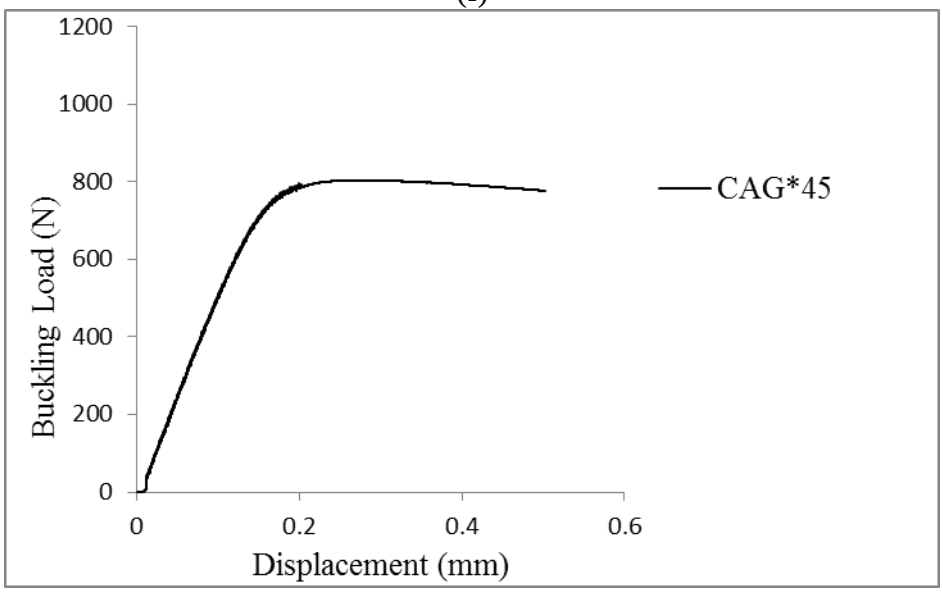
1200
1000
800
600
400
200
0
Buckling Load (N)
0
0.2
0.4
0.6
Displacement (mm)
CAG*45

(g)

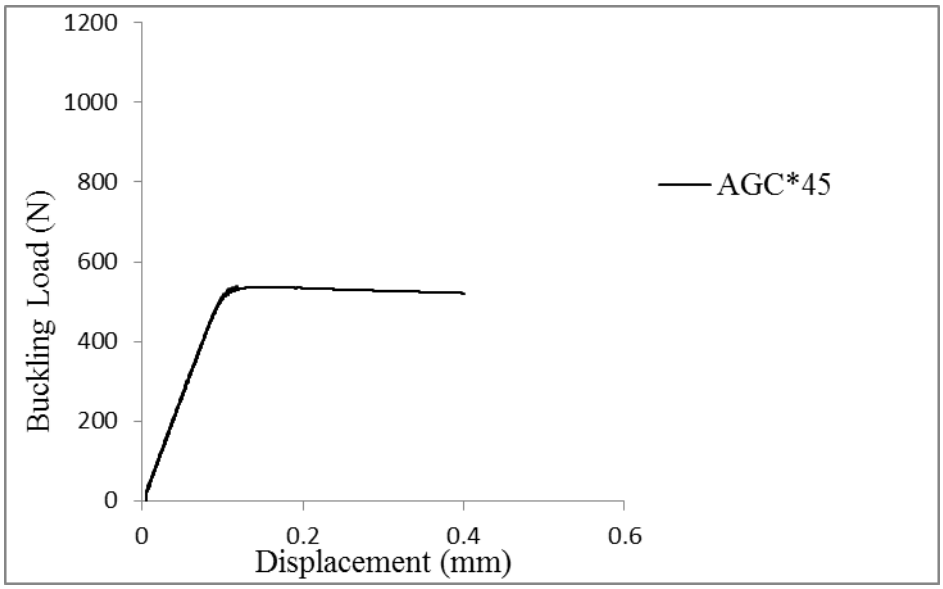

(h)

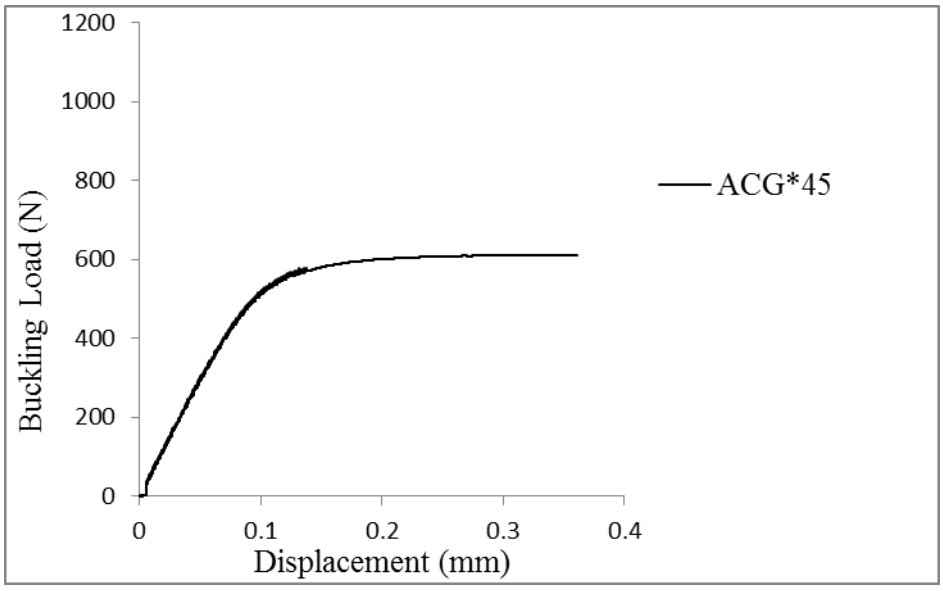

(ı)

Figure 5.9 Buckling load - displacement diagram of a) $(G_{12})^{45}$, b) $(A_{12})^{45}$, c) $(C_{12})^{45}$, d) GCA^{45}, e) GAC^{45}, f) CGA^{45}, g) CAG^{45}, h) AGC^{45}, ı) ACG^{45}

In the Figure 5.10, the buckling load-displacement curves of hybrid specimens GCA^{30}, GCA^{45}, GAC^{30}, GAC^{45}, CGA^{30}, CGA^{45}, CAG^{30}, CAG^{45}, AGC^{30}, AGC^{45}, ACG^{30} and ACG^{45} which have $[(30/-60)_3]_s$ and $[(45/-45)_3]_s$ stacking sequences are given together. The critical buckling load of the samples of CGA^{30} has highest buckling load and samples of AGC^{30} has the smallest buckling load for the $[(30/-60)_3]_s$ stacking sequences. Also CGA^{45} has the highest buckling load and AGC^{45} has minimum buckling loads for the $[(45/-45)_3]_s$ stacking sequences.

In the configurations having $[(30/-60)_3]_s$ stacking sequences, buckling load of CGA^{30} is nearly 36 % higher than buckling load of AGC^{30}. In the configurations having $[(45/-45)_3]_s$ stacking sequences, buckling load of CGA^{45} is nearly 43 % higher than buckling load of AGC^{45}.

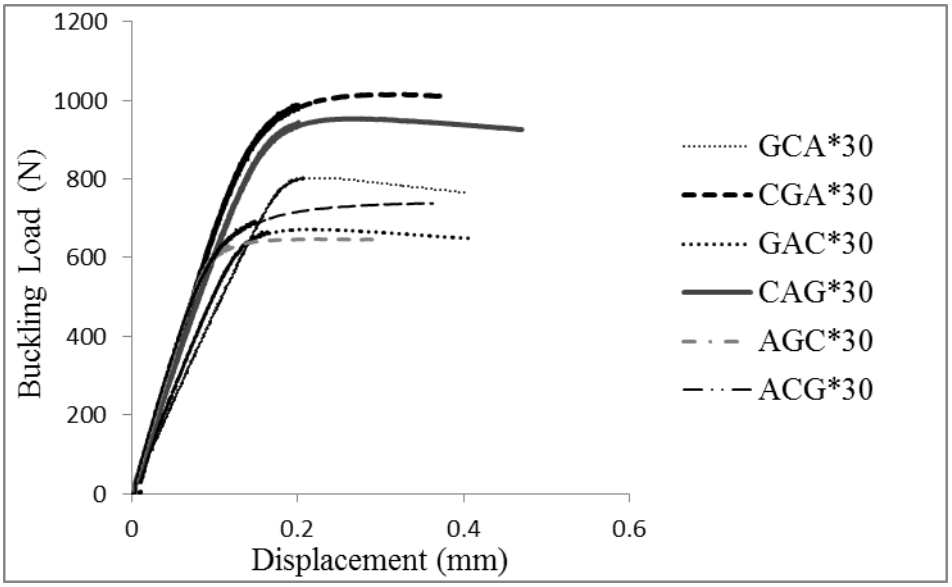

(a)

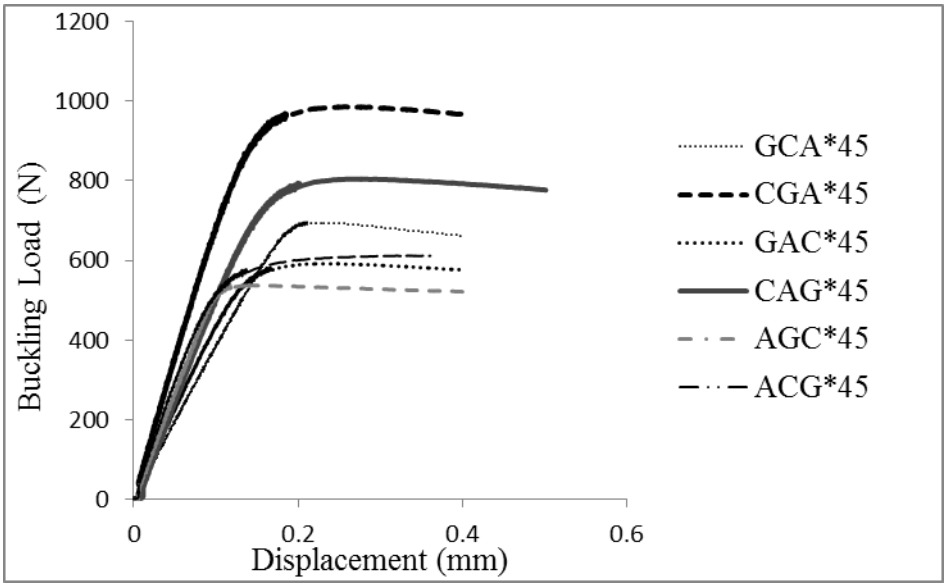

(b)

Figure 5.10 Comparison of buckling load- displacement curves of 6 different hybrid configurations having a) $[(30/-60)_3]_s$, b) $[(45/-45)_3]_s$ stacking sequences

Experiment results of 3 different specimens of each hybrid composite configurations having $[(30/-60)_3]_s$ and $[(45/-45)_3]_s$ stacking sequences are given in Figure 5.11 and Table 5.2 which shown that the results are in close agreement with each other.

Ordering to highest buckling load to smallest buckling load of hybrid samples (Table 5.2) having $[(30/-60)_3]_s$ stacking sequences is CGA^{30}, CAG^{30}, GCA^{30}, ACG^{30}, GAC^{30} and AGC^{30}, respectively. Also, ordering to the highest buckling load to the smallest buckling load of hybrid samples (Table 5.2) having $[(45/-45)_3]_s$ stacking sequences is CGA^{45}, CAG^{45}, GCA^{45}, ACG^{45}, GAC^{45} and AGC^{45}, respectively.

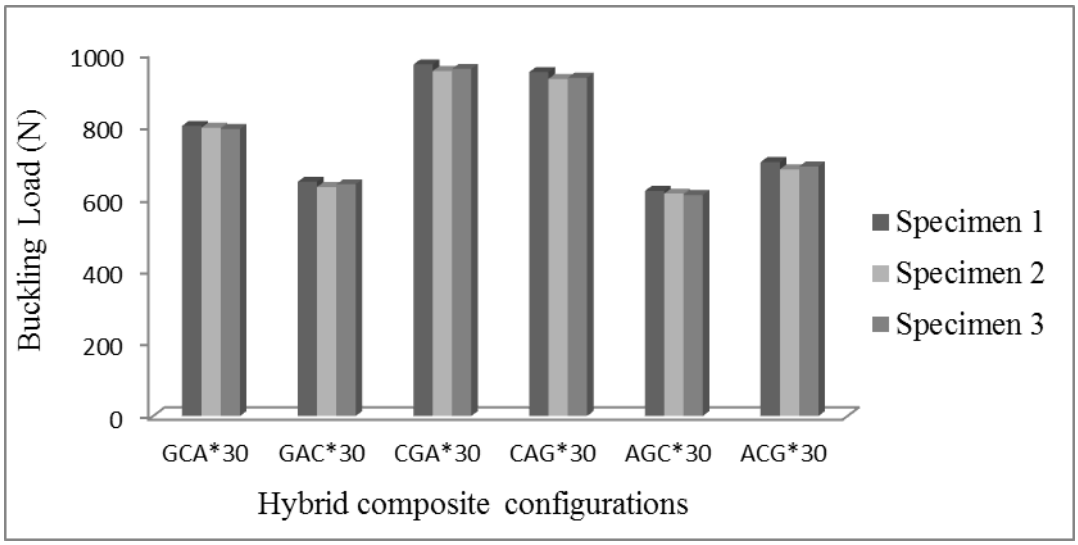

(a)

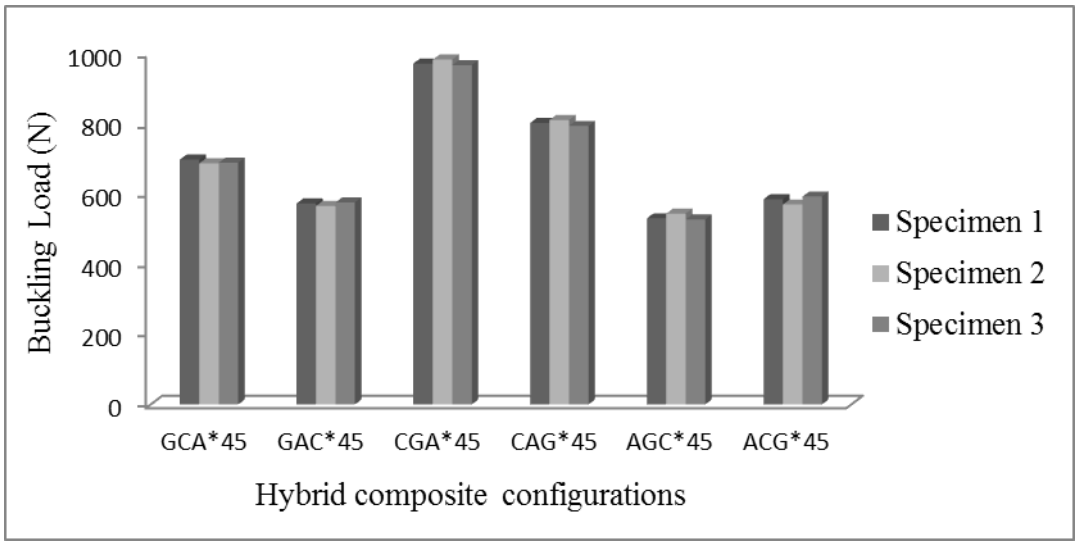

(b)

Figure 5.11 Comparison of buckling load- displacement curves of 6 different hybrid configurations having a) $[(30/-60)_3]_s$, b) $[(45/-45)_3]_s$ stacking sequences with 3 different specimens

Table 5.2 Critical buckling loads of Composite and hybrid composite specimens having $[(30/-60)_3]_s$ and $[(45/-45)_3]_s$ stacking sequences

	Buckling Load (N)		
Hybrid composite configurations	**Specimen 1**	**Specimen 2**	**Specimen 3**
$(G_{12})^{30}$	356.054	355.485	351.895
$(A_{12})^{30}$	1082.787	1067.062	1057.619
$(C_{12})^{30}$	1013.933	1005.282	1011.026
GCA^{30}	799.373	794.469	790.791
GAC^{30}	645.606	631.259	638.433
CGA^{30}	968.863	950.545	956.651
CAG^{30}	947.872	928.914	932.074
AGC^{30}	620.370	612.850	609.091
ACG^{30}	699.685	679.879	687.831
$(G_{12})^{45}$	318.688	312.643	321.304
$(A_{12})^{45}$	906.984	932.177	899.425
$(C_{12})^{45}$	867.911	860.505	865.423
GCA^{45}	697.240	686.418	688.201
GAC^{45}	572.293	565.139	575.154
CGA^{45}	970.514	981.800	966.100
CAG^{45}	801.203	809.727	792.680
AGC^{45}	529.875	543.375	526.500
ACG^{45}	584.424	569.342	591.965

5.4 Buckling Experiment Results of Composites Hybrid Composites having Un-symmetrical $[(0/90)_6]_{us}$ Stacking Sequence

Hybrid composites which have un-symmetrical $[(0/90)_6]_{us}$ stacking sequence are also examined to see effect of the un-symmetrical configurations on the buckling loads. In the Figure 5.12, buckling load - displacement diagrams of un-symmetrically produced hybrid composites (GCA*, GAC*, CGA*, CAG*, AGC* and ACG*) are given.

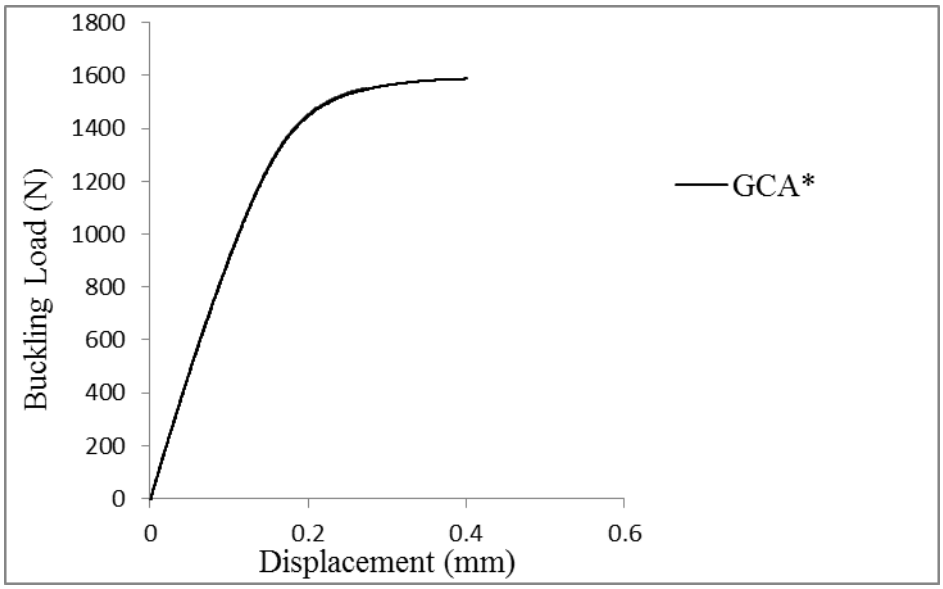
1800
1600
1400
1200
1000
800
600
400
200
0
Buckling Load (N)
0
0.2
0.4
0.6
Displacement (mm)
GCA*

(a)

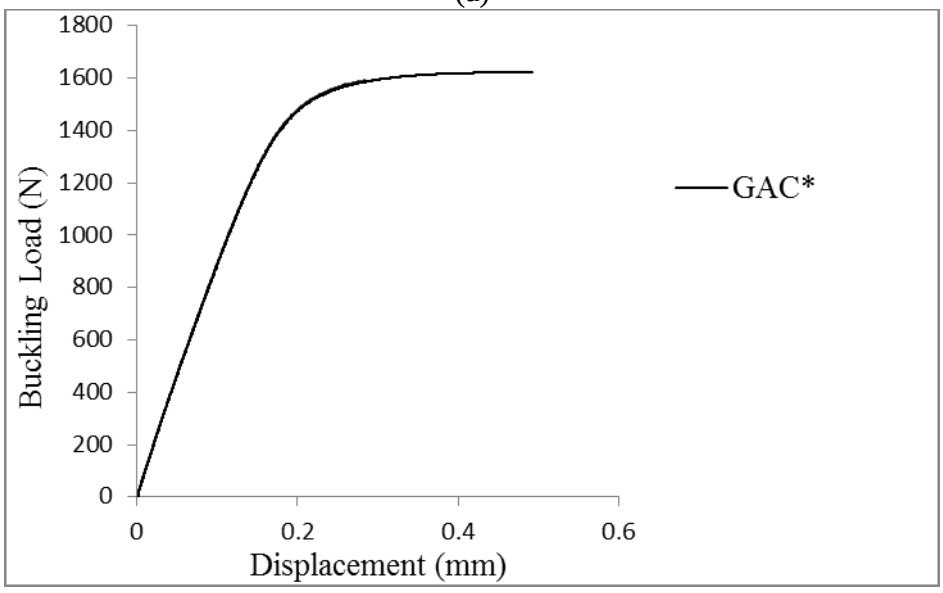
1800
1600
1400
1200
1000
800
600
400
200
0
Buckling Load (N)
0
0.2
0.4
0.6
Displacement (mm)
GAC*

(b)

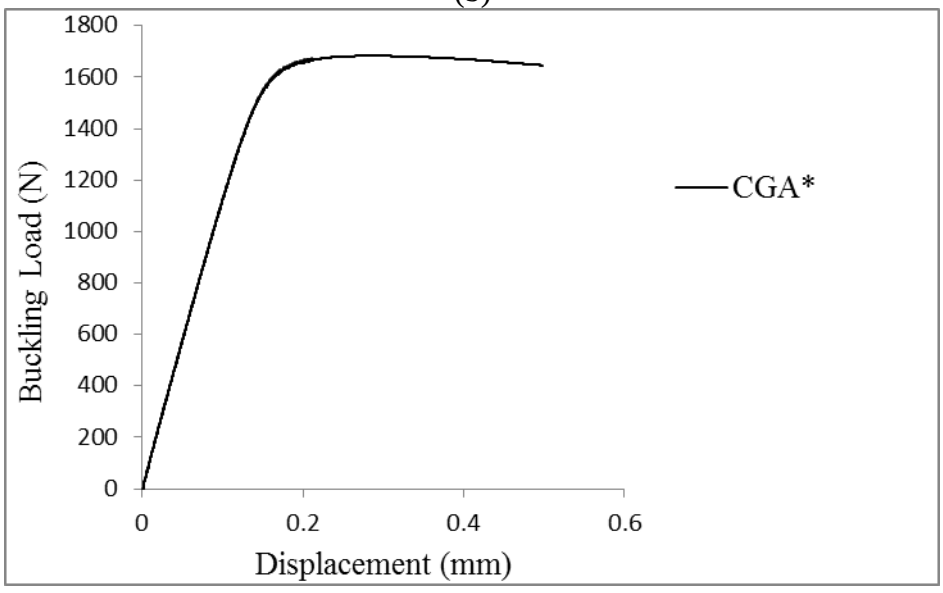
1800
1600
1400
1200
1000
800
600
400
200
0
Buckling Load (N)
0
0.2
0.4
0.6
Displacement (mm)
CGA*

(c)

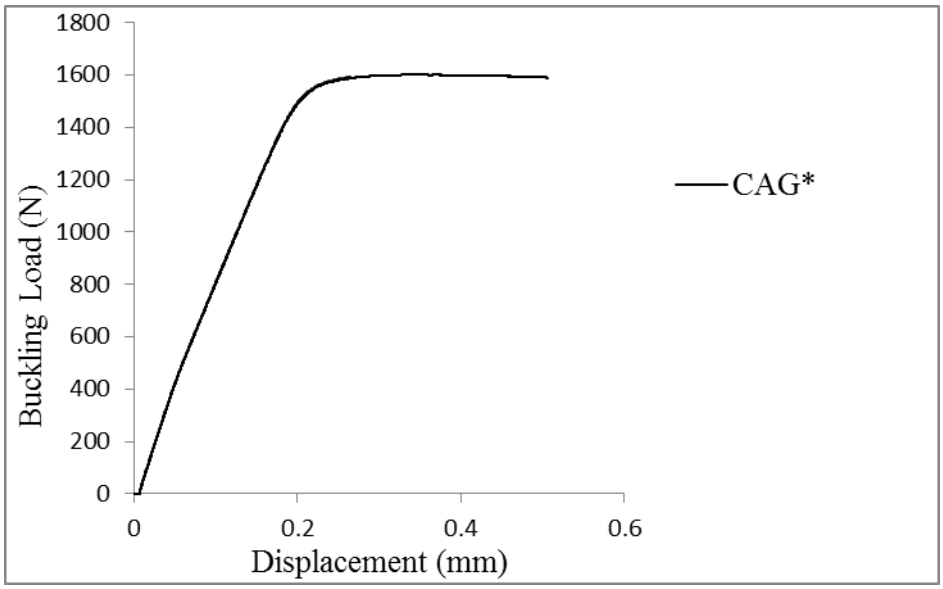
1800
1600
1400
1200
1000
800
600
400
200
0
Buckling Load (N)
0
0.2
0.4
0.6
Displacement (mm)
CAG*

(d)

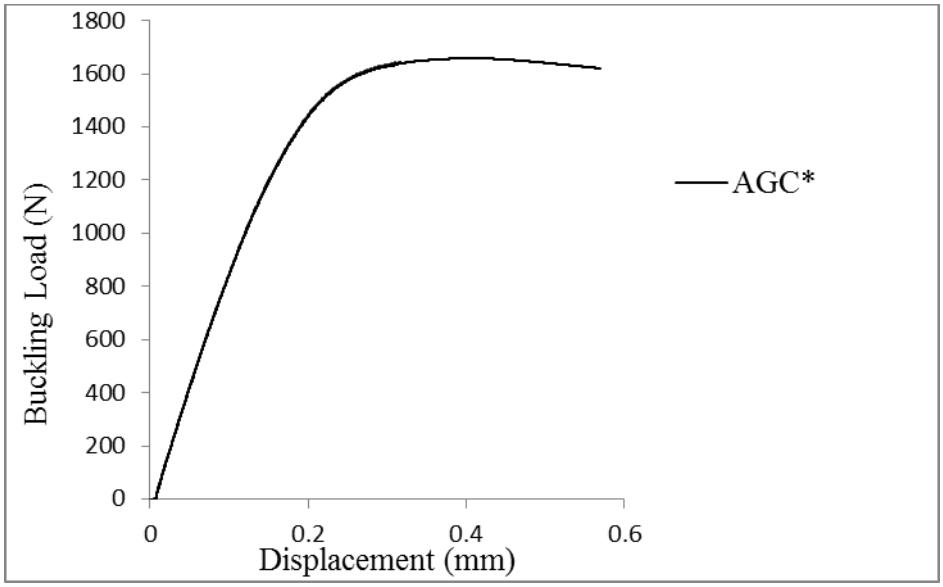
1800
1600
1400
1200
1000
800
600
400
200
0
Buckling Load (N)
0
0.2
0.4
0.6
Displacement (mm)
AGC*

(e)

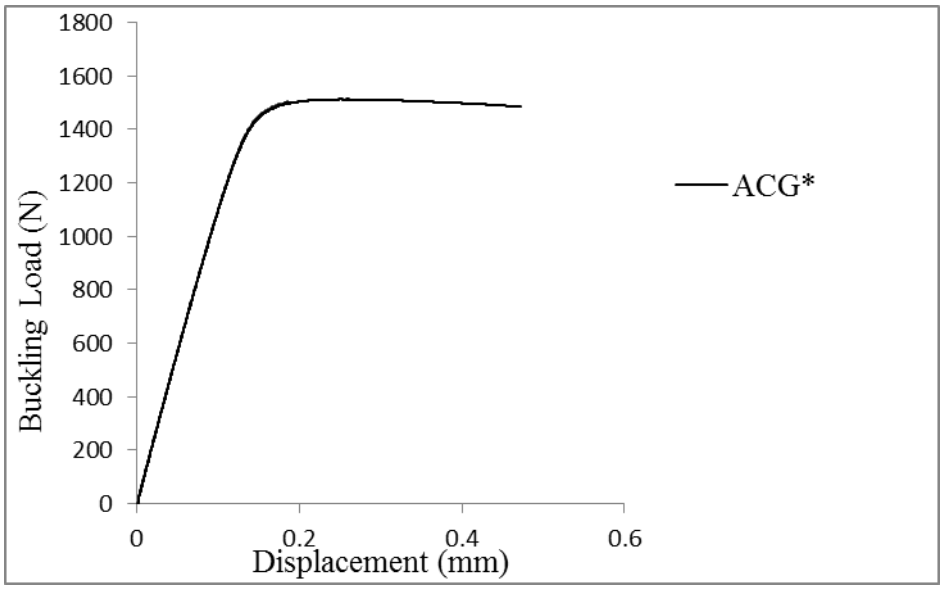

(f)

Figure 5.12 Buckling load - displacement diagram of a) GCA*, b) GAC*, c) CGA*, d) CAG*, e) AGC*, f) ACG*

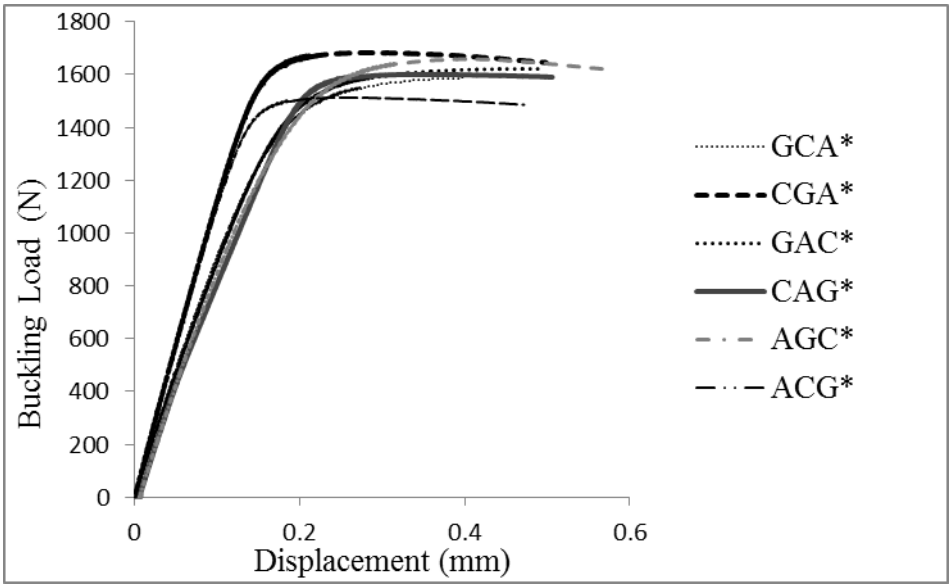

Figure 5.13 Comparison of buckling load- displacement curves of 6 different un-symmetrical hybrid composite configurations having $[(0/90)_6]_{us}$ stacking sequences

Experiment results of 3 different specimens which have un-symmetrical hybrid configurations are given in the Figure 5.14 and 5.14, and Table 5.3. It is shown (from Figures 5.13-5.14 and Table 5.3) that there is not huge difference between the buckling loads of these configurations. However, it can be ordered from the highest buckling load to the smallest buckling load as CGA*, AGC*, CAG*, GAC*, GCA*, ACG*, respectively.

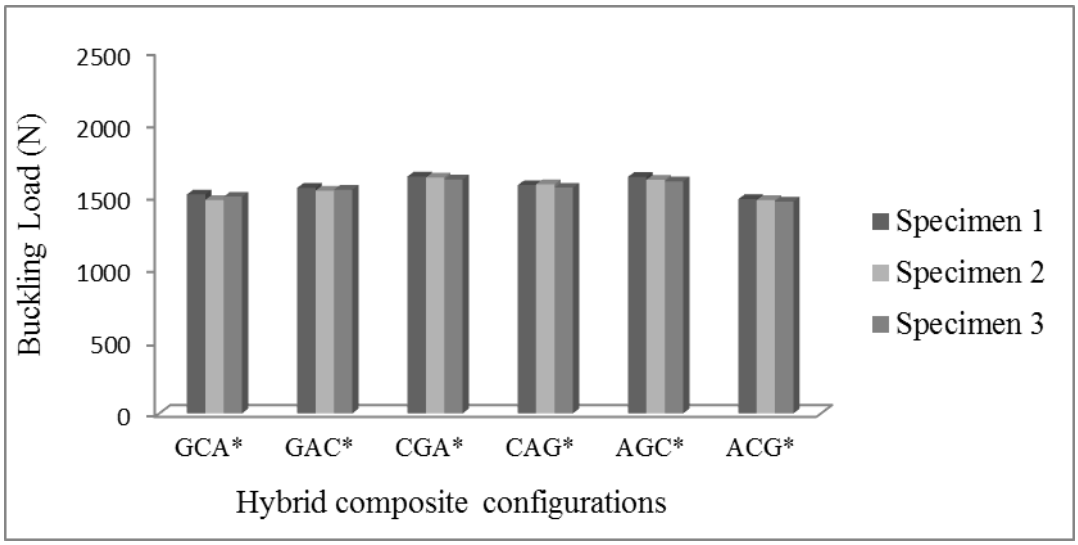

Figure 5.14 Comparison of buckling load- displacement curves of un-symmetrical hybrid composites with 3 different specimens

Table 5.3 Comparison of buckling load- displacement curves of un-symmetrical hybrid composites with 3 different specimens

	Buckling Load (N)		
Hybrid composite configurations	**Specimen 1**	**Specimen 2**	**Specimen 3**
GCA*	1512.836	1474.761	1497.210
GAC*	1558.235	1538.938	1545.470
CGA*	1636.209	1630.081	1615.574
CAG*	1577.076	1582.855	1559.210
AGC*	1634.322	1613.369	1602.892
ACG*	1479.927	1473.983	1463.630

5.5 Discussion on the Results of Buckling Experiments

Results of buckling experiments which were conducted to see effects of different hybrid configurations on buckling can be seen in the Figure 5.15 and 5.16. In the Figure 5.15 comparison of critical buckling loads of hybrid composites having symmetrical $[(0/90)_3]_s$, $[(30/-60)_3]_s$, $[(45/-45)_3]_s$ and un-symmetrical $[(0/90)_6]_{us}$ stacking sequences are given. It was concluded that for $[(0/90)_3]_s$ symmetrical hybrid configuration CAG, for $[(30/-60)_3]_s$ symmetrical hybrid configuration CGA^{30}, for $[(45/-45)_3]_s$ symmetrical hybrid configuration CGA^{45} and for un-symmetrical $[(0/90)_3]_s$ hybrid configuration CGA* has the highest buckling loads.

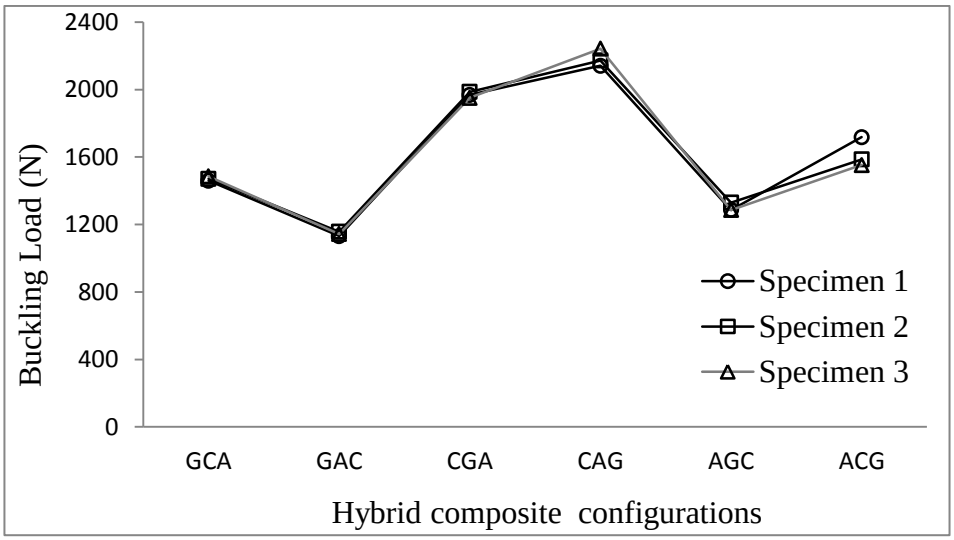
2400
2000
1600
1200
800
400
0
Buckling Load (N)
Specimen 1
Specimen 2
Specimen 3
GCA
GAC
CGA
CAG
AGC
ACG
Hybrid composite configurations

(a)

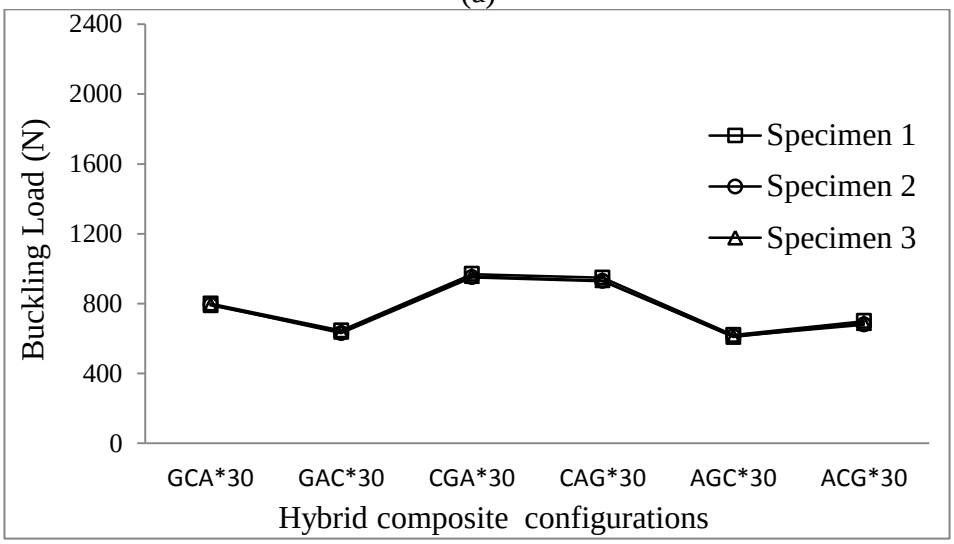
2400
2000
1600
1200
800
400
0
Buckling Load (N)
Specimen 1
Specimen 2
Specimen 3
GCA*30
GAC*30
CGA*30
CAG*30
AGC*30
ACG*30
Hybrid composite configurations

(b)

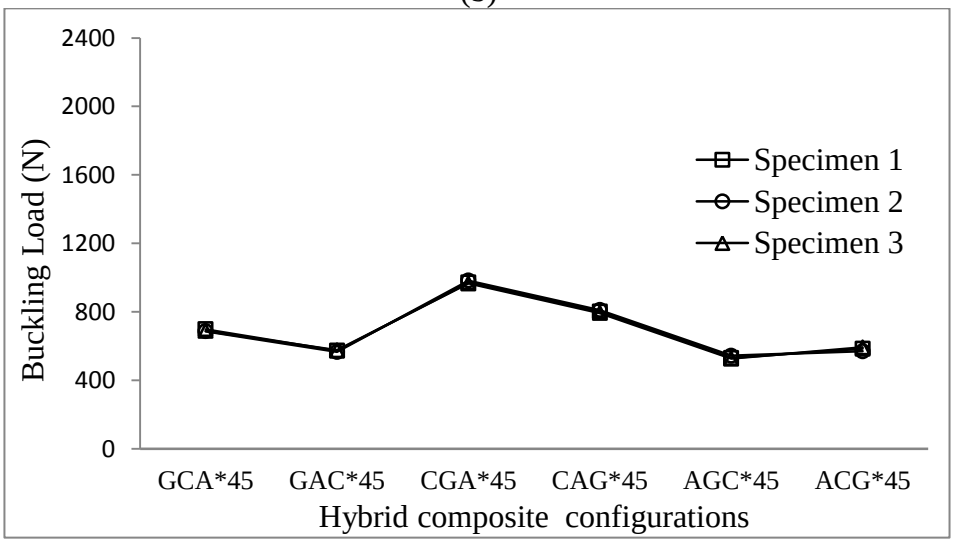
2400
2000
1600
1200
800
400
0
Buckling Load (N)
Specimen 1
Specimen 2
Specimen 3
GCA*45
GAC*45
CGA*45
CAG*45
AGC*45
ACG*45
Hybrid composite configurations

(c)

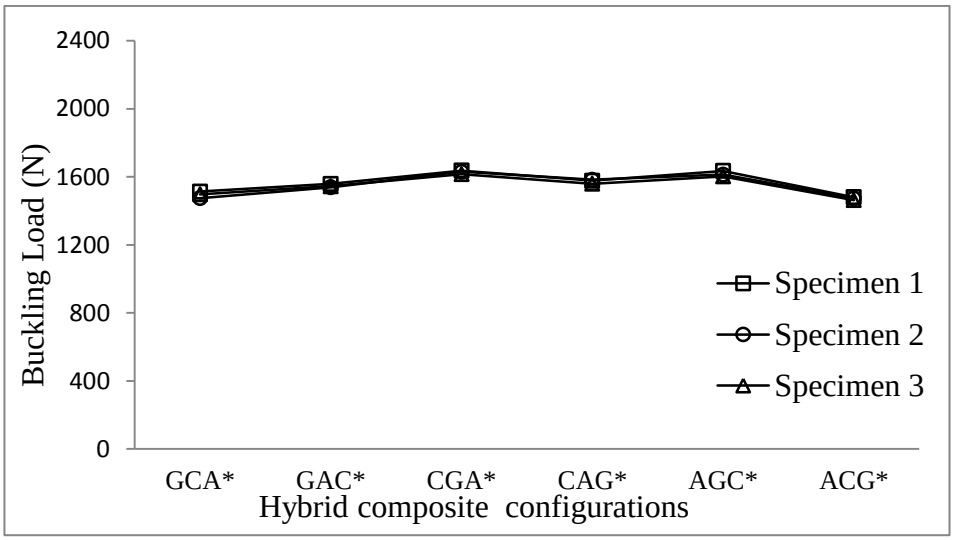

(d)

Figure 5.15 Comparison of critical buckling loads of hybrid composites having a) $[(0/90)_3]_s$ symmetrical , b) $[(30/-60)_3]_s$ symmetrical , $_c$) $[(45/-45)_3]_s$ symmetrical , d) $[(0/90)_6]_{us}$ un-symmetrical stacking sequences

It is seen that for $[(0/90)_3]_s$ symmetrical hybrid configuration GAC, for $[(30/-60)_3]_s$ symmetrical hybrid configuration GAC ^{30}, for $[(45/-45)_3]_s$ symmetrical hybrid configuration GAC ^{45} and for un-symmetrical $[(0/90)_6]_{us}$ hybrid configuration GAC* has the smallest buckling loads. So in the Figure 5.16, comparisons of critical buckling loads of these configurations (the best and the worst configurations) are considered.

As can be seen in Figure 5.16, CAG (having $[(0/90)_3]_s$ ply orientation) has the highest and CGA^{45} (close to CGA^{30}) has the lowest buckling load and CGA* has higher buckling load from CGA^{45} and CGA^{30}, and has smaller buckling load from CAG. In other words, CAG is the most designable with respect to buckling characteristic. Buckling load of CAG is nearly 55 % higher than CGA^{30} and CGA^{45}. It is also nearly 24 % higher than CGA*. Results also show that buckling characteristics are significantly effected by the replacement of fiber types and buckling loads are increased using fibers which have higher stiffness in the upper layers as being in the CAG. Moreover, it is concluded that hybrid plates which produced having $[(0/90)_3]_s$ stacking sequences have higher buckling strength.

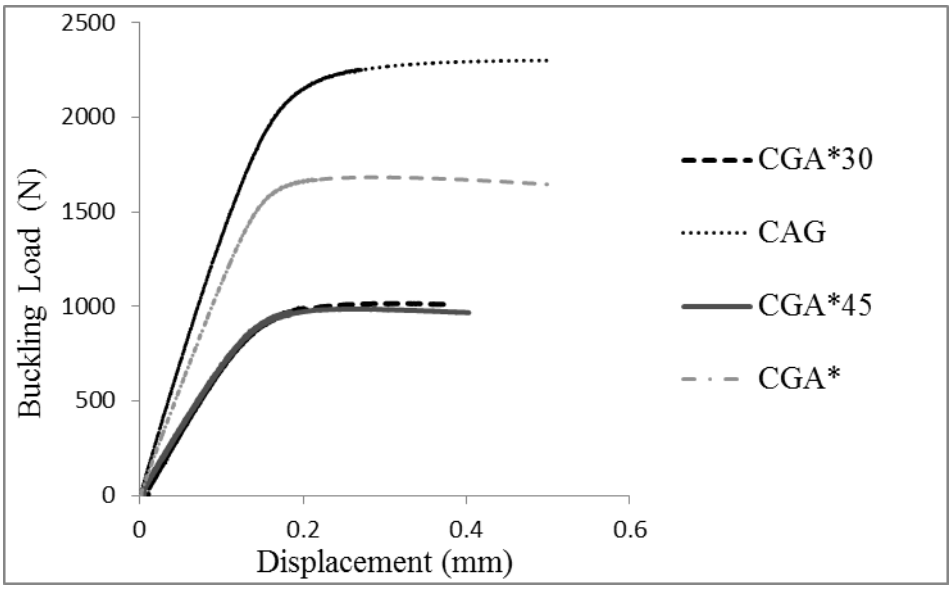

(a)

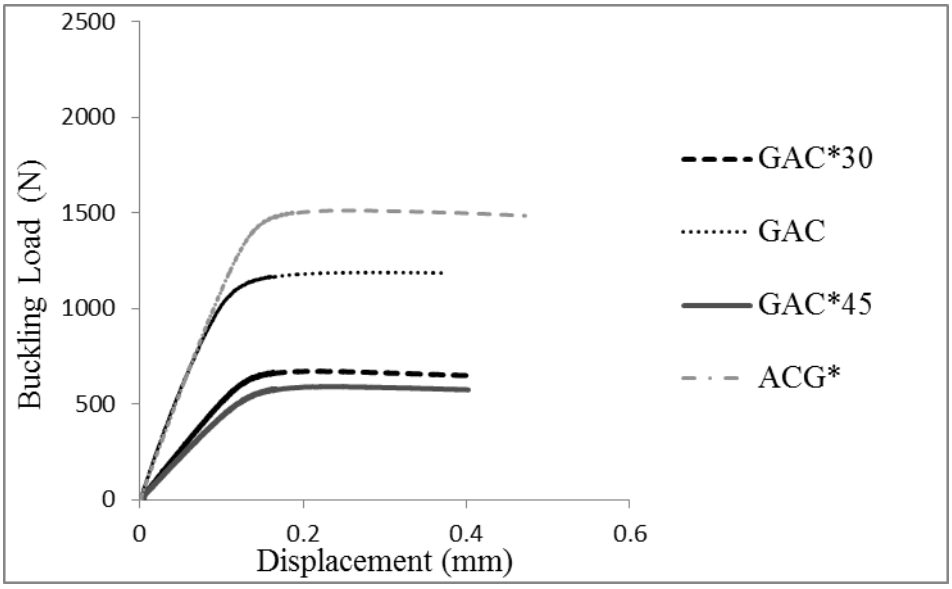

(b)

Figure 5.16 Comparison of critical buckling loads of a) the best configurations, b) the worst configurations

CHAPTER 6

EXPERIMENTAL STUDIES PART 3: LATERAL BUCKLING EXPERIMENTS

6.1. Introduction

In this chapter, lateral buckling experiments and their results are given. The specimens used in the experiments are prepared using composite and hybrid composite materials whose configurations G_{12}, A_{12}, C_{12}, GCA, GAC, CGA, CAG, AGC, ACG, $(G_{12})^{30}$,$(G_{12})^{45}$, $(A_{12})^{30}$, $(A_{12})^{45}$, $(C_{12})^{30}$,$(C_{12})^{45}$, GCA^{30} ,GCA^{45}, GAC^{30} , GAC^{45}, CGA^{30} ,CGA^{45}, CAG^{30}, CAG^{45}, AGC^{30} AGC^{45}, ACG^{30}, ACG^{45}, GCA^{*}, GAC^{*}, CGA^{*}, CAG^{*}, AGC^{*} and ACG^{*} and properties have been given in the previous chapter.

6.2 Lateral Buckling Experiment Results of Composites and Hybrid Composites Having $[(0/90)_3]_s$ Stacking Sequence

In the lateral buckling experiments, the specimens are loaded laterally from the free end with the 1 mm/min speed and the other end is fixed to provide a behavior like a cantilever beam. This test procedure is continued for all specimens and lateral buckling loads are determined.

The used specimen dimensions are taken as width (W) 20 mm, overall length (LO) 200 mm and gage length (G) 155 mm which equal to the dimensions of buckling specimens. Also the thicknesses of the composites and hybrid composites are the same as the dimensions of ones used in the buckling experiments (2.20 mm, 3.30 mm and 2.60 for G_{12}, A_{12} and $C_{12,}$ respectively and 2.70 ±0.2 mm for hybrid configurations).

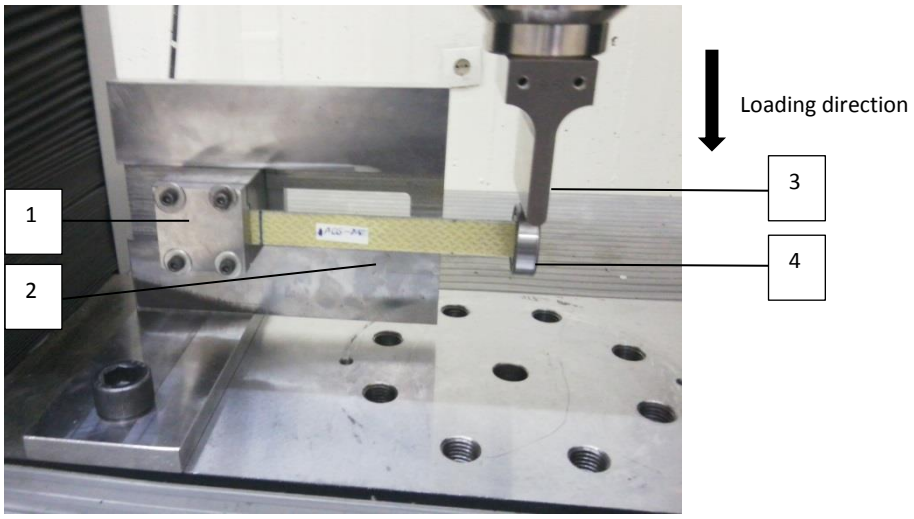

Figure 6.1 Lateral buckling test setup 1) Test fixture, 2) Specimen, 3) Loading unit, 4) Bearing

Lateral buckling test setup is given in the Figure 6.1. Friction is an important and opposite effect which cause increase of buckling load. So a bearing is placed to free end of the beam to minimize friction effect. Load-displacement diagrams of composite and hybrid composites specimens having $[(0/90)_3]_s$ stacking sequences are given in the Figure 6.2.

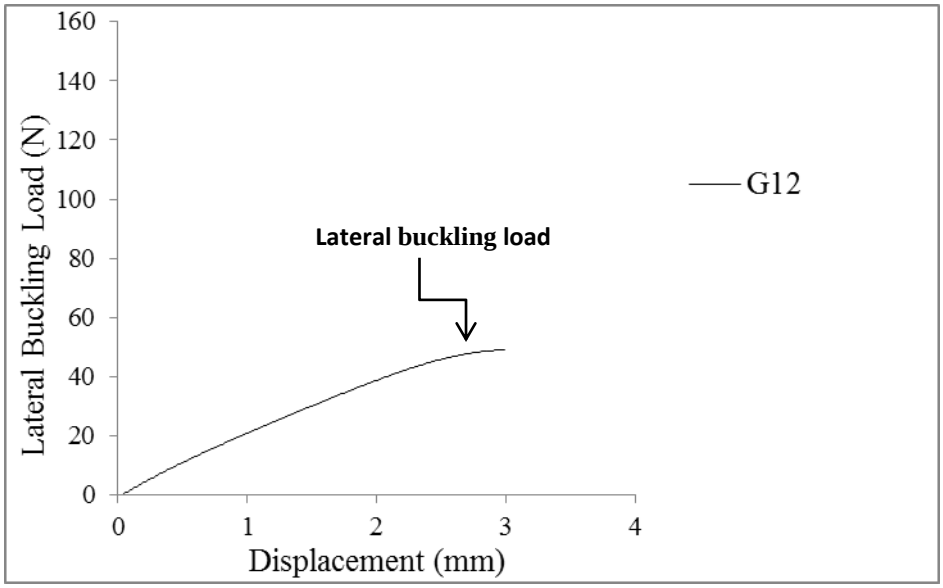

(a)

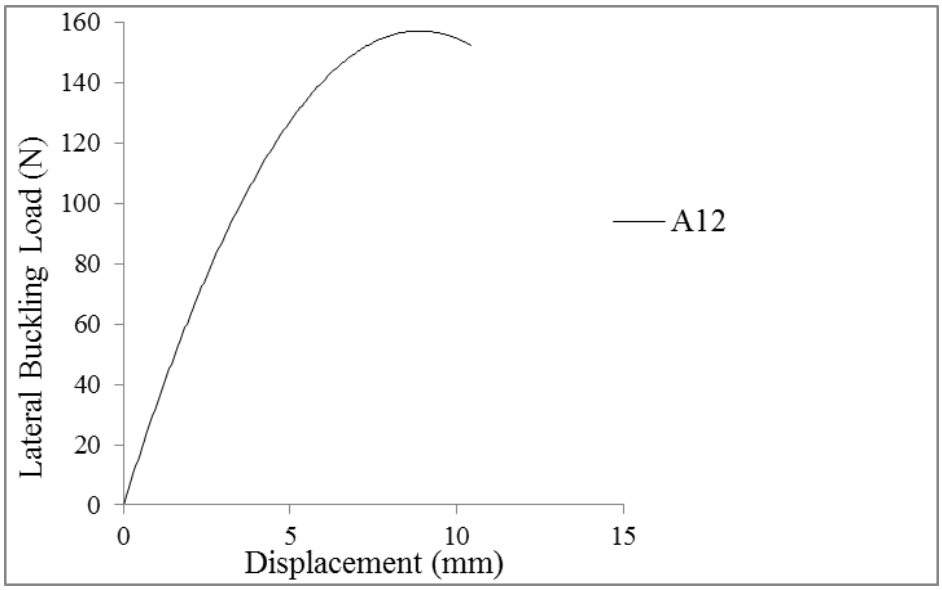
Lateral Buckling Load (N)
160
140
120
100
80
60
40
20
0
0
5
10
15
Displacement (mm)
A12

(b)

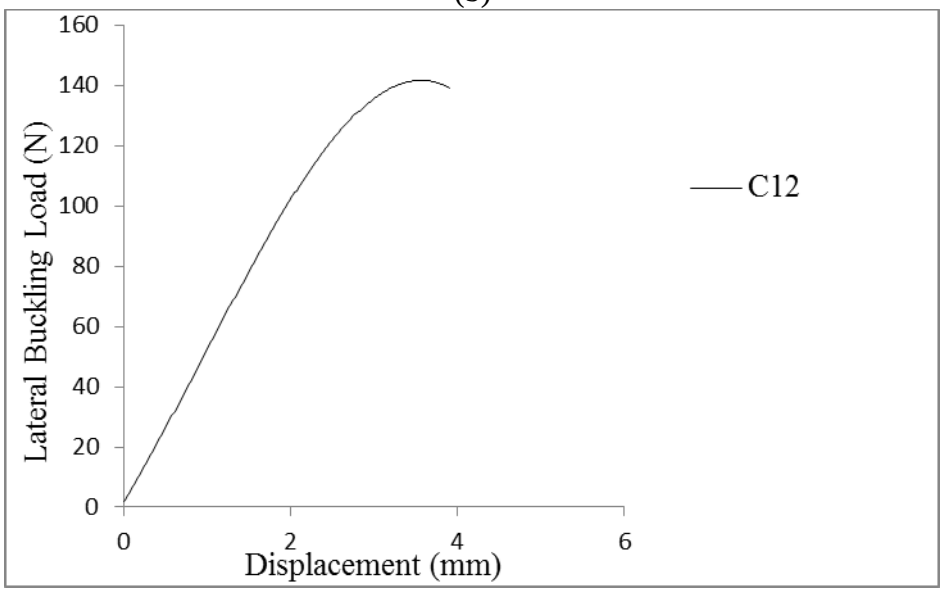
Lateral Buckling Load (N)
160
140
120
100
80
60
40
20
0
0
2
4
6
Displacement (mm)
C12

(c)

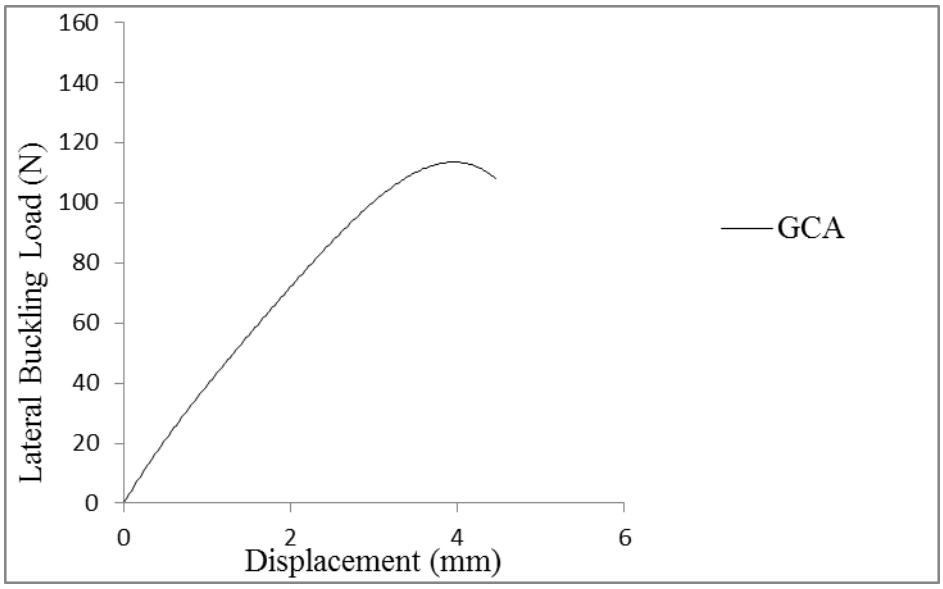
Lateral Buckling Load (N)
160
140
120
100
80
60
40
20
0
0
2
4
6
Displacement (mm)
GCA

(d)

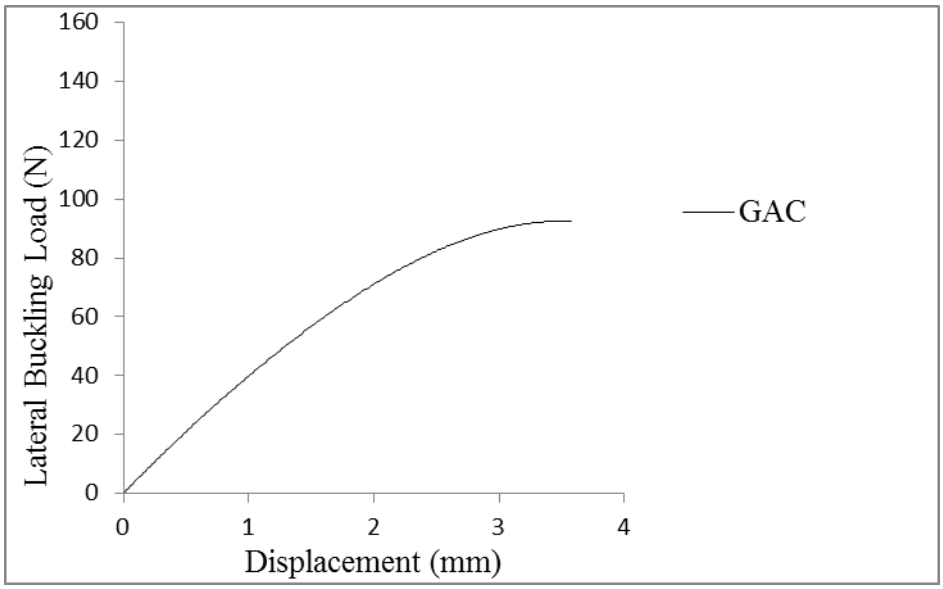
Lateral Buckling Load (N)
160
140
120
100
80
60
40
20
0
0
1
2
3
4
Displacement (mm)
GAC

(e)

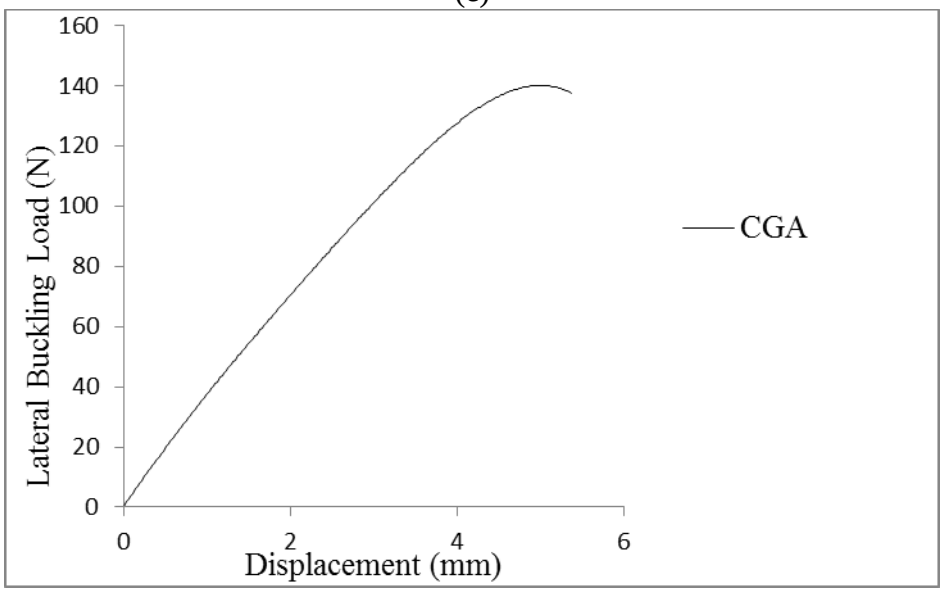
Lateral Buckling Load (N)
160
140
120
100
80
60
40
20
0
0
2
4
6
Displacement (mm)
CGA

(f)

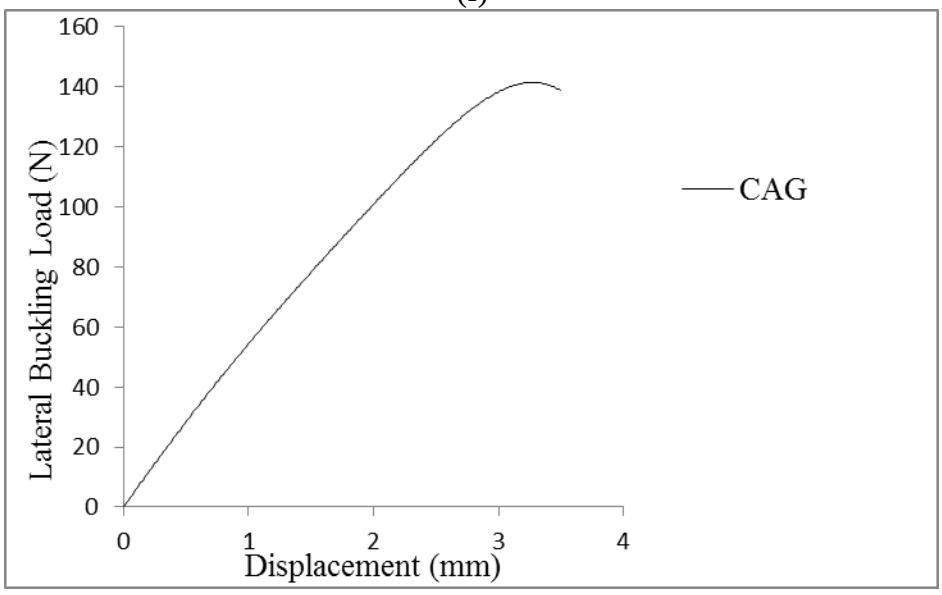
Lateral Buckling Load (N)
160
140
120
100
80
60
40
20
0
0
1
2
3
4
Displacement (mm)
CAG

(g)

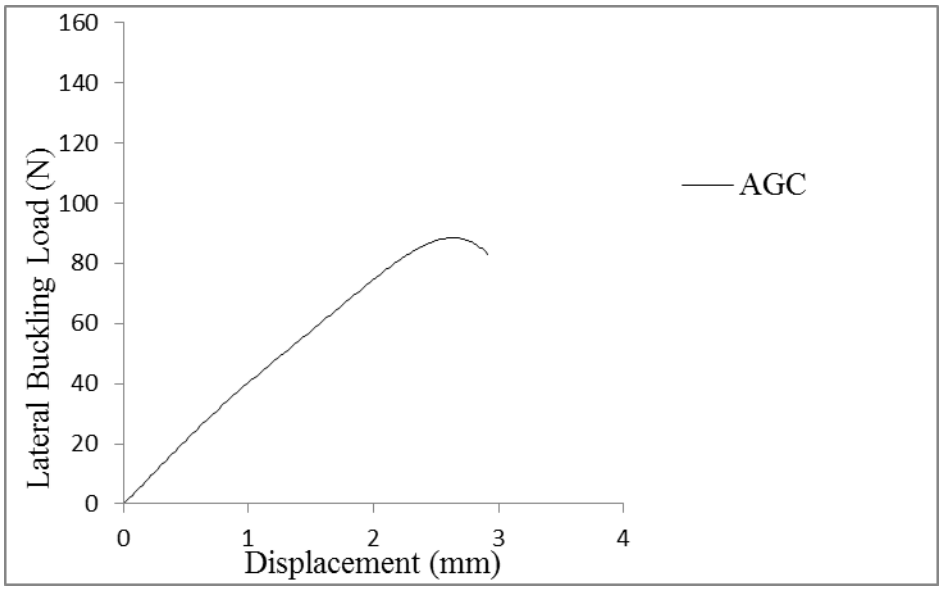

(h)

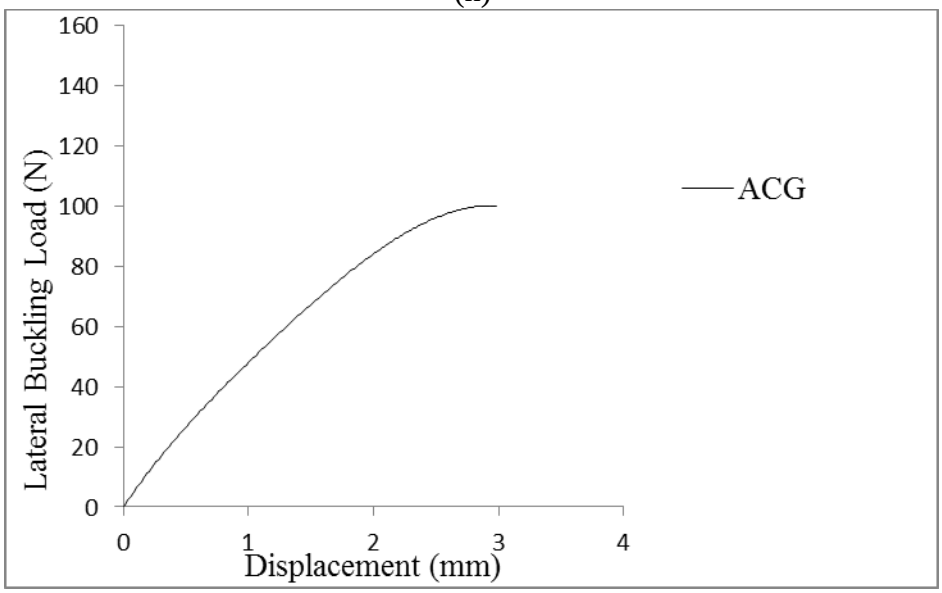

(ı)

Figure 6.2. Lateral buckling load - displacement diagram a) G_{12}, b) A_{12}, c) C_{12}, d) GCA, e) GAC, f) CGA , g) CAG , h) AGC , ı) ACG

Comparison of hybrid composite configurations having $[(0/90)_3]_s$ stacking sequence are given in Figure 6.3. It is seen that CGA has the highest lateral buckling load and AGC has the smallest lateral buckling load. Lateral buckling load of CGA is 34 % higher than AGC.

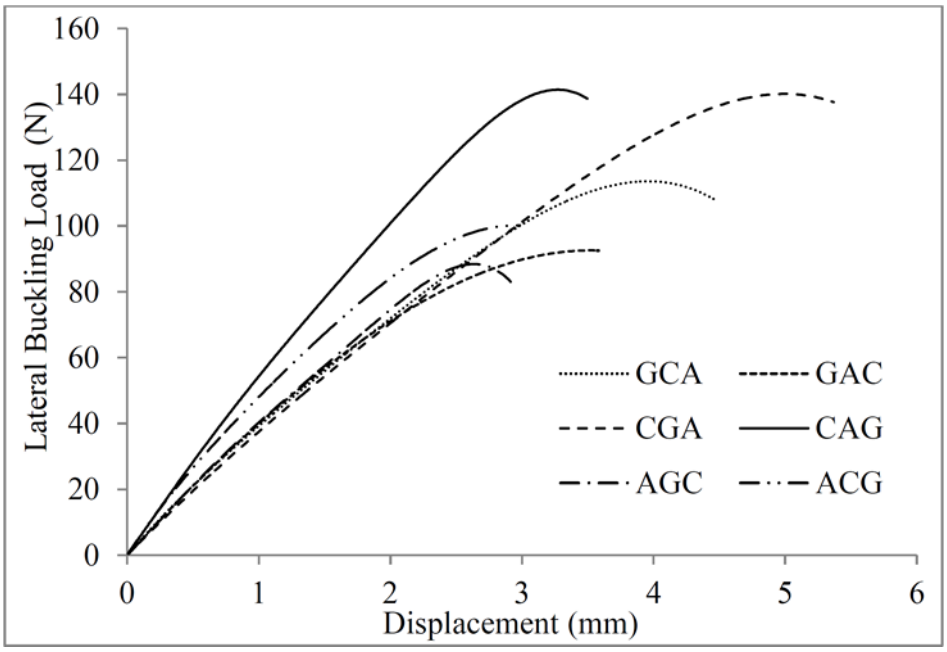

Figure 6.3 Comparison of buckling load- displacement curves of 6 different hybrid configurations

Comparisons of lateral buckling loads of 3 different specimens are given in Figure 6.4 and Table 6.1. As can be seen in the figure and the table, the results are in close agreement with each other. Ordering from the highest lateral buckling load to the smallest lateral buckling load of hybrid samples (Table 6.1) is CGA, CAG, GCA, ACG, GAC and AGC, respectively.

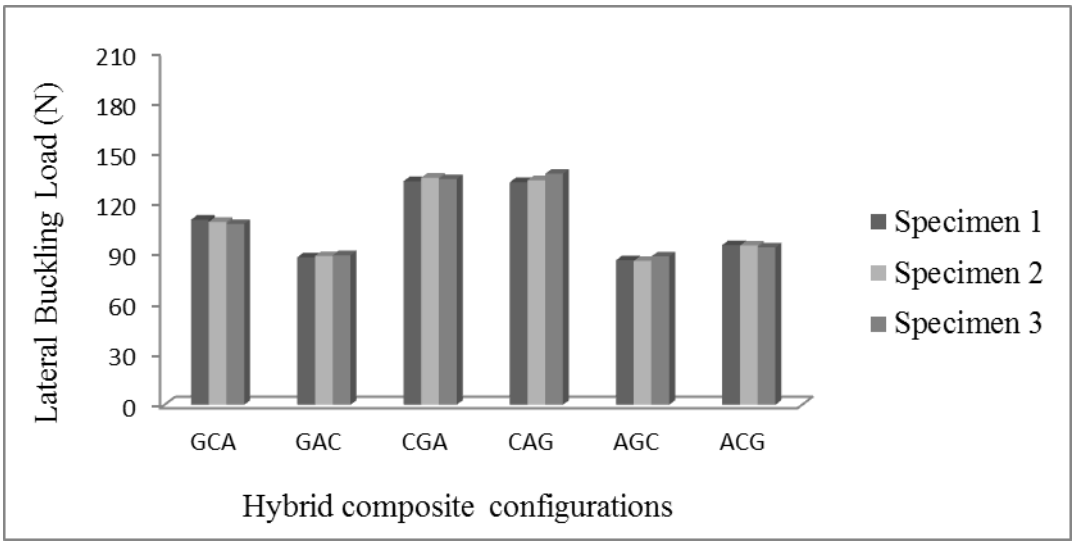

Figure 6.4. Comparison of lateral buckling load- displacement curves of 6 different hybrid configurations with 3 different specimens

Table 6.1 Critical lateral buckling loads of composite and hybrid composites

	Lateral Buckling Load (N)		
Hybrid composite configurations	**Specimen 1**	**Specimen 2**	**Specimen 3**
G_{12}	46.688	46.878	46.146
A_{12}	147.693	145.179	146.719
C_{12}	136.803	138.590	138.079
GCA	110.327	108.993	107.762
GAC	87.921	88.626	89.120
CGA	133.247	135.363	134.505
CAG	132.636	133.788	137.668
AGC	86.178	85.753	88.388
ACG	95.186	94.896	93.765

6.3 Lateral Buckling Experiment Results of Composites and Hybrid Composites having $[(30/-60)_3]_s$ and $[(45/-45)_3]_s$ Stacking Sequences

Lateral buckling experiments have also been conducted for the composite and hybrid composite having $[(30/-60)_3]_s$ and $[(45/-45)_3]_s$ stacking sequences. So in this part, lateral buckling experiment results are given for these ply orientations.

In Figure 6.5, the lateral buckling load-displacement diagrams of composite and hybrid composite specimens $(G_{12})^{30}$, $(A_{12})^{30}$, $(C_{12})^{30}$, GCA^{30} , GAC^{30} , CGA^{30} , CAG^{30}, AGC^{30} and ACG^{30} which have $[(30/-60)_3]_s$ stacking sequences are given.

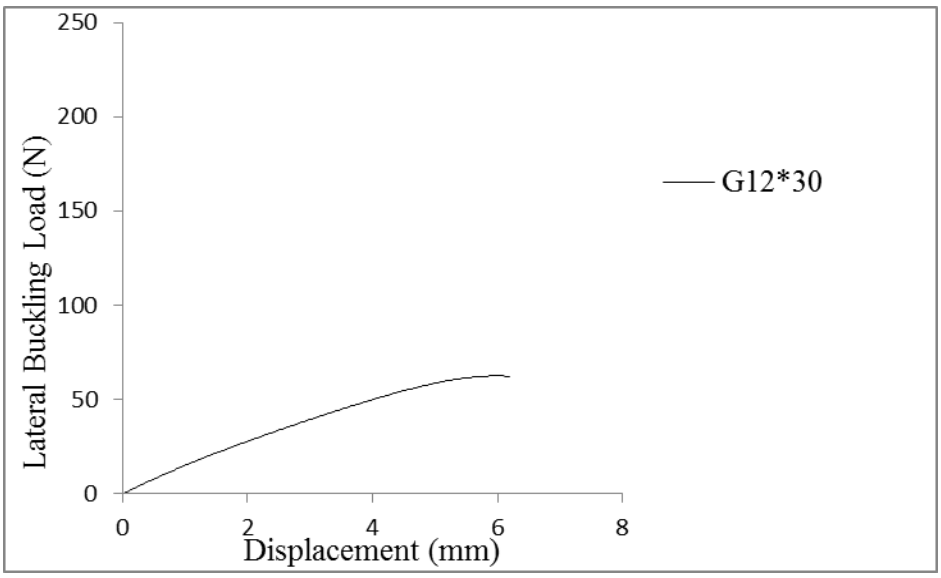

(a)

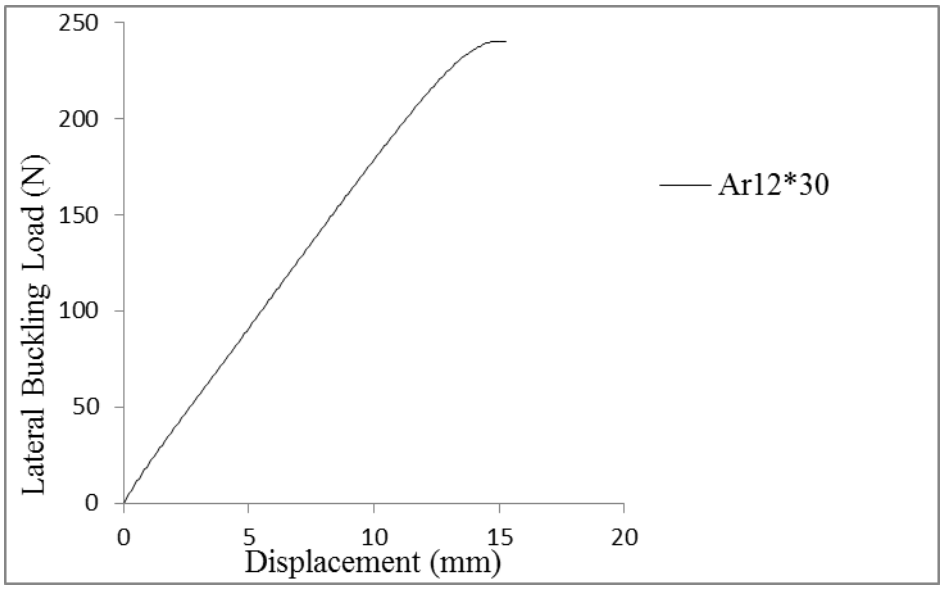
Lateral Buckling Load (N)
250
200
150
100
50
0
0
5
10
15
20
Displacement (mm)
Ar12*30

(b)

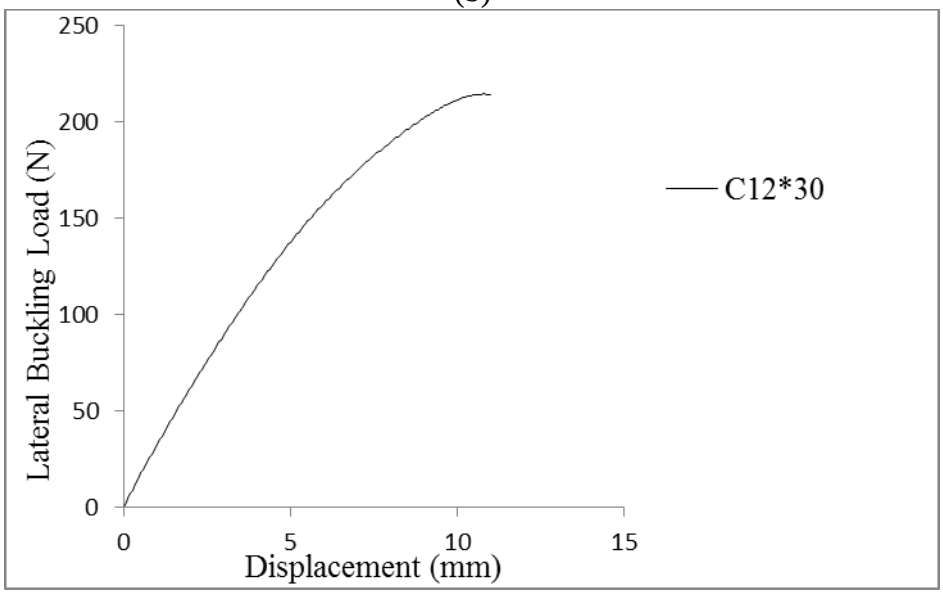
Lateral Buckling Load (N)
250
200
150
100
50
0
0
5
10
15
Displacement (mm)
C12*30

(c)

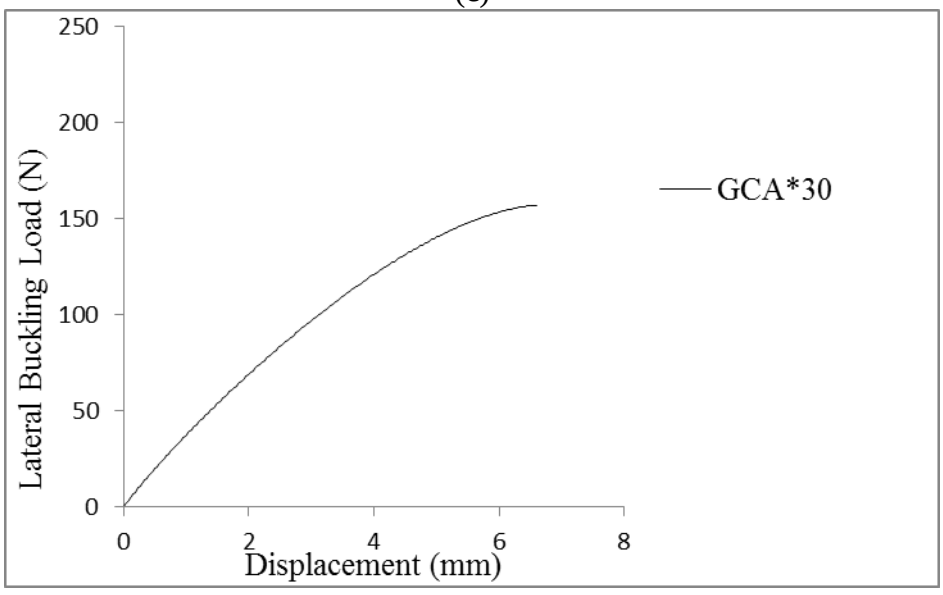
Lateral Buckling Load (N)
250
200
150
100
50
0
0
2
4
6
8
Displacement (mm)
GCA*30

(d)

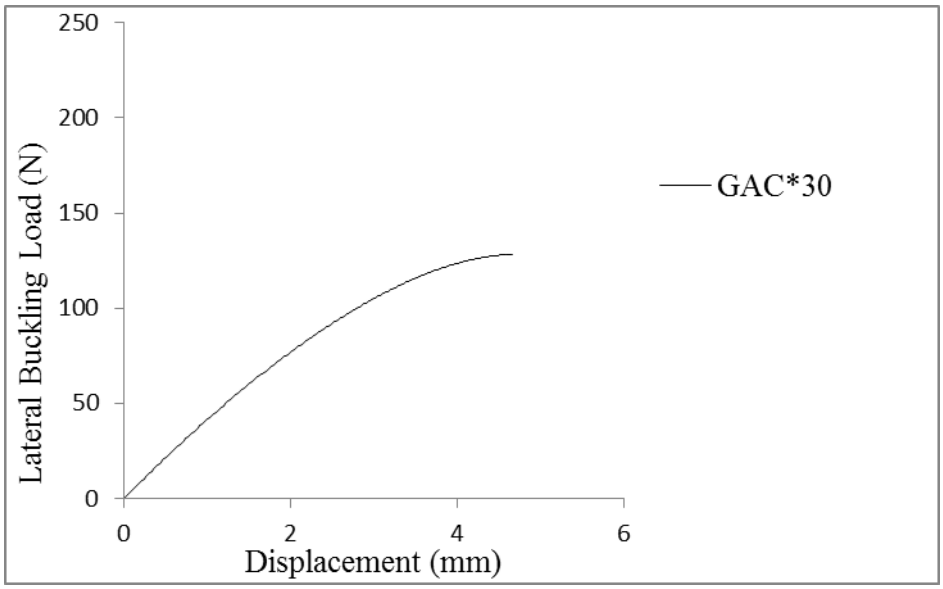
250
200
150
100
50
0
Lateral Buckling Load (N)
0
2
4
6
Displacement (mm)
GAC*30

(e)

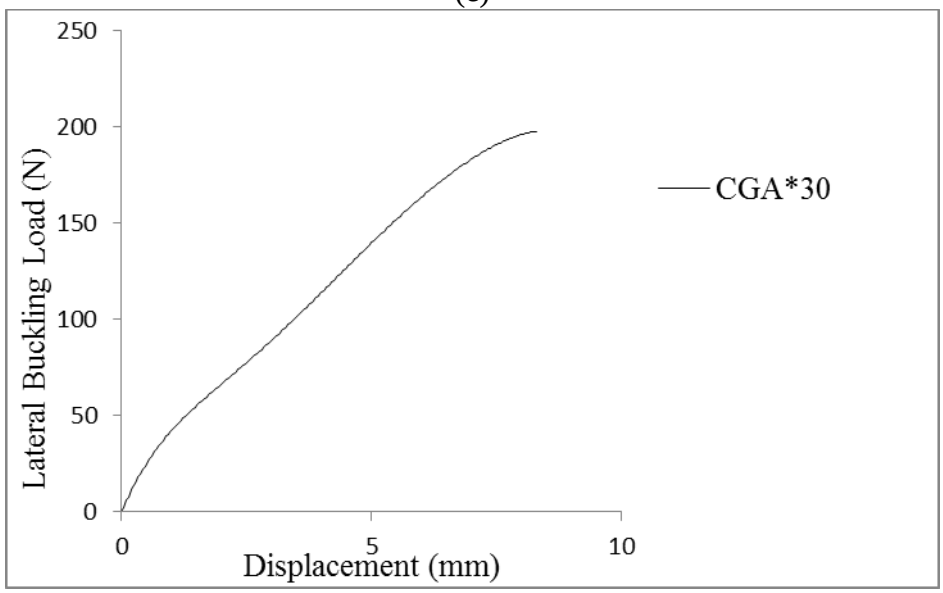
250
200
150
100
50
0
Lateral Buckling Load (N)
0
5
10
Displacement (mm)
CGA*30

(f)

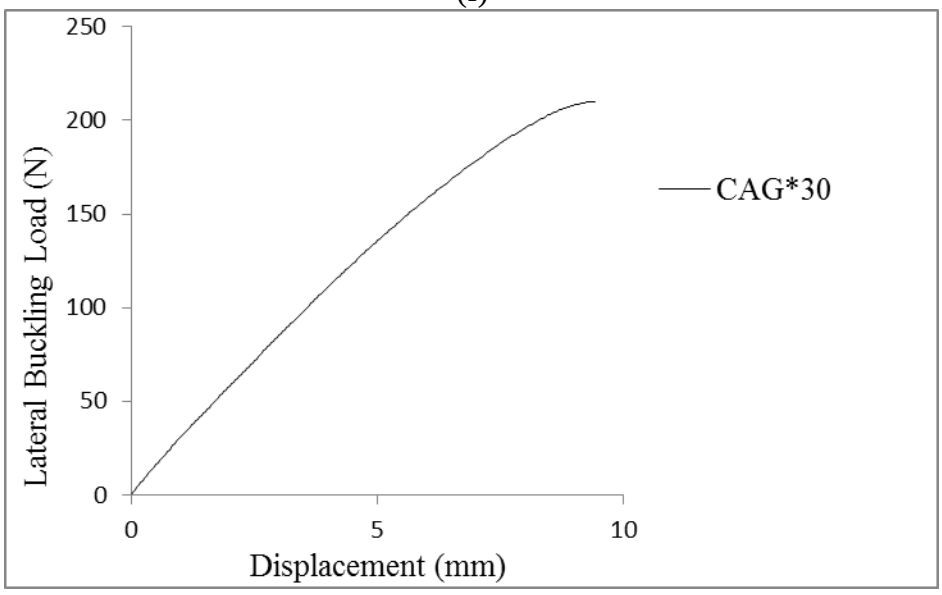
250
200
150
100
50
0
Lateral Buckling Load (N)
0
5
10
Displacement (mm)
CAG*30

(g)

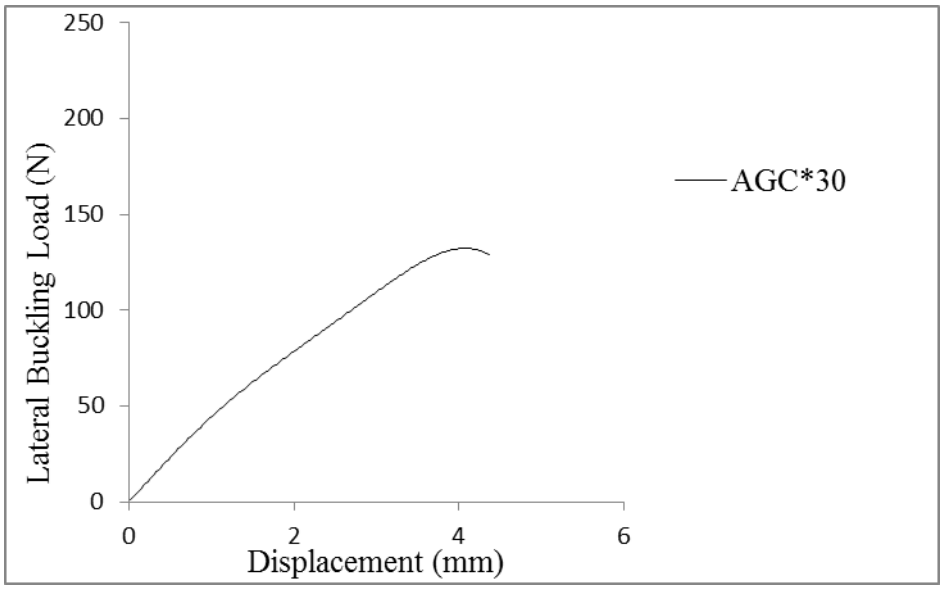

(h)

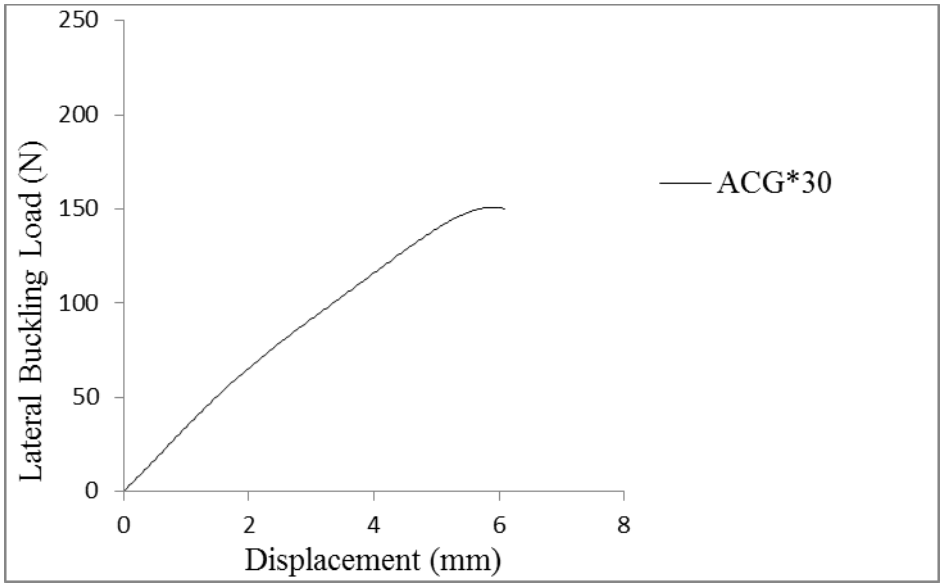

(ı)

Figure 6.5 Lateral Buckling load - displacement diagram a) $(G_{12})^{30}$, b) $(A_{12})^{30}$, c) $(C_{12})^{30}$, d) GCA^{30}, e) GAC^{30}, f) CGA^{30}, g) CAG^{30}, h) AGC^{30}, ı) ACG^{30}

Lateral buckling load-displacement diagrams for $(G_{12})^{45}$, $(A_{12})^{45}$, $C_{12})^{45}$, GCA^{45}, GAC^{45}, CGA^{45}, CAG^{45}, AGC^{45} and ACG^{45} (having $[(45/-45)_3]_s$ ply orientations) are given in Figure 6.6.

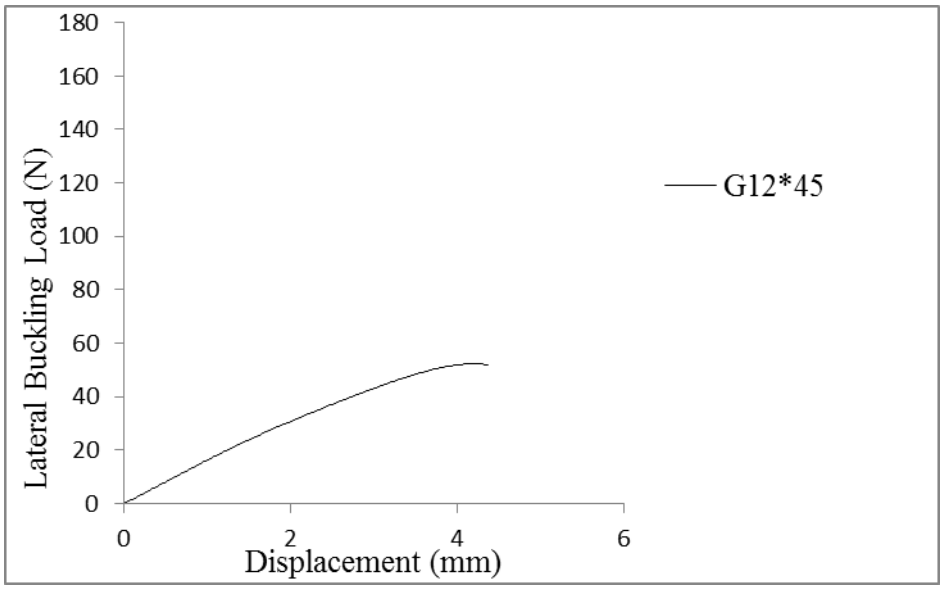
Lateral Buckling Load (N)
180
160
140
120
100
80
60
40
20
0
0
2
4
6
Displacement (mm)
G12*45

(a)

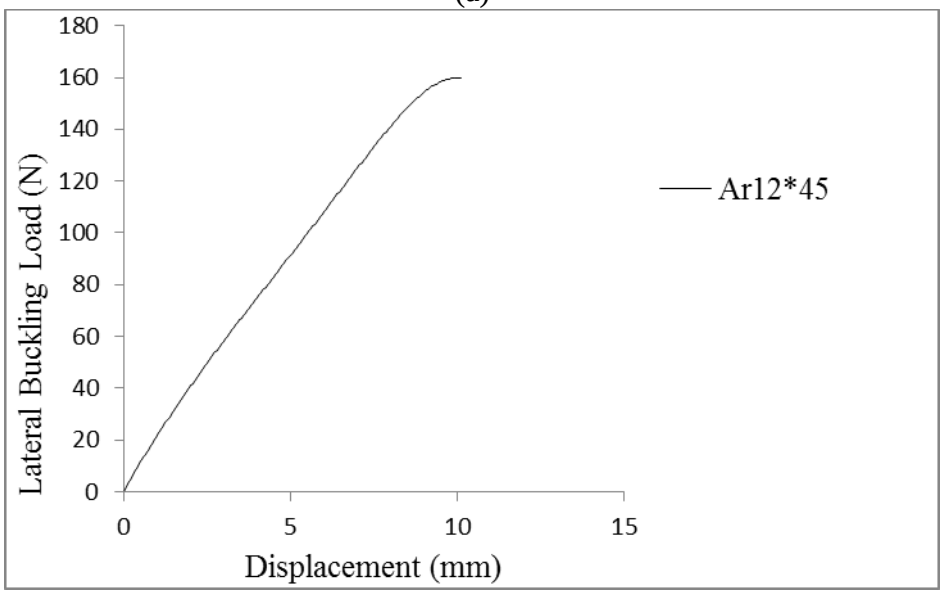
Lateral Buckling Load (N)
180
160
140
120
100
80
60
40
20
0
0
5
10
15
Displacement (mm)
Ar12*45

(b)

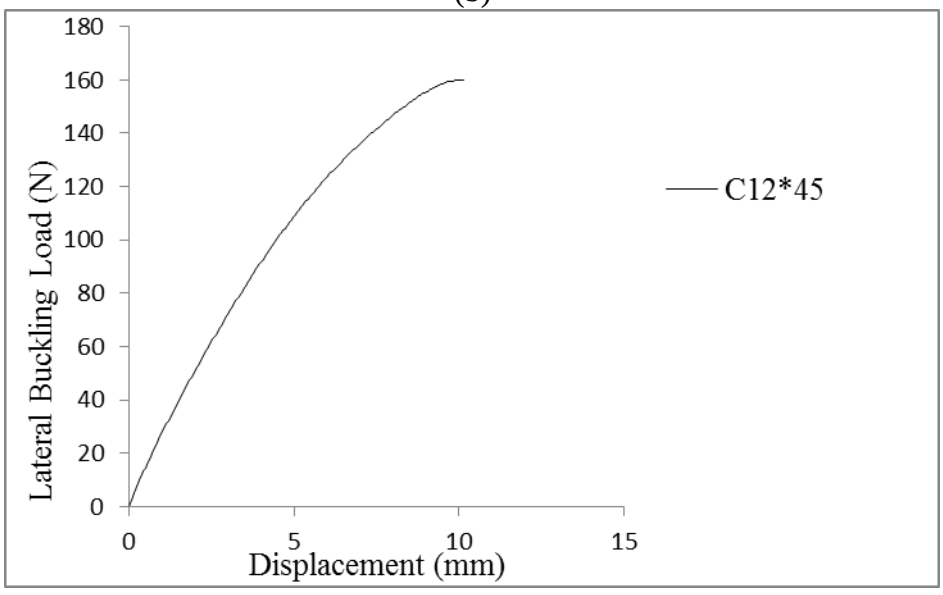
Lateral Buckling Load (N)
180
160
140
120
100
80
60
40
20
0
0
5
10
15
Displacement (mm)
C12*45

(c)

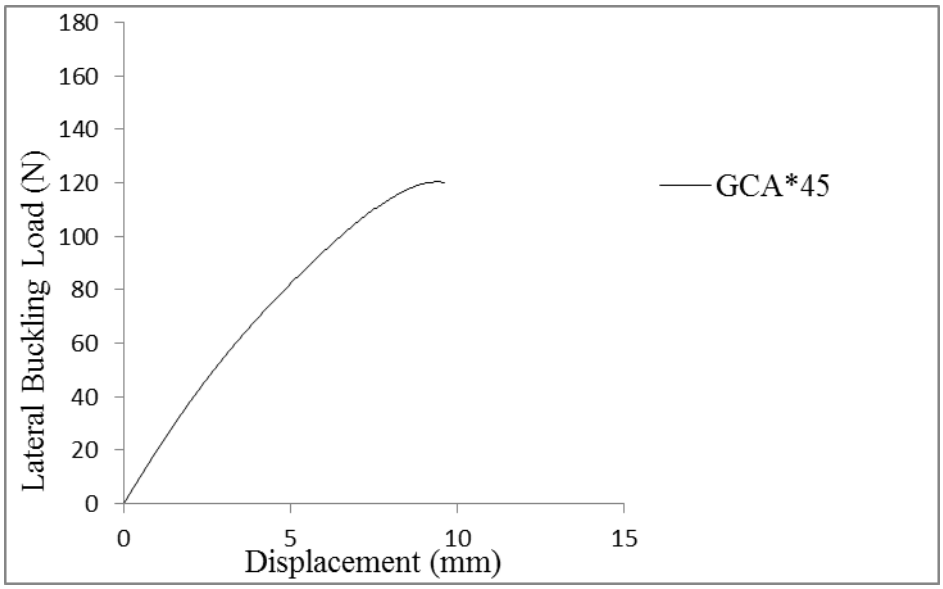
Lateral Buckling Load (N)
180
160
140
120
100
80
60
40
20
0
0
5
10
15
Displacement (mm)
GCA*45

(d)

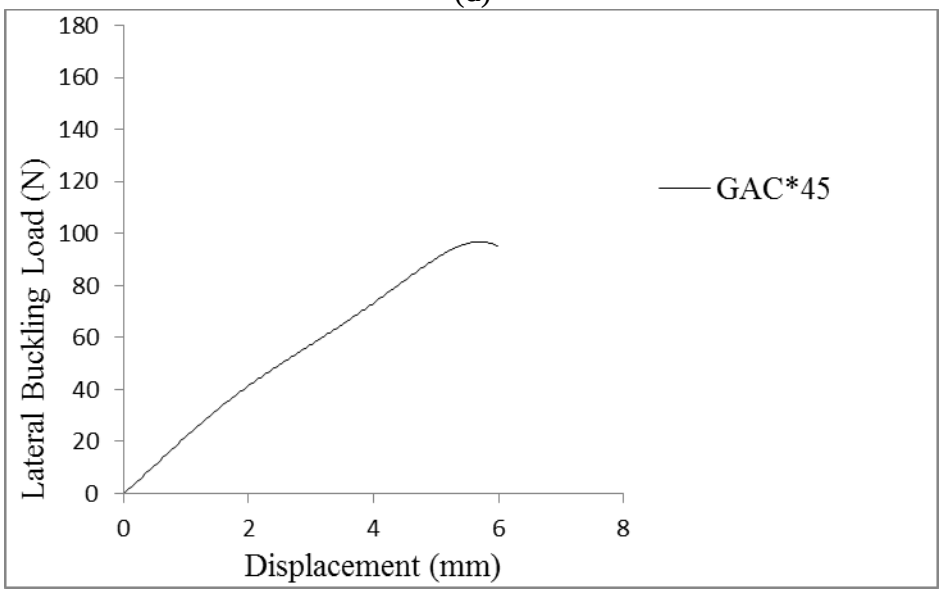
Lateral Buckling Load (N)
180
160
140
120
100
80
60
40
20
0
0
2
4
6
8
Displacement (mm)
GAC*45

(e)

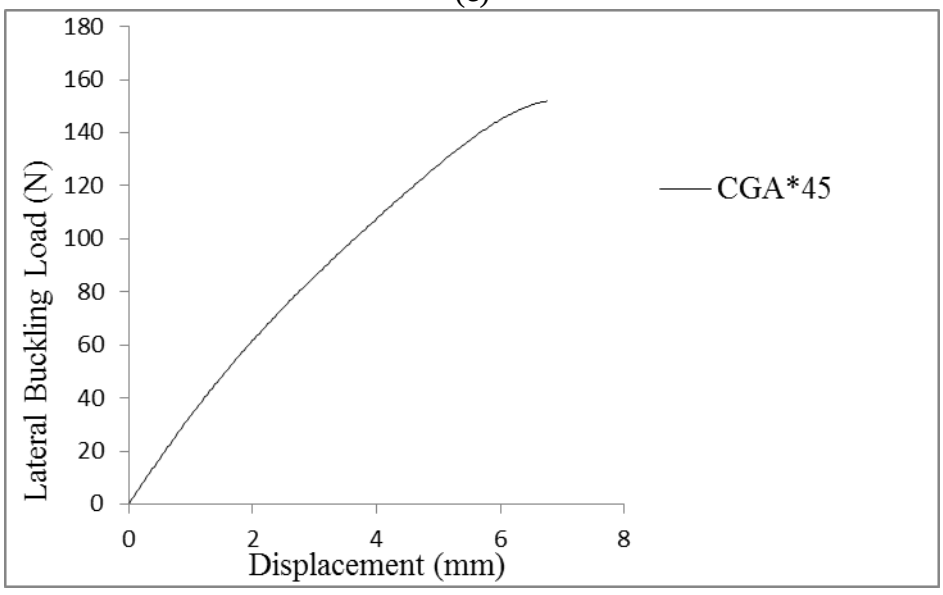
Lateral Buckling Load (N)
180
160
140
120
100
80
60
40
20
0
0
2
4
6
8
Displacement (mm)
CGA*45

(f)

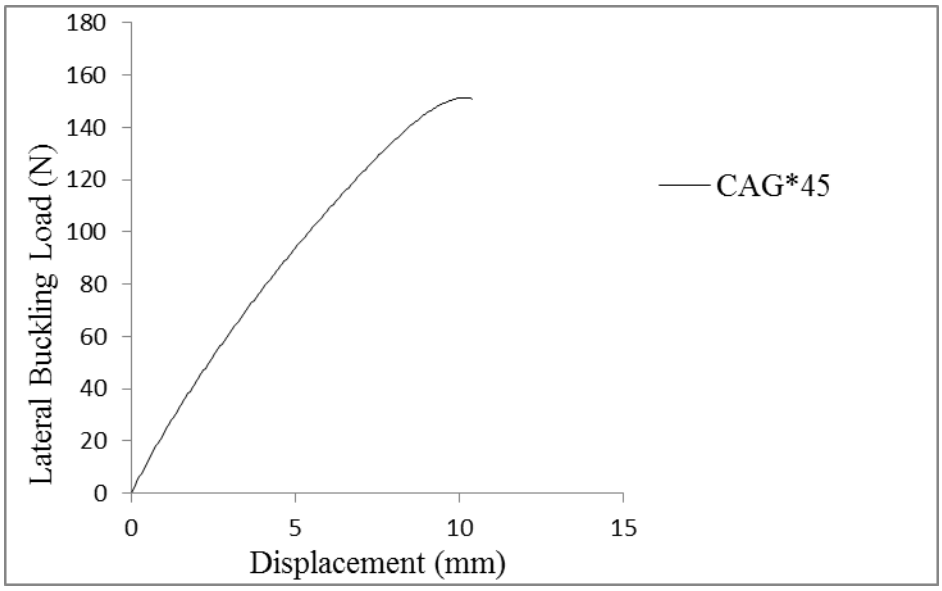
Lateral Buckling Load (N)
180
160
140
120
100
80
60
40
20
0
0
5
10
15
Displacement (mm)
CAG*45

(g)

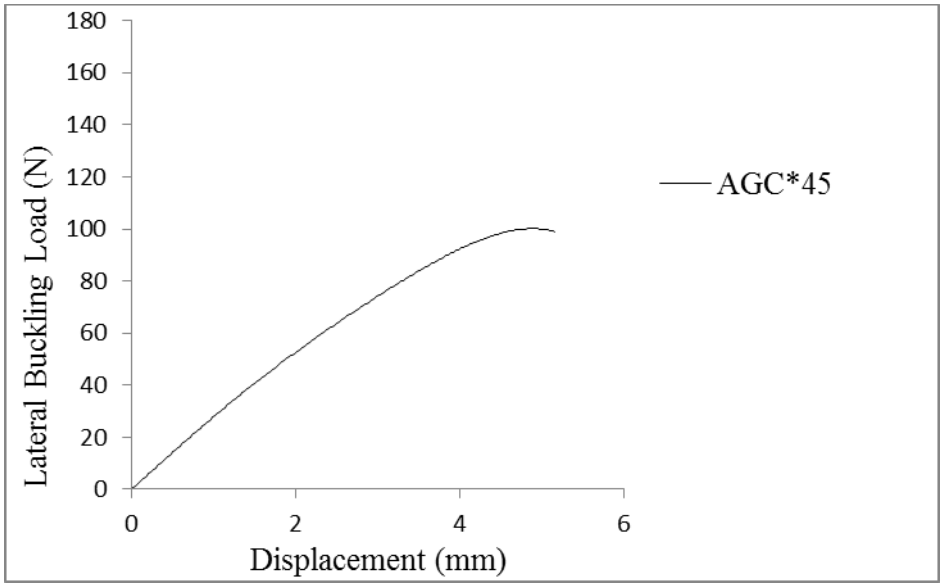
Lateral Buckling Load (N)
180
160
140
120
100
80
60
40
20
0
0
2
4
6
Displacement (mm)
AGC*45

(h)

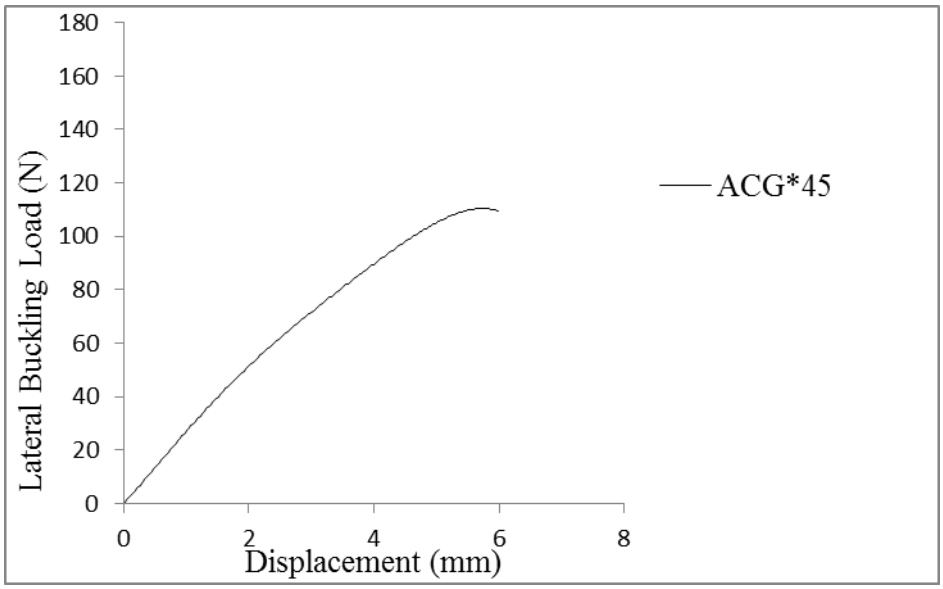

(ı)

Figure 6.6 Lateral Buckling load - displacement diagram a) $(G_{12})^{45}$, b) $(A_{12})^{45}$, c) $(C_{12})^{45}$, d) GCA^{45}, e) GAC^{45}, f) CGA^{45}, g) CAG^{45}, h) AGC^{45}, ı) ACG^{45}

Also hybrid composites which have $[(30/-60)_3]_s$ and $[(45/-45)_3]_s$ stacking sequences are given together in Figure 6.7. It is seen that CAG^{30} has the highest lateral buckling load and GAC^{30} has the smallest lateral buckling load for the $[(30/-60)_3]_s$ ply orientation and also CAG^{45} has the highest lateral buckling load and GAC^{45} has minimum lateral buckling load for the $[(45/-45)_3]_s$ ply orientation. For the $[(30/-60)_3]_s$ ply orientation, lateral buckling load of CAG^{30} is 40 % higher than GAC^{30}. For the $[(45/-45)_3]_s$ ply orientation, lateral buckling load of CAG^{45} is nearly 35 % higher than GAC^{45}.

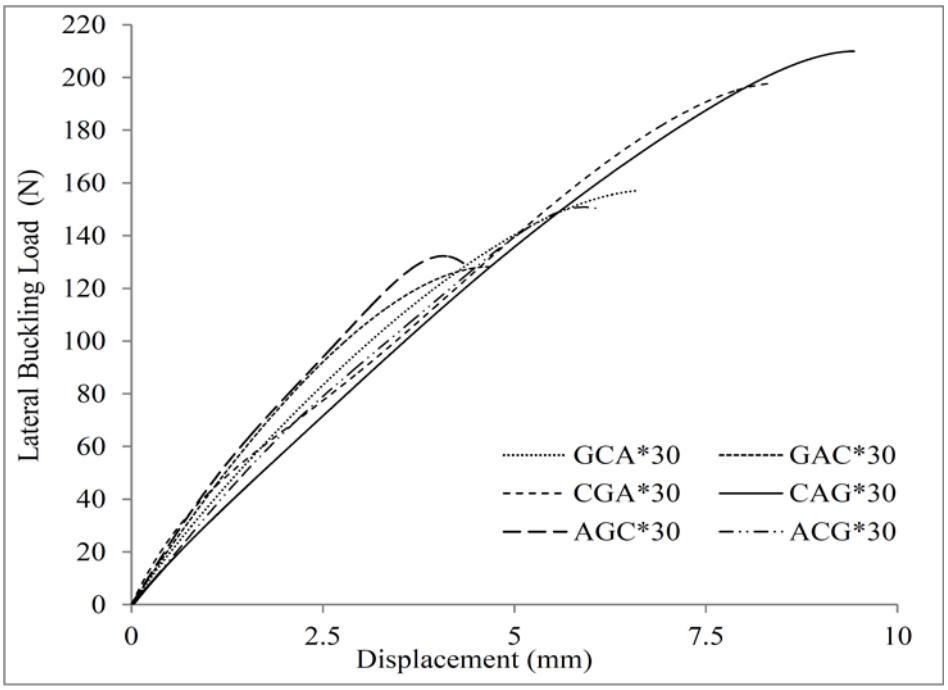

(a)

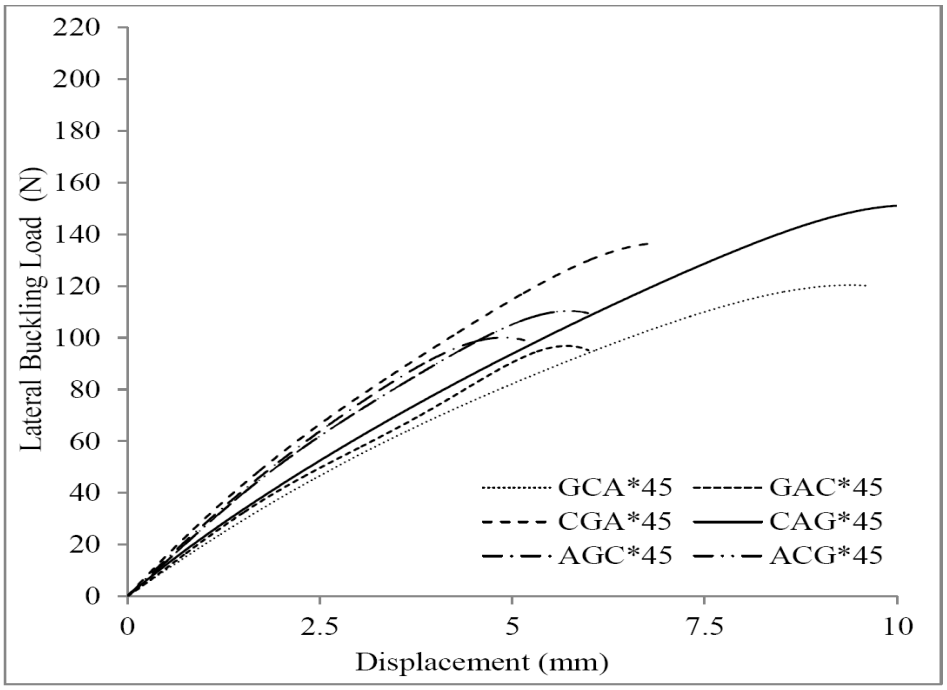

(b)

Figure 6.7 Comparison of lateral buckling load- displacement curves of 6 different hybrid configurations having a) $[(30/-60)_3]_s$, b) $[(45/-45)_3]_s$ stacking sequences

In Figure 6.8 and Table 6.2, lateral buckling experiment results of three different specimens of each hybrid composites are given for the $[(30/-60)_3]_s$ and $[(45/-45)_3]_s$ stacking sequences. As can be seen, the results are in close agreement with each other. Critical lateral buckling loads can be ordered from high value to small one for

$[(30/-60)_3]_s$ stacking sequences is CAG^{30}, CGA^{30}, GCA^{30}, ACG^{30}, AGC^{30} and GAC^{30}, respectively. Also for $[(45/-45)_3]_s$ stacking sequences, critical lateral buckling loads can be ordered as CAG^{45}, CGA^{45}, GCA^{45}, ACG^{45}, AGC^{45}, and GAC^{45} ,respectively.

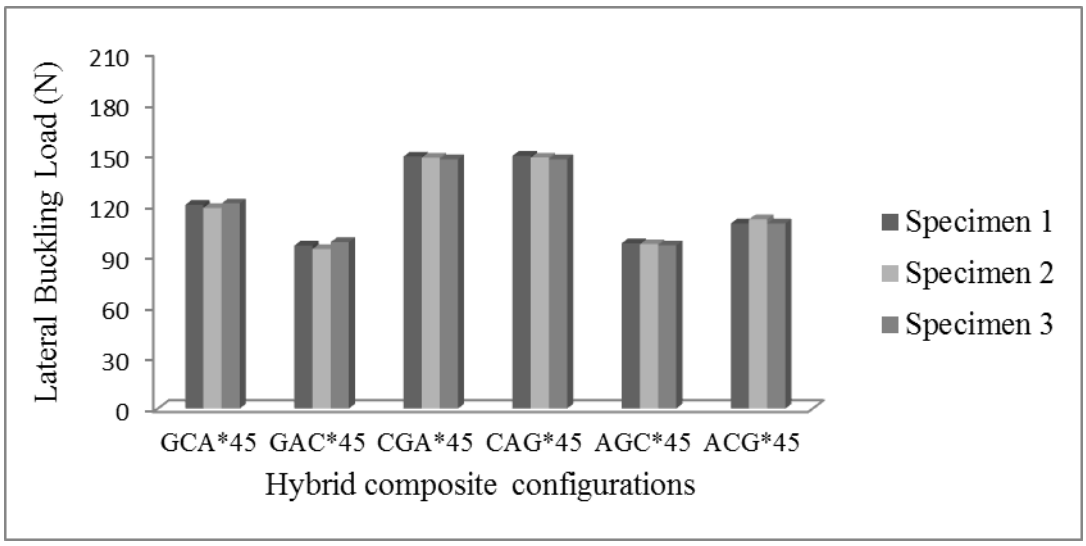

(a)

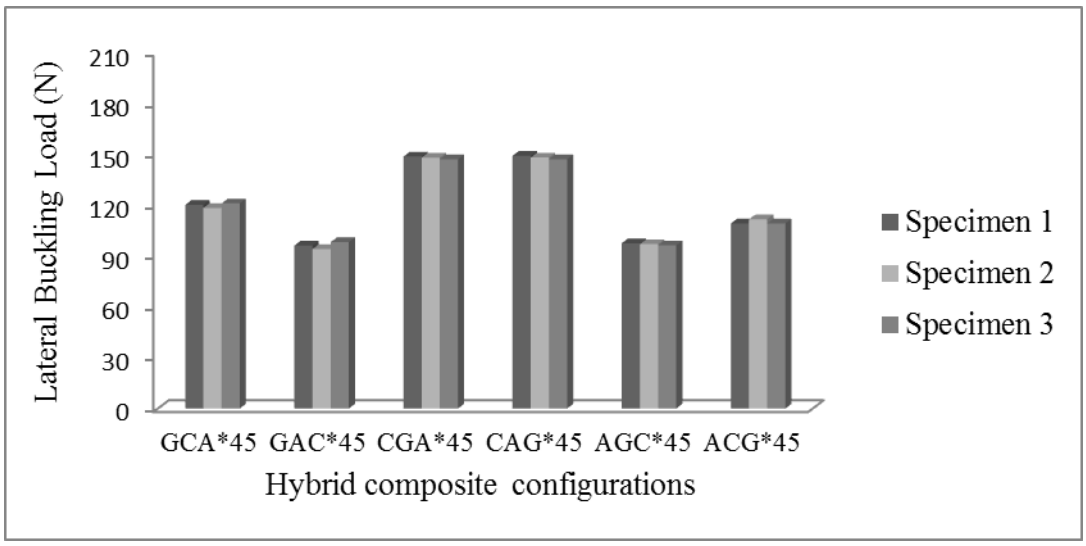

(b)

Figure 6.8 Comparison of lateral buckling load- displacement curves of 6 different hybrid configurations having a) $[(30/-60)_3]_s$, b) $[(45/-45)_3]_s$ stacking sequences with 3 different specimens

Table 6.2 Critical lateral buckling loads of Composite and hybrid composite specimens having $[(30/-60)_3]_s$ and $[(45/-45)_3]_s$ stacking sequences

	Lateral Buckling Load (N)		
Hybrid composite configurations	**Specimen 1**	**Specimen 2**	**Specimen 3**
$(G_{12})^{30}$	59.980	59.501	59.676
$(A_{12})^{30}$	227.663	225.336	226.076
$(C_{12})^{30}$	217.992	215.968	214.722
GCA^{30}	153.662	150.708	147.752
GAC^{30}	123.141	119.901	124.762
CGA^{30}	198.007	195.562	196.784
CAG^{30}	206.228	205.373	202.194
AGC^{30}	133.066	131.360	128.289
ACG^{30}	151.538	149.997	148.712
$(G_{12})^{45}$	50.130	50.277	50.424
$(A_{12})^{45}$	161.809	158.919	159.497
$(C_{12})^{45}$	158.162	159.743	158.953
GCA^{45}	120.062	118.271	120.958
GAC^{45}	96.095	94.051	98.140
CGA^{45}	148.576	147.931	146.962
CAG^{45}	149.018	147.983	146.948
AGC^{45}	97.458	96.945	96.175
ACG^{45}	109.117	111.596	109.117

6.4 Lateral Buckling Experiment Results of Composites and Hybrid Composites having un-Symmetrical $[(0/90)_6]_{us}$ Stacking Sequence

Lateral buckling experiments are also investigated for un-symmetrical $[(0/90)_6]_{us}$ stacking sequence like buckling phenomenon and results (lateral buckling load - displacement diagrams) are given in Figure 6.9, for these un-symmetrical configurations (GCA*, GAC*, CGA*, CAG*, AGC* and ACG*).

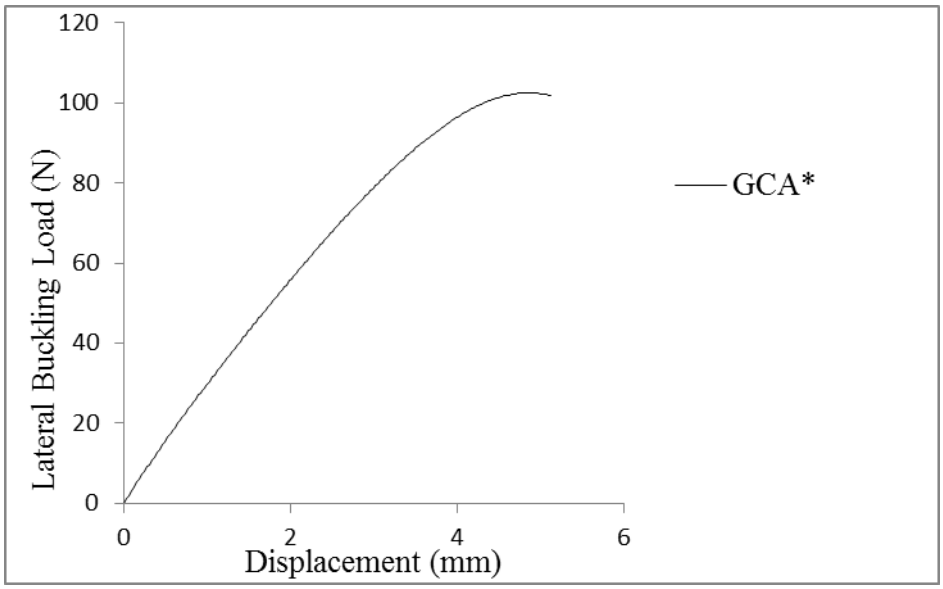
120
100
80
60
40
20
0
Lateral Buckling Load (N)
0
2
4
6
Displacement (mm)
GCA*

(a)

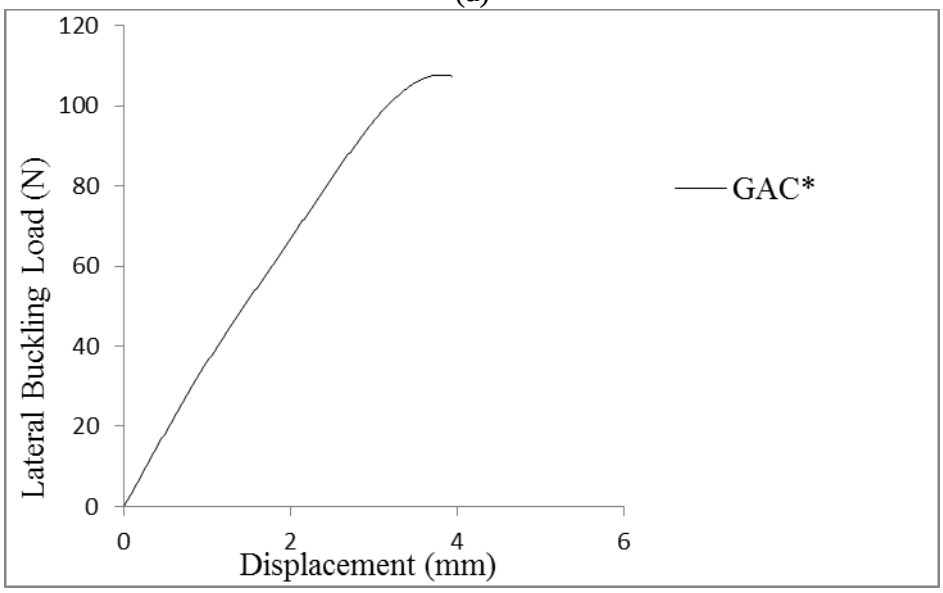
120
100
80
60
40
20
0
Lateral Buckling Load (N)
0
2
4
6
Displacement (mm)
GAC*

(b)

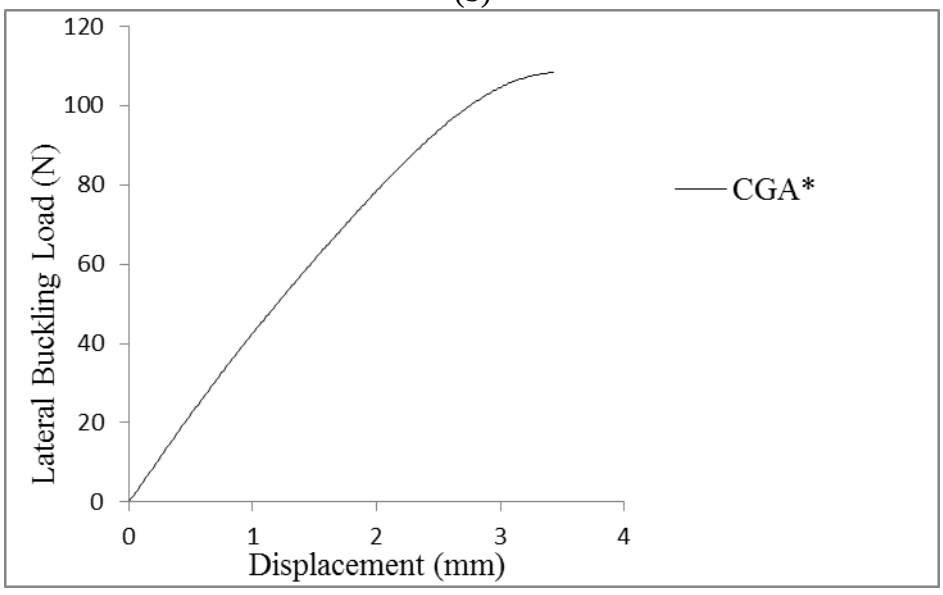
120
100
80
60
40
20
0
Lateral Buckling Load (N)
0
1
2
3
4
Displacement (mm)
CGA*

(c)

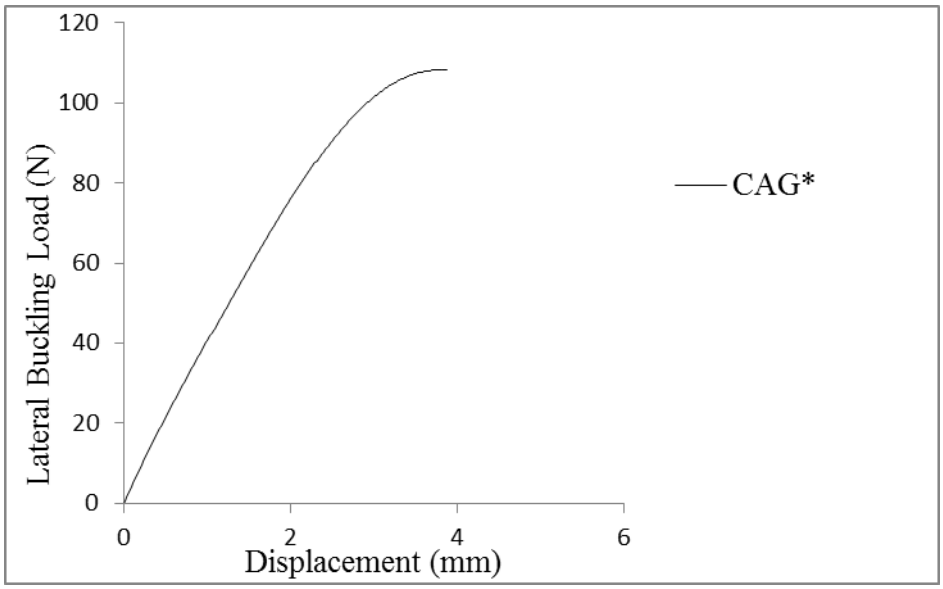
120
100
80
60
40
20
0
Lateral Buckling Load (N)
0
2
4
6
Displacement (mm)
CAG*

(d)

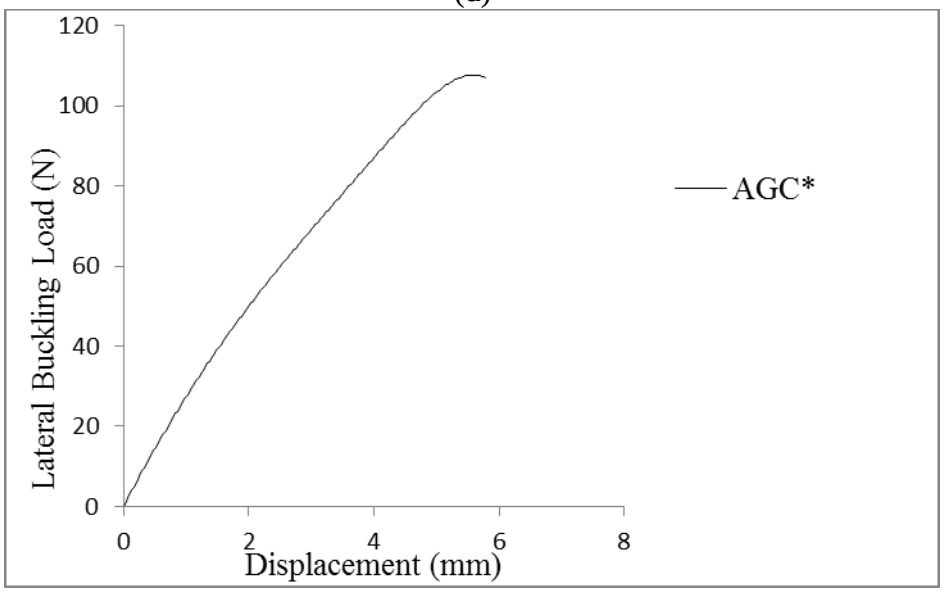
120
100
80
60
40
20
0
Lateral Buckling Load (N)
0
2
4
6
8
Displacement (mm)
AGC*

(e)

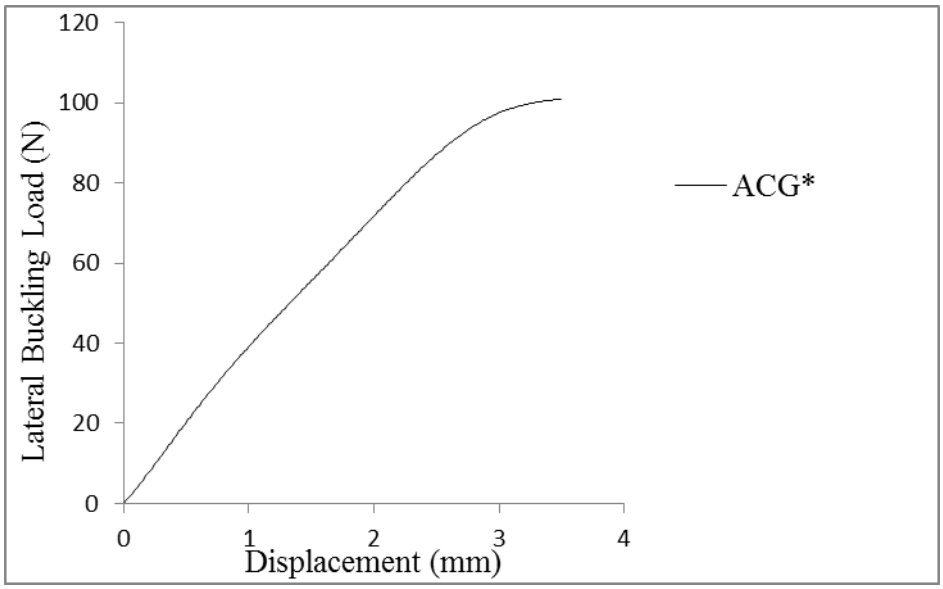

(f)

Figure 6.9 Lateral buckling load - displacement diagrams of a) GCA*, b) GAC*, c) CGA*, d) CAG*, e) AGC*, f) ACG*

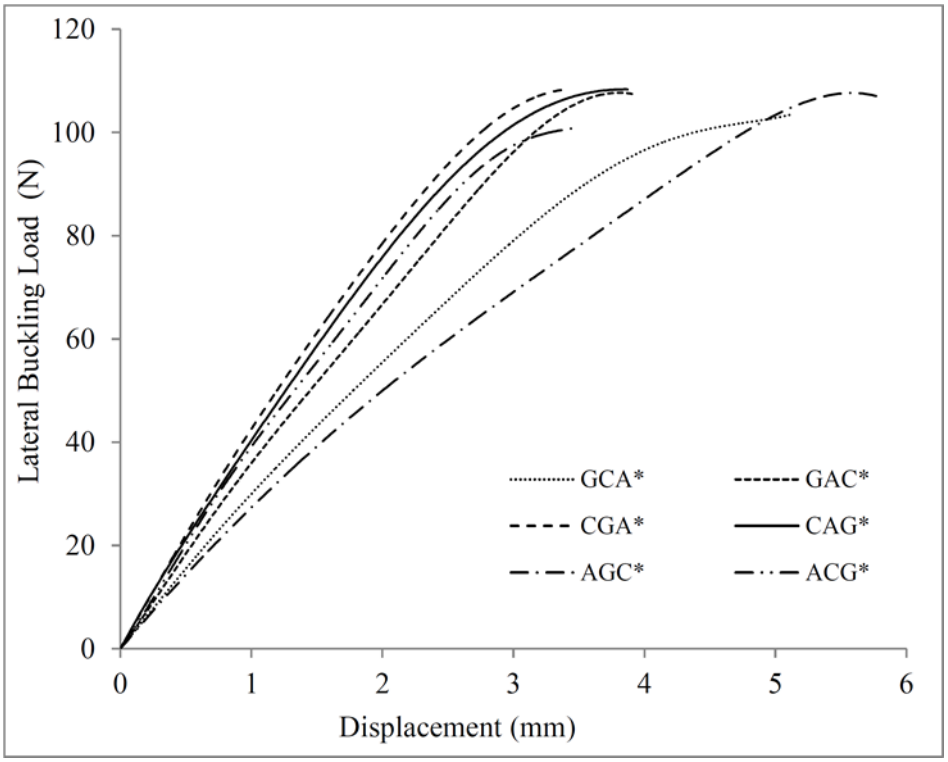

Figure 6.10 Comparison of lateral buckling load- displacement curves of 6 different un-symmetrical hybrid composite configurations having $[(0/90)_6]_{us}$ stacking sequences

Also for un-symmetrical hybrid configurations, the critical lateral buckling loads for 3 different specimens are given in Figure 6.11 and Table 6.3. Again like buckling

loads, there are not (in the Figure 6.11 and Table 6.3) huge difference between the critical loads of these configurations. However, it can be ordered from the highest lateral buckling load to the smallest lateral buckling load as GAC*, AGC*, CAG*, CGA*, GCA*, ACG*, respectively.

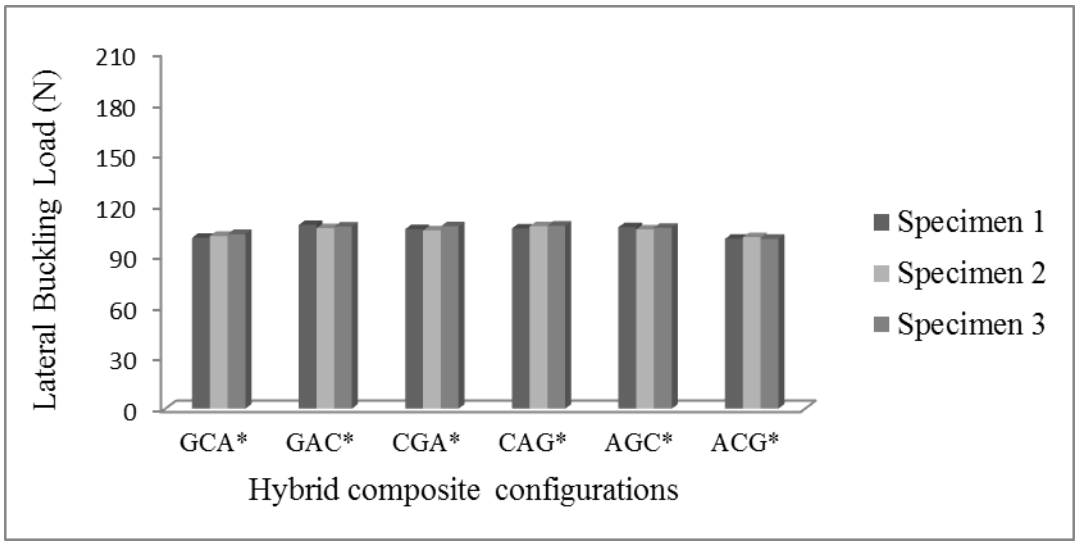

Figure 6.11 Comparison of lateral buckling load- displacement curves of un-symmetrical hybrid composites with 3 different specimens

Table 6.3 Comparison of lateral buckling load- displacement curves of un-symmetrical hybrid composites with 3 different specimens

	Lateral Buckling Load (N)		
Hybrid composite configurations	**Specimen 1**	**Specimen 2**	**Specimen 3**
GCA*	100.746	101.784	102.879
GAC*	108.250	106.334	107.292
CGA*	105.850	105.123	107.479
CAG*	106.225	107.513	107.786
AGC*	106.943	105.663	106.615
ACG*	100.137	101.048	100.086

6.5 Discussion on the Results of Lateral Buckling Experiments

General comparison for critical lateral buckling loads of different hybrid configurations on buckling can be seen in Figure 6.12 and 6.13. In Figure 6.12 comparison of critical lateral buckling loads of hybrid composites having symmetrical $[(0/90)_3]_s$, $[(30/-60)_3]_s$, $[(45/-45)_3]_s$ and un-symmetrical $[(0/90)_6]_{us}$

stacking sequences are given. It is seen that for $[(0/90)_3]_s$ symmetrical hybrid configuration CGA, for $[(30/-60)_3]_s$ symmetrical hybrid configuration CAG^{30}, for $[(45/-45)_3]_s$ symmetrical hybrid configuration CAG^{45} and for un-symmetrical $[(0/90)_3]_s$ hybrid configuration GAC* has the highest lateral buckling loads.

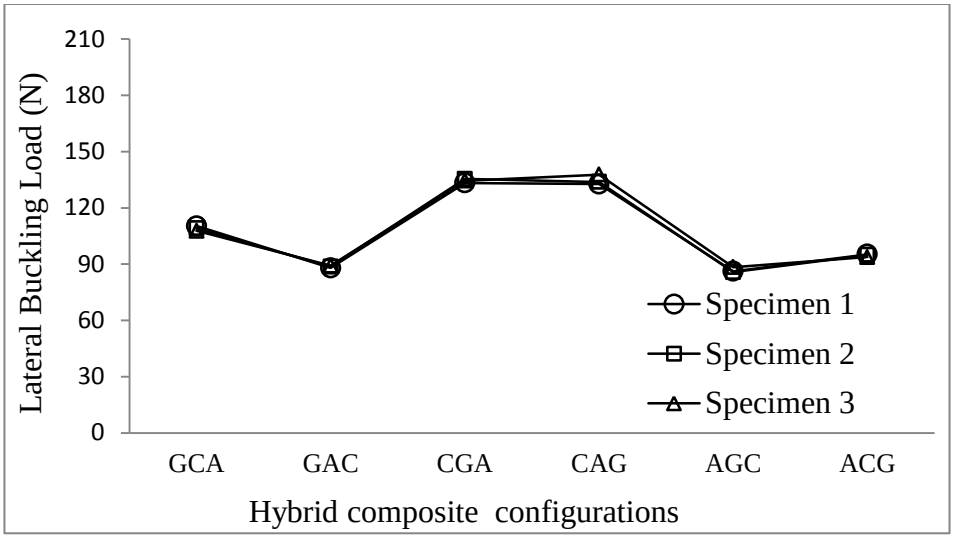

(a)

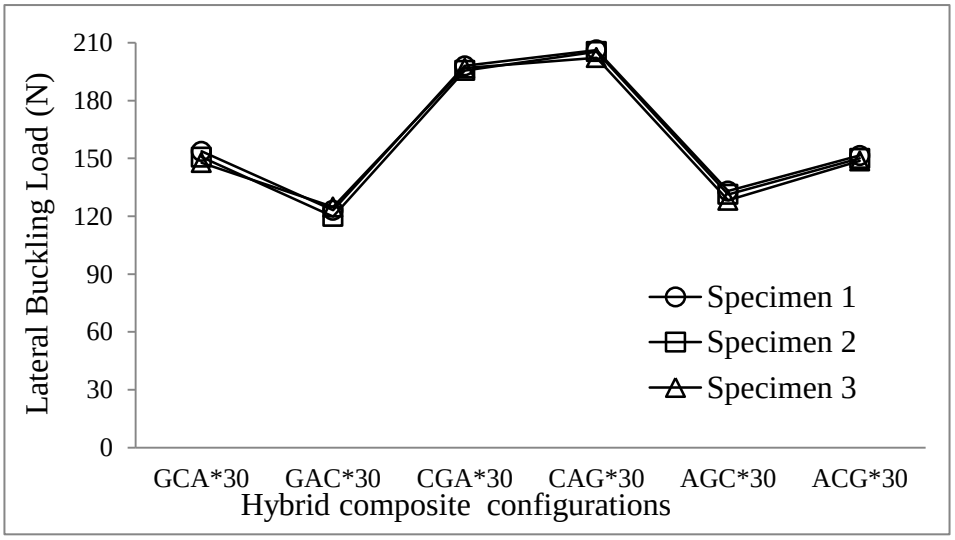

(b)

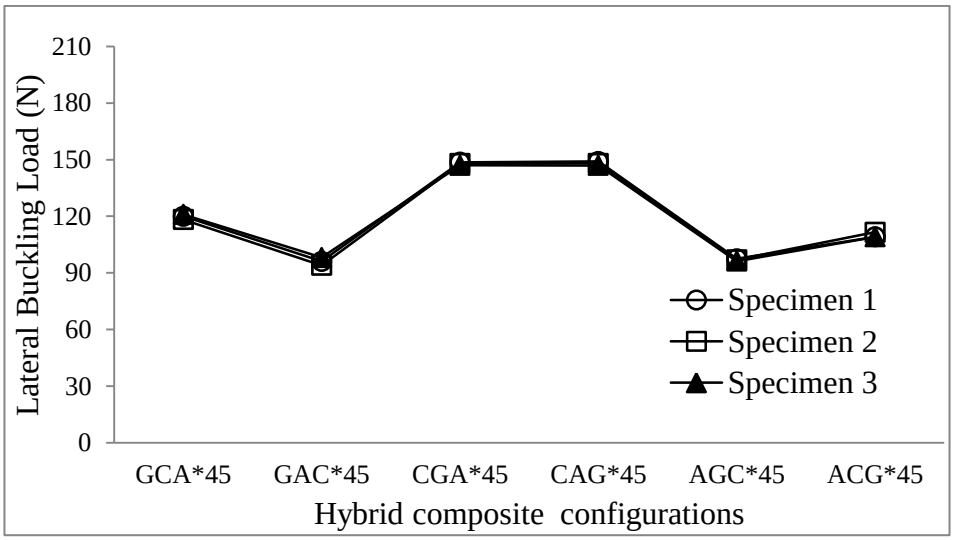

(c)

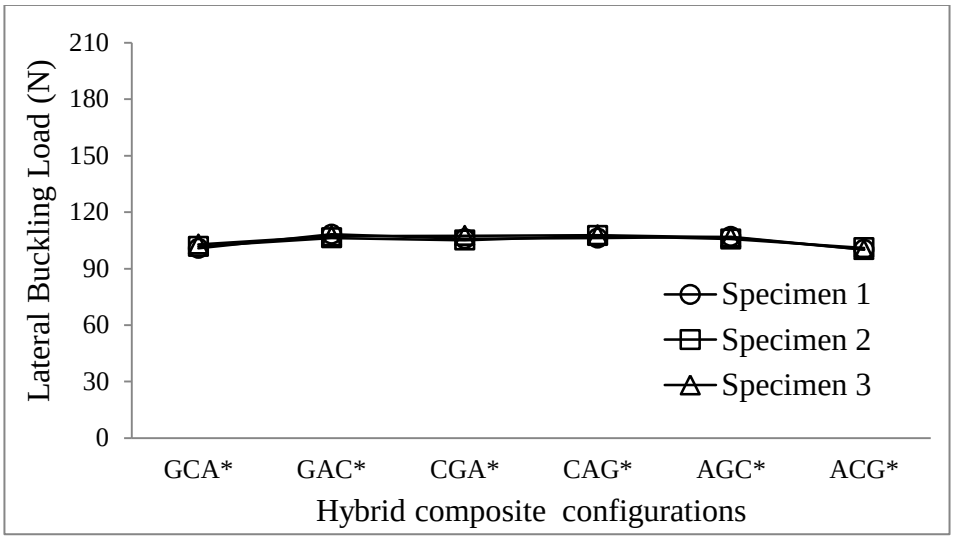

(d)

Figure 6.12 Comparison of critical lateral buckling loads of hybrid composites having a) $[(0/90)_3]_s$ symmetrical, b) $[(30/-60)_3]_s$ symmetrical, c) $[(45/-45)_3]_s$ symmetrical, d) $[(0/90)_6]_{us}$ un-symmetrical stacking sequences

It is also concluded that for $[(0/90)_3]_s$ symmetrical hybrid configuration AGC, for $[(30/-60)_3]_s$ symmetrical hybrid configuration GAC^{30}, for $[(45/-45)_3]_s$ symmetrical hybrid configuration GAC^{45} and for un-symmetrical $[(0/90)_6]_{us}$ hybrid configuration ACG* has the smallest lateral buckling loads. So in the figure 6.13, comparisons of critical lateral buckling loads of these configurations (the best and the worst configurations) are considered. As can be seen in this figure, CAG^{30} has the highest and GAC* has the lowest lateral buckling load and CAG^{45} has higher lateral

buckling load from GAC* and CGA. In other words, CAG^{30} is the most designable with respect to lateral buckling characteristic.

It is also seen that lateral buckling characteristics are significiantly effected by the replacement of fiber types like buckling characteristics. It is concluded that stiffness (Young modulus which effects stiffness) and shear properties (exactly shear modulus (G_{12})) are affecting lateral buckling characteristics. So configurations which produced using fibers which have higher stiffness and higher shear properties in the upper layers increase the lateral buckling strength. Moreover, hybrid plates having $[(30/-60)_3]_s$ and $[(45/-45)_3]_s$ stacking sequences have higher lateral buckling strength with respect to configurations which produced having $[(0/90)_3]_s$ stacking sequences (which is different than buckling in which hybrid plates which produced having $[(0/90)_3]_s$ stacking sequences have higher buckling strength).

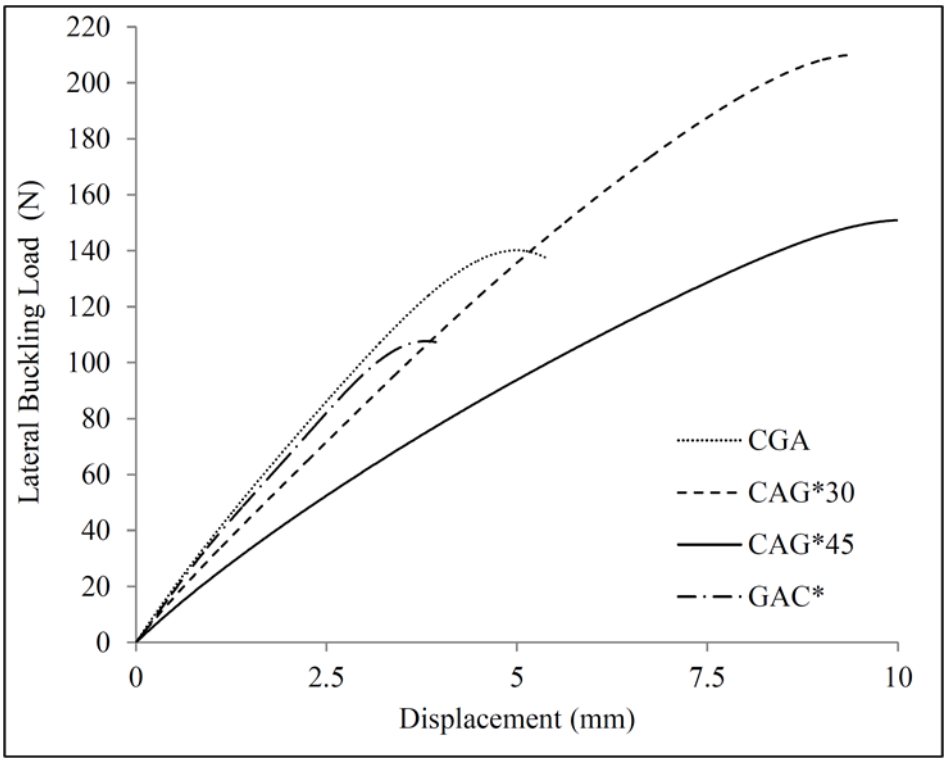

(a)

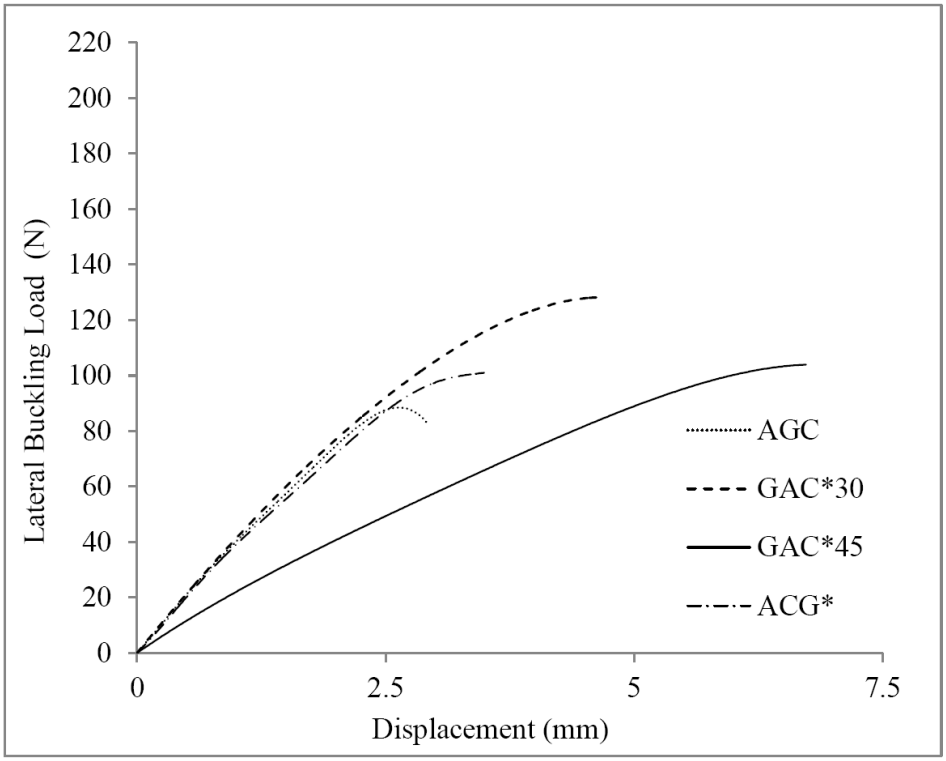

(b)

Figure 6.13 Comparison of critical lateral buckling loads of a) the best configurations, b) the worst configurations

CHAPTER 7

NUMERICAL STUDIES ON BUCKLING AND LATERAL BUCKLING

7.1 Introduction

This chapter deals with the numerical studies on the buckling and lateral buckling of hybrid composites and comparison with the results which determined from experiments. Numerical analyses were performed using ANSYS 12.0 (finite element analysis program). This chapter is divided into the three main sections; numerical buckling studies, numerical lateral buckling studies and parametric studies on numerical buckling and lateral buckling.

7.2 Numerical Buckling Studies

The produced G_{12}, A_{12} and C_{12} composite plate thicknesses are 2.20 mm, 3.30 mm and 2.60 mm, respectively. Thicknesses of hybrid composite plates (GCA, GAC, CGA, CAG, AGC, ACG, GCA^{30} ,GCA^{45}, GAC^{30} , GAC^{45}, CGA^{30} ,CGA^{45}, CAG^{30}, CAG^{45}, AGC^{30}, AGC^{45}, ACG^{30} and ACG^{45}) produced from different combinations of S-glass, Aramid and Carbon are 2.70 ±0.2 mm. Hybrid composites are modeled with the same thickness (2.70 mm) of produced plates. The models are totally 12 layers. Dimensions of models (Figure 7.1) are taken as width (W) 20 mm and length (L) 155 mm.

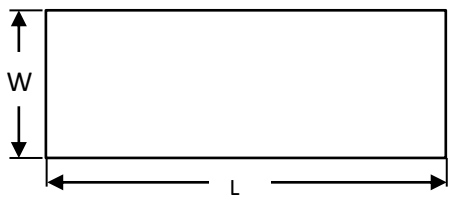

Figure 7.1 Dimensions of plates used in ANSYS

Plates are meshed with quadratic shell elements (SHELL91) based on first-order shear deformation theory. SHELL91 [152] element geometry illustrated in Figure 7.2

is used for layered applications to produce mesh structure. The element has six degrees of freedom at each node: translations in the nodal x, y and z directions and rotations about the nodal x, y and z axes.

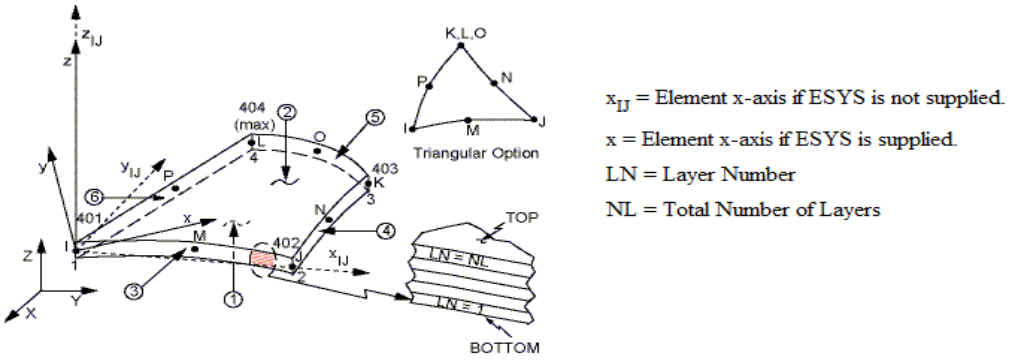

Figure 7.2 SHELL91element properties [152]

Sample mesh structure is shown in the Figure 7.3 for buckling. As can be seen in this figure, the model is meshed with quadrilateral elements for a good mesh generation. The boundary conditions and loadings of the models are also illustrated in Figure 7.3 (which has 84751 nodes and 27900 elements). The pre-buckled stress distribution is evaluated under 1 N/m uniform load and saved for the eigenvalue buckling solution. Then, the eigenvalue buckling load is determined. This procedure was carried out for all of the models.

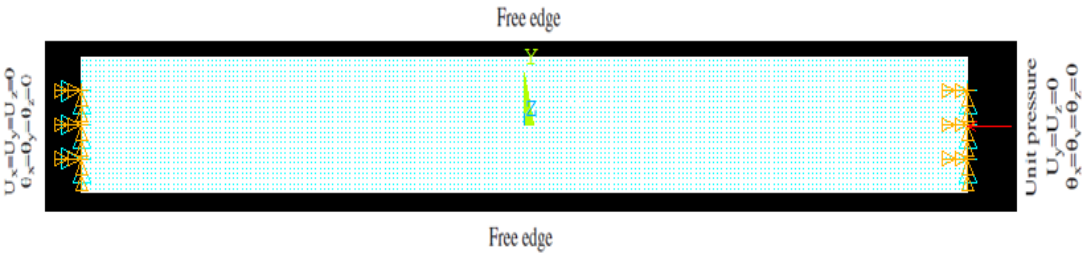

Figure 7.3 Mesh and boundary conditions

7.2. 1 Results of Numerical Studies of Buckling

Results of numerical and experimental studies of three different specimens of each hybrid composites are given together in Table 7.1 and Figure 7.4. In the Table 7.1, it is seen that experimental and numerical results are close to each other and in the Figure 7.4, it is seen that order of the critical buckling loads of hybrid configurations due to numerical results are in the same order with the results of experiments. For $[(0/90)_3]_s$ stacking sequences, this order is CAG, CGA, ACG, GCA, AGC, GAC, respectively. For $[(30/-60)_3]_s$ stacking sequences, this order is CGA^{30}, CAG^{30},

GCA^{30}, ACG^{30}, GAC^{30} and AGC^{30}, respectively. Finally for $[(45/-45)_3]_s$ stacking sequences, this order is CGA^{45}, CAG^{45}, GCA^{45}, ACG^{45}, GAC^{45} and AGC^{45}, respectively.

Table 7.1 Comparison of Critical buckling loads of experiments and numerical results for all hybrid configurations

	Buckling Loads (N)			
Hybrid composite configurations	**Specimen 1**	**Specimen 2**	**Specimen 3**	**ANSYS**
G_{12}	578.022	524.502	513.798	564.000
A_{12}	2347.177	2355.115	2380.154	2577.987
C_{12}	2280.469	2292.633	2234.237	2380.000
GCA	1459.624	1471.356	1485.189	1587.052
GAC	1131.577	1157.074	1143.718	1239.635
CGA	1968.691	1986.26	1951.44	2159.770
CAG	2141.485	2172.078	2188.406	2242.441
AGC	1286.164	1329.657	1286.164	1403.192
ACG	1775.299	1585.998	1552.592	1644.439
$(G_{12})^{30}$	356.054	355.486	351.895	387.998
$(A_{12})^{30}$	1082.787	1067.062	1057.619	1197.929
$(C_{12})^{30}$	1013.933	1005.282	1011.026	1124.396
GCA^{30}	799.373	794.469	790.791	904.818
GAC^{30}	645.606	631.259	638.433	732.596
CGA^{30}	968.863	950.545	956.651	1091.104
CAG^{30}	947.872	928.914	932.074	1069.161
AGC^{30}	620.370	612.850	609.091	702.108
ACG^{30}	699.685	679.879	687.831	777.377
$(G_{12})^{45}$	318.688	312.643	321.304	351.575
$(A_{12})^{45}$	906.984	932.177	899.425	1011.637
$(C_{12})^{45}$	867.911	860.505	865.423	956.624
GCA^{45}	697.240	686.418	688.201	790.668
GAC^{45}	572.293	565.139	575.154	644.512
CGA^{45}	970.514	981.800	966.100	1091.103
CAG^{45}	801.203	809.727	792.680	908.394
AGC^{45}	529.875	543.375	526.500	601.835
ACG^{45}	584.424	569.342	591.965	660.801
GCA*	1512.837	1474.762	1497.210	1622.175
GAC*	1558.235	1538.939	1545.470	1700.703
CGA*	1636.210	1630.081	1615.575	1762.072
CAG*	1577.076	1582.855	1559.211	1700.703
AGC*	1634.322	1613.369	1602.893	1762.072
ACG*	1479.927	1473.984	1463.631	1622.175

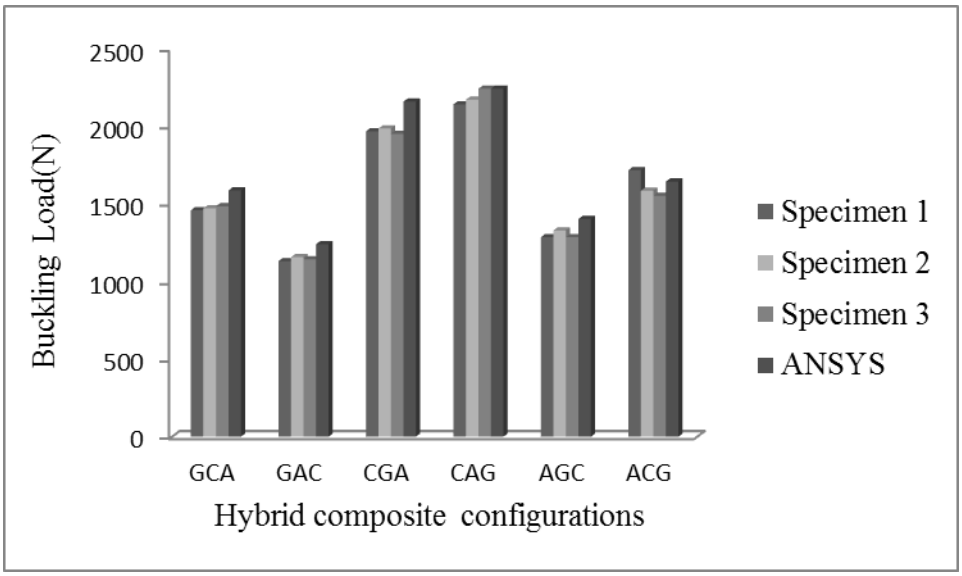
Buckling Load(N)
2500
2000
1500
1000
500
0
GCA
GAC
CGA
CAG
AGC
ACG
Hybrid composite configurations
Specimen 1
Specimen 2
Specimen 3
ANSYS

(a)

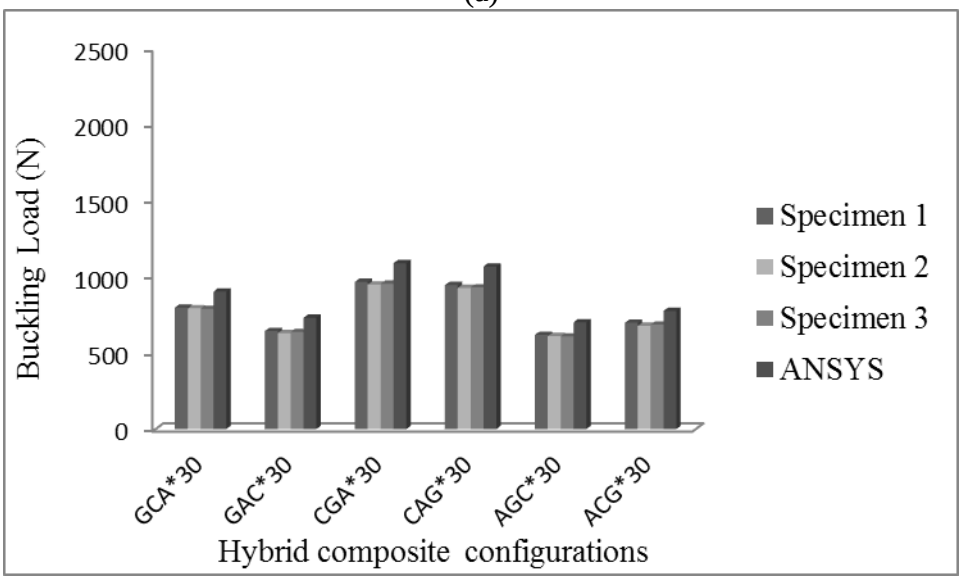
Buckling Load (N)
2500
2000
1500
1000
500
0
GCA*30
GAC*30
CGA*30
CAG*30
AGC*30
ACG*30
Hybrid composite configurations
Specimen 1
Specimen 2
Specimen 3
ANSYS

(b)

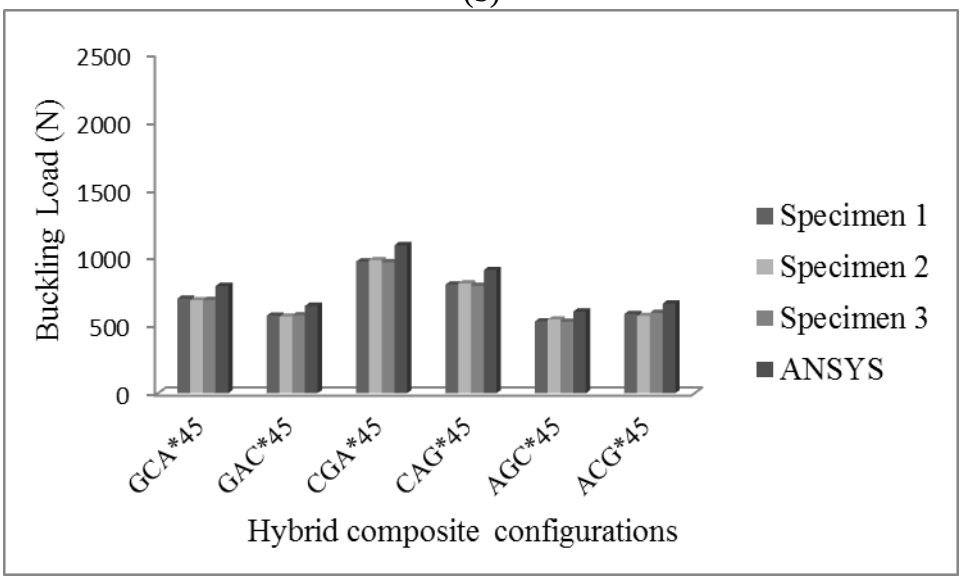
Buckling Load (N)
2500
2000
1500
1000
500
0
GCA*45
GAC*45
CGA*45
CAG*45
AGC*45
ACG*45
Hybrid composite configurations
Specimen 1
Specimen 2
Specimen 3
ANSYS

(c)

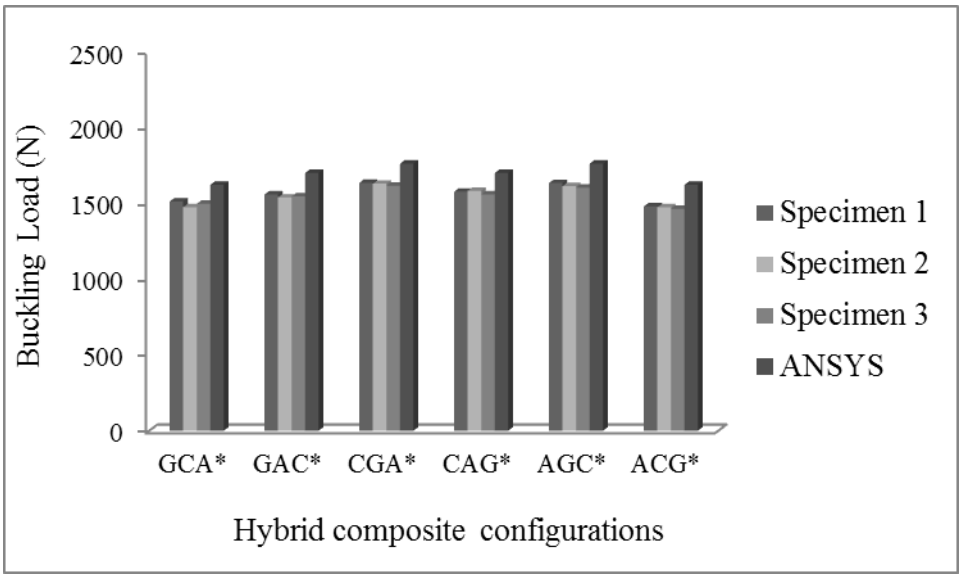

(d)

Figure 7.4 Comparison of experimental and numerical (ANSYS) results for configurations of a) $[(0/90)_3]_s$, b) $[(30/-60)_3]_s$, c) $[(45/-45)_3]_s$, d) $[(0/90)_3]_s$ un-symmetrical.

7.3. Numerical Lateral Buckling Studies

Lateral Buckling test specimen dimensions are taken as width (W) 20 mm, gage length (G) 155 mm. Models are meshed with quadrilateral elements (SHELL91) for a good mesh generation. Sample mesh structure, boundary conditions and loadings of the models are shown in Figure 7.5 (which has 84751 nodes and 27900 elements). The pre-buckled stress distribution is evaluated under 1 N uniform transverse load and saved for the eigenvalue buckling solution. Then, the eigenvalue buckling load is determined. This procedure is carried out for all models.

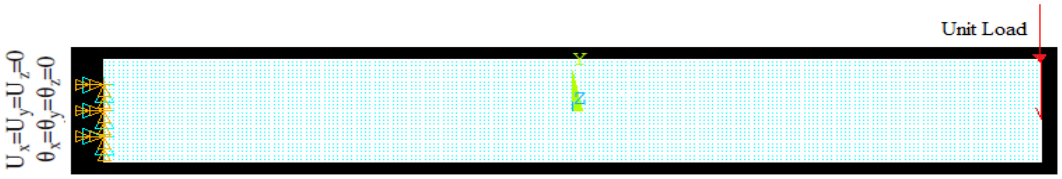

Figure 7.5 Mesh and boundary conditions

7.3. 1 Results of Numerical Studies of Lateral Buckling

Results of numerical and experimental studies of three different specimens of each hybrid composites are given together in the Table 7.2 and Figure 7.6. In the Table 7.2, it is seen that experimental and numerical results are close to each other. For

$[(0/90)_3]_s$ stacking sequences, they can be ordered from the highest lateral buckling load to the smallest buckling load as CGA, CAG, GCA, ACG, GAC and AGC, respectively. For $[(30/-60)_3]_s$ stacking sequences, this order is CAG^{30}, CGA^{30}, GCA^{30}, ACG^{30}, AGC^{30} and GAC^{30}, respectively. Finally for $[(45/-45)_3]_s$ stacking sequences, this order is CAG^{45}, CGA^{45}, GCA^{45}, ACG^{45}, AGC^{45}, and GAC^{45}, respectively.

Table 7.2 Experimental and Numerical Lateral Buckling loads of 6 different hybrid configurations

	Lateral Buckling Loads (N)			
Hybrid composite configurations	**Specimen 1**	**Specimen 2**	**Specimen 3**	**ANSYS**
G_{12}	46.688	46.878	46.146	48.968
A_{12}	147.693	147.379	147.719	143.687
C_{12}	136.803	138.590	138.079	152.644
GCA	110.327	108.993	107.762	113.262
GAC	87.921	88.626	89.120	91.682
CGA	133.247	135.363	134.505	138.037
CAG	132.636	133.788	137.668	136.215
AGC	86.178	85.753	88.388	89.324
ACG	95.186	94.896	93.765	99.375
$(G_{12})^{30}$	59.980	59.501	59.676	66.074
$(A_{12})^{30}$	227.663	225.336	226.077	254.362
$(C_{12})^{30}$	217.992	215.968	214.722	241.016
GCA^{30}	153.663	150.708	147.753	170.529
GAC^{30}	123.142	119.901	124.762	135.833
CGA^{30}	198.007	195.562	196.784	221.809
CAG^{30}	206.229	205.373	202.195	226.575
AGC^{30}	133.066	131.360	128.289	147.191
ACG^{30}	151.538	149.997	148.713	168.798
$(G_{12})^{45}$	50.130	50.277	50.424	55.792
$(A_{12})^{45}$	161.809	158.919	159.497	182.385
$(C_{12})^{45}$	158.162	159.743	158.953	174.400
GCA^{45}	120.062	118.271	120.958	133.093
GAC^{45}	96.095	94.051	98.140	107.513
CGA^{45}	148.576	147.931	146.962	164.695
CAG^{45}	149.018	147.983	146.948	164.114
AGC^{45}	97.458	96.945	96.175	108.351
ACG^{45}	109.117	111.596	109.117	121.354
GCA*	100.746	101.784	102.879	106.366
GAC*	108.250	106.334	107.292	112.770
CGA*	105.850	105.123	107.479	112.004
CAG*	106.225	107.513	107.786	112.770
AGC*	106.943	105.663	106.615	112.004
ACG*	100.137	101.048	100.086	106.366

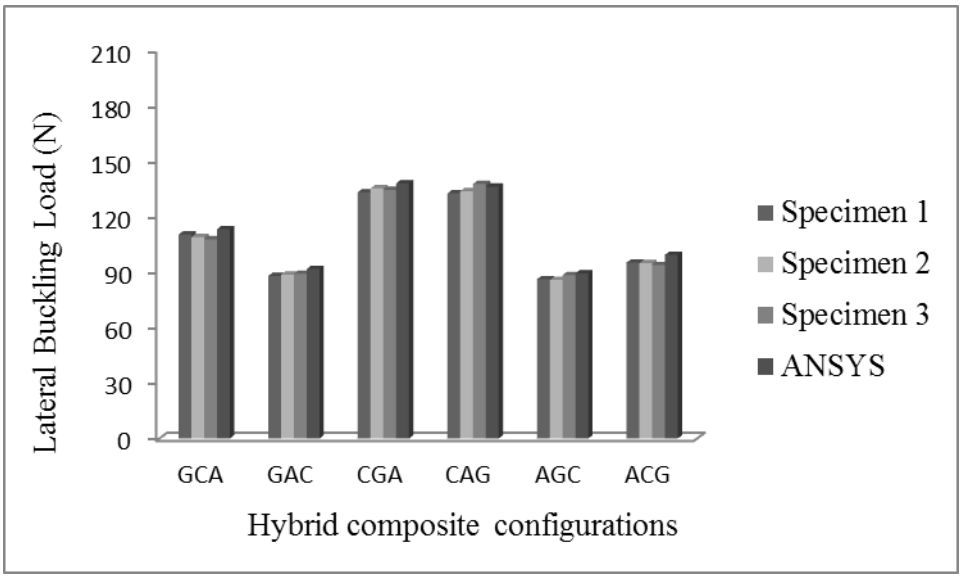
Lateral Buckling Load (N)
210
180
150
120
90
60
30
0
GCA
GAC
CGA
CAG
AGC
ACG
Hybrid composite configurations
Specimen 1
Specimen 2
Specimen 3
ANSYS

(a)

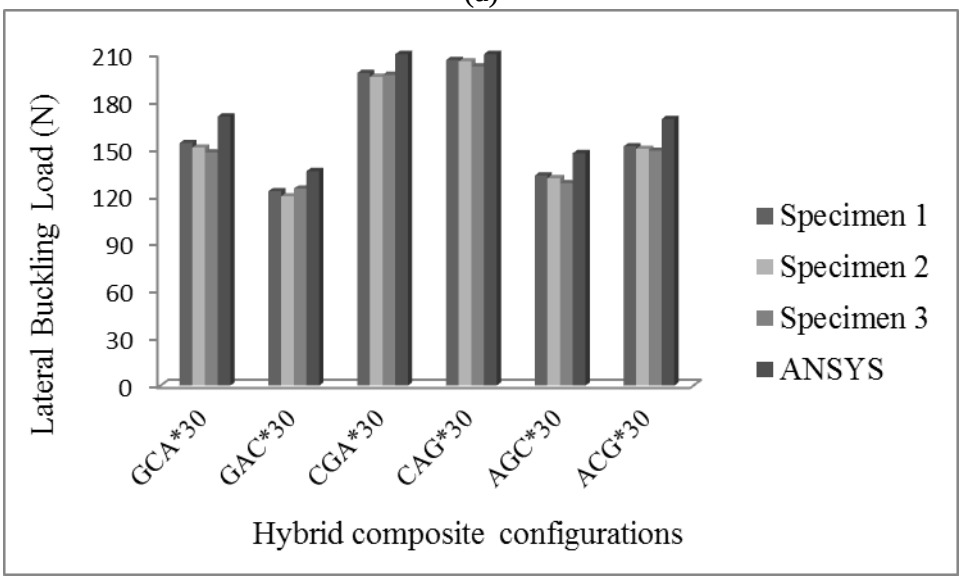
Lateral Buckling Load (N)
210
180
150
120
90
60
30
0
GCA*30
GAC*30
CGA*30
CAG*30
AGC*30
ACG*30
Hybrid composite configurations
Specimen 1
Specimen 2
Specimen 3
ANSYS

(b)

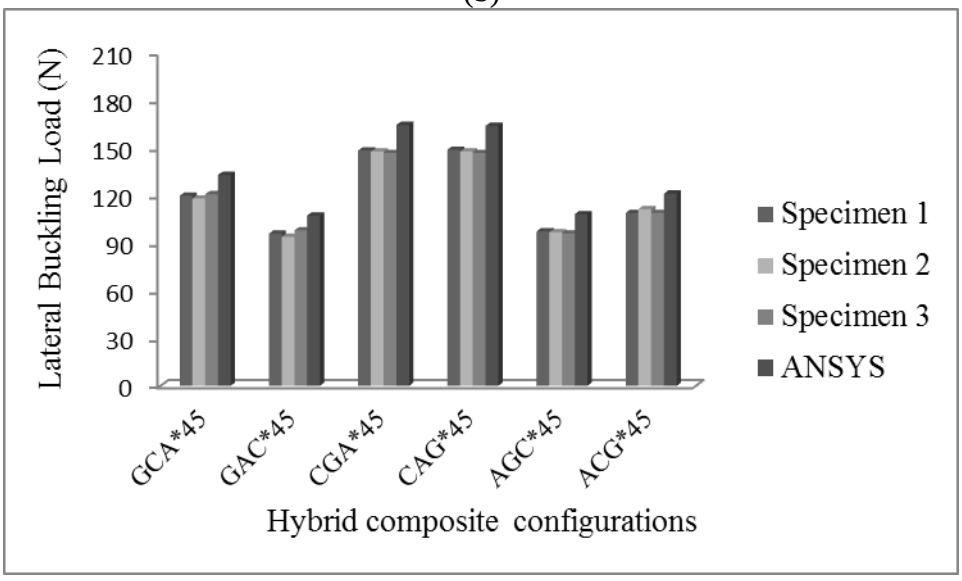
Lateral Buckling Load (N)
210
180
150
120
90
60
30
0
GCA*45
GAC*45
CGA*45
CAG*45
AGC*45
ACG*45
Hybrid composite configurations
Specimen 1
Specimen 2
Specimen 3
ANSYS

(c)

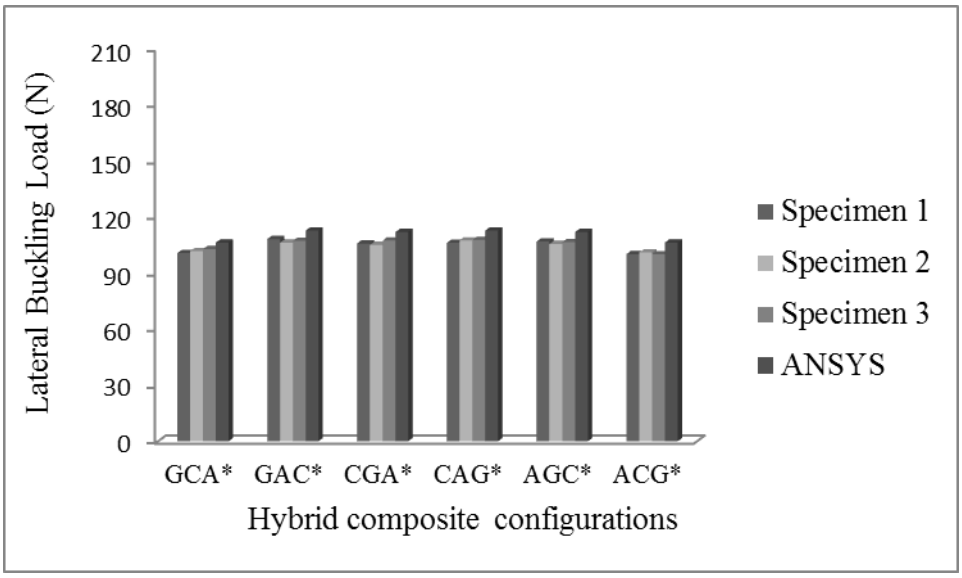

(d)

Figure 7.6 Comparison of lateral buckling experimental and numerical (ANSYS) results for configurations of a) $[(0/90)_3]_s$, b) $[(30/-60)_3]_s$, c) $[(45/-45)_3]_s$, d) $[(0/90)_3]_s$ un-symmetrical.

7.4 Parametric Study on Numerical Buckling and Lateral Buckling

A parametric study is also performed to see effects of various parameters such as hybrid plate thickness, plate aspect ratio, type, size and location of cutouts on buckling and lateral buckling are examined. Plates containing various cut-outs have been modeled and effects of singularity (since cutout causes the singularity and generally used as a design requirement) on buckling and lateral buckling loads are investigated. Square, circular, triangular and elliptical cutouts are used by considering different sizes. Hybrid configurations are abbreviated again as given Table 7.3 to prevent confusion on the graphics.

Table 7.3 New Abbreviations of Hybrid Composite Configurations

Naming	Abbreviations	Naming	Abbreviations
GCA	4	GCA*	10
GAC	5	GAC*	11
CGA	6	CGA*	12
CAG	7	CAG*	13
AGC	8	AGC*	14
ACG	9	ACG*	15

7.4. 1 Numerical Parametric Study on Buckling

In this section, effects of different parameters on buckling are given. To see different effects of various parameters such as hybrid plate thicknesses (HTK), plate aspect ratio (L/W and W/L), cutout type, size and location of cutouts, they are investigated separately and given the below sub-sections.

7.4.1.1 The effects of hybrid plate thickness on buckling

Influences of HTK on lateral buckling are examined taking width (W) equals to 30 mm and length (L) equals to 150 mm. Thicknesses of all hybrid configurations are increased by changing number of layers as; 12, 24, 36 and 48 layers. Change of buckling load in terms of increase of HTK is given in the Figure 7.7. It is seen in the Figure 7.7 that buckling load increases nonlinearly with increasing HTK for both un-symmetrical and symmetrical configurations. It can be concluded that 6 and 7 have the highest buckling loads and 8 has the smallest buckling loads for symmetrical configurations. For un-symmetrical configurations, it can be concluded that their values change nearly the same ratio with respect to HTK increase but their maximum values are smaller than the ones of symmetrical configurations.

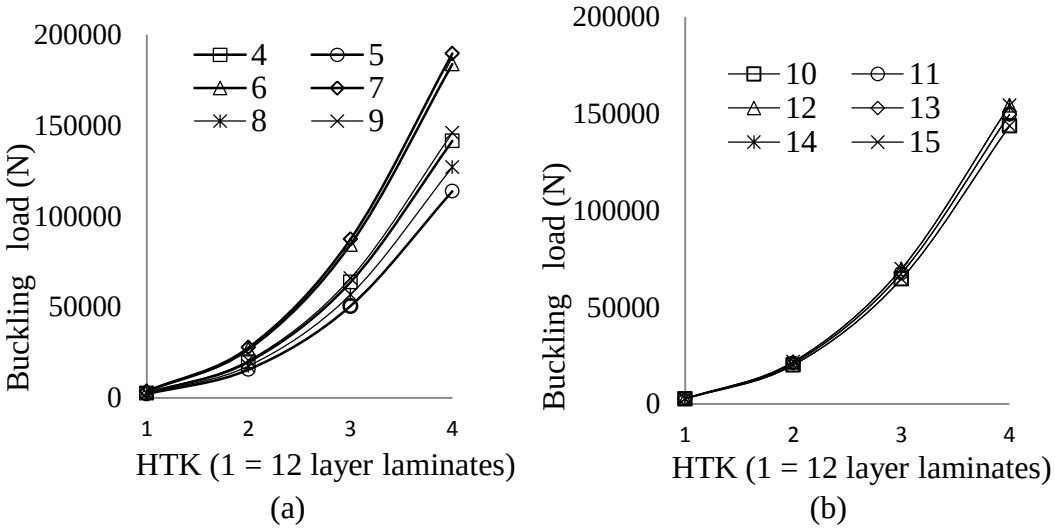

Figure 7.7 The effects of HTK on buckling load (a) symmetrical hybrid configurations, (b) unsymmetrical hybrid configurations.

7.4.1.2 The effect of Hybrid plate sizes on buckling

Effects of hybrid plate sizes are examined by considering width of hybrid plates (W) constant and length (L) changing and vice versa.

Four different widths (15, 30, 45 and 60 mm) are used in the analyses considering L equal to 150 mm. Also four different lengths (150, 300, 450 and 600 mm) are used in the analysis considering W equals to 30 mm. Change of buckling load in terms of W/L ratio is given in Figure 7.8 and change of buckling load in terms of L/W ratio is given in Figure 7.9.

It is seen in the Figure 7.8 that buckling load increases with increasing of W/L ratio and 6 and 7 have the highest buckling loads and 8 has the smallest buckling load. Also it is seen in the Figure 7.9 that buckling load decreases with increasing of L/W ratio and 7 has the highest buckling load and 5 has the smallest buckling load.

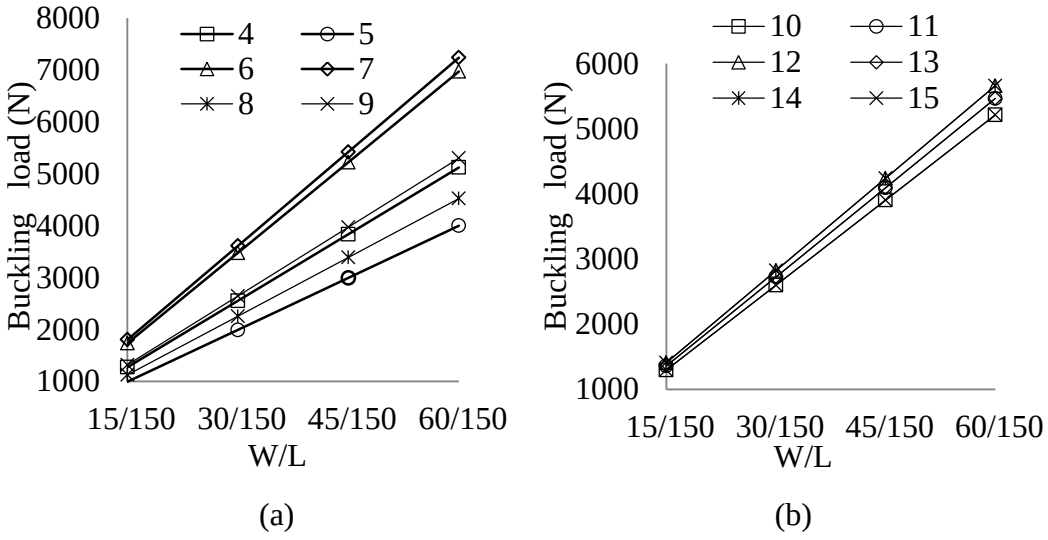

Figure 7.8 The effects of W/L ratio on buckling load (a) symmetrical hybrid configurations, (b) un-symmetrical hybrid configurations.

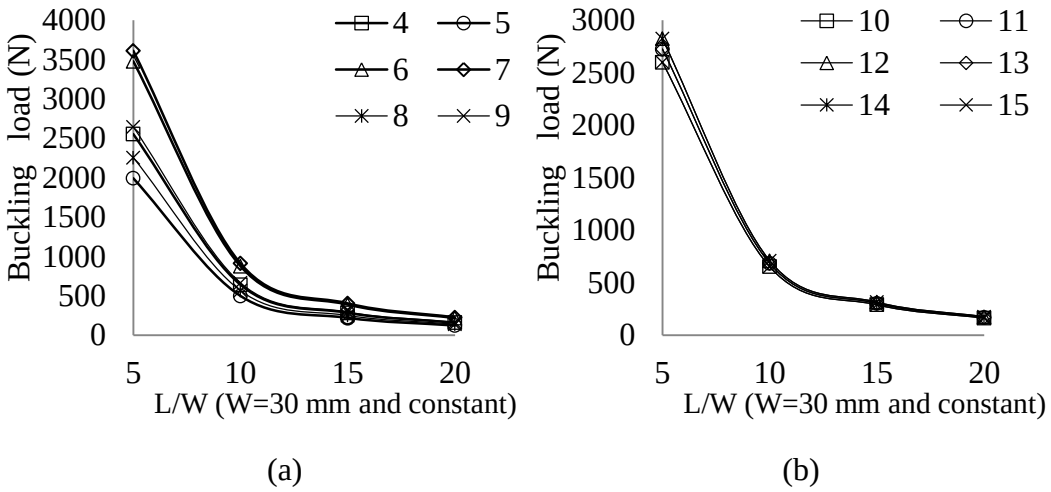

Figure 7.9 The effects of L/W ratio on buckling load (a) symmetrical hybrid configurations, (b) un-symmetrical hybrid configurations.

7.4.1.3 The effects of cutout type, size and location of cutouts on buckling of hybrid plates

Effects of various cutouts on buckling loads are also investigated for all hybrid configurations. Square, circular, triangular and elliptical cutouts are used by considering different sizes (A is used for the size of a cutout). Cut-outs used in the analyses are given in Figure 7.10. P_{cr} is used for critical buckling load of hybrid plates with cutout and $P_{cr}^{w\text{-}c}$ is used for critical buckling loads of plates without a cutout. Also w-c, s-c, c-c, t-c and e-c stand for without cutout, square cutout, circular cutout, triangular cutout and elliptical cutout, respectively.

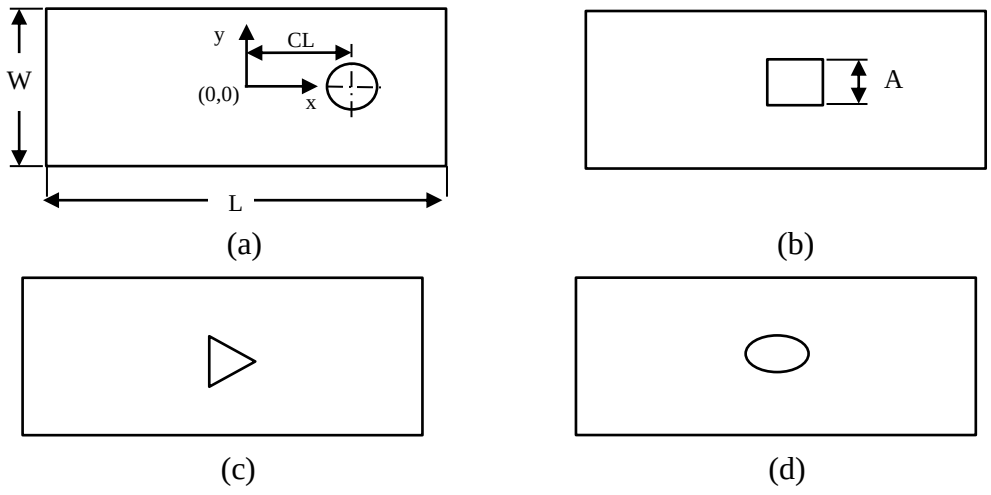

Figure 7.10 Cutouts used in the analyses (a) circular, (b) square, (c) triangular, (d) elliptical

Change of P_{cr}/P_{cr}^{w-c} ratio with respect to cutout types are given in Figure 7.10. In this Figure, 0, 1, 2, 3 and 4 are used for circular, square, triangular and elliptical cutouts, respectively. One side (A) of the square cutout is taken as 15 mm and for the other cutout types, areas are kept constant using suitable side parameters. The elliptic cutout aspect ratio is taken as 0.5.

As can be seen in the Figure 7.11, for all hybrid configurations, P_{cr}/P_{cr}^{w-c} ratio decreases when a cut-out is opened. In other words, opening a cut-out decreases the buckling strength of the plate. But, it is also seen that decrease of buckling load having elliptical cutout (4) is less than the others and decrease with square cutout is the highest. So it can be concluded that the elliptical cutout is the best and square cutout is the worst cutout type for buckling load. And if hybrid configurations are compared, it is seen that P_{cr}/P_{cr}^{w-c} for 4 and 5 is higher than the others which means their buckling strength is decreased less than the others when a cutout is opened.

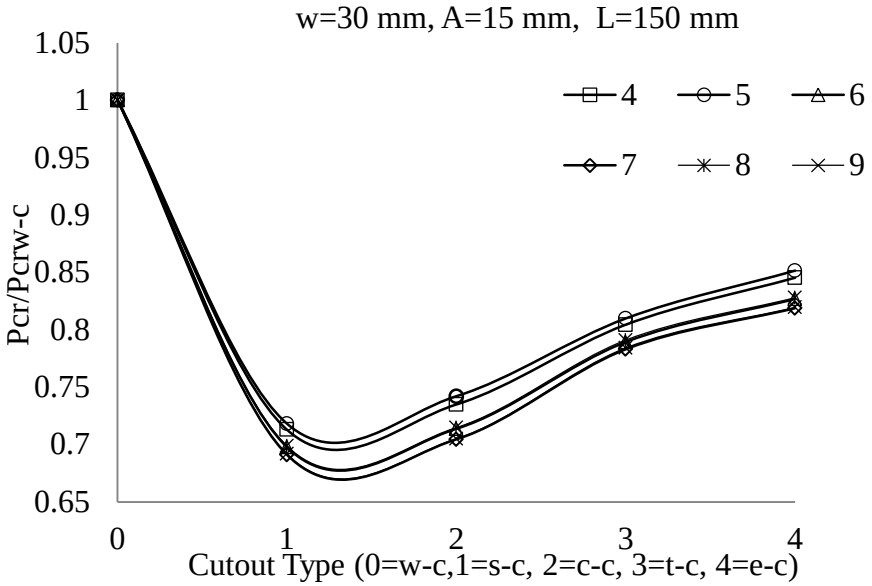

(a)

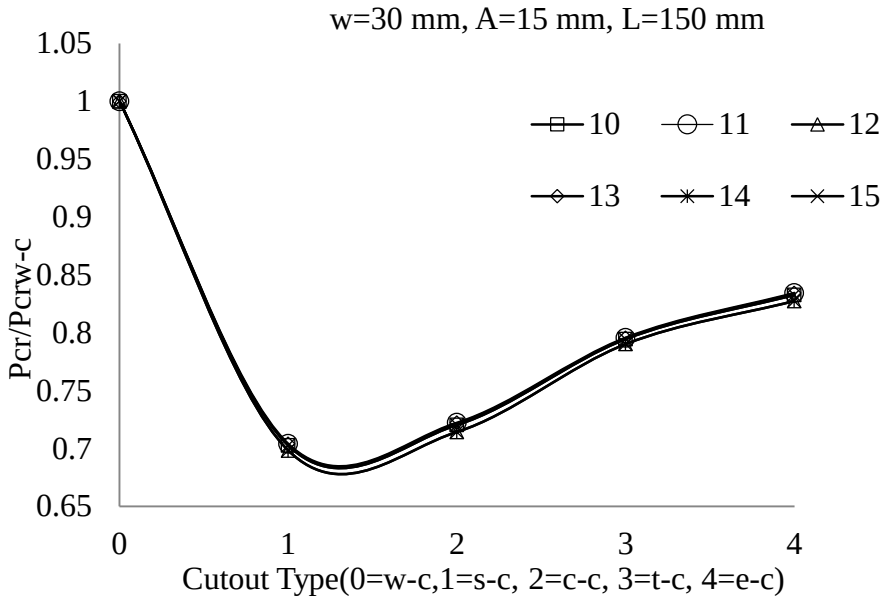

(b)

Figure 7.11 The effects of cutout type on buckling load (a) symmetrical hybrid configurations, (b) un-symmetrical hybrid configurations.

Also effects of cutout sizes on buckling are investigated. For this purpose, square cutout type is used and 4 different cutout sizes are used considering W and L constant (30 mm and 150 mm, respectively). The used sizes of cutouts are 5, 10, 15, 20 mm.

Change of $P_{cr}/P_{cr}^{w\text{-}c}$ ratio for square cutout with respect to increase of A/W ratio is given in Figure 7.12. As can be seen in this figure, for hybrid configurations, $P_{cr}/P_{cr}^{w\text{-}c}$ ratio decreases when cutout size (A/W ratio) is increased. 7 is the best and 5 is the worst configurations for buckling load with respect to increase of A/W ratio. So the effects of cutout size (importance of cutout size) on buckling increases when A/W ratio is increased.

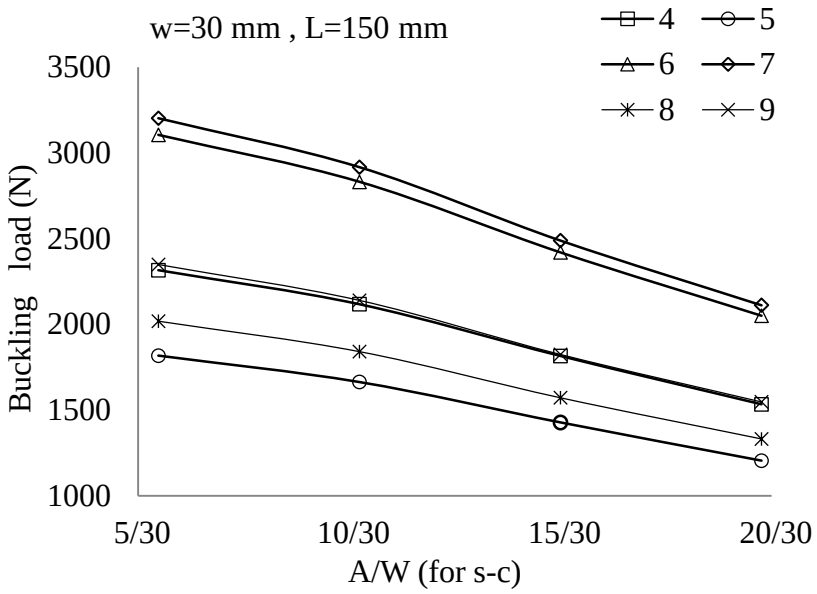

(a)

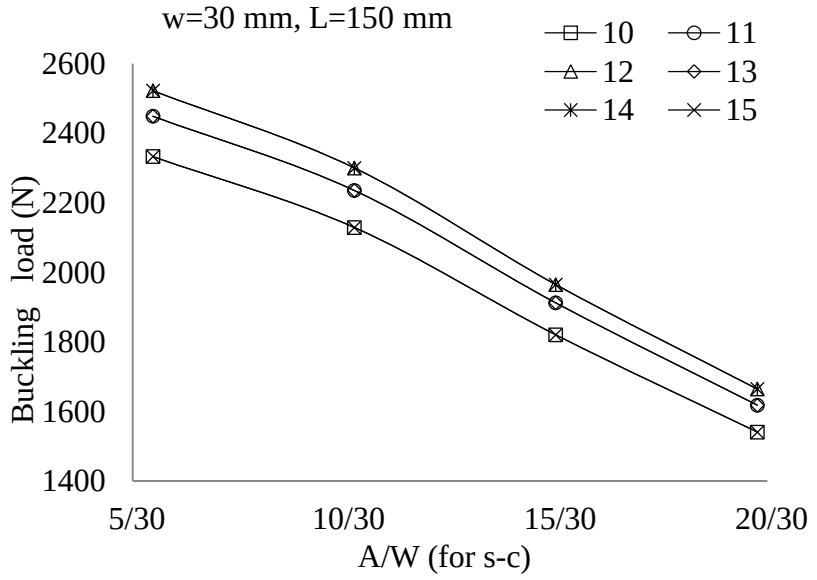

(b)

Figure 7.12 The effects of A/W ratio on buckling load for square cutout (a) symmetrical hybrid configurations, (b) un-symmetrical hybrid configurations.

In order to investigate the effect of cutout location (CL), center of the plate (L=150 mm and W= 30 mm) is taken as origin and cutout is moved on x direction from -60 mm to +60 mm as given in Figure 7.10. The effects of CL on the buckling load are given in Figure 7.13. It is seen that lateral buckling loads and $P_{cr}/P_{cr}^{w\text{-}c}$ ratio are minimum at center of the plate and maximum at the center of half plate (nearly) from left side and right side. As can be seen in Figure 7.13 (a) and Figure 7.13 (c), buckling loads of symmetrical and un-symmetrical configurations change with

change of CL. For symmetrical configurations, 6 and 7 have highest buckling loads, and 5 and 8 have smaller buckling loads in all locations. However, when Pcr/P_{cr}^{w-c} is considered (Figure 7.13 (b) and 7.13(d)), it can be concluded that 5 has highest P_{cr}/P_{cr}^{w-c} ratio. In other words, decrease of buckling strength of 5 with cutout is less than the others.

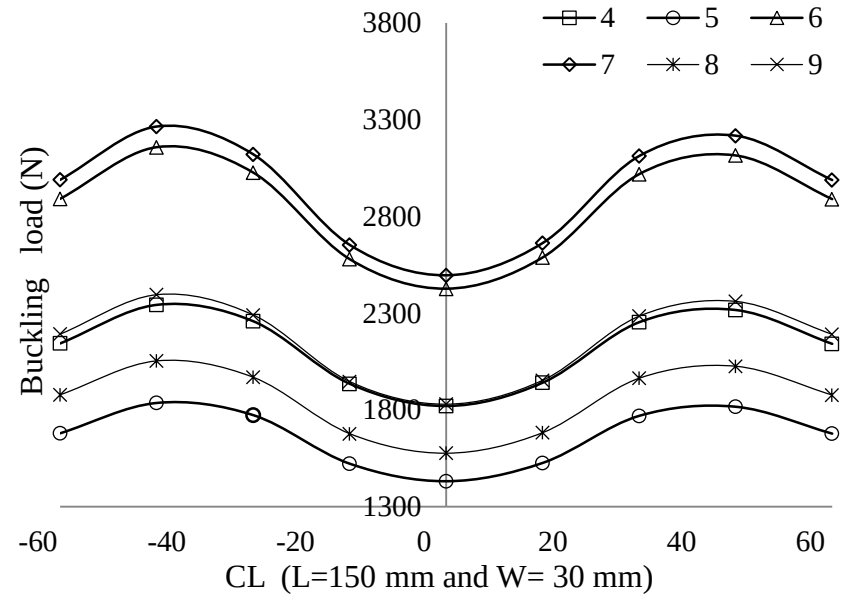

(a)

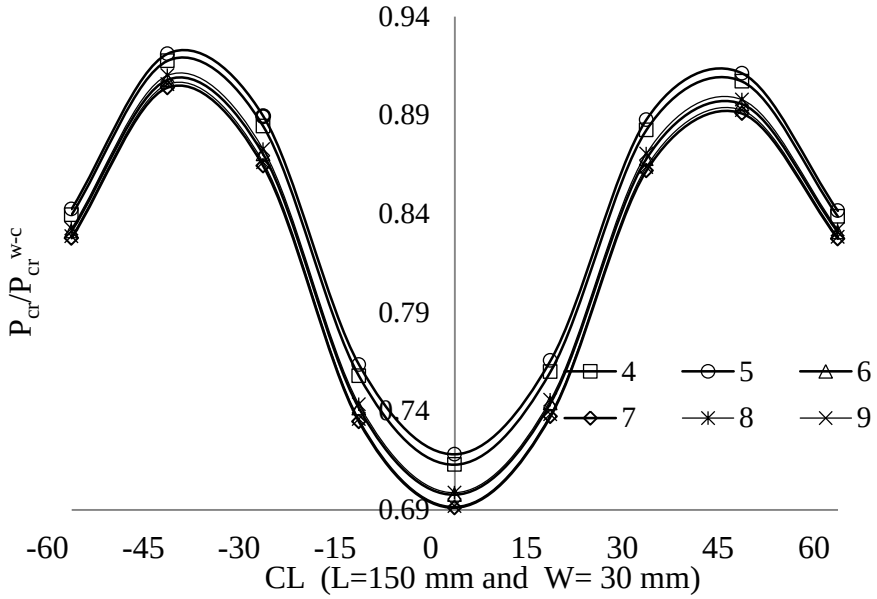

(b)

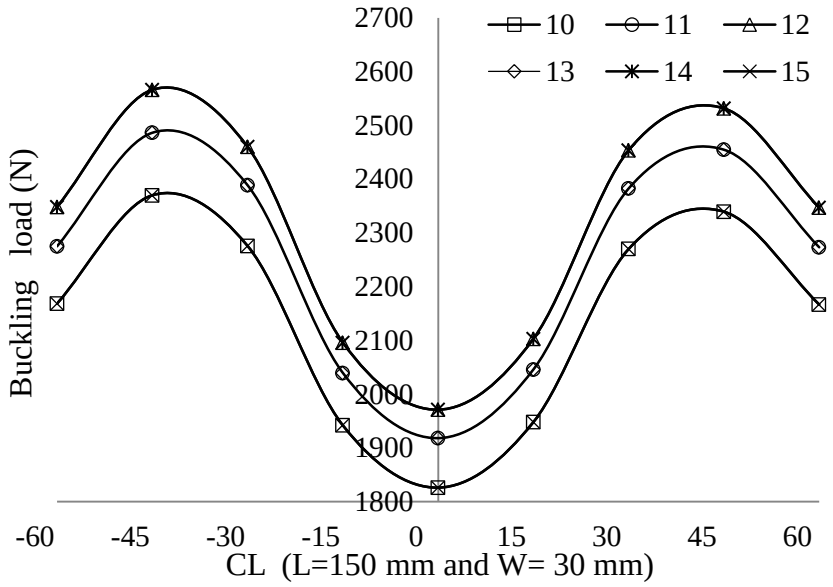

(c)

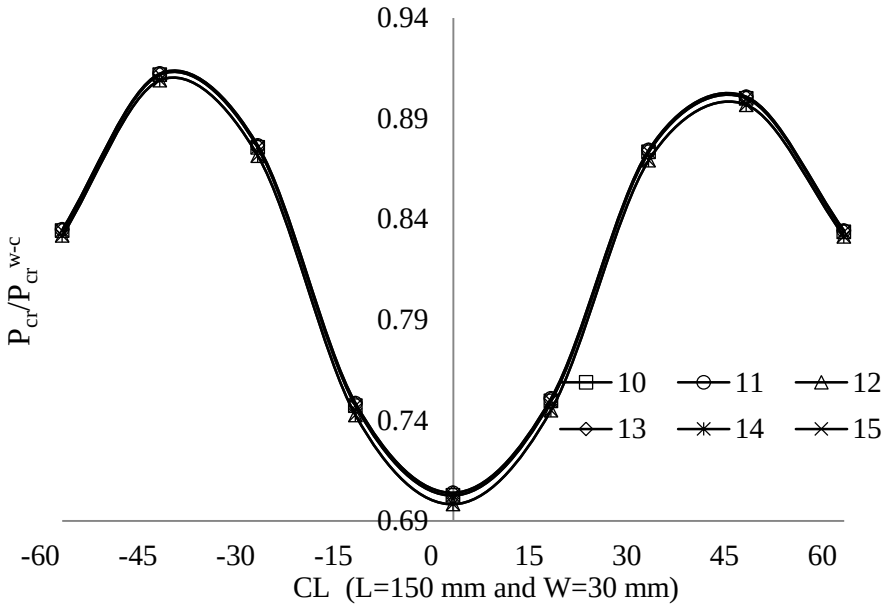

(d)

Figure 7.13 The effects of cut-out location on buckling load for square cutout (a) buckling loads of symmetrical hybrid configurations, (b) P_{cr}/P_{cr}^{w-c} ratio of symmetrical hybrid configurations, (c) buckling loads of un-symmetrical hybrid configurations, (d) P_{cr}/P_{cr}^{w-c} ratio of un-symmetrical hybrid configurations

7.4.2 Numerical Parametric Study on Lateral Buckling

Effects of various parameters such as hybrid plate thickness, plate aspect ratio, cutout type, size and location of cutouts on lateral buckling are also examined. In this section, these effects are given.

7.4.2.1 The effect of hybrid plate thickness on lateral buckling

Influences of HTK on lateral buckling are examined taking W equals to 30 mm and L equals to 150 mm. Thicknesses of all hybrid configurations are increased by changing number of layers as; 12, 24, 36 and 48 layers. In the Figure 7.14, lateral buckling loads with respect to HTK increase are given. This figure shows that lateral buckling load increase nonlinearly with increasing HTK for both un-symmetrical and symmetrical configurations as being in buckling phenomenon given in the previous section. It is seen that 6 and 7 have the highest lateral buckling loads, 5 and 8 have the smallest lateral buckling load for symmetrical configurations (Figure 7.14 (a)). For un-symmetrical configurations, again as being in buckling, lateral buckling loads are changing nearly the same ratio with respect to HTK increase but their maximum values are smaller than the ones of symmetrical configurations (Figure 7.14 (b)).

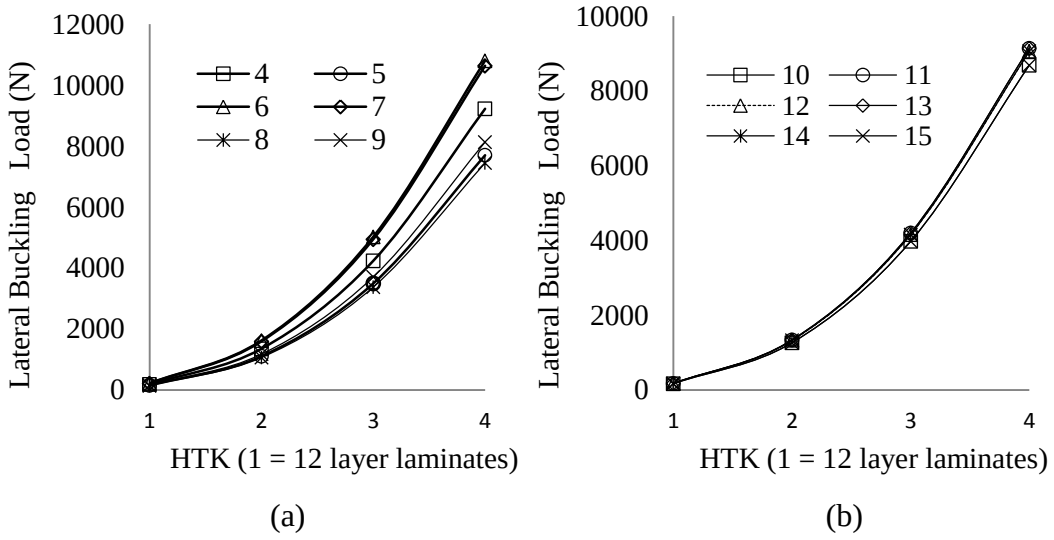

Figure 7.14 The effects of HTK on lateral buckling load (a) symmetrical hybrid configurations, (b) un-symmetrical hybrid configurations.

7.4.2.2 The effects of hybrid plate sizes on lateral buckling

Effects of various plate aspect ratios on lateral buckling are examined considering W constant and L changing and vice versa. The same dimensions which are used in buckling study are considered (W = 15, 30, 45 and 60 mm considering L equals to 150 mm and L = 150, 300, 450 and 600 mm considering W equals to 30 mm).

Effects of W/L ratio on lateral buckling is given in the Figure 7.15 and effects of L/W ratio on lateral buckling is given in the Figure 7.16. It is seen in the Figure 7.15 that lateral buckling loads increase with the increase of W/L ratio. 6 and 7 have the highest lateral buckling loads, 8 has the smallest lateral buckling load with respect to increase of W/L ratio. Also it is seen that lateral buckling load decreases with increase of L/W ratio. 7 has the highest lateral buckling load, 5 and 9 have the smallest lateral buckling loads with respect to increase of L/W ratio.

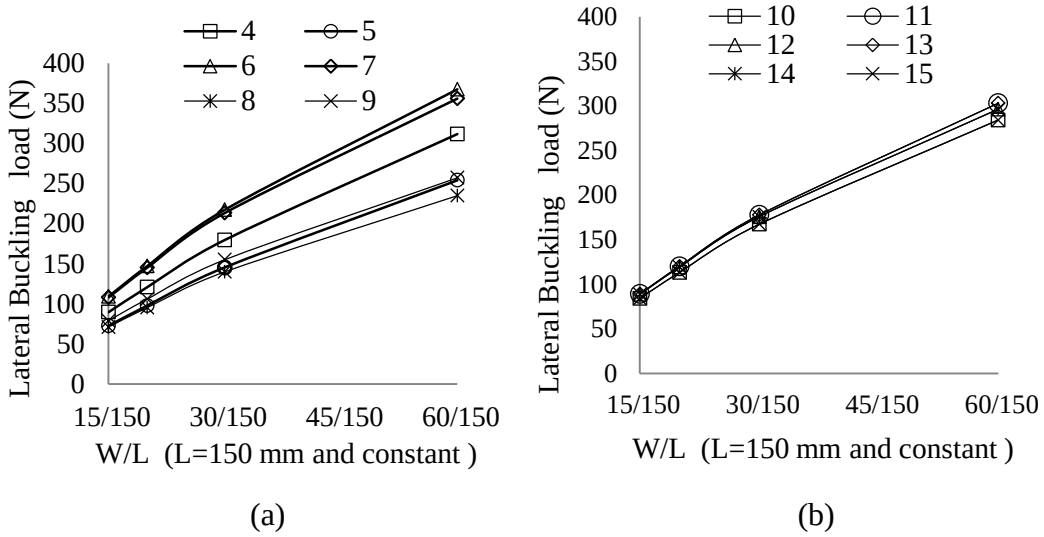

(a) (b)

Figure 7.15 The effects of W/L ratio on lateral buckling load (a) symmetrical hybrid configurations, (b) un-symmetrical hybrid configurations.

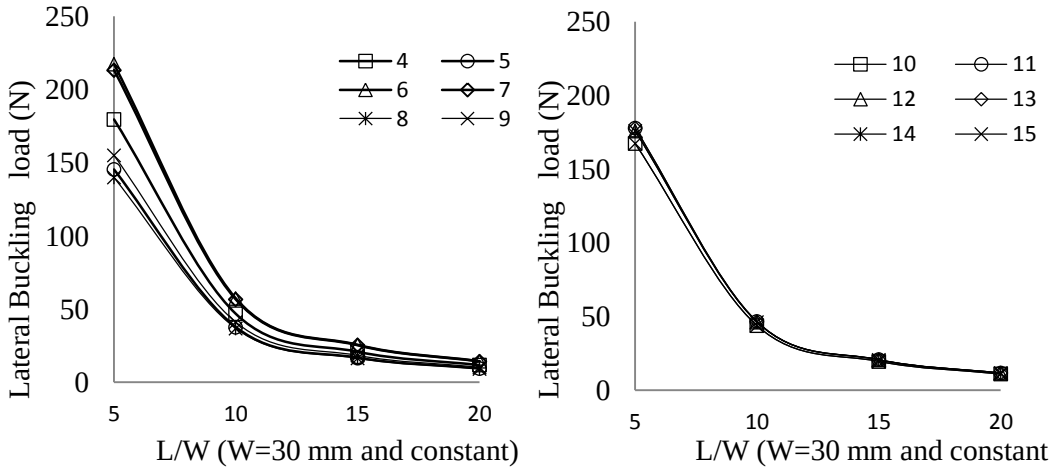

(a) (b)

Figure 7.16 The effects of L/W ratio on lateral buckling load (a) symmetrical hybrid configurations, (b) un-symmetrical hybrid configurations.

7.4.2.3 The effects of cutout type, size and location of cutouts on lateral buckling of hybrid plates

Effects of type, size and location of cutouts on lateral buckling are also investigated. The same cutout types (square, circular, triangular and elliptical) are used again to see effects on lateral buckling. For square cutout one side (A) is taken as 15 mm and for the other cutout types, areas are kept constant using suitable side parameters.

$P_{cr}/P_{cr}^{w\text{-}c}$ ratio with respect to cut-out types are given in the figure 7.17 (0, 1, 2, 3 and 4 are again used for circular, square, triangular and elliptical cutout as in buckling). Figure 7.17 shows that, for all hybrid configurations, opening cut-out causes to decrease of lateral buckling strength of plates as in buckling. It is seen that the elliptical cutout is the best and square and circular cutouts are the worst cutout types for lateral buckling. And if hybrid configurations are compared, it is seen that $P_{cr}/P_{cr}^{w\text{-}c}$ for 9 is higher (different from buckling in which 4 and 5 were best) than the others which means their buckling strength is decreased less than the others.

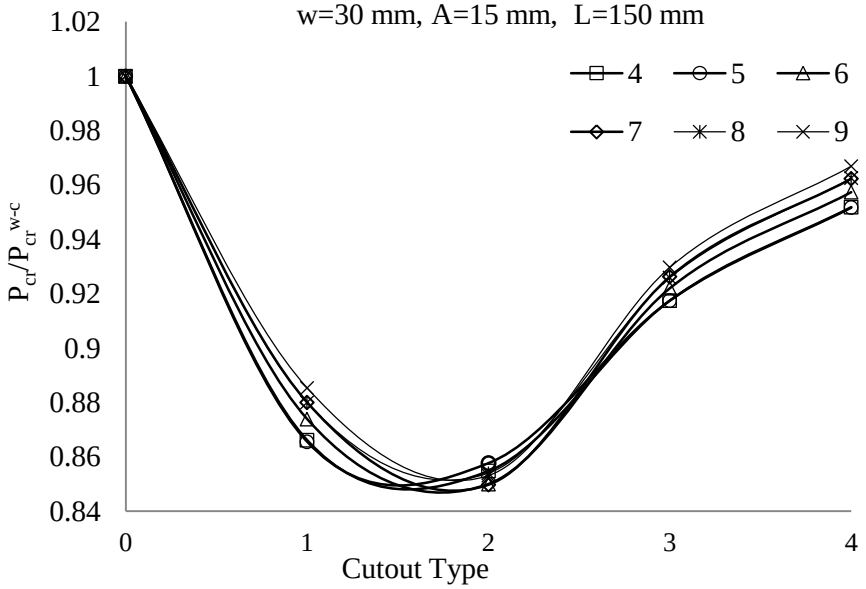

(a)

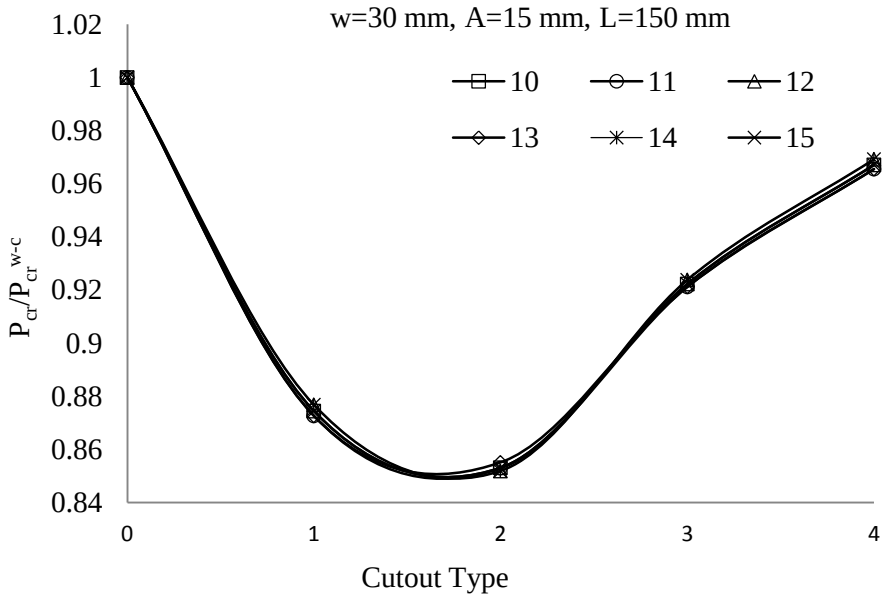

(b)

Figure 7.17 The effects of cutout type on lateral buckling load (a) symmetrical hybrid configurations, (b) un-symmetrical hybrid configurations.

The same cutout sizes which used in buckling are used again to see effects on lateral buckling. For this purpose, square cutout type is used and 4 different cutout sizes are used considering W and L constant (30 mm and 150 mm, respectively). The used sizes of cutouts are 5, 10, 15, 20 mm.

Effects of increase of A/W ratio on lateral buckling for square cutouts with respect to increase of A/W ratio are given in Figure 7.18. As can be seen in this figure, for hybrid configurations, P_{cr}/P_{cr}^{w-c} ratio decreases when cutout size (A/W ratio) is increased. 6 and 7 are the best, 5 and 8 are the worst configurations for lateral buckling load with respect to increase of A/W ratio.

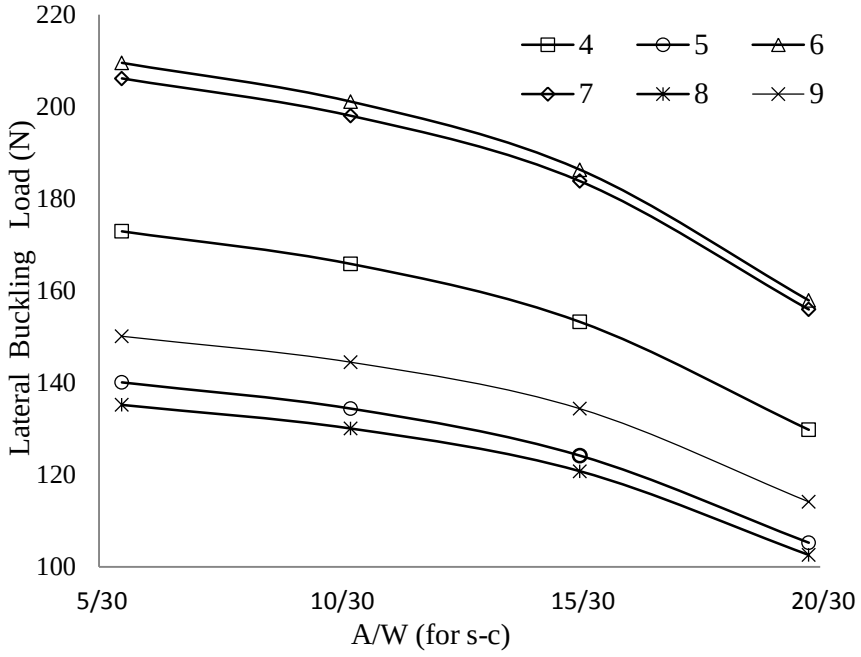

(a)

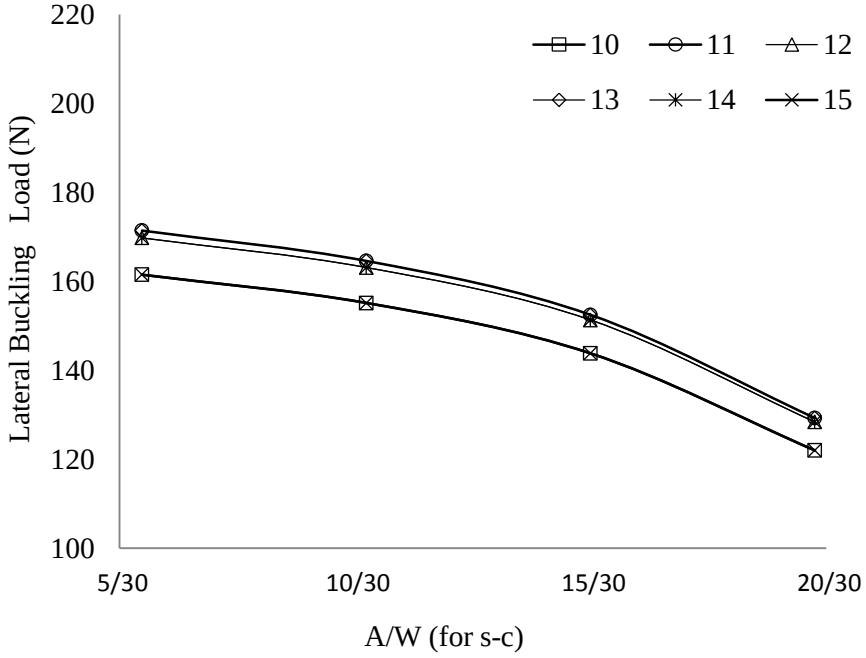

(b)

Figure 7.18 The effects of A/W ratio on lateral buckling load for square cutout (a) symmetrical hybrid configurations, (b) un-symmetrical hybrid configurations.

In order to investigate the effect of cutout location (CL), center of the plate (L=150mm and W=30 mm) is taken as origin. Cutout is moved on x direction from -60 mm to +60 mm. The effects of CL on the lateral buckling load are given in Figure 7.19. It is seen that lateral buckling loads and $P_{cr}/P_{cr}^{w\text{-}c}$ ratio are minimum near the

center of plate and maximum at free side of the plate. As can be seen in Figure 7.19 (a) and Figure 7.19 (c), lateral buckling loads of symmetrical and un-symmetrical configurations change with change of CL. For symmetrical configurations, 6 and 7 have higher buckling loads, and 5 and 8 have smaller lateral buckling loads in all locations. However, when Pcr/P_{cr}^{w-c} is considered (Figure 7.19 (b) and 7.19(d)), It can be concluded that 9 has highest P_{cr}/P_{cr}^{w-c} ratio. In other words, decrease of buckling strength of 9 with cutout is less than the others.

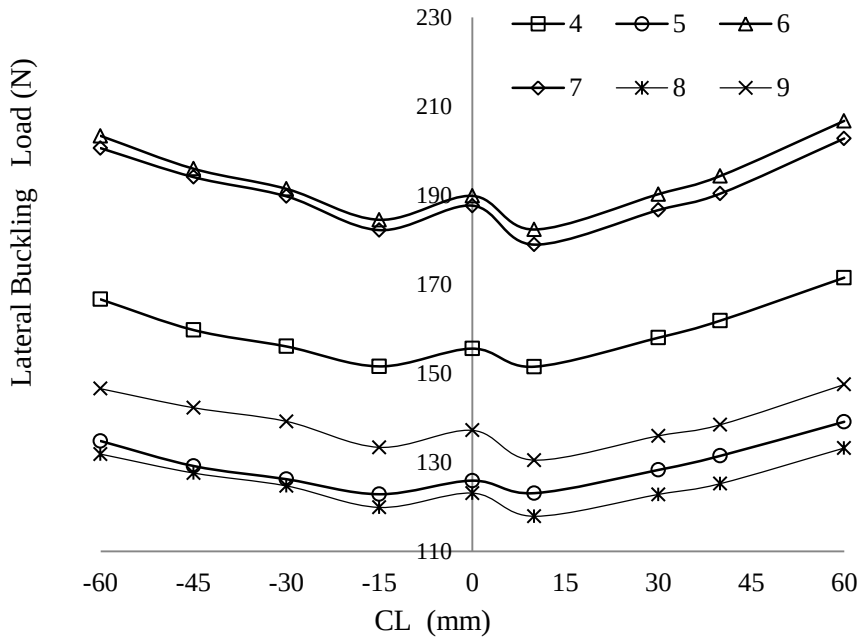

(a)

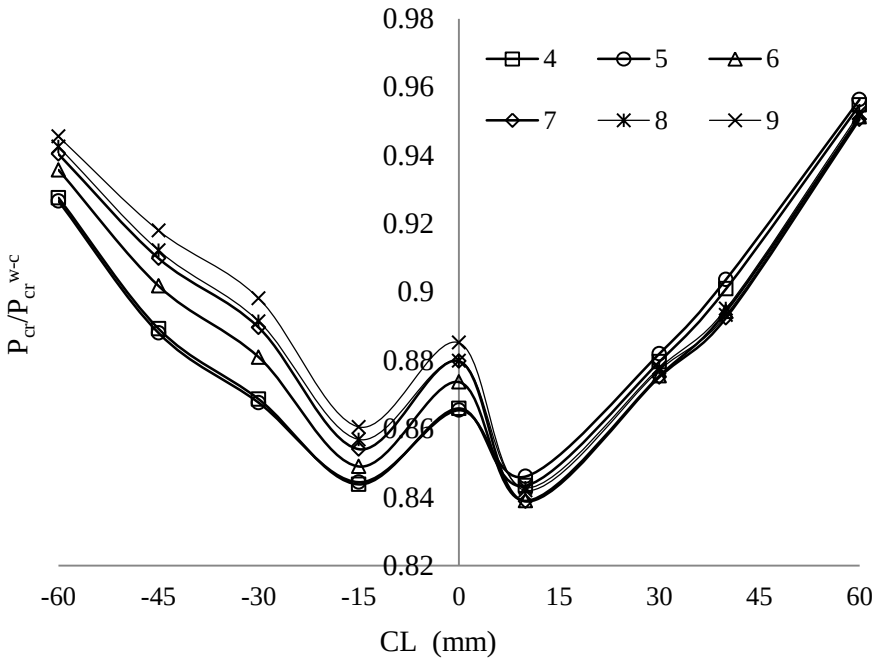

(b)

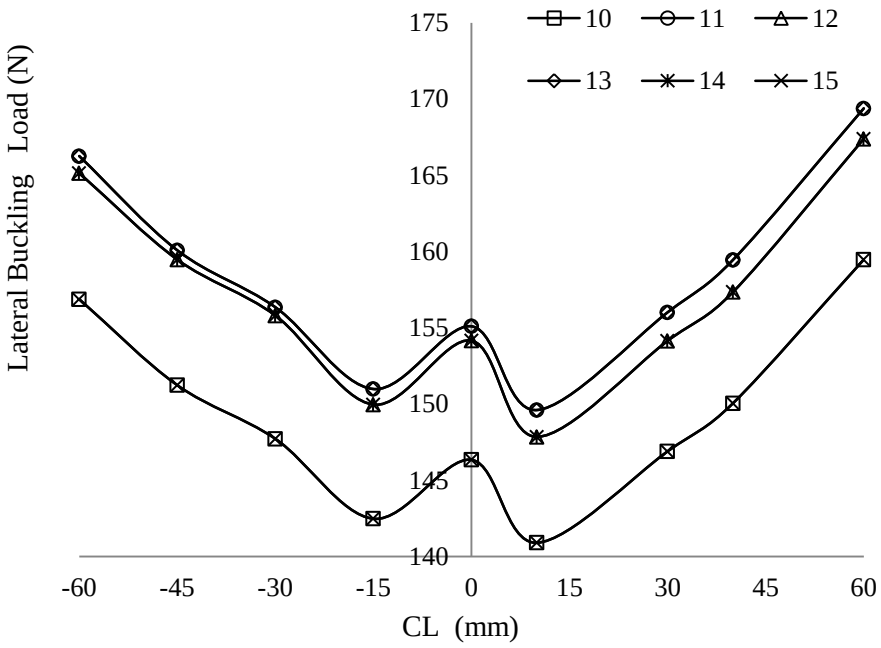

(c)

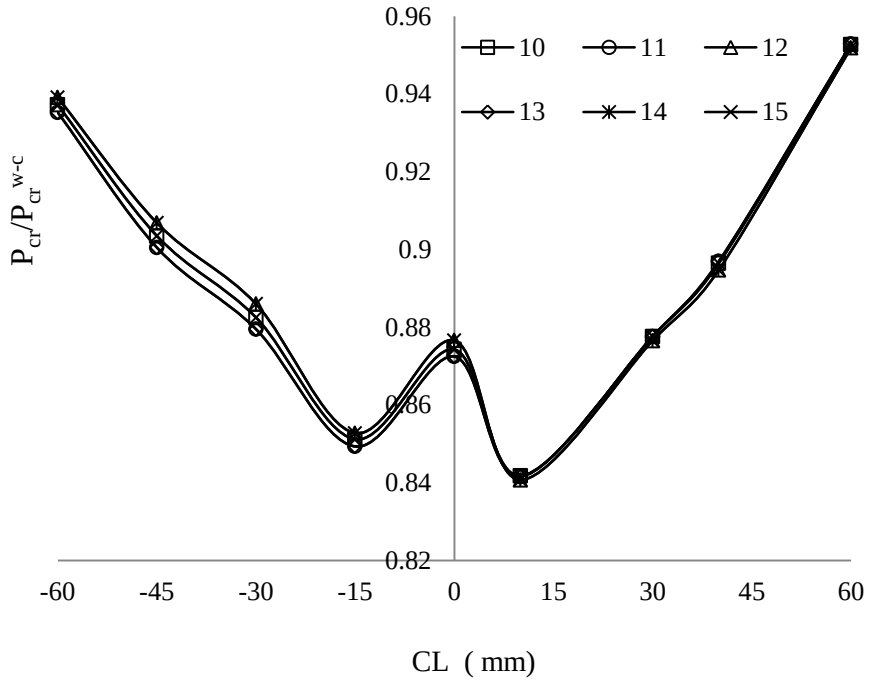

(d)

Figure 7.19 The effects of cut-out location on lateral buckling load for square cutout (a) lateral buckling loads of symmetrical hybrid configurations, (b) P_{cr}/P_{cr}^{w-c} ratio of symmetrical hybrid configurations, (c) lateral buckling loads of un-symmetrical hybrid configurations, (d) P_{cr}/P_{cr}^{w-c} ratio of un-symmetrical hybrid configurations

CHAPTER 8

CONCLUSION

In this study, hybrid composite plates have been produced using different combinations of Carbon, S-glass and Aramid fibers with epoxy resin and effects of fiber types and their combinations on the buckling and lateral buckling have been investigated. In the production part, vacuum supported production unit (has been designed and produced) is used. Then buckling and lateral buckling loads of produced hybrid composite plates have been determined with different fiber orientation angles with symmetrical and unsymmetrical ply orientations. Also numerical studies have been performed to compare with experimental studies. A parametric study is also performed to see effects of effects of hybrid plate thickness, plate aspect ratio, cutout type, size and location of cutouts on buckling and lateral buckling are also examined. Plates containing various cut-outs have been modeled and effects of singularity on buckling and lateral buckling loads for all hybrid configurations are investigated. Main results can be summarized as:

- Buckling and lateral buckling characteristics were significantly affected by the replacement of fiber types.
- For $[(0/90)_3]_s$ symmetrical hybrid configuration CAG, for $[(30/-60)_3]_s$ symmetrical hybrid configuration CGA^{30}, for $[(45/-45)_3]_s$ symmetrical hybrid configuration CGA^{45} and for un-symmetrical $[(0/90)_6]_{us}$ hybrid configuration CGA* has the highest buckling loads.
- For $[(0/90)_3]_s$ symmetrical hybrid configuration GAC, for $[(30/-60)_3]_s$ symmetrical hybrid configuration GAC ^{30}, for $[(45/-45)_3]_s$ symmetrical hybrid configuration GAC ^{45} and for un-symmetrical $[(0/90)_3]_s$ hybrid configuration GAC* has the smallest buckling loads.
- CAG (having $[(0/90)_3]_s$ ply orientation) has the highest and CGA^{45} (close to CGA^{30}) has the lowest buckling load and CGA* has higher buckling load

- from CGA^{45} and CGA^{30}, and has smaller buckling load from CAG. In other words, CAG is the most designable with respect to buckling characteristic.
- Buckling load of CAG is nearly 55 % higher than CGA^{30} and CGA^{45}. It is also nearly 24 % higher than CGA*.
- Buckling loads were increased using fibers which have higher stiffness in the upper layers as being in the CAG and plates which produced having $[(0/90)_3]_s$ stacking sequences have higher buckling strength
- For $[(0/90)_3]_s$ symmetrical hybrid configuration CGA, for $[(30/-60)_3]_s$ symmetrical hybrid configuration CAG^{30}, for $[(45/-45)_3]_s$ symmetrical hybrid configuration CAG^{45} and for un-symmetrical $[(0/90)_6]_{us}$ hybrid configuration GAC* has the highest lateral buckling loads.
- $CAG^{30\ has}$ the highest and GAC* has the lowest lateral buckling load and CAG^{45} has higher lateral buckling load from GAC* and CGA. In other words, CAG^{30} is the most designable with respect to lateral buckling characteristic.
- Stiffness (Young modulus which effects stiffness) and shear properties (exactly shear modulus (G_{12})) are affecting lateral buckling characteristics. So configurations which produced using fibers which have higher stiffness and higher shear properties in the upper layers increase the lateral buckling strength.
- Hybrid plates having $[(30/-60)_3]_s$ and $[(45/-45)_3]_s$ stacking sequences have higher lateral buckling strength with respect to configurations which produced having $[(0/90)_3]_s$ stacking sequences
- Critical buckling loads of hybrid configurations due to numerical results are in the same order with the results of experiments. For $[(0/90)_3]_s$ stacking sequences, this order is CAG, CGA, ACG, GCA, AGC, GAC, respectively. For $[(30/-60)_3]_s$ stacking sequences, this order is CGA^{30}, CAG^{30}, GCA^{30}, ACG^{30}, GAC^{30} and AGC^{30}, respectively. Finally for $[(45/-45)_3]_s$ stacking sequences, this order is CGA^{45}, CAG^{45}, GCA^{45}, ACG^{45}, GAC^{45} and AGC^{45}, respectively.
- For $[(0/90)_3]_s$ stacking sequences, they can be ordered from the highest lateral buckling load to the smallest buckling load as CGA, CAG, GCA, ACG, GAC and AGC, respectively. For $[(30/-60)_3]_s$ stacking sequences, this order is

CAG^{30}, CGA^{30}, GCA^{30}, ACG^{30}, AGC^{30} and GAC^{30}, respectively. Finally for $[(45/-45)_3]_s$ stacking sequences, this order is CAG^{45}, CGA^{45}, GCA^{45}, ACG^{45}, AGC^{45}, and GAC^{45}, respectively.

- Buckling load increases nonlinearly with increasing HTK for both un-symmetrical and symmetrical configurations. 6 (CGA) and 7 (CAG) have the highest buckling loads and 8 (AGC) has the smallest buckling loads for symmetrical configurations. For un-symmetrical configurations, their values change nearly the same ratio with respect to HTK increase but their maximum values are smaller than the ones of symmetrical configurations.
- Buckling load increases with increasing of W/L ratio and 6 and 7 have the highest buckling loads and 8 has the smallest buckling load.
- Buckling load decreases with increasing of L/W ratio and 7 has the highest buckling load and 5 has the smallest buckling load.
- For all hybrid configurations, P_{cr}/P_{cr}^{w-c} ratio decreases when a cut-out is opened. In other words, opening a cut-out decreases the buckling strength of the plate. Decrease of buckling load having elliptical cutout (4) is less than the others and decrease with square cutout is the highest. Elliptical cutout is the best and square cutout is the worst cutout type for buckling load. And if hybrid configurations are compared, it is seen that P_{cr}/P_{cr}^{w-c} for 4 and 5 is higher than the others which means their buckling strength is decreased less than the others when a cutout is opened.
- For hybrid configurations, P_{cr}/P_{cr}^{w-c} ratio decreases when cutout size (A/W ratio) is increased. 7 (CAG) is the best and 5 is the worst configurations for buckling load with respect to increase of A/W ratio. So the effects of cutout size (importance of cutout size) on buckling increases when A/W ratio is increased.
- For buckling phenomenon, P_{cr}/P_{cr}^{w-c} ratio is minimum at center of the plate and P_{cr}/P_{cr}^{w-c} ratio is maximum at the center of half plate (nearly) from left side or right side. For symmetrical configurations, 6 and 7 have highest buckling loads, and 5 and 8 have smaller buckling loads in all locations. However, when Pcr/P_{cr}^{w-c} is considered, it can be concluded that 5 has highest P_{cr}/P_{cr}^{w-c} ratio. In other words, decrease of buckling strength of 5 with cutout is less than the others.

- Lateral buckling load increase nonlinearly with increasing HTK for both un-symmetrical and symmetrical configurations as being in buckling phenomenon given in the previous section. 7 (CAG) and 6 (CGA) have the highest lateral buckling loads, and 5 (GAC) and 8 (AGC) have the smallest lateral buckling load for symmetrical configurations. For un-symmetrical configurations, again as being in buckling, lateral buckling loads are changing nearly the same ratio with respect to HTK increase but their maximum values are smaller than the ones of symmetrical configurations.
- Lateral buckling loads increase with the increase of W/L ratio. 6 (CGA) and 7 (CAG) have the highest lateral buckling loads and 8 has the smallest lateral buckling load with respect to increase of W/L ratio. Lateral buckling load decreases with increase of L/W ratio. 7 has the highest lateral buckling load and 5 (GAC) and 9 (ACG) have the smallest lateral buckling loads with respect to increase of L/W ratio
- For all hybrid configurations, opening cut-out causes to decrease of lateral buckling strength of plates as in buckling. Elliptical cutout is the best and square cutout is the worst cutout type for lateral buckling. And if hybrid configurations are compared, it is seen that P_{cr}/P_{cr}^{w-c} for 9 (ACG) is higher (different from buckling in which 4 (GCA) and 5 (GAC) were best) than the others which means their buckling strength is decreased less than the others.
- For hybrid configurations, P_{cr}/P_{cr}^{w-c} ratio decreases when cutout size (A/W ratio) is increased. 7 (CAG) is the best and 8 (AGC) and 5 (GAC) are the worst configurations for lateral buckling load with respect to increase of A/W ratio.
- For lateral buckling phenomenon, P_{cr}/P_{cr}^{w-c} ratio is minimum near the center of plate and maximum at free side of the plate. 9 (ACG) has higher P_{cr}/P_{cr}^{w-c} ratio at these points.

CHAPTER 9

FUTURE WORKS

This study can be extended in the following aspects:

- Impact and fatigue characteristics of hybrid plates can be determined.
- Hybrid plates can be produced containing different particulate additives to increase mechanical properties of hybrid composites.

CURRICULUM VITAE

PERSONAL INFORMATION

Name and Surname: Eyüp YETER

Natioality: T.C

Email: eyeter@gantep.edu.tr

EDUCATION

	Graduate school	Year
Master	University of Gaziantep Mechanical Eng. Dept.	2010
Bachelor	University of Gaziantep Mechanical Eng. Dept.	2007
High School	Gaziantep Anatolian High school	2002

Work experience

	Place	Enrollment
2010-Present (35.)	University of Gaziantep Mechanical Eng. Dept.	Research assistant
2009- Present	Bitlis Eren University Mechanical Eng. Dept.	Research assistant
2007-2009	Sanko Makina	Product development Engineer

PUBLICATIONS

1. Erklig A., Yeter E., Bulut M. (2013). The effects of cut-outs on lateral buckling behavior of laminated composite beams, *Composite Structures*, **104**, 54–59.

2. Erklig A., Yeter E. (2012). The Effects of Cut-outs on Buckling Behavior of Composite Plates, *Science and Engineering of Composite Materials*, **19(3),** 323–330.

3. Erkliğ A, Yeter E. (2013). On the thermal buckling behavior of laminated hybrid composite plates due to square/circular cut-outs, *Mathematical and Computational Applications* , **18(3),** 548-557.

4. Erklig A., Yeter E. (2013). The Improvements of the Backhoe-Loader Arms, *Modeling and Numerical Simulation of Material Science* , **3(4**), 142-148.

5. Erklig A., Bulut M., Yeter E. (2013). Effects of cutouts on natural frequency of laminated composite plates, *Science and Engineering of Composite Materials*, **20(2)**,179–185.

6. Erklig A., Yeter E. (2011). Kompozit Malzemelere Açılan Dairesel, Kare, Üçgen ve Eliptik Kesitlerin Burkulmaya Etkisinin Sonlu Eleman Yöntemiyle Araştırılması, proceeding of 17th national mechanic conference, Nov., Elazığ, Türkiye.

7. Erklig A., Yeter E., Gülbay M. (2010). Finite Element Analysis of Backhoe-Loader Front Arm, proceeding of 5. Automotive Technologies conference, Bursa, Türkiye, June, 445-452.

FOREIGN LANGUAGE

English

REFERENCES

[1] Kaw, A. K. (2006). Mechanics of Composite Materials. 2nd Edition. London: Taylor & Francis, Inc.

[2] Jones, R.M. (1999). Mechanics of Composite Materials. 2nd Edition. NY: Taylor & Francis.

[3] Armstrong, K. B., Barrett, R. T. (1998). Care and Repair of Advanced Composites. Warrendale, PA: SAE (Society of Automotive Engineers), Inc.

[4] Vinson, JR, Sierakowski, RL. (2004). The Behavior of Structures Composed of Composite Materials. 2nd edition. London: Kluwer Academic Publishers.

[5] Becenen N. (2008). A study for improving structural properties of composite materials with plastic matrix used in tractor companions, a Major Project Report for the Degree of doctor of philosophy in Mechanical Engineering, Namık Kemal University.

[6] Aktas M., Karakuzu R. (2009), Determination of mechanical properties of glass-epoxy Composites in High Temperatures, *Polymer Composites*, **30**, 1437-1441.

[7] Kus R. (2006). Investigation of mechanical properties of gray cast iron composites reinforced with low carbon steel fiber, a Major Project Report for the Degree of doctor of philosophy in Mechanical Engineering, Selçuk University.

[8] Okutan B. (2002). Effects of geometric parameters on the failure strength for pin-loaded multi-directional fiber-glass reinforced epoxy laminate, *Composites: Part B*, **33**, 567–578.

[9] Okutan B., Karakuzu R. (2003). The strength of pinned joints in laminated composites, *Composites Science and Technology*, **63**, 893–905.

[10] Icten B. M., Karakuzu R. (2002). Progressive failure analysis of pin-loaded carbon–epoxy woven composite plates, *Composites Science and Technology*, **62**, 1259–1271.

[11] Icten B. M., Karakuzu R., Toygar M. E. (2006). Failure analysis of woven kevlar fiber reinforced epoxy composites pinned joints, *Composite Structures*, **73**, 443–450.

[12] Karakuzu R., Gulem T., Icten B. M. (2006). Failure analysis of woven laminated glass–vinylester composites with pin-loaded hole, *Composite Structures*, **72**, 27–32.

[13] Karakuzu R., Taylak N., Icten B. M., Aktas M. (2008). Effects of geometric parameters on failure behavior in laminated composite plates with two parallel pin-loaded holes, *Composite Structures*, **85**, 1–9.

[14] Whitworth H. A, Othieno M., Barton O. (2003). Failure analysis of composite pin loaded joints, *Composite Structures*, **59**, 261–266.

[15] Ahn H. S., Kweon J. H., Choi J. H. (2005). Failure of unidirectional-woven composite laminated pin-loaded Joints, *Journal of Reinforced Plastics and Composites*, **24**, 735.

[16] Yılmaz T. (2006). Load bearing properties of pin connected polymer composites, a Major Project Report for the Degree of doctor of philosophy in Mechanical Engineering, Kocaeli University.

[17] Dursun T. (2006). Failure analysis of bolted laminated composite plates, a Major Project Report for the Degree of doctor of philosophy in Mechanical Engineering, Gazi University.

[18] Adin H. (2007). Mechanical analysis of adhesive with bonded inverse z type ties of composite materials, a Major Project Report for the Degree of doctor of philosophy in Mechanical Engineering, Fırat University.

[19] Sen F. (2007). Failure analysis of composite pin-loaded joints under preload moments, a Major Project Report for the Degree of doctor of philosophy in Mechanical Engineering, Dokuz Eylul University.

[20] Sen F., Sayman O. (2009). Experimental Failure Analysis of Two-Serial-Bolted Composite Plates, *Journal of Applied Polymer Science*, **113**, 502–515.

[21] Koruvatan A. (2008). Failure analysis of the laminated composite plates with pin/bolt loaded joints manufactured under various cure temperatures and periods, a Major Project Report for the Degree of doctor of philosophy in Mechanical Engineering, Balıkesir University.

[22] Atas A., Arslan N., Sen F. (2009), Failure analysis of laminated composite plates with two parallel pin-loaded holes, J*ournal of Reinforced Plastics and Composites*, **28**, 1265-1276.

[23] Icten B. M. (2006). Damage in laminated composite plates subjected to low-velocity impact, a Major Project Report for the Degree of doctor of philosophy in Mechanical Engineering, Dokuz Eylul University.

[24] Aktas M. (2007). Temperature effect on impact behavior of laminated composite plates, a Major Project Report for the Degree of doctor of philosophy in Mechanical Engineering, Dokuz Eylul University.

[25] Khalili S. M. R., Mittal R. K., Panah N. M. (2007). Analysis of fiber reinforced composite plates subjected to transverse impact in the presence of initial stresses, *Composite Structures*, **77**, 263–268.

[26] Cırak I. F. (2004). Homojen olmayan ortotrop kompozit malzemelerden olusan dikdörtgen plakların enine kayma deformasyonunu içeren titresim analizi, a Major Project Report for the Degree of master in Civil Engineering, Süleyman Demirel University.

[27] Gharagoni V. A. M. (2005). Vibration analysis of composite plates by finite element method (fem), a Major Project Report for the Degree of master in Mechanical Engineering, İstanbul University.

[28] Özakıncı M. (2006). Free vibration analysis of laminated composite plates, a Major Project Report for the Degree of master in Mechanical Engineering, İstanbul Teknik University.

[29] Eren A. (2007). Çatlak içeren kompozit şerit levhada levhanın doğal frekanslarına çatlağın etkisi, a Major Project Report for the Degree of master in Mathematical Engineering, Yıldız Teknik University.

[30] Eruslu S. Ö. (2008). Vibration analysis of short fiber reinforced composite plates, a Major Project Report for the Degree of doctor of philosophy in Mechanical Engineering, Trakya University.

[31] Tolun C. (2008). Load dynamic analysis of rectangular elastoplastic composite plates, a Major Project Report for the Degree of doctor of philosophy in Mechanical Engineering, Gazi University.

[32] Grimmer C. S. (2008). The cyclic strength of carbon Nanotube / Glass Fiber Hybrid Composites, a Major Project Report for the Degree of doctor of philosophy in Mechanical Engineering, University of California.

[33] Erkal S., Sayman O., Benli S., Dogan T., Yeni E. C. (2010). Fatigue Damage in Composite Cylinders, *Polymer Composites,* **31**,707–713.

[34] Rezaeepazhand J., Javari M. (2005). Stress analysis of perforated composite plates, *Composite Structures*, **71**, 463–468.

[35] Rezaeepazhand J., Javari M. (2010). Stress Analysis of Composite Plates with a Quasi-Square Cutout subjected to uniaxial tension, *Journal of reinforced plastics and composites*, **29**,2015-2026.

[36] Walker A. C. (1984). A brief review of plate buckling research. In: Rhodes J, Spence J, editors. *Behaviour of thin-walled structures*. London: Elsevier

[37] Bryan, G. H. (1891). On the Stability of a Plane Plate under Thrusts in its own Plane, with Applications to the Buckling of the Sides of a Ship, *Proc. London Math. Soc*., **22**, 54-67.

[38] Papila M., Akgün M. A. (2001). Post-Buckling of composite I-sections. Part 1: Theory, *Journal of Composite Materials*, **35**, 774-796.

[39] Zou G. P., Lam S. S. E. (2002). Buckling analysis of composite laminates under end shortening by higher-order shear deformable finite strips, *International Journal for Numerical Methods in Engineering*, **55**,1239–1254.

[40] Elaldı F. (2010). Structural efficiency and post-buckling strength of J- and Hat-stiffened Composite Panels, *Journal of Reinforced Plastics and Composites*, **29**, 1590-1594.

[41] Ray C. (2004). An Investigation on the effect of fiber weight fraction on buckling of laminated composite plates, *Journal of Reinforced Plastics and Composites*, **23**,951-957

[42] Wiedenman N., Dharan C. K. H. (2006). Ballistic penetration of compressively loaded composite plates, *Journal of Composite Materials*, **40**, 1041–1061.

[43] Chakrabarti A., Sheikh H. A. (2006). Buckling of composite laminates subjected to in-plane partial edge compression using a refined plate theory, *Journal of Reinforced Plastics and Composites*, **25**,1189-1204.

[44] Singh B.N., VermaV.K. (2009). Hydrothermal effects on the buckling of Laminated composite plates with random geometric and material properties, *Journal of Reinforced Plastics and Composites*, **28**, 409-427.

[45] Tarjan G., Sapkas A. K., Kollar (2010). Local web buckling of composite (FRP) Beams, *Journal of Reinforced Plastics and Composites*, **29**,1451-1462.

[46] Kim M., Cho J., Bae W. , Kweon J., Choi J. H., Cho S.,Cho Y. (2010). Buckling analysis of filament-wound thick composite cylinder under hydrostatic pressure, *International Journal of Precision Engineering and Manufacturing*, **11**, 909-913.

[47] Lin C.C., Kuo C.S. (1989). Buckling of laminated plates with holes, *Composite Materials*, **23,** 536–553.

[48] Britt, V. O. In: AIAA/ASME/ASCE/AHS/ASC Structures, Structural Dynamics, and Materials Conference, 34th and AIAA/ASME Adaptive Structures Forum, La Jolla, CA, Apr. 19-22, (1993), Technical Papers. Pt. 4 (A93-33876 13-39), p. 2240-2249.

[49] Srivatsa K.S., Murty A.V.K. (1993). Stability of Laminated Composite Plates with Cut-outs, *Computer and Structures*, **43(2)**, 273–279.

[50] Lee H. H., Hyer M. W. (1993). Postbuckling failure of composite plates with holes. *AIAA J*, **31(7)**, 1293–1298.

[51] Akbulut H., Sayman O. (2001). An Investigation on buckling of laminated plates with central square hole, *Journal of Reinforced Plastics and Composites*, **20**, 1112-1124.

[52] Kong C., Hong C., Kim C. (2001). Post buckling strength of composite plate with a hole, *Journal of Reinforced Plastics and Composites*, **20**, 466-481.

[53] Yazıcı M., Ozcan R., Ulku S., Okur I. (2003). Buckling of composite plates with u-Shaped cutouts, *Journal of Composite Materials*, **37**, 2179-2195.

[54] Yazıcı M. (2008). Buckling of square perforated thermoplastic composite plates, *Journal of Reinforced Plastics and Composites*, **27**, 1059-1070.

[55] Yazıcı M. (2009). Influence of cutout variables on buckling behavior of composite plates, *Journal of Reinforced Plastics and Composites*, **28**, 2325-2339.

[56] Jain P., Kumar A. (2004). Postbuckling response of square laminates with a central circular/elliptical cutout, *Composite Structures*, **65**, 179–185.

[57] Ghannadpour S. A. M., Najafi A., Mohammadi B. (2006). On the buckling behavior of cross-ply laminated composite plates due to circular/elliptical cutouts, *Composite Structures*, **75**, 3–6.

[58] Baltacı A. Sarıkanat M., Yıldız H. (2006). Buckling analysis of laminated composite circular plates with holes, *Journal of Reinforced Plastics and Composites*, **25**, 733-744.

[59] Elaldi F., Alecakir S. (2006). Damage tolerance of stiffened composite panels with cutouts, *Journal of Reinforced Plastics and Composite*, **25**, 1341-1351.

[60] Baba B. O. (2007). Buckling behavior of laminated composite plates, *Journal of Reinforced Plastics and Composites*, **26**, 1637-1655.

[61] Baba B. O., Baltacı A. (2007). Buckling characteristics of symmetrically and anti-symmetrically laminated composite plates with central cutout, *Appl. Compos. Mater.*, **14**, 265–276.

[62] Yeh H., Ryan Minh Le R. M. and Yeh H. (2007), Buckling of metal-matrix composite plate with a square hole, *Journal of Reinforced Plastics and Composites*, **26**, 525-540.

[63] Yapıcı A., Sahin Ö. S., Arıkan H. (2005). Buckling of Metal-reinforced Thermoplastic Composite Laminated Plates with holes, *Journal of Reinforced Plastics and Composites*, **24**, 1379-1386.

[64] Akbulut H., Ural T. (2007). An Investigation on buckling of composite laminated plates with corner circular notches, *Journal of Thermoplastic Composite Materials*, **20**, 371-387.

[65] Sahin M. (2008). Experimental and numerical analyses of laminated composite plates subjected to buckling Load., a Major Project Report for the Degree of master in Mechanical Engineering, Cumhuriyet University.

[66] Topal U., Uzman U. (2008), Maximization of buckling load of laminated composite plates with central circular holes using MFD method, *Struct Multidisc Optim*, **35**, 31–139.

[67] Kumar A. R. (2009). Analytical and experimental vibration analysis of e-glass epoxy woven type composite plate, a Major Project Report for the Degree of master in Civil Engineering, National Institute of Technology Rourkela.

[68] Selek K. (2009). Investigating of buckling effects in plates with and without hole, a Major Project Report for the Degree of master in Civil Engineering, Zonguldak Karaelmas University.

[69] Qablan H. A., Katkhuda H., Dwairi H. (2009). Assessment of the Buckling Behavior of Square Composite Plates with Circular Cutout Subjected to In-Plane Shear, *Jordan Journal of Civil Engineering*, **3(2)**, 184-195.

[70] Komur M. A., Sen F., Atas A., Arslan N. (2010). Buckling analysis of laminated composite plates with an elliptical/circular cutout using FEM, *Advances in Engineering Software*, **41**, 161–164.

[71] Kumar D., Singh S. B. (2010). Effects of boundary conditions on buckling and postbuckling responses of composite laminate with various shaped cutouts, *Composite Structures*, **92**, 769–779

[72] Sun X., Tong L., Chen H. (2001). Progressive Failure Analysis of Laminated Plates with Delamination, *Journal of Reinforced Plastics and Composites*, **20**, 1370-1389.

[73] Hwang S., Mao C. (2001). Failure of delaminated Carbon/Epoxy composite plates under compression, *Journal of Composite Materials*, **35**, 1634-1653.

[74] Hwang S., Liu G. (2002). Experimental Study for Buckling and post buckling behaviors of composite laminates with multiple delaminations, *Journal of Reinforced Plastics and Composites*, **21**, 333-349.

[75] Zor M. (2003). Delamination width effect on buckling loads of simply supported woven laminated composite plates made of carbon/Epoxy, *Journal of Reinforced Plastics and Composites*, **22**, 1535-1546.

[76] Zor M., Çallioglu H., Akbulut H. (2004). Three-dimensional buckling analysis of thermoplastic composite laminated with single vertical or horizontal Strip Delamination, *Journal of Thermoplastic Composite Materials*, **17**, 557-568.

[77] Zor M. (2009). Determination of critical width of multiple delaminations in laminated composite plate under buckling Load, *Journal of Reinforced Plastics and Composites*, **28**, 305-316.

[78] Msrao P., Hao S., Shu D. *(*2005). Buckling Analysis of Tri-layer Beams with Overlapped Delaminations, *Journal of Composite Materials*, **39**, 109-125.

[79] Wright J. E. (2006). Compound bifurcations in the buckling of a delaminated omposite strut , *Nonlinear Dynamics*, **43**,59–72.

[80] Arman Y., Zor M., Aksoy S., (2006). Determination of critical delamination diameter of laminated composite plates under buckling loads, *Composites Science and Technology*, **66**, 2945–2953.

[81] Yap C. W., Chai G. B. (2007). Analytical and numerical studies on the buckling of delaminated composite beams, *Composite Structures*, **80**, 307–319.

[82] Suemasu H., Irie T., TIshikawa T. (2009). Buckling and Post-buckling Behavior if Composite Plates Containing Multiple Delaminations, *Journal of Composite Materials*, **43**, 191-202.

[83] Sahin M. (2008). Experimental and numerical analyses of laminated composite plates subjected to buckling Load., a Major Project Report for the Degree of master in Mechanical Engineering, Cumhuriyet University.

[84] Aslan Z., Sahin M. (2009). Buckling behavior and compressive failure of composite laminates containing multiple large delaminations, *Composite Structures*, **89**, 382–390.

[85] Hosseini-Toudeshky H., Hosseini S., Mohammadi B. (2010). Buckling and delamination growth analysis of composite laminates containing embedded delaminations, *Appl Compos Mater*., **17**, 95–109.

[86] Kharazi M., Ovesy H.R., Taghizadeh M. (2010). Buckling of the composite laminates containing through-the-width delaminations using different plate theories, *Composite Structures*, **92**, 1176–1183.

[87] Ovesy H. R., Kharazi M., Taghizadeh M. (2010). Semi-analytical Buckling Analysis of Clamped Composite Plates Containing Embedded Rectangular and Circular Delaminations, *Mechanics of Advanced Materials and Structures*, **17**, 343–352.

[88] Chirica I. and Beznea E. (2011), Buckling analysis of the composite plates with delaminations, *Computational Materials Science*, **50**, 1587–1591.

[89] Damghani M., Kennedy D., Featherston C. (2011). Critical buckling of delaminated composite plates using exact stiffness analysis, *Computers and Structures*, **89**, 1286–1294.

[90] Kroflic A., Saje M., Planinc I., Zupan D. (2011). Buckling of asymmetrically delaminated three-dimensional composite beam: Analytical solution, *Composites: Part B*, **42(7)**, 2047‑2054.

[91] Schnabl S., Planinc I. (2011). The effect of transverse shear deformation on the buckling of two-layer composite columns with interlayer slip, *International Journal of Non-Linear Mechanics*, **46**, 543–553.

[92] Li S.R., Batra R. C., Sheng L. (2007). Vibration of thermally post-buckled orthotropic circular plates, *Journal of Thermal Stresses*, **30**, 43-57.

[93] Laura P. A. A., Rossit C.A. (1999). Thermal bending of thin, anisotropic, clamped elliptic plates, *Ocean Engineering*, **29**, 485-488.

[94] Lee J. (1997). Thermally induced buckling of laminated composites by a layer wise theory, *Computers and Structures*, **65(6)**, 917-922.

[95] Singha M. K., Ramachandra L. S., Bandyopadhyay J. N. (2000). Optimum design of laminated composite plates for maximum thermal buckling loads, *Journal of Composite Materials*, **34**, 1982-1997

[96] Kabir H. R. H., Askar H., Chaudhuri R. A. (2003). Thermal buckling response of shear flexible laminated anisotropic plates using a three-node isoparametric element, *Composite Structures*, **59**, 173–187.

[97] Kabir H. R. H. (1992). A shear locking free isoparametric three-nodetriangular finite element for moderately-thick and thin plates, *Int J Numer Meth Eng*, **35**,503–19.

[98] Le-Chung S., Shih-Yao K. (2004). Thermal buckling of composite sandwich plates, *Mechanics Based Design of Structures and Machines*, **32**, 57–72

[99] Shariyat M. (2007). Thermal buckling analysis of rectangular composite plates with temperature-dependent properties based on a layer wise theory, *Thin-Walled Structures*, **45**, 439–452.

[100] Barton O. JR. (2009). Approximate method for buckling of symmetric composite Laminates under thermal loading, *Journal of Thermoplastic Composite Materials*, **22(3)**, 305-320.

[101] Le-Chung S., Shih-Yao K., Cheng-Yuan C. (2010). Thermal buckling behavior of composite laminated plates, *Composite Structures*, **92**, 508–514.

[102] Aydogdu M. (2007). Thermal buckling analysis of cross-ply laminated composite beams with general boundary conditions, *Composites Science and Technology*, **67**, 1096-1104.

[103] Yapici A. (2005). Thermal buckling behavior of hybrid-composite angle-ply laminated plates with an inclined crack, *Mechanics of Composite Materials*, **41**, 131-138.

[104] Avci A., Sahin O.S., Ataberk N. (2006). Thermal buckling behavior of cross-ply hybrid composite laminates with inclined crack, *Composites Science and Technology*, **66**, 2965-2970.

[105] Avci A., Kaya S., Daghan B. (2005). Thermal buckling of rectangular laminated plates with a hole, *Journal of Reinforced Plastics and Composites*, **24**, 259-272.

[106] Avci A., Sahin O.S., Uyaner M. (2005). Thermal buckling of hybrid laminated composite plates with a hole, *Composite Structures*, **68**, 247-254.

[107] Sahin O. S. (2005). Thermal buckling of hybrid angle-ply laminated composite plates with a hole, *Composite Science and Technology*, **65**, 1780-1790.

[108] Bauld N. R., Tzeng L. S. (1984). Vlasov theory for fiber-reinforced beams with thin-walled open cross sections, *Int J Solids Struct*, **20**, 277-297.

[109] Ma M., Hughes O. (1996). Lateral distortional buckling of monosymmetric I-beams under distributed vertical load, *Thin Walled Structures*, **26(2)**, 123-145

[110] Mottram J.T. (1992). Lateral-torsional buckling of a pultruded I-beam, *Composites*, **23(2)**, 81-92.

[111] Davalos J. E., Qiao P., Salim H. A. (1997). Flexural-torsional buckling of pultruded fiber reinforced plastic composite I-beams: experimental and analytical evaluations, *Composite Structures*, **38(1-4)**, 241-250.

[112] Roberts T. M., Al-Ubaidi H. (2001). Influence of shear deformation on restrained torsional warping of pultruded FRP bars of open cross-section, *Thin Walled* Struct,**39**, 395–414.

[113] Qiao P., Zou G. and Davalos J. F. (2002). Lateral buckling of FRP composite cantilever I-beams. In: 15th ASCE Engineering Mechanics Conference, Columbia University, June 2-5, New York: NY.

[114] Brooks R. J., Turvey G. J. (1995). Lateral buckling of pultruded GRP I-section cantilever, *Composite Structures*, **32**, 203–15.

[115] Turvey G. J. (1996). Effects of load position on the lateral buckling response of pultruded GRP cantilevers-comparisons between theory and experiment, *Composite Structures*, **35**, 33–47.

[116] Roberts T. M., Masri T. M., H. M. (2003). Section Properties and Buckling Behavior of Pultruded FRP Profiles, *Journal of Reinforced Plastics and Composites*, **22**, 1305-1317.

[117] Silva N. F., Silvestre N. (2007). On the Influence of Material Couplings on the Linear and Buckling Behaviour of I-section Composite Columns, *International Journal of Structural Stability and Dynamics* , **7**, 243-272.

[118] Correia J. R., Branco F. A., Silva N. F., Camotim D., Silvestre N. (2011). First-Order, Buckling and Post-Buckling Behaviour of GFRP Pultruded Beams-Part 1: Experimental Study, *Computers & Structures*, **89**, 2052-2064.

[119] Silva N. F., Camotim D., Silvestre N., Correia J. R., Branco F. A. (2011). First-Order, Buckling and Post-Buckling Behaviour of GFRP Pultruded Beams-Part 2: Numerical Simulation, *Computers and Structures*, **89**, 2065-2078.

[120] Kabir M. Z., Sherbourne A. N. (1998). Optimal fiber orientation in lateral stability of laminated channel section beams, *Composites Part B*, **29(1)**, 81–87

[121] Kabir M. Z., Sherbourne A. N. (1998). Lateral-torsional buckling of post-local buckled fibrous composite beams, *J Eng Mech* , **124 (7)**, 754-764.

[122] Lee J., Kim S. (2001). Flexural-torsional buckling of thin-walled I-section composites, *Computers and Structures*, **79(10)**, 987–95.

[123] Lee J, Kim S., Hong K. (2002). Lateral buckling of I-section composite beams, *Eng Struct* , **24**, 955–964

[124] Sapkas A., Kollar L. P. (2002). Lateral-torsional buckling of composite beams, *Int J Solids Struct*, **39**, 2939–2963.

[125] Lee J., Lee S. (2004). Flexural–torsional behavior of thin-walled composite beams, *Thin Walled Struct*, **42**, 1293–1305.

[126] Mohri F., Azrar L., Potier-Ferry M. (2002). Lateral post-buckling analysis of thin-walled open sections beams, *Thin Walled Struct*, **40**, 1013–1036.

[127] Machado S. P., Cortinez V. H. (2005). Lateral buckling of thin-walled composite bisymmetric beams with prebuckling and shear deformation, *Eng Struct*, **27**, 1185–1196.

[128] Machado S. P. (2007). Geometrically non-linear approximations on stability and free vibration of composite beams, *Eng Struct*, **29**, 3567–3578.

[129] Lawson R. M., Lim J., Hicks S. J., Simms W. I. (2006). Design of composite asymmetric cellular beams and beams with large web openings, *J Constr Steel Res*, **62**, 614–629.

[130] Kim N., Shina D. K., Kim M. (2007). Exact lateral buckling analysis for thin-walled composite beam under end moment. *Eng Struct*, **29**, 1739–1751.

[131] Kim N., Shina D. K., Kim M. (2007). Improved flexural–torsional stability analysis of thin-walled composite beam and exact stiffness matrix, *Int J Mech Sci*, **49**, 950–969.

[132] Minghini F., Tullini N., Laudiero F. (2008). Buckling analysis of FRP pultruded frames using locking-free finite elements, *Thin Walled Struct* ,**46**, 223–241.

[133] Kabir M. Z., Seif A. E. (2010). Lateral-Torsional Buckling of Retrofittted Steel I-Beams Using FRP Sheets, *Transaction A: Civil Engineering*, **17(4)**, 262-272.

[134] Lee J. (2006). Lateral buckling analysis of thin-walled laminated composite beams with monosymmetric sections, *Eng Struct*, **28**, 1997–2009

[135] Machoda SP. (2008). Non-linear buckling and postbuckling behavior of thin-walled beams considering shear deformation, *Int J Non Linear Mech*, **43**, 345 –365.

[136] Karaagac C., Ozturk H., Sabuncu M. (2009). Free vibration and lateral buckling of a cantilever slender beam with an edge crack: Experimental and numerical studies. *J Sound Vib*, **326**, 235–250.

[137] Eryigit E. (2006). Surveying buckling with the effect of lateral load at laminated composite beam, a Major Project Report for the Degree of master in Mechanical Engineering, Dokuz Eylul University.

[138] Eryigit E., Zor M., Arman Y. (2009). Hole effects on lateral buckling of laminated cantilever beams, *Composites: Part B*, **40**, 174–179.

[139] Hwang S. F., Mao C. P. (2001). Failure of delaminated interply hybrid composite plates under compression, *Composites Science and Technology*, **61**, 1513–1527.

[140] Önal G. (2006), Mechanical buckling behavior of hybrid laminated composite plates with inclined crack, *Journal of Reinforced Plastics and Composites*, **25**, 1535-1544.

[141] Kar N.K., Barjasteh E., Hu Y. and Nutt S.R. (2011). Bending fatigue of hybrid composite rods, *Composites: Part A*, **42**, 328–336.

[142] Hosur M. V., Adbullah M., Jeelani S.(2005). Studies on the low-velocity impact response of woven hybrid composites, *Composite Structures*, **67**, 253–262.

[143] Sayer M. and Bektaş N. B. (2009). Temperature effects on hybrid composite plates under impact loads, *Pamukkale University Journal of Engineering Sciences*, **15**, 337-343.

[144] Sevkat E., Liaw B., Delale F., Raju B. B. (2009). Drop-weight impact of plain-woven hybrid glass–graphite/toughened epoxy composites, *Composites: Part A*, **40**, 1090–1110.

[145] Sayer M., Bektas N. B., Sayman O. (2010). An experimental investigation on the impact behavior of hybrid composite plates, *Composite Structures*, 92, 1256–1262.

[146] Ghasemnejad, H., Furquan, A. S. M., Mason, P. J. (2010). Charpy impact damage behaviour of single and multi-delaminated hybrid composite beam structures, *Materials and Design*, **31**, 3653–3660.

[147] Durao, L. M., Magalhaes, A. G., Marques A. T. and Tavares J. M. R. S. (2008). Damage assessment of drilled hybrid composite laminates, proceeding of 13th European conference on composite materials, June 2-5, Stockholm, Sweden, 1-10.

[148] Don O. Brush, Bo O. Almroth (1975). Buckling of Bars, Plates, and Shells. 1st Edition. United States: McGraw-Hill, Inc.

[149] ASTM Standards and Literature References for Composite Materials. (2010) Standard Test Method for Tensile Properties of Plastics D 638-10. American Society for Testing and Materials, Philadelphia, PA.

[150] ASTM Standards and Literature References for Composite Materials. (2008) Standard Test Method for Compressive Properties of Polymer Matrix Composite Materials with Unsupported Gage Section by Shear Loading D3410/D3410M–03. American Society for Testing and Materials, Philadelphia, PA.

[151] ASTM Standards and Literature References for Composite Materials. (2008) Standard Test Method for In-Plane Shear Response of Polymer Matrix Composite Materials by Tensile Test of a ±45° Laminate D3518/D3518M – 94. American Society for Testing and Materials, Philadelphia, PA.

[152] ANSYS Procedures. Engineering analysis system verification manual, vol. 1. (1993), Houston, PA, USA: Swanson Analysis System Inc.